To the Graduate Council:

I am submitting herewith a thesis written by Douglas Stewart Falcon entitled "The Determination of Specific Heat and Electrical Resistivity of an Alloy with Nickel and Molybdenum in the Ratio of 4:1 Using a Pulse-Heating Calorimeter". I have examined the final copy of this thesis for form and content and recommend that it be accepted in partial fulfillment of the requirements for the degree of Master of Science, with a major in Metallurgical Engineering.

C.R. Brooks, Major Professor

We have read this thesis
and recommend its acceptance:

E.E. Stansbury

B.F. Oliver

Accepted for the Council:

Associate Vice Chancellor and
Dean of the Graduate School

DETERMINATION OF SPECIFIC HEAT AND ELECTRICAL RESISTIVITY OF AN ALLOY WITH NICKEL AND MOLYBDENUM IN THE RATIO OF 4:1 USING A PULSE-HEATING CALORIMETER

A Thesis
Presented for the
Master of Science
Degree
The University of Tennessee, Knoxville

Douglas Stewart Falcon
December 1998

This thesis is dedicated

to my wife

April

and

to my daughter

Jessica

who have given me encouragement and

enthusiasm to continue my education.

ACKNOWLEDGMENTS

There are several people who have contributed to this project, to whom the author expresses his appreciation.

I would first like to thank his major professor, Dr. Charlie Brooks, for his continuous assistance in reviewing the data and providing advice. I could not have completed this work without Dr. Brooks' help. I would also like to thank the other members of his thesis committee, Dr. Gene Stansbury and Dr. Ben Oliver, for their continued interest in the pulse-heating calorimeter project.

I also received assistance from the University of Tennessee Materials Science and Engineering Department and Chemical Engineering Department machine shop and electronics shop members. I am especially grateful to Doug Fielden and Raymond Bellamy from the machine shop, and Mark Potter and Greg Jones from the electronic support shop. Among other things, the machine shop personnel provided prompt construction of many prototype parts for the calorimeter and provided precision sample measurements. The electronic shop personnel helped keep certain parts of the pulse-calorimeter operational and properly calibrated.

I would also like to acknowledge tremendous support from the Materials Science & Engineering department secretaries, Sandy Maples and Carla Lawrence, and from the Chemical Engineering secretaries, Sancy Hail and Betty Frazier.

ABSTRACT

The Ni_4Mo alloy goes through an order-disorder phase transformation at 1141 K. Specific heat and electrical resistivity data were obtained on three states of the alloy: equilibrium LRO β from 300 to 1141 K, equilibrium SRO α from 1141 K to 1400 K, and metastable SRO α from 300 to 1141 K.

The method used to obtain the data was a pulse-heating calorimeter, which allowed data to be obtained at heating rates over 200 K/s. Two different heating rates were used; 60 to 75 K/s (30 amp pulses) and 120 to 220 K/s (65 amp pulses). These high heating rates suppressed certain aspects of the transformations that were not suppressed at very slow heating rates (0.2 K/s) used by other researchers. These differences were apparent in comparing the specific heat data and electrical resistivity data of specimens in the SRO α initial condition. The specific heat data at very slow heating rates showed two minimums due to heat release affects between 300 K and 1141 K whereas the heating rates used here did not show these affects. The electrical resistivity data of the very slow heating rates showed a minimum prior to the critical temperature upon heating, wheras the heating rates used here did not indicate any mimimum in that region.

There was a slight shift in the thermal arrest portion of the initial LRO β temperature-time plot from 1141 K at pulses of about 60 to 75 K/s to about 1160 K at pulses of about 200 K/s. This indicates that higher heating rates than those used here may suppress the order-to-disorder transformation. This would allow data on the metastable LRO β phase to be obtained further above 1141 K.

The Gibbs free energy change of the transformation was evaluated from 300 to 1141 K based on the specific heat data obtained in this study. The free energy change was

found to be primarily due to the heat of transformation term (ΔH_0 times the supercooling divided by the transformation temperature), which was found from the literature. The integral terms were small (less than 1 %) compared to this term because the ΔCp term was small.

TABLE OF CONTENTS

LIST OF FIGURES

LIST OF TABLES

Chapter 1. Introduction

This research was primarily based on recommendations from other projects that were conducted at the University of Tennessee. The goals of this thesis were to obtain specific heat data and electrical resistivity data over the temperature range from 300 to 1400 K on alloy Ni_4Mo.

The Ni-Mo alloys are often the alloy of choice for certain high temperature corrosion resistance applications. Examples of an industrial alloys based primarily on this composition is the Hastalloy™ B series alloys. Of particular interest is the order-disorder phase transformation which the Ni4Mo alloy undergoes upon heating above a critical temperature of 1141 K. One further goal of the thesis was to use the specific heat data to calculate the Gibbs free energy change of the phase transformation over the 300 to 1400 K temperature range. In order to determine the free energy, it was necessary to obtain specific heat data in both the equilibrium and metastable phases.

The specific heat, discussed in detail in Section 2.5, is a fundamental thermodynamic property. It is especially useful in deriving several other thermodynamic quantities. One of these quantities, the Gibbs free energy, is determined in Chapter 4 from the specific heat data that was found. Other thermodynamic relationships are discussed in Chapter 2. The specific heat and electrical resistivity data that were obtained are presented in Chapter 4.

The electrical resistivity, which is discussed in detail in Section 2.4, is a fundamental physical property that is useful in detecting changes in the atomic structure. The data may be used to test certain theories of solid state behavior. The change in resistivity during ordering is sufficiently large that resistivity measurements have been

used to monitor the kinetics of both LRO and SRO in alloys. The electrical resistivity also gives information on the impurity of the material, detection of phase and magnetic transitions, and information on defect production and migration. It can be used in prediction of thermal conductivity through the Wiedmann-Franz law, and it can be used to calculate magnetoresistivity. Other practical aspects of knowing the electrical resistivity include applications for strain gauges and thermometers.

The method chosen to obtain the specific heat data and electrical resistivity data is by pulse-heating calorimetry. This method is discussed in detail in Chapter 3. It has several advantageous over other calorimetric techniques. The high heating rate and short time of the pulse give it high accuracy due to the minimal heat losses. The specific heat data and electrical resistivity data are obtained simultaneously during the pulse. The high heating rate of the pulse-heating calorimeter also makes it applicable to the measurement of specific heat and electrical resistivity on metastable states. Because of the high heating rate for such a short period of time, the specimen heats up while the surrounding materials stay at a much lower temperature. Hence the calorimeter components do not have to be made of extremely high-temperature materials.

The method basically consists of passing a high current for a short period of time through an electrical conductor. The specimen, usually in the shape of a round wire, heats up due to the resistive self-heating. The electrical potential at different points of the circuit along with the temperature of the sample are measured as a function of time during the pulse. From these values, the electrical resistivity and specific heat of the material can be determined.

Chapter 2. Literature Review of the Nickel-Molybdenum Binary System

2.1 Equilibrium Phase Diagram

Numerous investigators have researched various portions of the phase diagram and other aspects of the Ni-Mo system. The works mentioned in this review are by no means a complete list.

A current equilibrium phase diagram by Singleton and Nash [1] is shown in Figure 2.1. This diagram was obtained by using a least-squares-optimization method of thermodynamic modeling. The assessed diagram is based primarily on data by Casselton and Hume-Rothery [2] and Wicker et al. [3] for the liquidus/solidus lines, and the solid-state equilibrium was based on those of Casselton and Hume-Rothery [2], Heijwegan & Rieck [4], and Katayanama et al. [5].

The main features of the phase diagram are described as follows. The nickel phase (designated as α) is a fairly extensive terminal solid solution. The Mo phase, however, is a very limited terminal solid solution. The Mo solidus was studied by Kang et al. [6] and their results indicate that the maximum solubility of Ni in Mo is 2.8 wt% at 2450 K. There are three equilibrium intermetallic compounds at or near the stoichiometric ratios of Ni_4Mo (20 at%), Ni_3Mo (25 at%), and NiMo (50 at%), which are designated as β, γ, and δ, respectively. β and γ are closely stoichiometric and have a narrow composition range, but δ has a range of existence of about 2 at%. Upon heating, β and γ decompose by a peritectoid reaction, while δ decomposes peritectically. A eutectic occurs at about 35 at% Mo and 1318 °C, and a peritectic occurs at about 38 at% Mo and 1362 °C.

Some of the earlier phase diagrams were from Ellinger [7], Elliot [8] and Hansen [9]. Casselton and Hume-Rothery [2] is still one of the more frequently cited works.

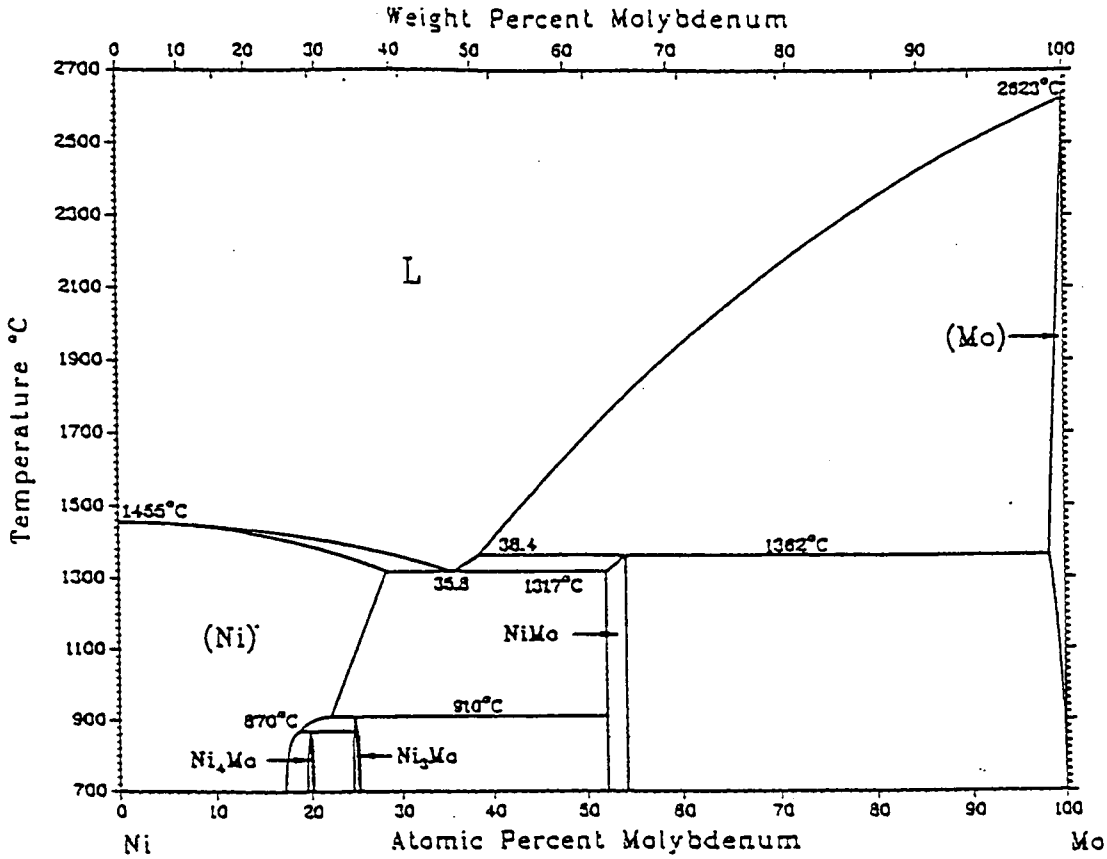

Figure 2.1 Equilibrium phase diagram of the nickel-molybdenum binary system. From Singleton and Nash [1].

They re-evaluated Hansen's diagram and using thermal, microscopical, and x-ray methods, found slightly different results. Their samples were from high purity powder material that was pressed and sintered, and then either induction melted in a vacuum or arc melted on a Cu hearth in an Ar atmosphere. A single β phase was not obtained in their 80.4 at% Ni sample, and so they placed the β region at 80.5 to 81.0 at% Ni. This does not include the exact Ni_4Mo stoichiometry. The γ phase was placed as including Ni_3Mo, and as varying less than 1 at%. The δ phase is placed at about 47 at% Ni, but has a width of about 2 at%.

Bloom and Grant [10] looked at the Ni-Mo-Cr ternary system, and re-evaluated Ellinger's [7] system. They found a few differences in the diagram.

1. The eutectic was found to be closer to 57.5 wt% instead of 54 wt%.
2. They found the peritectic temperature to be 1350 °C instead of 1370 °C.
3. The liquid composition in equilibrium with the Mo solid solution at the peritectic reaction of 1350 was closer to 53 % Ni instead of 48% Ni.

Heijwegan & Rieck [4], determined the phase diagram between 800 and 1295 °C using microscopic and electron probe micro-analysis. Their samples were prepared by both the diffusion-couple method and the equilibriated-alloy method. Both of their methods yielded the same phase diagram results. The β phase was found to be 80.0 to 80.5 at% Ni, the γ phase was found to be 75.5 to 76.0 at% Ni, and the δ phase ranged from 48 to 52 at% Ni.

Guthrie and Stansbury [11] investigated the 12-48% Mo and 700-1000°C region, and these results are consistent with Heijwegan & Rieck [4] on the three intermediate phases, which is the composition region of most of the important commercial alloys.

They found the β phase to be in the region of 20 to 20.5 at% Mo, which does include Ni_4Mo.

Gust et al. [12] place the β phase in agreement with Casselton and Hume-Rothery [2] using metallographic methods. They used samples ranging from 18 to 23 at % Mo, and aged samples at 550, 605, and 827 °C for very long times. Ellinger [7] put the β phase at 80 at% Ni and the δ phase at 48.9 to 51.0 at% Mo.

Brooks, Spruiell, and Stansbury [13] reviewed the overall physical metallurgy of the Ni-Mo system. They contrasted the β phase location graphically (see Figure 2.2) from data by Guthrie and Stansbury [11], Casselton and Hume-Rothery [2], and Heijwegan and Rieck [4]. They pointed out that diffusion-couple and metallographic techniques by Heijwegan and Rieck [4] only allowed some boundaries to be determined within 5 at% Mo.

Brooks et al. [13] used electrical resistivity measurements and specific heat measurements to determine the β decomposition temperature as 868 ± 3 °C. This is in contrast to data by Kozlov and Kusharennko [14], who place the temperature at 876 ± 5 °C, with a composition of about 20.7 at% Mo. Guthrie and Stansbury [11] place the composition of this point at between 19.2 and 20.8 at % Mo. Casselton & Hume-Rothery [2] and Heijwegan and Rieck [4] put this value closer to 18 at% Mo.

Frisk [15] calculated the phase diagram. A subregular model was used to determine the FCC Ni and BCC Mo phases and the liquid phase. The δ phase region was determined based on the crystal structure, determined by Shoemaker and Shoemaker [16] (see Section 2.3). The β and γ phases were assumed to be stoichiometric Ni_4Mo and Ni_3Mo, respectively.

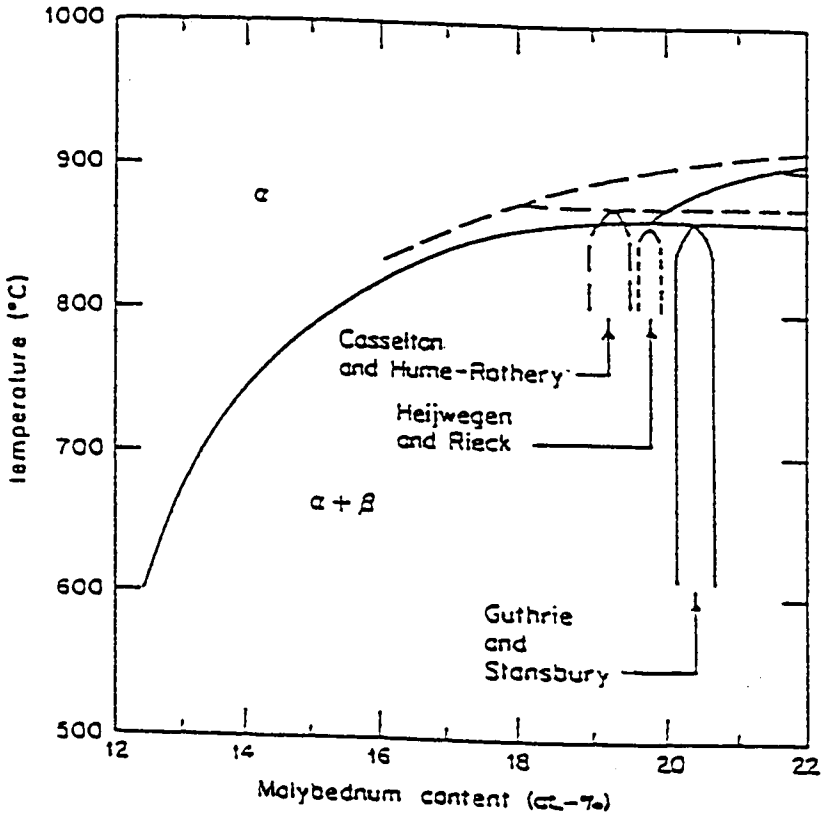

Figure 2.2 Graphical contrast of the β phase composition according to different investigators [13].

Some other diagrams of the Ni-Mo system which were calculated or partially calculated were presented by Kang et al. [6] and Kaufman and Nesor [17]. Computer advances have aided in calculating phase equilibria. Caution must be used however. Okamoto [18] points out that it is not rare to find phase diagrams that involve functions with parameters with hardly credible magnitude. Okamoto and Massalski [19] discuss thermodynamically improbable phase diagrams.

2.2 Crystal Structures

2.2.1 α *Phase*

As can be seen by Figure 2.1, the intermetallic phases β and γ transform to the alpha (α) phase if the temperature is high enough. α is also the equilibrium phase at room temperature below approximately 19 at% Mo. The α phase is a solid solution of Mo in Ni and is the Struchturbericht A1 type of structure, which is a standard FCC unit cell.

Harker [20] worked on a 18.7 at% Mo alloy, and found the lattice parameter to be 3.612 Å. Brooks et al. [13] found the lattice parameter to be:

$$a = 0.00406 \text{ at\% Mo} + 3.5242 \text{ (Å)} \qquad \textbf{(2.1)}$$

This empirical relationship was based on a least-squares fit of data from Casselton and Hume-Rothery [2], Guthrie and Stansbury [11], and Nosova and Polyakova [21].

The α phase is also a short-range ordered (SRO) solid solution. This was observed by Spruiell and Stansbury [22] in the quenched Ni_4Mo alloy using x-ray diffuse scattering methods. More details of the SRO phenomena will be discussed in Section 2.3 on the SRO (α) to LRO (β) phase transformation.

2.2.2 β *Phase*

The β phase occurs below 1141 K (868 °C) at compositions near Ni_4Mo as discussed in the previous section. It is now accepted as a long-range ordered (LRO) structure of the D1a type of superlattice, which is a body-centered tetragonal (BCT) structure. Figure 2.3 shows the unit cell.

Grube and Schlect [23] first reported the existence of β, and they reported the crystal structure to be tetragonal. Harker [20] later used x-ray diffraction methods on a 18.7 at% Mo sample quenched from 1200 °C , which showed an FCC pattern. He then held the alloy at temperature ranges between 700 and 825 °C, and found a similar pattern to what he previously observed from an AuCu alloy. Thus he suggested that there was an ordering reaction occurring. The lattice parameters were determined to be a = 3.618 Å , c = 3.567 Å , with c/a = 0.986. The structure was found to be body-centered tetragonal (BCT), with 8 Ni atoms and 2 Mo atoms per unit cell. He determined the crystal structure to be of the C_{4h}^5 type of space group (D1a). This was later confirmed by Casselton and Hume-Rothery [2] and by Guthrie and Stansbury [11], although they reported different lattice parameters: a = 5.683 Å , c = 3.592 Å with c/a = 0.632 and a = 5.727 Å, c = 3.566 Å with c/a = 0.623, respectively.

Harker also showed how there could be 30 ways in which the Ni_4Mo structure could be situated in a region that was originally a single FCC crystal. Thus the solid solution becomes a very complicated array of Ni_4Mo crystals as the reaction proceeds. Slip becomes much more difficult because of the complex arrangement of tetragonal regions.

Brooks et al. [13] give the specific atom coordinates of the Ni_4Mo ordered phase:

2 Mo atoms at
(0,0,0) and (1/2, 1/2, 1,2)

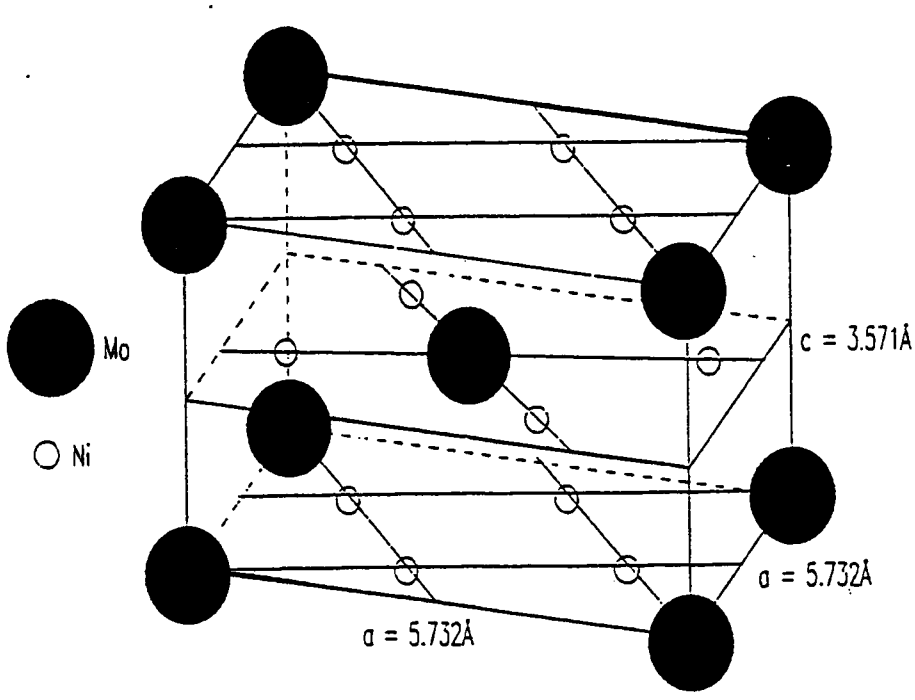

Figure 2.3 β phase crystal structure. The structure is body-centered tetragonal. Adapted from Brooks et al. [13].

8 Ni atoms at

(x,y,0), (-x, -y, 0), (-y,x,0), (y,-x,), (x+1/2,y+1/2,1/2)
(-x+1/2,-y+1/2,1/2), (-y+1/2,x+1/2,1/2), and (y+1/2,-x+1/2,1/2)

where x = 1/5 and y = 2/5.

For a more detailed discussion of some general aspects of the D1a structure, see Matveeva and Kozlov [24].

Other alloys of the D1a AB_4 tetragonal type are alloys of Au with Group IV and VII transition metals and Ni with tungsten. More specifically, WNi_4, $TiAu_4$, VAu_4, $CrAu_4$, and $MnAu_4$.

The Mo atoms occupy the BCT sublattice while the Ni atoms form 4 sublattices, so the structure can be considered as 5 interpenetrating BCT sublattices. With a slight adjustment of the average inter-atomic distance, FCC (α) is formed. An equivalent way of deriving the BCT crystal structure from the α phase would be to order the Mo atoms in the lattice, and then allow a slight shift in innerplanar spacing. Figure 2.4 shows the relationship between the β and FCC lattice. This will be discussed further in the phase transformations review section. On the (001) plane, Mo atoms are on successive {110} rows and are arranged such as to maximize the distance between like atoms on a previous {110} row. When a second plane is placed on top, the Mo atoms occupy the positions marked by an 'X' in Figure 2.4.

2.2.3 γ Phase

Grube and Winkler [25] determined that the γ Ni_3Mo alloy had an HCP lattice with a = 2.545 Å and c/a = 1.65. Saito and Beck [26] later determined that the crystal structure could be considered as an ordered orthorhombic structure of a disordered HCP structure. It is actually isotypic with the ordered $TiCu_3$ structure type (Struchturbericht

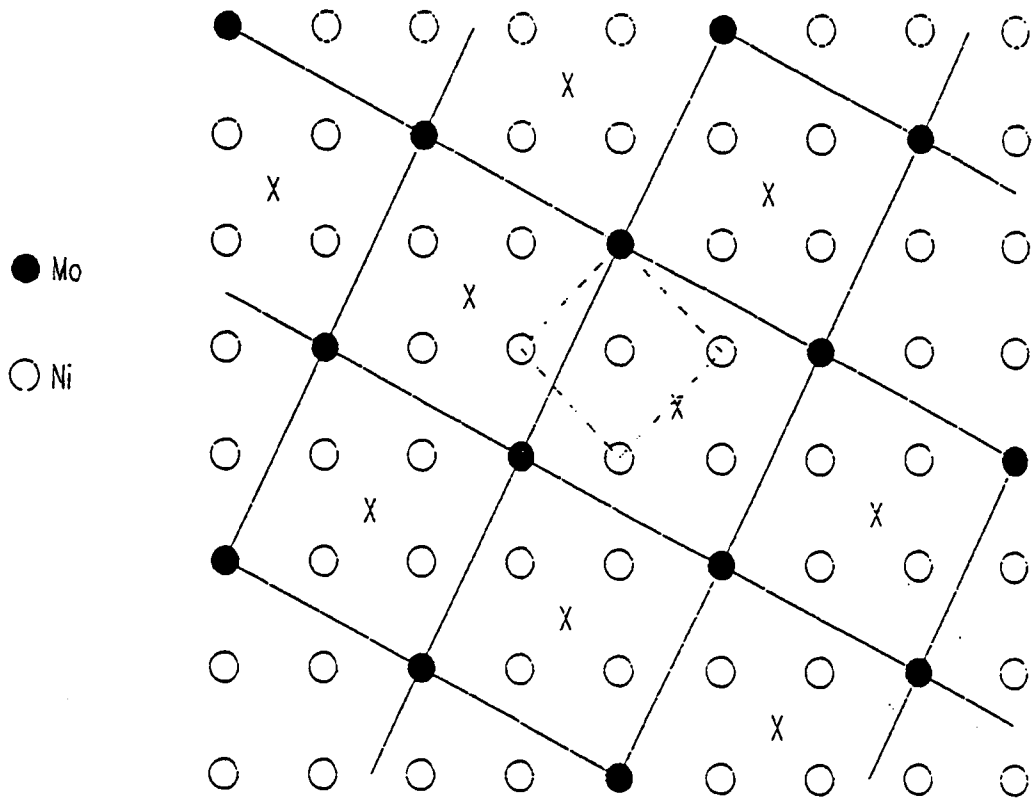

Figure 2.4 View of the (001) plane of the β phase. The dark circles represent Mo atoms and the open circles represent Ni atoms. The 'X' represents Mo atoms one half plane above and below the (001) plane. The dashed line shows the outline of the FCC unit cell of the α phase. After Guthrie and Stansbury [11].

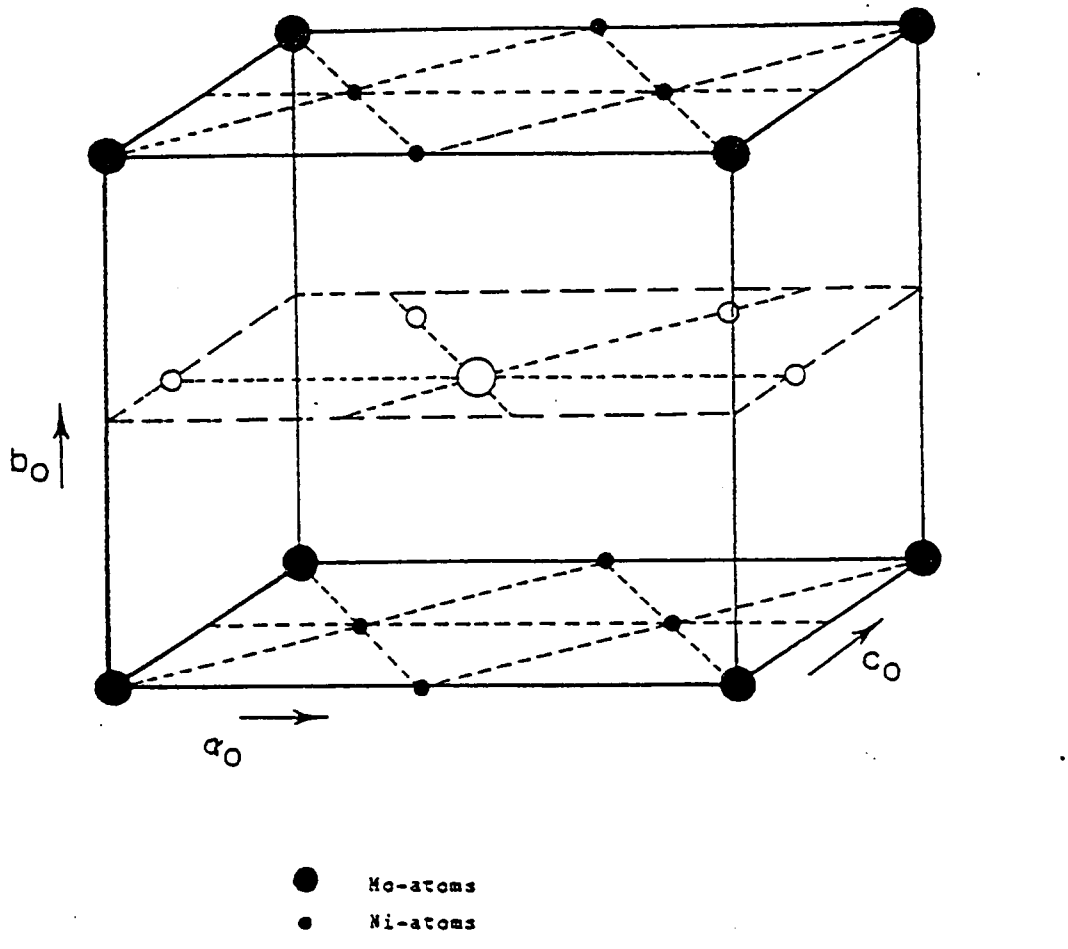

Figure 2.5 γ phase crystal structure. After Van Tendeloo and Amelinckx [27].

D0a [24]). The crystal structure is shown in Figure 2.5 from Van Tendeloo and Amelinckx [27]. This unit cell has a = 5.064 Å, b = 4.448 Å, and c = 4.224 Å. There are 6 Ni atoms and 2 Mo atoms per unit cell.

There are 3 orientations of the γ phase that can form within the FCC matrix [13]. Quenched alloys of Ni_3Mo composition have SRO α structure similar to that found in the Ni_4Mo, and γ transforms to LRO. It gives complex orientation relationships of domains during the transformation. These were investigated by Ruedl and Amelinckx [28] in more detail.

2.2.4 δ Phase

The δ phase is close to NiMo stoichiometry, but has a range of compositions. This structure was determined by Shoemaker & Shoemaker [16] to be an orthorhombic cell with tetragonal symmetry, shown in Figure 2.6. They used single crystal x-ray analysis on a sample of composition 49.2 ± 0.2 at% Mo. The lattice parameters are a = b = 9.108 ± 0.005 Å and c = 8.852 ± 0.005 Å. The δ phase is complicated, belonging to the P-$2_12_12_1$ space group (it was originally assumed [29] to be of the P-$4_22_12(D^6_4)$).

It is completely ordered upon quenching from 1350 °C (α region) and the domain structure was investigated by Van Tendeloo and Amelinckx [30] using electron microscopy and diffraction. It shows three types of predicted domain boundaries; anti-phase boundaries, inversion boundaries, and permutation twins.

Obrowski [31] reported that the δ phase has a tetragonal structure with a primitive cell of parameters a= 9.36 Å, c = 4.85 Å, and a space group of P-$4_22_12_1$. Nash et al. [32] and Miracle et al. [33] support the findings of Shoemaker and Shoemaker [16].

Jin et al. [34] studied the δ phase using SEM, EDS, and TEM. They determined

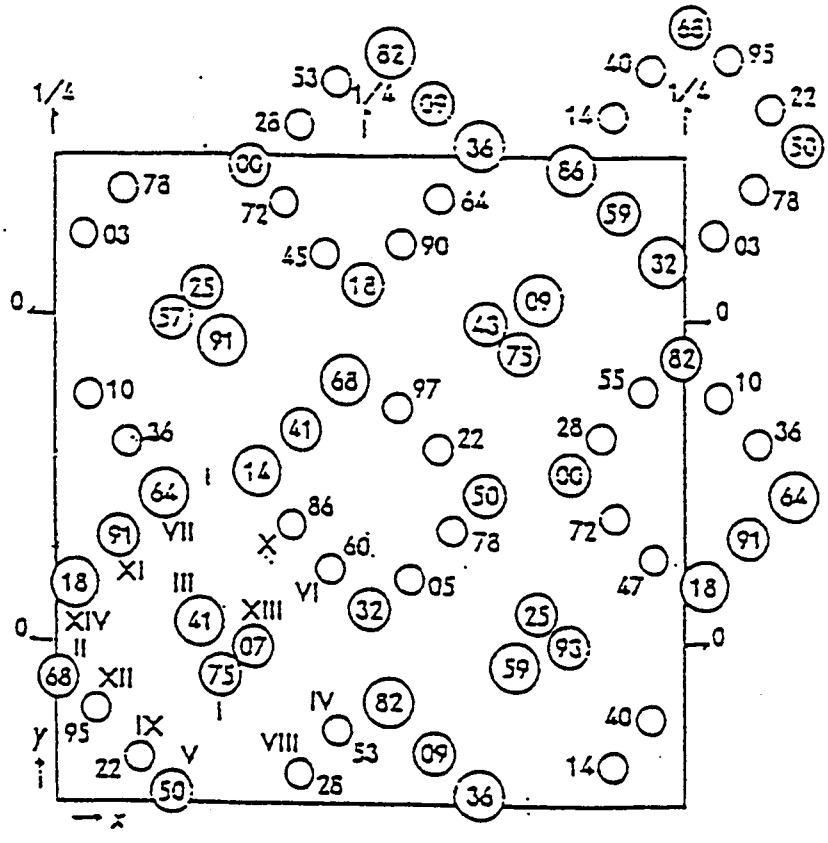

Figure 2.6 Structure of the NiMo δ phase looking down the 'z' axis. Large circles represent Mo atoms. Small circles repesent Ni atoms. Intermediate circle sizes represent a mixture of Ni and Mo atoms. The numbers inside the circles are z coordinates in hndredths of the unit cell length, c. After Shoemaker and Shoemaker [16].

the structure to be tetragonal with a = b = 9.108 Å, c = 8.852 Å, and belonging to the P4/mmm space group using a convergent beam electron diffraction method.

2.2.5 Ni_2Mo Metastable Phase

There are two other known phases not shown on the equilibrium diagram that are involved in some phase transformations: the Ni_2Mo metastable phase and the DO_{22} metastable phase.

Saburi et al. [35] noted the existence of a Pt_2Mo type superlattice (possibly ordered Ni_2Mo) in the early stages of decomposition of regions of a quenched sample. The $MoPt_2$ type is a $D^{25}{}_{2h}$-Immm structure [24]. They used alloy samples of 20.1, 22.7, and 24.4 at% Mo, which were quenched and then annealed at a temperature below the peritectoid temperature (assumed to be 865 °C) for various times. Optical and electron microscopy was used to investigate the transition. They found four stages in the transformation from FCC in the 22.7 at% sample:

1. Decomposition of α into small β domains and coaguration of Ni_2Mo uniformly throughout the matrix.
2. Growth of β domains and coaguration of Ni_2Mo along β domain boundaries.
3. Nucleation of aggregate of γ phase and β phase blocks.
4. Growth of aggregate to consume the existing β + Ni_2Mo region.

The second, third, and fourth stages overlap.

Das and Thomas [36] also did TEM and diffraction studies in the initial stages of ordering in Ni_3Mo and Ni_4Mo alloys, and confirmed that Ni_3Mo LRO development involves the formation of metastable Ni_2Mo and Ni_4Mo. Figure 2.7 shows a schematic diagram of the unit cell, and the relationship to the FCC structure. The projection of atoms onto the (001) FCC plane is shown in Figure 2.7(b). The dashed lines outline the

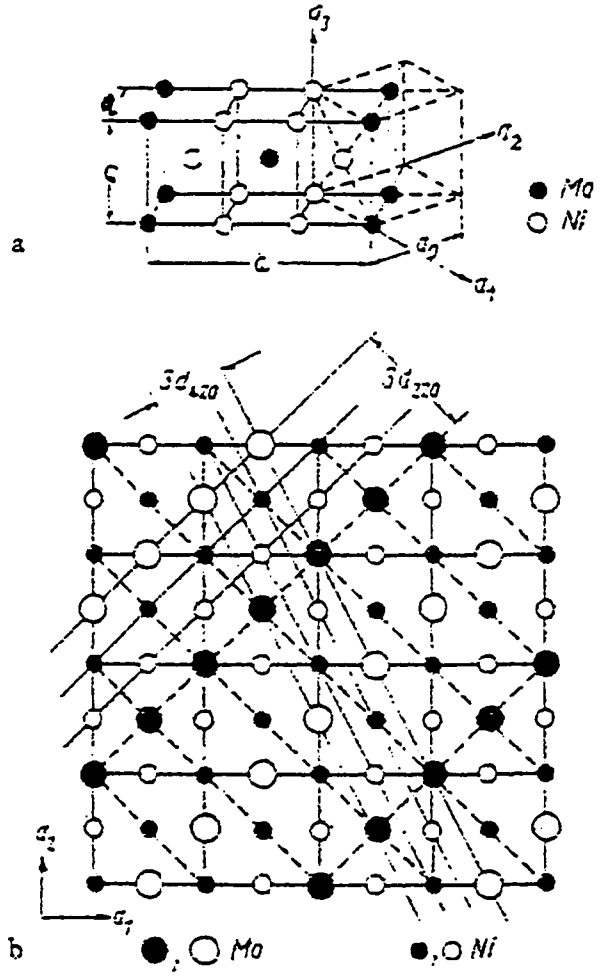

Figure 2.7 Crystal Structure of the ordered Ni_2Mo metastable phase. Part a) shows the orthorhombic unit cell and its relationship to the original FCC (dashed lines) lattice. Part b) shows the atomic packing along the (001) plane. The dashed lines are the outline of the orthorhombic Ni_2Mo lattice. Open circles are atoms on a layer a/2 above. After Das and Thomas [36].

orthorhombic Ni_2Mo cell. All open circles represent projected atoms on a layer a/2 above. The approximate dimensions can be derived [37] from the dimensions of the parent FCC α phase:

$$a = \frac{\sqrt{2}}{2} a_{FCC}, \quad b = \frac{3\sqrt{2}}{2} a_{FCC}, \text{ and } c = a_{FCC} \qquad \textbf{(2.2)}$$

The Ni_2Mo phase is related [38] to the FCC phase by:

[100] Ni_2Mo // [110]α
[010]Ni_2Mo // [-110]α
[001]Ni_2Mo // [001]α

The Ni_2Mo phase occurs as a metastable phase during ordering of Ni_4Mo, but it has a restricted volume fraction. Das and Thomas concluded that their results supported the predictions by Richards and Cahn [39] and thermodynamic calculations explain why Ni_2Mo occurs as metastable phase during ordering of Ni-Mo alloys. They also demonstrated a model based on the presence of non-conservative APB's and showed that such APB's are nuclei for the Ni_2Mo phase in stoichiometric Ni_4Mo.

2.2.6 DO_{22} and $Ni_{17}Mo_5$ Metastable Phases

Van Tendeloo, Ridder, and Amelinckx [40], using electron microscopy and electron diffraction methods, found a new metastable phase having a $D0_{22}$ superstructure. They mention that it is only observed under certain circumstances, generally only immediately from the SRO state. They attempted to determine how the ordered Ni_3Mo structure at room temperature formed out of the disordered FCC matrix at high temperature. It was found that $D0_{22}$ is an intermediate step in ordering of the Ni_3Mo alloy. A flow chart [40] in Figure 2.8 shows the steps of Ni_3Mo formation from SRO α.

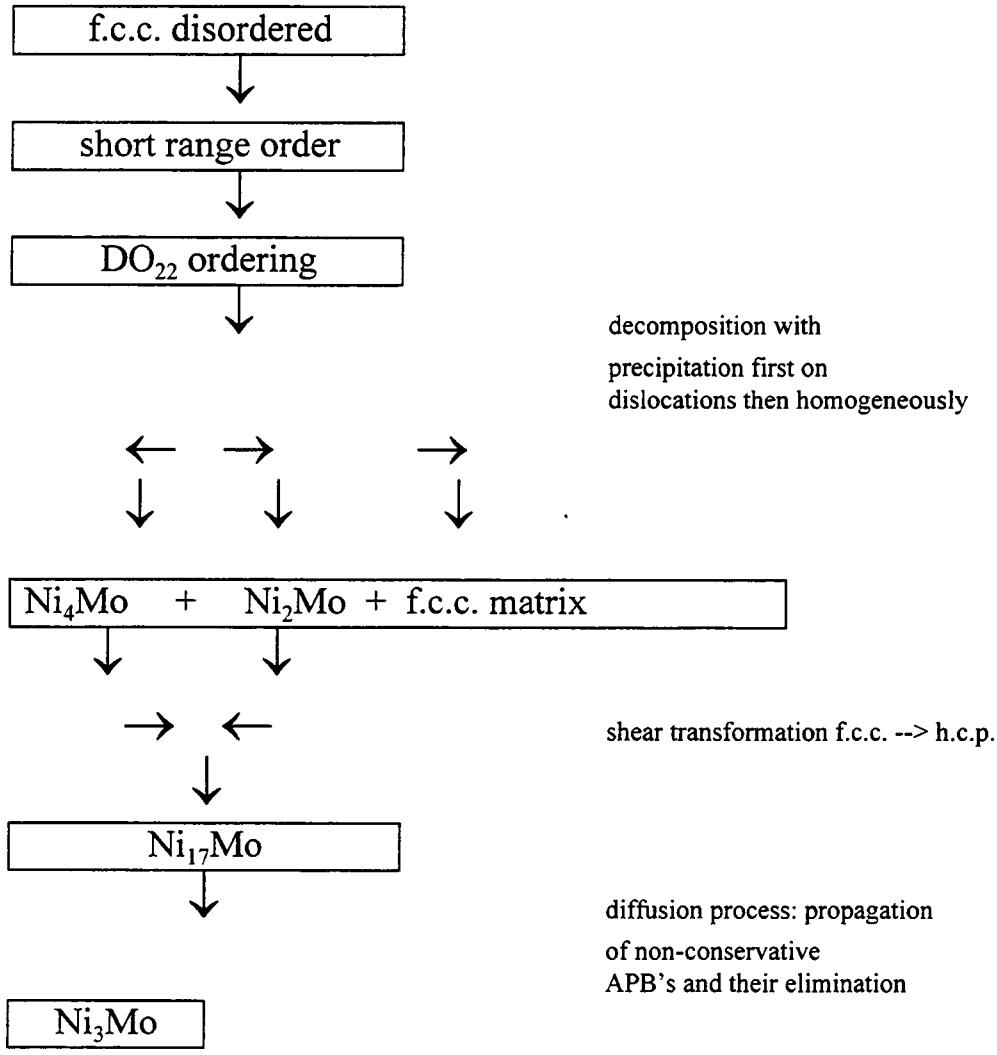

Figure 2.8 Flowchart showing the stages involved in the formation of the ordered Ni_3Mo γ phase from the disordered FCC phase. Three metastable phases, $D0_{22}$, Ni_2Mo, and $Ni_{17}Mo_5$, form and then disappear during the process. Adapted from Van Tendeloo et al. [40].

Van Tendeloo previously showed that a shear transformation takes place along the (010) Ni_3Mo planes transforming the ABC stacking of the close-paced planes into AB stacking. This leaves a dense array of non-conservative quasi-periodic APB's that is a new long period superstructure with $Ni_{17}Mo_5$ composition. $D0_{22}$ is then considered a basis for the formation of Ni_4Mo, Ni_3Mo, and Ni_2Mo. It is described as a sequence of pure Ni planes and pure Mo planes in the $[210]_{FCC}$ direction. The $D0_{22}$ structure is shown in Figure 2.9.

2.3 Ni_4Mo Alloy α to β Phase Transformation and Thermophysical Properties

2.3.1 Theoretical Relationships Between Thermodynamic Quantities

The relationships described here allow determination of the Gibbs free energy of the α to β phase transition in Ni_4Mo from the data of specific heat at constant pressure for the different equilibrium and metastable phases. Most material here is from DeHoff [41].

The state functions in thermodynamics are temperature T, pressure P, volume V, internal energy U, enthalpy H, Hemholtz free energy F, Gibbs free energy G, and entropy S. Because these are state functions, they satisfy Cauchy-Riemann relations [41], and satisfy the exact differential condition. This leads to Maxwell relations, which help describe relationships between thermodynamic functions in terms of partial derivatives. The Maxwell relations are too numerous to show here. Other mathematical relationships such as the reciprocal relation

$$\left(\frac{\partial Z}{\partial X}\right)_Y = \frac{1}{\left(\frac{\partial X}{\partial Z}\right)_Y} \qquad \textbf{(2.3)}$$

and the ratio relation:

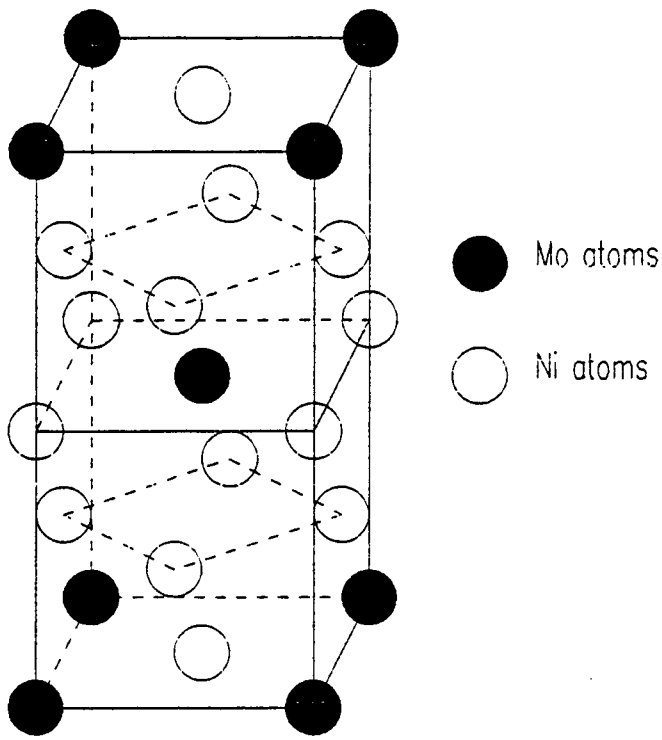

Figure 2.9 Crystal Structure of the $D0_{22}$ metastable phase. Adapted from Matveeva and Kozlov [24].

$$\left(\frac{\partial Z}{\partial X}\right)_Y \left(\frac{\partial X}{\partial Y}\right)_Z \left(\frac{\partial Y}{\partial Z}\right)_X = -1 \qquad \textbf{(2.4)}$$

allow developmental relationships between the thermodynamic state functions and help manipulate the partial derivatives. Some common relationships between the energy functions are

$$G = H - TS \qquad \textbf{(2.5)}$$

$$F = U - TS \qquad \textbf{(2.6)}$$

$$H = U + PV \qquad \textbf{(2.7)}$$

The equations of state P, V, and T are usually determined experimentally. Some other experimentally determined variables are the coefficient of thermal expansion, β, the coefficient of isothermal compressibility, κ, and the specific heat at constant pressure, C_P.

Using the laws of thermodynamics in conjunction with the above mathematical tools allows useful relationships to be derived. One relationship is from the combined statement of the first and second laws:

$$C_P = T\left(\frac{dS}{dT}\right)_P \qquad \textbf{(2.8)}$$

Also under isobaric conditions, specific heat is related to enthalpy as

$$C_P = \left(\frac{dH}{dT}\right)_P \qquad \textbf{(2.9)}$$

Another relationship is the specific heat at constant volume

$$C_V = \left(\frac{dU}{dT}\right)_V \qquad \textbf{(2.10)}$$

which comes from the first law, assuming P-V work only. Also from the combined statement of first and second laws

$$C_V = T\left(\frac{dS}{dT}\right)_V \tag{2.11}$$

C_V is of interest in theoretical work since a change in the internal energy of a substance with temperature can be related by statistical methods to the changes in rotational, translational, vibrational, electronic, and magnetic energies in terms of its atoms [42]. C_V is more difficult than C_P to obtain experimentally, hence relationships have been derived to convert between the two.

If β, κ, and C_P are known for any simple system (where there is no other work besides P-V work), then changes in all the state functions can be computed for any arbitrary process through which the system may be taken. Therefore, these values are the center of the strategy for solving practical problems requiring thermodynamics. The thermodynamic state functions expressed in differential form in terms of temperature and pressure are [41]

$$dV = (V\beta)dT - (V\kappa)dP \tag{2.12}$$

$$dS = \left(\frac{C_P}{T}\right)dT - (V\beta)dP \tag{2.13}$$

$$dU = (C_P - PV\beta)dT + V(P\kappa - T\beta)dP \tag{2.14}$$

$$dH = (C_P)dT + V(1 - T\beta)dP \tag{2.15}$$

$$dF = -(S + PV\beta)dT - (PV\kappa)dP \tag{2.16}$$

$$dG = -(S)dT + (V)dP \tag{2.17}$$

These allow calculation of all changes of state functions accompanying a process if the initial and final temperatures and pressures (along with β, κ, and C_P) are known.

The Gibbs free energy for the Ni_4Mo α to β phase transition is determined as follows. A mathematical expression (polynomial) for C_P as a function of temperature for each of the two phases will be developed based on the experimental data. The equation will be continuous through the complete range of temperature (approximately 25 to 1200 °C) either by extrapolation or by measurement. The free energies of the individual phases are

$$G^{\alpha} = H^{\alpha} - T S^{\alpha} \quad \textbf{(2.18)}$$

$$G^{\beta} = H^{\beta} - T S^{\beta} \quad \textbf{(2.19)}$$

The change in free energy through the transition is

$$\Delta G^{\alpha \rightarrow \beta} = G^{\beta} - G^{\alpha} = (H^{\beta} - H^{\alpha}) - T(S^{\beta} - S^{\alpha}) \quad \textbf{(2.20)}$$

where the enthalpies and entropies are calculated as follows

$$H^{\alpha} = H_0^{\alpha} + \int_{T_0}^{T} C_P^{\alpha} \, dT \quad \textbf{(2.21)}$$

$$H^{\beta} = H_0^{\beta} + \int_{T_0}^{T} C_P^{\beta} \, dT \quad \textbf{(2.22)}$$

$$S^{\alpha} = S_0^{\alpha} + \int_{T_0}^{T} \frac{C_P^{\alpha}}{T} dT \quad \textbf{(2.23)}$$

$$S^{\beta} = S_0^{\beta} + \int_{T_0}^{T} \frac{C_P^{\beta}}{T} dT \quad \textbf{(2.24)}$$

Where H_0, and S_0 are the enthalpy and entropy, respectively, at a reference temperature T_0. Since the specific heat equations are polynomials, the integrals are relatively simple to evaluate analytically. Thus, $\Delta G^{\alpha \rightarrow \beta}$ as a function of temperature is determined.

2.3.2 Long-Range Order and Short-Range Order Theory

The concept of order in alloys can be traced back to Tammann [43]. Bain [44], soon after Tammann, detected the ordered arrangements by x-ray methods. The presence of order is conclusively demonstrated through the appearance of "superlattice lines" in x-ray diffraction (XRD) patterns, in addition to the fundamental lines [45].

In an ideal solid solution, the different types of atoms are randomly arranged on the lattice. Ideal solution theory assumes that the probability of finding a solute atom at any specified point in the crystal is equal to the atom fraction of the solute atoms [41].

When the atomic bond energies are considered to be different between different species in the lattice, i.e., in the case of a binary solution where the AA bond energies, BB bond energies, and AB bond energies are all different, then there is behavior that is different than that for an ideal solution model. The simplest step beyond the ideal model is the regular solution model (quasi-chemical theory), where the enthalpy of mixing, ΔH_m is no longer zero. When ΔH_m is negative Ω is also negative, then

$$\Delta H_m = \Omega x_A x_B \qquad \textbf{(2.25)}$$

where

$$\Omega = N_A z \varepsilon \qquad \textbf{(2.26)}$$

The coordination number is z, N_A is Avagradro's number, and ε is the bond energy defined as

$$\varepsilon = \varepsilon_{AA} + \varepsilon_{BB} - 2\varepsilon_{AB} \quad (2.27)$$

If ε is negative, then Ω is also negative (since N_A and z are always positive), and

$$\varepsilon_{AB} < \frac{1}{2}(\varepsilon_{AA} + \varepsilon_{BB}) \quad (2.28)$$

makes ε positive. Thus the energy of the unlike bonds is lower than the energy of the like bonds. The actual number of AB bonds will then tend to be greater than the expected number of AB bonds, and the atoms will tend to order [41].

The concept of SRO, first introduced by Bethe [46], describes local deviations from randomness. The amount of SRO can be described by a short-range order parameter,

$$\sigma = \frac{q - q_r}{q_m - q_r} \quad (2.29)$$

where q is the fraction of unlike (AB) pairs, q_m is the maximum number of bonds possible for the perfectly ordered case, and q_r is the number of bonds in the random case. The SRO parameter is zero for a completely random solution. The short-range order parameter was later re-defined by Cowley [47] as a series of successive shells of atoms surrounding a B atom

$$\alpha_i = 1 - \frac{n_i}{m_A c_i} \quad (2.30)$$

where there are c_i atoms in the *i*th shell surrounding a B atom, n_i is the average number of A atoms in the shell, and m_A is the atom fraction of A. The principal feature of these results, as Guttmann points out [48], is the remarkably high degree of nearest-neighbor

order retained well above the critical temperature. Even atoms in the 10th shell still show a small effect on the presence of a simple atom.

It is frequently possible to obtain structures in which the A atoms preferentially locate themselves with respect to the B atoms. These are known as long-range order (LRO) solid solutions, or superlattices. This usually occurs in compositions near stoichiometric compositions like AB or A_3B, but also occurs for the case of Ni_4Mo.

Consider a binary alloy [49]. If there are N sites total, then there are Nx_A A sites and Nx_B B sites, where x_A and x_B are mole fractions. In perfectly ordered alloys, the A atoms are on A sites and B atoms are on B sites. In disordered states, the A and B atoms are distributed randomly on A and B sites. In completely disordered states, $N(x_A)^2$ is the number of A atoms occupying A sites and Nx_Ax_B is the number of B atoms occupying A sites. The number of wrong A atoms on B sites is Nx_w. The probability of this occurring is $w_A = x_w/x_A$. The probability of an A atom on a right (correct) site is $r_A = 1 - w_A$. The probability of a B atom on a B site is r_B. The probability of a B atom on an A site is w_B. The long-range order parameter, L, introduced by Bragg and Williams [50], can be described in various ways:

$$\eta = \frac{r_A - x_A}{1 - x_B} = \frac{r_B - x_B}{1 - x_B} = 1 - \frac{x_w}{x_A x_B} \qquad \textbf{(2.31)}$$

For perfect order η is unity, and η is zero for a random solid solution. Above the critical temperature of ordering, Tc, η is zero but σ is not zero. This is because when $\Omega < 0$, there is still some tendency for unlike atoms to attract [51].

The entropy of mixing of structures with LRO is extremely small and entropy increases as temperature increases. η decreases with increasing temperature until there is

no LRO at all at Tc. The critical temperature increases with increasing Ω or ΔH_m. Therefore in many systems the ordered phase is stable all the way to the melting temperature.

In ordered structures, atoms of a given kind occupy specific sites. The size of the unit cell is increased because differentiation is made between the different sites [49]. For a description of some of the more common ordering superlattices, the reader is referred to [51]. Some basic information on the formation of common types of superlattices is as follows [51].

1. $L2_0$ (also known as B2): a disordered AB BCC orders to a cubic structure.
2. $L1_0$: an FCC disordered AB structure orders into a tetragonal structure.
3. $L1_2$: an FCC disordered A_3B goes to a cubic structure.
4. DO_3 : a disordered A_3B BCC goes to an FCC ordered structure.
5. DO_{19}: an HCP disordered A_3B structure goes to an HCP ordered structure.

The important type of ordering superlattice for the Ni_4Mo alloy is the D1a type, in which an FCC disordered A_4B structure goes into a tetragonal structure. Matveeva and Kozlov refer to this as the $MoNi_4$ type [24]. All of the above superlattices can be considered in terms of two sublattices (in a binary solution), one occupied by A atoms and one occupied by B atoms.

The SRO parameter by Bethe [46] took into account just the surrounding atoms and is not associated with the different types of sites. This is opposed to the LRO parameter by Bragg and Williams, which considered each lattice site to be influenced by every other site in the crystal. It should be mentioned that σ also has a critical temperature associated with it.

Figure 2.10 shows a plot of η and σ as a function of temperature for two types of order-disorder alloys. This plot was derived from the quasi-chemical approach [51].

The CuZn type of transition is shown in 2.10a. At all temperatures above a critical temperature, T_C, the superlattice is destroyed. Upon cooling below T_C, the same alloy then re-orders. Above T_C, L is zero. As the alloy temperature approaches T_C , L drops to zero very rapidly upon heating. The order becomes more and more perfect with decreasing temperature. At 0 K, there is perfect order ($\eta = 1$). At the critical temperature, η is zero. As can be seen, in this case, the transformation from 0 K to Tc is continuous. Also note that σ is non-zero above Tc.

The same type of plot is shown in Figure 2.10b for the Cu_3Au type of alloy. In this case, the LRO gradually decreases until Tc is reached, when η drops abruptly to 0. The

SRO parameter is non-zero above Tc, and it is also shown that the SRO parameter has a critical temperature as well.

A discontinuous drop to zero at Tc implies that the transformation requires a latent heat. This latent heat must be added or subtracted at Tc. Thus the change in enthalpy at Tc is discontinuous [48]. Take for example the melting of a pure solid. The addition of a small quantity of heat converts more solid to liquid but during the process, the temperature remains constant [51]. In melting a pure solid, you also have two phases co-existing in equilibrium at the transition (melting) temperature. As heat is supplied, the relative amounts of the two phases changes. This is the situation described in Figure 2.10b of the Cu_3Au type of transition.

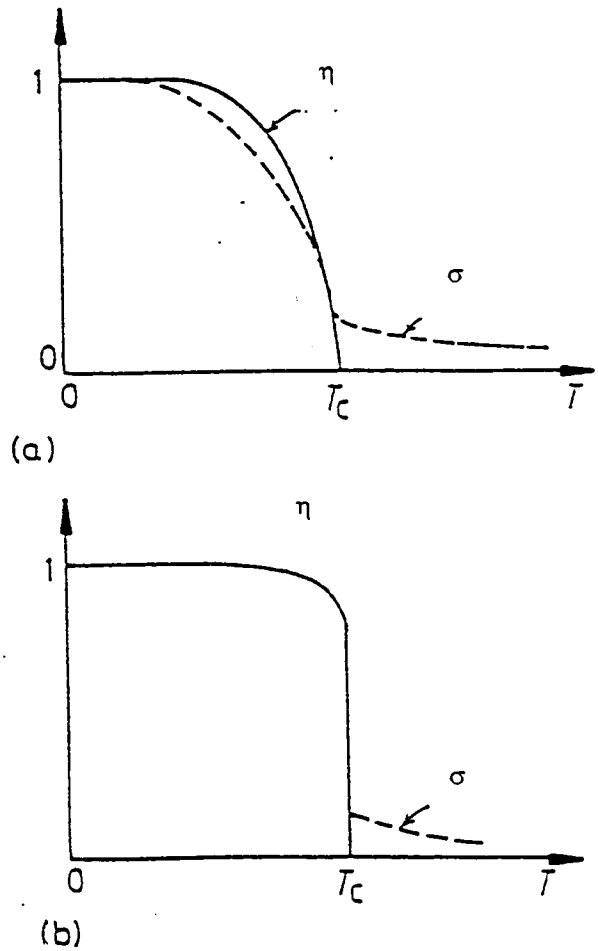

Figure 2.10 Long-range (η) order and short-range (σ) order parameters as functions of temperature for different types of ordering reactions. The CuZn-type of reaction is shown in 2.10a and the Cu_3Au-type of reaction is shown in 2.10b. From Porter and Easterling [37].

There are several approaches to classifying phase transitions [24]. Since the Gibbs free energy function is always continuous through a transition at the transformation temperature, this function is often used to define the order of a phase transformation. One way to define the order of a phase transformation is as the lowest derivative of the Gibbs free energy that shows a discontinuity. Two common thermodynamic relationships are the first derivatives of G with respect to temperature and pressure, respectively:

$$\left(\frac{\partial G}{\partial T}\right)_P = -S \tag{2.32}$$

where S is entropy, and the volume, V, is

$$\left(\frac{\partial G}{\partial T}\right)_P = V \tag{2.33}$$

The second derivatives of G are

$$\left(\frac{\partial^2 G}{\partial T^2}\right)_P = -\left(\frac{\partial S}{\partial T}\right)_P = -\frac{C_P}{T} \tag{2.34}$$

$$\left(\frac{\partial^2 G}{\partial P^2}\right)_T = \left(\frac{\partial V}{\partial P}\right)_T = -\beta V \tag{2.35}$$

where Cp is the constant pressure specific heat and β is the isothermal compressibility.

For a first order transformation then, entropy and volume as functions of temperature are discontinuous. Since the disordered state will have a higher internal energy and enthalpy than the ordered state due to the greater number of high energy like-like atom bonds, then there also will be a discontinuous change in enthalpy at Tc due to the evolution of heat. This is the case as described above for melting a solid. Thus melting a solid is a first order phase transformation. Landau and Lifshitz [52] further state

that for a first order phase transformation there are no restrictions on the change of symmetry of the body and the two phases may have nothing in common.

Figure 2.10a shows η to be decreasing continuously all to the way to zero at Tc. In second degree transitions the addition of any heat raises the temperature at all temperatures including the critical temperature. Hence the two phases never co-exist, but only one or the other is present, according to whether T is above or below Tc [48]. Second order transformations also require identical composition of the phases [51]. In a second order transition there is no latent heat or a high specific heat associated with the transformation, as opposed to a first order, where Cp becomes infinite at Tc.

The behavior of first and higher degree transitions produces different phase relationships as described in phase diagrams. This general trend is shown in Figure 2.11 [48]. This is due to second order transformations requiring identical compositions of the two phases, but a first order does not require this. Thus a first order transition appears as two lines bounding the region where there are two phases with two compositions can coexist in equilibrium, but a second order transition appears as a single line.

It should be noted that it is difficult to establish the fact that a transition is second degree. The main current belief is that transitions from $L2_0$ or DO_3 structures to A2 (BCC) are second order phase transformations, and all others are probably first order. For a more detailed discussion of second order transitions, the reader is referred to Landau and Lifshitz [52].

There is also an effect of "purity" or nearness to ideal stoichiometry that should be mentioned that can be seen in some order-disorder transformations. When an ordering alloy is at the ideal composition required for the superlattice, then the critical temperature

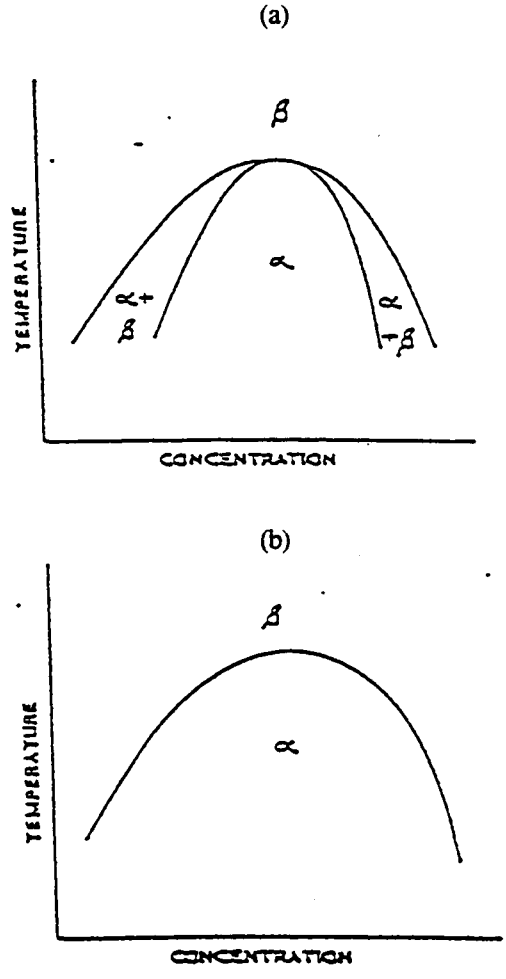

Figure 2.11 Relation of first degree and higher degree transitions to the phase diagram. The first order relationship is shown in 2.11a and the higher degree relationship is shown in 2.11b. Adapted from Guttmann [48].

is at the maximum. The LRO can still be maintained when the composition deviates from this ideal value. One way for this to occur is if some of the sites are left vacant. Another way is when some of the "wrong" atoms occupy the sites. When either of these situations occurs, it is easier to disrupt the order as the temperature is increased, and Tc is less. When the composition is not ideal in a first order transition there is a two phase field associated with the transformation. The disordered phase transforms on cooling to an ordered phase in addition to a disordered matrix. The composition changes, and LRO must be involved. There is never a two-phase field associated with a second order transformation, regardless of how close to stoichiometry the alloy is.

When heating an ordering alloy from 0 K to up through the critical temperature, the LRO decreases from unity to zero. This is related to the entropy increase. Porter and Easterling [51] state that "The mechanism by which order is lost is most likely the interchange of atoms by diffusion processes occurring homogeneously throughout the crystal".

Upon cooling, there are two possible mechanisms for creating an ordered superlattice from a disordered solution. The more common is where there is an energy barrier to the formation of ordered domains, in which case the transformation must take place by nucleation and growth processes. Another way is to have a continuous increase in the SRO by local rearrangements occurring homogeneously throughout the crystal which finally leads to LRO.

Most experimental evidence suggests that most of the superlattices are nucleated in the disordered phase. The activation energy barrier to nucleate ordered domains should be rather small even at low undercoolings below Tc because the nuclei and matrix have

essentially the same crystal structure and will be coherent with low interfacial energies [51]. Also, since the compositions are nearly the same between the two phases and the strain energy to overcome the transition is small, thus nucleation is expected to be homogeneous and independent of lattice defects such as dislocations and grain boundaries. Also at low ΔT the nucleation rate will be low and large domains will grow. At large ΔT, many domains will grow but will be smaller. High LRO will be associated with larger, but fewer, domains.

In the local rearrangement type of mechanism, no distinct interface exists analogous to a homogeneous chemical reaction. It is mentioned [51] that this mechanism may only be able to operate by either second-order phase transformations or by conditions of very large amounts of supercooling.

Once independently ordered domains are nucleated inside the same parent crystal, they will often be out-of-phase. That is, they may grow like grains until they impinge on each other. When they do this, they may have a boundary that is out of step with the regular chemical periodicity but in-phase crystallographically. These boundaries are called anti-phase boundaries, or APB's. The degree of order within the domain will vary according to the LRO parameter versus temperature behavior described above for different alloys. As the temperature is decreased, the LRO will increase by homogeneous diffuse rearrangements within the domain. Then the APB's coarsen in a manner similar to grain growth. The type of APB structure that forms is dependent on the sublattice type. For example, the CuZn type structure only has two types of sites upon ordering, thus this limits the way that the separate ordered domains can come together. On the other hand,

the Cu_3Au structure has four ways that the domains can start. This increases the number of ways the domains can impinge on each other.

A metastable structure can form in some of these complex sublattice situations. The structure is considered metastable because it is at a higher energy state than the equilibrium case due to an increased number of like bonds. The structure still has a tendency to reduce the energy as much as possible by maximizing the distance between the like bonds.

In the $L2_0$ superlattice (CuZn) only two possible sublattices exist. Thus only two type of ordered domains are possible. It is impossible for such a metastable APB structure to form in this situation, and it is relatively easy for a APB structure to coarsen. Hence the long-range order can increase.

The rate at which APB structure coarsening occurs depends on the superlattice type. The rate at which ordering occurs varies greatly from one alloy to another. One example is in the CuZn alloy, which orders so rapidly that it is almost impossible to quench in the disordered BCC structure because of the second order continuous ordering process. In the Cu_3Au system ordering is relatively slow, and occurs by nucleation and growth. The LRO transformation is impeded by the presence of a metastable APB networks.

The relative speed of disordering may be judged from the observations of Cowley [47], who found that the intensity of a superlattice reflection from Cu_3Au became immeasurably small within 15 minutes of the time exceeding Tc, but that 70 hours or more were needed to reach equilibrium below Tc once the crystal had been disordered [48].

2.3.3 The Ni_4Mo α to β Phase Transformation

The α to β transformation involves a SRO to LRO transformation. As mentioned previously, the β phase is a D1a LRO structure, and the α phase is a FCC (A1) SRO structure. According to Hume-Rothery [53], the important feature of the order-disorder transformation is that there be essentially no change in the lattice in which the atoms are placed in the two states. In line with this definition, the α→β transformation in Ni_4Mo is a disorder-to-order transformation.

Several investigators have obtained order-parameter data for the Ni_4Mo alloy. The SRO parameter in a 20.7 at% Mo alloy was determined by Kozlov and Kushnarenko [54]. Kao [55] studied the LRO parameter as a function of temperature for Ni_4Mo for quenched samples. The ordering reaction for the Ni_4Mo alloy was studied by Matveeva and Kozlov [24]. They measured the LRO parameter as a function of temperature, shown in Figure 2.12. The D1a to A1 type of ordering reaction is similar to the first-order transition that proceeds through a two-phase region. Matveeva and Kozlov have summarized some data on this particular transformation in Table 2.1.

The structural relationship between the α and β crystal structures was briefly

Table 2.1. Data on the D1a to A1 transformation for the Ni_4Mo alloy [24,56,54].

Tc (K):	1148 ±3
Boundaries of two-phase regions (K):	1133-1148
Jump in the degree of order	
At beginning of two-phase region:	0.93
At end of two-phase region:	0.85
ΔT in two-phase region (K):	15
$\delta(T/T_k)/\delta\eta$	
At beginning of two-phase region:	0.50
At end of two-phase region:	0.33
c/a:	0.968±0.001

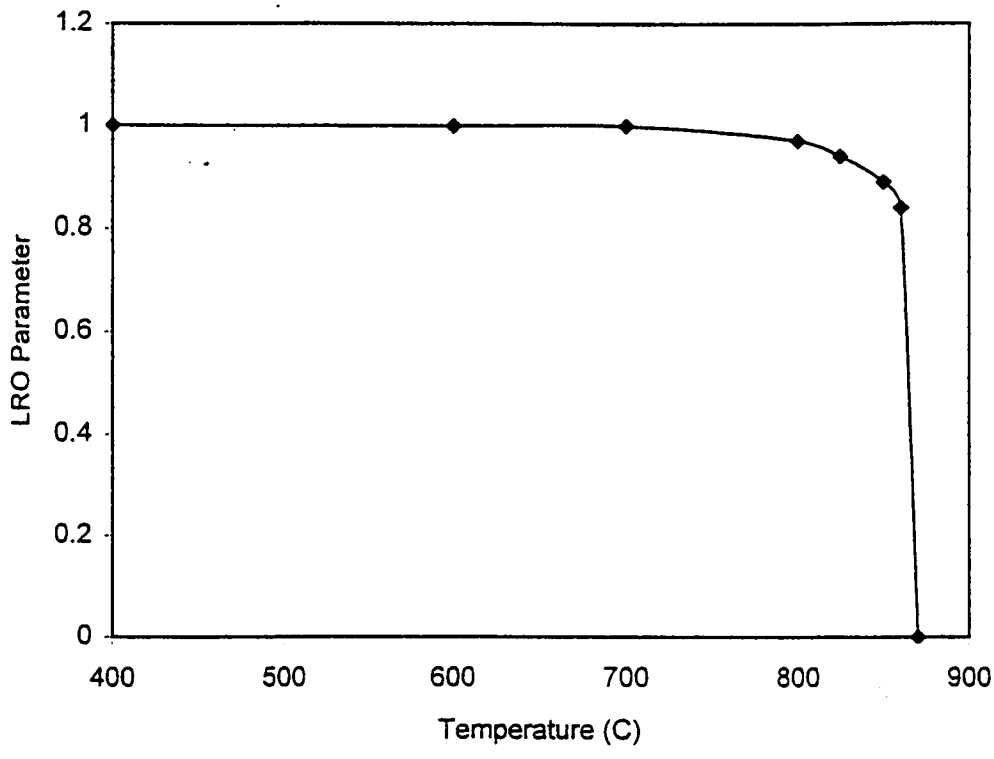

Figure 2.12 Long-range order parameter as a function of temperature for the Ni_4Mo alloy. Adapted from Matveeva and Kozlov [24].

mentioned in Section 2.2 and shown in Figure 2.4. It is further described [57] as follows. Lattice sites of the initial FCC lattice are initially preserved, with only a 1.16 % contraction in the c axis and a 0.4% expansion along the a and b axis. Ni_2Mo and $D0_{22}$ phases can be generated by occupying the {420} FCC planes with Mo atoms at spacings of $3d_{420}$ and $4d_{420}$, respectively. One theory is that β possibly nucleates and grows with a crystallographic relationship to the α matrix, with coherency existing between the ordered plates of β and the disordered α matrix. With a further growth of a β plate, both laterally and in thickness, β plates will finally impinge [36]. Orientation relationships that exist between β and the parent FCC phase are shown in Figure 2.4 [11], which shows the FCC (100) plane. There are Mo atoms every fifth position and there is ABAB stacking. The c axis of the BCT cell is perpendicular to the (001), and parallel to one of the FCC alpha cube edges. The c axis of the tetragonal cell can be any one of the three original cube axes of the original FCC cell, and the tetragonal a axis can be inclined positively or negatively to the original cell. This can be seen in Figure 2.13 [58]. Each one of the first five atoms in the [110] row could serve equally well as the origin. Thus there are 3x2x5 = 30 ways for β to nucleate from a single lattice. Only 6 of the 30 possibilities produce different orientations of β, and each of these of these can result in a differently oriented LRO domain. There are 3 different types of domain interfaces [13]. These can be classified as antiphase boundaries (APB's), antiparallel twins (APT's), and parallel twins (PT's). In APB's, the unit cell axes of the superlattice in the adjacent domains are parallel to one another, but there is a lattice displacement. APT's correspond to interfaces between two orientation variants in which the c axes of the superlattices are antiparallel. The domain lattices may be displaced relative to each other, generating a combination

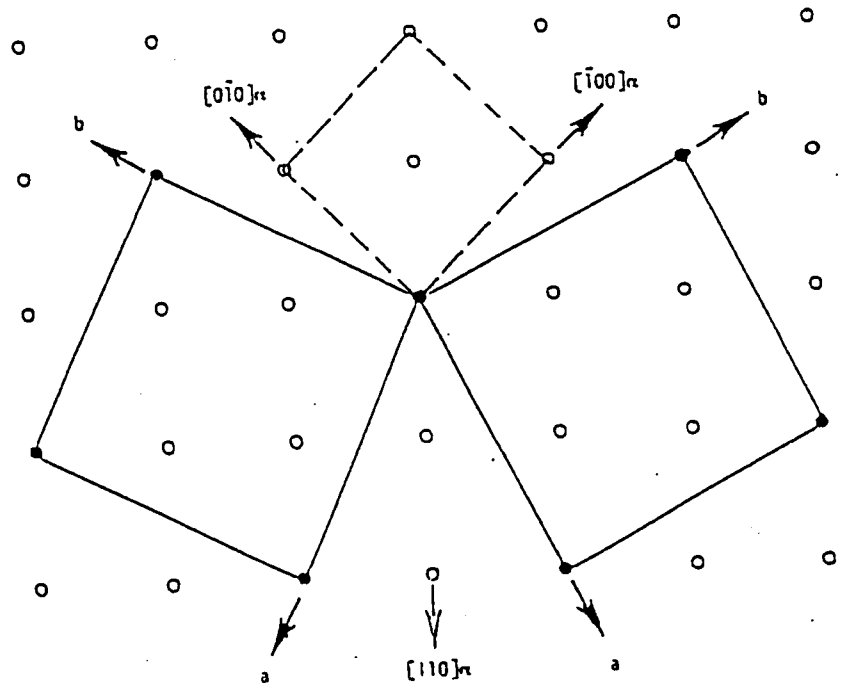

Figure 2.13 Schematic diagram of anti-phase twin formation in the Ni_4Mo FCC lattice. The c axis is parallel to the [001] α direction, showing how two anti-parallel twins (APT's) of the ordered Ni_4Mo phase can form from different orientations. After Lei [58].

APB/APT. PT's exist when the c axis of the adjacent superlattice domains are roughly perpendicular to each other [13].

Numerous other studies have been done on the domain structure and on the SRO-LRO transition. Dienes [59], Vineyard [60], Sato and Kikuchi [61], Yamuchi and de Fontaine [62], and Cohen [63] wrote on general order-disorder kinetics. Cook [64, 65] studied the kinetics of clustering and SRO in terms of lattice diffusion theory, and suggested that the Ni_4Mo transformation could be continuous at lower aging temperatures. Irani [66] studied ordering systems in terms of thermodynamics and mechanisms. Some early kinetic studies were also done on Ni-Mo alloys by Kiriyenko and Potapov [67, 68, 69], Vlasova et al. [70], Tyapkin et al. [71], Artsishevskaya et al. [72], Saburi et al. [73], Amelinckx [74], Yamamoto et al. [75], and Ling et al. [76].

The SRO phase exists in Ni_4Mo quenched from 1000 °C, and probably exists up to the melting point. The development of SRO in Ni_4Mo is somewhat controversial. Experimental determination of SRO coefficients for Ni_4Mo using diffuse x-ray intensity distribution around the {1 1/2 0} positions have been performed by Spruiell and Stansbury [77], and later by Chakravarti et al. [78]. Spruiell and Stansbury suggested that domains, about the size of 10 times the distance of the FCC lattice parameter, a_0 , having the LRO structure must exist in order to have the observed splitting of (001) spots in the diffraction pattern. They further suggested that the SRO state could be caused by either micro-domains less than 10 times the lattice parameter, or by a statistically non-random solution in which the number of neighbors in shells about a given atom is statistically similar to that found in the LRO phase. This model was supported by Clapp and Moss [79, 80], who predicted positions of the diffuse maxima based on statistical

thermodynamic models involving first and second neighbor interactions. Thomas and Sinclair [81] promoted the multiple micro-domain model.

Brooks et al. [13] mention that there is some reasonable agreement on the general microscopical features of the SRO to LRO Ni_4Mo phase transformation:

1. SRO maxima first become more intense, and then there is an increase in the diffuse streaking.
2. There is then a formation of three-dimensional isolated scattering at the D1a positions. These first appear to co-exist with the SRO maxima, but the SRO maxima soon disappear.
3. Once the D1a reflections appear, β domains are clearly visible in DF images. This suggests that the domains already posess a high degree of order.
4. All orientation variants of β appear simultaneously.
5. The number density of domains increases as the aging temperature decreases.
6. Small domains give a 'basket-weave' pattern in bright field images, which is attributed by Tanner and Leamy [82] to be from elastic coherent strains.
7. Further aging produces a 'soap-froth' structure of antiphase domains.

Banerjee [83] reviewed some of the recent thinking on structural models and mechanisms that have been proposed for the SRO-LRO transitions in the Ni-Mo system and discussed the conflict between the continuous transformation mechanism and the discrete (nucleation and growth) mechanism. Several structural descriptions of the SRO state and the transitional states between SRO and LRO have been proposed. These are shown schematically in Figure 2.14.

The concentration-wave model was proposed by de Fontaine [84]. This theory, which is based on earlier theories of Landau and Lifshitz [52], Clapp and Moss [79, 80] and Khachaturyan [85], establishes the k-space configurational energy as a function of the atom pair interaction parameters. A statistical expression for the atomic distribution results, where the lattice positions are expressed in terms of waves varying in

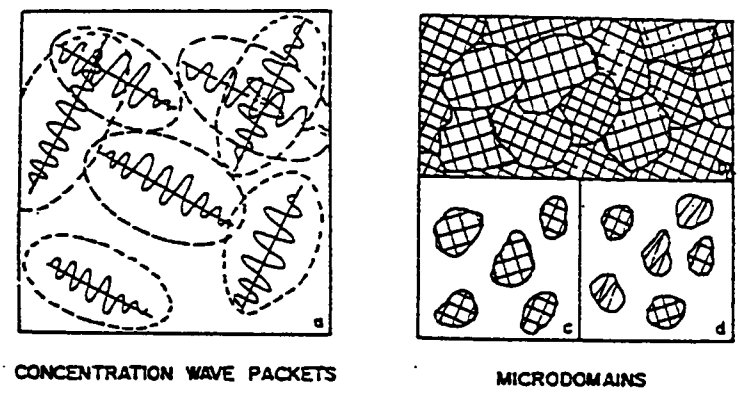

Figure 2.14 Schematic diagram of various short-range models in Ni_4Mo. The wave packet model in 1) shows regions bounded by dashed lines where a single variant of concentration wave is localized. The amplitude of the concentration wave taper off as the boundary is approached. Overlapping of such waves leads to the formation of the N_3M structure. The microdomain model in b) shows a continuous arrangement of microdomains, each with a few unit cells of nearly fully ordered domains. Another microdomain model, shown in c), is with the same type of microdomains, but separated by disordered regions. The last model shown, d), is a multiple microdomain model, in which the microdomains contain different types of superstructures. From Banerjee [83].

concentration in different directions. Characteristic diffraction effects are present in the reciprocal lattice. In terms of the Ni_4Mo ordering transition, de Fontaine lists three conclusions:

1. SRO diffuse intensity is predicted for the {1 1/2 0} position as observed.
2. All ordering reactions of the 420 series must occur at equilibrium by nucleation and growth.
3. A spinodal ordering temperature concept is developed.

The spinodal defines [86] a region in the phase diagram where the FCC solid solution becomes unstable with respect to the concentration waves with k-vectors equal to <1 1/2 0>. Mayert and Urban [87] have since determined a spinodal ordering temperature to be about 1150 ± 30 K. This is somewhat higher than the first order critical ordering temperature of 1141 K.

A concentration-wave-packet model has been proposed by Chevalier and Stobbs [88, 89], who continued the theory of de Fontaine. They propose that the attenuation of the concentration wave by exponential decay leads to a static concentration wave packet. These packets can form on all {420} planes, leading to a 'speckle' pattern in the microstructure which is observed experimentally. This would indicate that the micro-domains of small bounded regions of D1a, $D0_{22}$, or Ni_2Mo do not constitute the SRO state.

A cluster model was proposed by De Ridder et al. [90]. This is a description of SRO based on small sub-unit size (< 6 atom) clusters. They also suggested a similar cluster variational method (CVM) which was first introduced by Kikuchi [91].

A multiple micro-domain model was proposed by Okamoto and Thomas [92] and Das et al. [93]. They examined how a distribution of diffuse intensity relates to the {420}

stacking sequence on Ni and Mo atoms which result in the Ni_2Mo, Ni_4Mo, and $D0_{22}$ structures. The model relates how some of these structures are dispersed in the disordered matrix. Order may be imperfect within these structures and the subsequent transformation involves the increase in perfection and final conversion to the stable D1a structure. In this view, the Ni_2Mo, and $D0_{22}$ structures are intermediate and unstable. The {1 1/2 0} intensity is attributed to non-conservative APB's formed between micro-domains as a result of adjacent micro-domains impinging with Mo atoms at every $3d_{420}$ or $4d_{420}$ rather than the equilibrium $5d_{420}$ sequence.

Banerjee [83] mentioned that many first-order order transformations could occur in either a discrete or continuous mode, depending on the extent of supercooling provided. First-order, by definition, occurs by nucleation and growth at temperatures near Tc, but at high supercoolings, an instability is developed in the system at $\eta = 0$, and the transformation can proceed in the initial stages in a continuous manner. The Ni_4Mo transformation seems to be a mixed-mode transformation [94] where there is a competition between first and second order transitions.

Banerjee [83] also mentions a few points regarding the SRO state in Ni-Mo alloys. On quenching from the completely disordered state, Ni-Mo alloys from 8 to 33 at% Mo exhibit maximum of diffraction intensity at all {1 1/2 0} positions, and complete extinction at {2 1 0 } positions of the reciprocal space. Interpretations of these effects vary. Okamoto and Thomas [92] suggested that the SRO state possibly consisted of micro-domains of the $D0_{22}$ structure, and proposed non-conservative APB's along the {4 2 0} plane. de Fontaine's [84] statistical thermodynamic description of the SRO state in Ni-Mo alloys is based on the appearance of the 1 1/2/ 0 intensity maxima as a

manifestation of the minimization of the second derivative of G with respect to η of the solid solution at the special points in reciprocal space. For a further interpretation of superlattice reflections. See Thomas and Goringe [96].

Dark field micrographs taken with [1 1/2 0} reflections show a "speckle" contrast, the size and sharpness depending on (increasing with) quenching rate. In fast quenched samples, Chevalier and Stobbs [89] found that very fine speckles are not seen to be distributed within the thickness of the sample. This contrast has been described as due to static-concentration-wave-packet. Coarse dots are observed in samples exposed to temperatures above 1000 K for a few seconds, and are attributed to micro-domains. Chevalier [97] concluded that in quenched Ni_4Mo there was no micro-domains, and that the 'speckle' pattern was due to the superposition of static concentration wave packets (SCWP), and concluded that in Ni_4Mo quenched and then aged at 1023 K for 60 s that there was a two-phase system consisting of a SRO matrix (SCWP) with imperfectly ordered D1a micro-domains. He used dark-field stereomicroscopy to distinguish between 3D bound scattering regions (micro-domains) and other scattering regions due to the superposition of scattering from several locally correlated groups of atoms.

Kulkarni et al. [86] tried to simulate the SRO state and the SRO to LRO transition at the atomistic level with computer modeling. They felt that the concentration wave model and the cluster model of Amelinckx et al. [98, 99] fit well with their results. The cluster model is characterized by small locally ordered atomic configurations representing motifs of the coherent LRO structure(s). The micro-domain model due to Das et el. [93] and Das and Thomas [36] predicts the sizes of locally ordered domains to be the size of

several unit cells of LRO domains. Amelinckx [99, 98] attribute streaking in diffraction patterns to the formation of atomic clusters.

They [86] conclude that the concentration wave model and the cluster/micro-domain model appear to be relevant to two different regimes of the ordering process. The concentration wave model is more appropriate for the SRO state, but are expected to be present as packets. The cluster/micro-domain model describes the nature of the transitional states which give rise to the various patterns of diffuse intensity. The overall SRO to LRO transition involves the formation of degenerate clusters of N_3M, D1a, Pt_2Mo, and $D0_{22}$ structures, and the clusters can arise from the secondary ordering process in the SRO state consisting of <1 1/2 0> concentration waves. There is a continuous increase in the numbers and sizes of such clusters during the transition.

Stobbs and Stobbs [100] also feel that the cluster approach and SCWP approach should be jointly applicable. They used HREM methods and dark-field imaging, but feel that neither method provides evidence for the presence of micro-domains of D1a or $D0_{22}$. They state that their data and data by Van Tendeloo [99] preclude any physical predictive application of a well-defined micro-domain model for the description of the SRO of the <1 1/2 0>special point alloys. They also mention that the CVM method of Kikuchi [91] is more appropriate for real space while the SCWP model of de Fontaine is more appropriate for reciprocal space.

Banerjee [83] concluded that the controversy as to whether the SRO-LRO transition occurs by continuous transition or by nucleation and growth transition has been resolved using high resolution electron microscope (HREM) experiments, which have been done over a wide range of temperatures and have been carried out in order to resolve

the structure of the SRO state on an atomic resolution. Van Tendeloo et al. [99] found that bright spots arranged in small clusters in two-dimensional patterns representing the [001] projection of the real lattice, which were often found to be arranged in diamond-shaped or in square-shaped clusters. The cluster orientations and dimensions matched with the motifs corresponding to $D0_{22}$ and D1a structures, respectively. Optical processing of HREM micrographs has revealed (Lee et al. [101]) the presence of wave packets corresponding to different variants of <1 1/2 0> waves and their frequent interference. HREM images of SRO to LRO transitional structures, which exhibit D1a and $D0_{22}$ motifs, show that these motifs are generated by the superimpostion of wave packets associated with different variants of <1 1/2 0> wave vectors. Hata et al. [102] have even more recently investigated the transformation using Monte Carlo simulation based on an FCC Ising model and TEM techniques. The TEM samples were quenched and then aged at 873 K for various durations. They found that micro-clusters of D1a, $D0_{22}$, and Pt_2Mo structure unit cells are simultaneously formed in the early stages of SRO. The features of the HRTEM images and diffraction patterns of SRO are explained in terms of the projection of mixed micro-clusters. The SRO to LRO transformation in the subsequent stage is characterized by the preferential growth of D1a subunit cells into extended domains. Hence they feel that the SRO to LRO is attributed to continuous growth of D1a segments into ordered domains.

Most evidence points to the fact that there is no unique mechanism which is operative over the entire temperature range and order parameter range. These mechanisms [83] have been mapped for the case of an irradiated sample, as shown in Figure 2.15.

As Banerjee mentioned [83], the temperature range over which the α to β

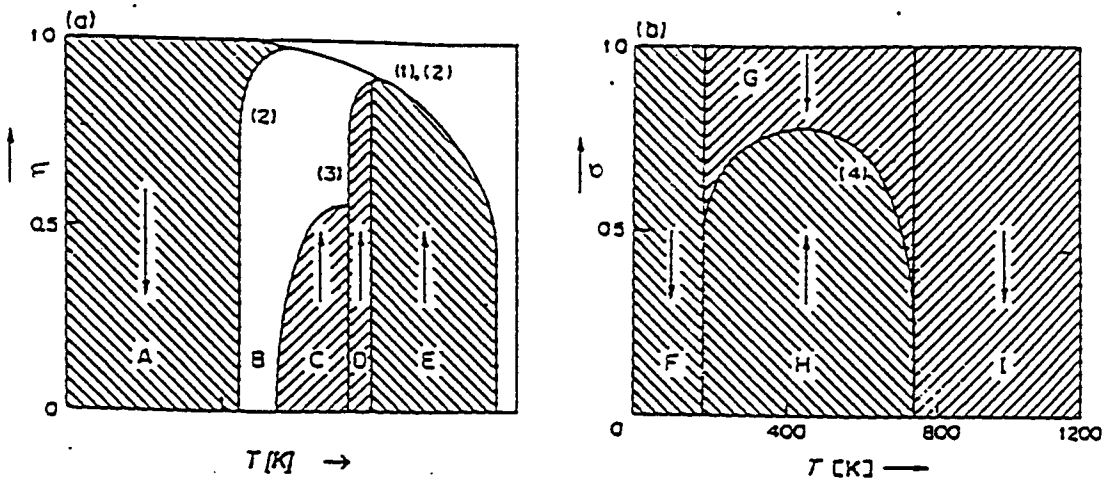

Figure 2.15 Different ordering mechanisms of Ni_4Mo under irradiation at different temperatures. Diagram a) is the long-range order parameter as a function of temperature and Diagram b) is the short-range order parameter as a function of temperature.

Region A Destruction of LRO
Region B No significant change if the initial state corresponds to $\eta=1$ or $\eta=0$
Region C Continuous ordering by decay of the SRO waves and simultaneous amplification of the LRO waves
Region D Initially as in Region C, after SRO is destroyed completely LRO develops by domain formation and growth
Region E Nucleation and growth of D1a microdomains from the beginning of the transition
Region F destruction of SRO
Region G Reduction of the degree of SRO and at $T > 550$ K transition to LRO
Region H Development of SRO
Region I Destruction of SRO and transition to LRO
Region J Development of SRO from completely disordered state in the early stage of ordering in the absence of irradiation (not shown on map)

(Adapted from Banerjee et al. [100])

transition has been studied is restricted in the absence of irradiation because the ordering kinetics below 1000 K is too slow to follow experimentally. The formation of β from α upon re-heating the quenched alpha in the Ni_4Mo alloy transformation from LRO to SRO follows a classic 'C' shape curve. Stansbury [103] mentions that classical first-order phase transformations typically occur by nucleation and growth leading to this type of TTT curve. This 'C' shape results from two main factors. One is due to transformation times approaching infinity at the equilibrium transition temperature due to the absence of a free energy driving force. The other factor is the transformation times at low temperatures being long due to the low atom mobility. The two factors cause a maximum transformation rate at intermediate temperatures at some critical degree of undercooling. Figure 2.16 [103] shows a TTT curve that has been determined by electrical resistivity methods. The start curve was defined in this case as a 0.5 μΩ cm change from the initial value, and the end curve was defined by a 75% change in initial resistivity. The resistivity changes of the SRO and LRO changes have been investigated by Lei et al. [104], and their results are discussed in more detail in section 2.4.

Brooks and Cao [105] studied the development of LRO from cold-worked SRO α in Ni_4Mo. This allowed them to examine the effects of recrystallization on the ordering kinetics. They cold-worked quenched samples by swaging to 43 % R.A and then aged the samples at 1123 K and 973 K for up to 48 hours. The α phase recrystallized with accompanying softening, the ordered β domains formed with an increase in hardness. At 973 K, the α phase first changed to deformed β, with an increase in hardness. Then recrystallized β domains formed in the deformed β , and eventually hardness decreased as the domain sizes increased.

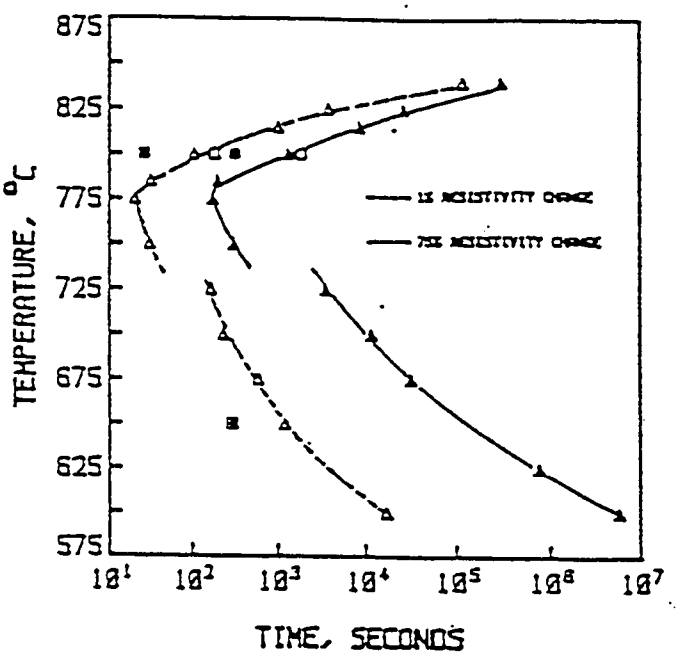

Figure 2.16 Time-temperature-transformation (TTT) diagram for the Ni_4Mo alloy α to β phase transformation. The data was obtained using direct current electrical resistivity measurements. The start curve was assumed from a 1% change in resistivity, and the end curve was assumed from a 75% change in initial resistivity. Note the displacement in the curve near 735 °C. From Lei [58].

Stansbury [103] reviewed the kinetics of the Ni_4Mo SRO to LRO phase transformation, and provided the TTT diagram in Figure 2.16. He points out that because of the diversity of identified structures associated with the SRO/LRO states of the Ni_4Mo alloy, the identification of structural changes under specific conditions is complicated. The ability to develop quantitative kinetic mechanisms for the transformations as functions of initial states and time is severely limited. Phenomenological beginning and ending states are well established by x-ray and electron diffraction and by changes in properties such as electrical resistivity, volume, and hardness.

There is strong evidence that the transformation occurs by nucleation and growth above about 700 to 750 °C, but homogeneously at lower temperatures. Field ion microscopy observations of Yamamoto [106] show exceptions to this. The mechanism of the transformation below 750-725 °C is less certain. Stansbury [103] notes a possible change in reaction mechanism and hence in morphology as indicated by the time displacement of the TTT diagram near 735 °C .

Banerjee et al. [107] observed that radiation and thermal exposure from 200 to 500 K lead to three main conclusions:

1. SRO forms only from a more highly disordered state.
2. In the presence of LRO, SRO does not form.
3. LRO does not nucleate from SRO.

From 550 to 720 K, they found that the continuous diffraction intensity shift indicates that no D1a micro-domains are present, and the alloy existed in a single phase transitional state. At higher temperatures LRO nucleates discretely, and a mechanism involving pre-existing micro-domains is not involved. At 770 K the initial SRO disappears with the formation of LRO with $\eta = 0.85$, and at temperatures above 850 K, the SRO intensity

disappears continuously as LRO appears, with no intensity between diffraction spots. This indicates that LRO nucleates discretely, and a mechanism involving pre-existing LRO is not involved. Some evidence for a change in mechanism around 750 °C is evident from the isothermal resistivity data of Lei [58] in Figure 2.16. Banerjee et al. [107] feel that nucleation and growth occurs as low as 550 °C. Stobbs and Chevalier [108] imply there is no strong reason to preclude these mechanism at low temperatures.

Once the domains form, It was found by Vasudevan et al. [109] that the domain growth is analogous to metallurgical grain growth, and can be described by

$$D^n = kt \qquad \textbf{(2.32)}$$

where D is the average grain size, t is the aging time, k is a constant, and n is the reciprocal of the slope of the Log D versus t plot. They studied by TEM the growth of domains in Ni_4Mo in the range of 600 to 850 °C and times up to 4500 hours. They found n = 2.0 at 850 °C and 800 °C , and n = 2.9 at 600 °C and 700 °C. This change was attributed to domain orientation effects. The domain growth activation energy was found to be 290 kJ/mole from 800 to 850 °C, and 390 kJ/mole from 600 to 700 °C.

A schematic diagram of the structural changes during the transition from SRO to LRO are shown in Figure 2.17 [110]. Changes in the LRO parameter and in ductility are also correlated to the changes in morphology.

2.3.4 Anomalies in Some Thermophysical Behavior

Electrical Resistivity measurements were made by Thomas [111] which provided early evidence that there is a structural variance within the α phase region. The electrical resistivity of quenched or cold worked structures was observed to be higher than for the slowly cooled ordered condition. Thomas attributed the high electrical resistivity of the

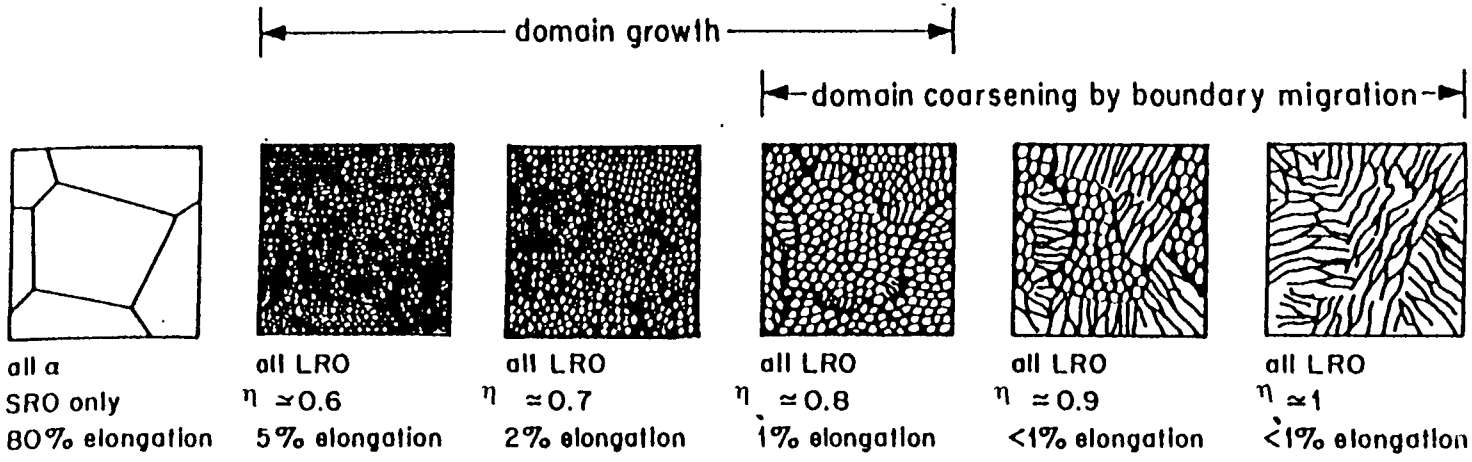

Figure 2.17 Schematic diagram of the microstructural changes that occur during the Ni_4Mo α to β phase transformation. The long-range order parameter data and ductility data also accompany the diagram. Adapted from Brooks and Sanganeria [156].

non-deformed alloy to a distinct structural state which he called the "komplex" state, or 'K' state, which we now know is SRO (see below). In Ni_4Mo, the decrease of electrical resistivity with cold work is due to the removal of the high degree of SRO. SRO increases the electrical resistivity in many systems, but there are systems where ρ decreases as SRO increases. Most Ni-based solid solution alloys exhibit K-state phenomena, an equilibrium structural feature. Upon cold working, ρ decreases. Thomas theorized that one of the elements must be a transition element for K-state formation.

Chang [57] mentions that the K-state is a state of SRO clustering. These SRO clusters form in the microstructure and act as sites for scattering the electrons. SRO clusters are non-random atom configurations which provide more effective electron scattering as compared to a random solid solution [112].

According to Vasudevan [37], it is not quite clear how SRO might increase electrical resistivity. One possible explanation is related to the transition element electron configuration, namely the unfilled d state. Another explanation is considering the SRO state as micro-domains of non-random atom configurations providing a higher amount of electron scattering.

Brooks et al. [13] point out that SRO can be accepted as the major contributor to the K-state since it correlates to x-ray data. Other possible contributors may be LRO, clustering, precipitation reactions, and transfer of electrons to d shells of the transition elements.

2.4 Determination of Electrical Resistivity

2.4.1 Electrical Resistivity Theory

2.4.1.1 Classical Models

The theories of electrical resistivity started soon after the discovery of the electron by Thomson [113]. The first important model was proposed by Drude in 1900 and was developed by Lorentz around 1909.

According to the classical model of conduction, the electrons in a metal are treated like an ideal gas [114]. The electrons, which are detached from the atoms, are considered responsible for the transport of current, and collisions with the lattice are the cause of the electrical resistivity. The electrons are assumed not to interact with each other. The methods of the kinetic theory of gases, including Maxwell-Boltzmann statistics, are applicable [113].

Under the influence of an electric field, $\vec{E}$, which in the interior of the metal is assumed to be uniform, the electrons experience a force, $\vec{F} = -q\vec{E}$ where q is the charge of the electron. The force results in an acceleration, $\vec{a} = q\vec{E} / m_e$, where m_e is the electron mass [115]. The kinetic energy is quickly dissipated by the collisions. If the collisions did not occur, the acceleration of electrons would continue. Without an electric field, the electrons move about randomly between the fixed metal ions of the lattice with a mean velocity dependent on temperature. The application of an electric field in conjunction with the collisions causes a steady state drift velocity where the electrons take on a velocity in the direction opposite to $\vec{E}$.

The average speed of electrons from thermal motion determined from the Maxwell-Boltzmann distribution is [113]:

$$\bar{v} = \sqrt{\frac{8k_B T}{\pi m_e}} \qquad \textbf{(2.33)}$$

where T is absolute temperature, k_B is boltzmann's constant, and m_e is the electron rest mass. This expression is the same as for an ideal gas. If τ is taken as the average time between collisions, then the drift velocity v_d can be expressed as

$$v_d = \frac{qE}{m_e}\tau \tag{2.34}$$

v_d is much less than the average thermal velocity. If the mean free path λ is assumed to be the average distance between collisions, then

$$v_d = \frac{qE\lambda}{m_e\bar{v}} \tag{2.35}$$

and the current is

$$I = \frac{ne^2\lambda}{m_e\bar{v}}EA \tag{2.36}$$

where n = the number of electrons per unit volume and A is the cross-sectional area of the conductor. This classical model successfully predicts Ohm's law, i.e., current proportional to voltage [64]. The electrical resistivity is then given as the proportionality constant

$$\rho = \frac{m_e\bar{v}}{ne^2\lambda} \tag{2.37}$$

This is the classical model prediction. λ can be related to the metal ion size as

$$\lambda = \frac{1}{n_a\pi r^2} \tag{2.38}$$

where r = ion radius and n_a = the number of ions per unit volume. This assumes that the electron size is negligible and that there is one free electron per atom.

There are many attractive features of the Drude model. One is that given the above assumptions, a reasonable order of magnitude value for the electrical resistivity of metal elements at room temperature is given. Another important result of the classical model is that it predicts the Weidmann-Franz Law [115]:

$$\frac{\kappa}{\sigma} = 3\left(\frac{k_B}{q}\right)^3 \qquad \textbf{(2.39)}$$

where κ is the thermal conductivity and σ is the electrical conductivity, $1/\rho$. This relationship is in modest agreement with experimental results. This result confirms that thermal conductivity is mainly an electronic phenomena. The classical model has underlying components used in subsequent theories. Some of the earlier theories by Sommerfeld and Lorentz did not improve the experimental agreement by that much for electrical conductivity [116]. We now know that the free electron concept is correct and that the neglect of the electron-electron interactions is also a correct assumption.

There are some problems associated with the classical model, and quantum mechanics models give results much closer to the experimental observations. Some of the problems with the classical theory are that the electrical resistivity calculated is much greater than the experimentally observed values, and the electrical resistivity varies linearly with temperature experimentally but the theory predicts that $\rho \propto \sqrt{T}$. The model does not provide a realistic mechanism for conduction in materials; i.e., it does not explain why some materials are insulators while others are conductors [113]. One other

discrepancy is that the electronic contribution of the specific heat is predicted classically to be composed of all electrons, but experimentally it is composed of only a small fraction of the total electrons [117].

2.4.1.2 Quantum Mechanical Models

Quantum theory predicts that the electrons do not obey the equipartition theory, but quantum theory still gives the resistivity proportional to the electron mass and average velocity. One difference between classical and quantum theory is that in the quantum theory, the average velocity is based on the quantum model. Thus the mean free path is a function of the wave nature of the electron and the electrons are thought to obey the Fermi-Dirac distribution instead of the Maxwell-Boltzmann distribution.

A quantum free-electron theory electron theory was proposed by Sommerfeld in 1928, after the introduction of wave mechanics and the recently developed Fermi quantum statistics [60]. Sommerfeld treated the electrons as a gas and employed Fermi-Dirac statistics and the Pauli exclusion principle to show that only a fractional number of the conduction electrons are affected by thermal energy [115]. This fractional number is $k_B T/E_F$, where E_F is the Fermi energy. The Fermi energy is the energy of the highest occupied energy level at T = 0 K. The theory assumed a uniform electric field and ordinary plane waves to describe the electrons and also assumed that the conduction electrons are not influenced by the ionic field or by electron-electron interactions.

The Pauli exclusion principle was the key (only one free electron per quantum state). At absolute zero, all of the electrons fill those states which are the lowest ones available; below the Fermi energy, all states are occupied and above it, all states are vacant [117]. Since the electrons are confined to the space of the metal, the Heisenberg

uncertainty principle shows that at absolute zero the kinetic energy is not zero as predicted by the classical theory. At T > 0 K, only the few electrons that have an empty energy state within their reach are allowed to change states. Some of these electrons then acquire an additional energy of k_BT. Only those with energy within k_BT of the Fermi energy can gain energy as the temperature increases [56].

In a quantum mechanical theory of electrical conduction, under an applied electric field, the electrical resistivity is still given by

$$\rho = \frac{m_e \bar{v}}{n e^2 \lambda} \tag{2.40}$$

but the electron velocity and mean free path are interpreted differently than in the classical model. The velocity is essentially independent of temperature because the electron speeds follow the Fermi-Dirac distribution:

$$v_F = \sqrt{\frac{2E_F}{m_e}} \tag{2.41}$$

The mean free path, λ, is calculated in terms of the wave nature of the electron; the scattering of electrons by phonons is treated similarly to that of x-rays. The mean free path can be as much as hundreds of atomic distances if n is taken as one free electron per atom, and at low temperatures λ can exceeded millions of atomic distances. The wavelength describing an electron was shown by DeBroglie to be

$$\lambda = \frac{2\pi\hbar}{m_e v} \tag{2.42}$$

For a one-dimensional case, the wave number, k, which is the number of waves in a length 2π, is

$$k = \frac{2\pi}{\lambda} = \frac{m_e v}{\hbar} \tag{2.43}$$

and k is shown to be proportional to the momentum. The kinetic energy of a free electron with wave number k is given by:

$$E_K = \frac{\hbar^2}{2m_e} k^2 \tag{2.44}$$

The potential energy is assumed to be constant and taken to be zero. Hence the total energy is the kinetic energy. Problems dealing with wave motion are often described with the Schrödinger equation [118]:

$$\nabla^2 \psi + \frac{\hbar^2}{2m_e}\left(E - U(\bar{r})\right)\psi = 0 \tag{2.45}$$

where E is the total energy, $U(\bar{r})$ is the potential energy as a function of position, and $\nabla^2\psi$ is the Laplacian of the eigen (wave) function. The probability that an electron is present in a volume element dV is

$$|\psi|^2 \, dV \tag{2.46}$$

As mentioned previously, the Fermi energy is the energy of the highest occupied energy level at T = 0 K. In three dimensions at absolute zero temperature, the Fermi energy is

$$E_F = \frac{h^2}{8m_e}\left(\frac{3N}{\pi V}\right)^{2/3} \tag{2.47}$$

where V is the volume, and N/V is the number density of states. The average energy at absolute zero is $3/5E_F$.

The Fermi factor, F, is the probability that an energy level will be occupied. At T = 0 K, F = 0 if $E > E_F$ and F=1 if $E < E_F$. At T > 0 K, the Fermi factor is

$$F = \frac{1}{\exp\left(\frac{E - E_F}{k_B T}\right) + 1} \tag{2.48}$$

and the Fermi energy for T > 0 K is defined as the energy when F = 1/2.

The Sommerfeld model is an intermediate stage between the classical physics and the more modern quantum mechanical models. The theory gives a good agreement between theory and experiment for the specific heat and the Lorentz number (Weidmann-Franz law). The model, however, does not give agreement with the experimental results of the electrical conductivity [118].

A great advance in theory occurred when it was assumed that the potential to which the electrons are subjected varies periodically as a result of atoms arranged on a space lattice [118]. Bloch introduced this essential new feature. The waves are no longer ordinary plane waves because they are modulated by a function which is the period of the lattice [115]. The Bloch model suggests that the electrical resistivity is a consequence of disturbances in the atomic periodicity in the crystal. Bloch used the Fermi-Dirac distribution as the electron occupational probability function. The theory demonstrates that in a perfect metal at 0 K, λ approaches infinity and ρ approaches zero. He also showed that the appropriate solutions to the Shrödinger equation for the case of a periodic potential were of the form

$$\psi\left(\vec{k}\right) = U\left(\vec{r}\right)\exp\left(i\vec{k} \bullet \vec{r}\right) \tag{2.49}$$

and $U(\vec{r}) = U\left(\vec{r} + \vec{R}\right)$ where $\vec{R}$ is the identity period of the lattice in the $\vec{k}$ direction. The Bloch functions represent plane waves modulated with the lattice periodicity and having

the mean free path as $\lambda = \frac{2\pi}{k}$ traveling in the $\vec{k}$ direction. If the lattice is periodic with no imperfections, the electron waves will propagate through the lattice without loss of energy because there is zero resistance to the motion of the conduction electrons [60]. When electrons interact with electric and magnetic fields, they respond as if they have an effective mass given by:

$$m^* = \frac{h^2}{\left(\frac{d^2E}{dk^2}\right)} \tag{2.50}$$

The interaction of an electron with the periodic field occurs when Bragg's law, $n\lambda = 2d\sin\theta$, is satisfied [12]. Total diffraction then occurs when

$$k_d = \frac{n\pi}{d_{hkl}} \tag{2.51}$$

There are certain k values which are not permitted, and propagation of these waves cannot occur [117]. The wave vector ends on a plane perpendicular to k and at a distance of $\frac{n\pi}{d_{hkl}}$ from the origin. Thus there are zones of allowed energy between the critical values of k. These zones are known as Brillouin zones, each of which contains a band of allowed energies. Each zone is separated by a gap of forbidden energy levels. There are some circumstances where those bands overlap. At 0 K there are two electrons in each of the allowed energy levels. At higher temperatures some of the electrons are excited into states slightly above the Fermi energy (the energy representing electrons of maximum energy). The Fermi surface may lie partly in one zone and partly in another. The electrical conductivity of a solid is essentially determined by how completely filled the Brillouin zones are. When an electric field is applied, the balance of momentum is upset, and there

is a net drift. This drift will occur if there are some unoccupied states with energies just above the occupied levels so that the applied field can accelerate some of the electrons. In a metal, there is always these unfilled states. Monovalent metals have enough valence electrons to fill half the states of the first zone, hence they are good conductors. In divalent metals, conduction occurs by zone overlap [118].

A knowledge of the location and shape of the Brillouin surface is important to understanding the conductive properties of the metal. Metals of high valence have complex band structures, with Fermi surfaces crossing several zones. Spill-over also occurs when the gaps between the zones are small.

Bloch's solutions only describe the experimental values at high and low temperatures. Gruneisen suggested that Bloch's low temperature form could be used for all temperatures [115]:

$$\rho(T) = 4\left(\frac{T}{\theta_R}\right)\rho(\theta_R)\int_0^{\frac{\theta_R}{T}} \frac{x^5}{\left(e^x - 1\right)\left(1 - e^{-x}\right)}dx \qquad \textbf{(2.52)}$$

where θ_R is a characteristic temperature chosen to fit the experimental data. This Bloch-Grünisien model is the only widely used equation that moderately well describes the temperature variation of the resistivity of a large number of metals over a wide range of temperatures. The integral is proportional to T^5 at low temperatures and at high temperatures becomes linear with temperature. The Bloch-Grünisien equation provides a valuable tool for discussing experimental data [117]. The resistivity of monovalent elements are in reasonable agreement with this expression. The multivalent elements and transition elements are often in substantial disagreement with this expression.

Refinement of the Bloch equation still remains at the heart of most modern theories of electrical resistivity [115]. A calculation of ρ requires a knowledge of the Bloch wave functions and the potentials on the atoms. It is relatively easy to calculate ρ within a factor of 2 or 3, but getting within 10% is very difficult [119].

It is generally agreed that the electrical resistance arises from two primary sources [117]. A major source is the vibrations of the lattice ions as a consequence of the thermal energy they gain with temperature. This portion of the total resistivity is referred to by many names; thermal, phonon, lattice, intrinsic, or ideal. The other source of resistivity is the presence of chemical or physical imperfections in the lattice, which are relatively few and independent of temperature. There are increases in ρ when an impurity atom replaces a solvent atom [115]. Alloying or impurity elements destroy the perfect periodicity in the potential, and this gives rise to elastic scattering. This is often referred to as the residual resistivity or sometimes the impurity resistivity. This proposal will refer to the former as the thermal resistivity, ρ_T, and the latter as the impurity resistivity, ρ_i . Mattheissen's rule expresses the total resistivity as the sum of these two contributions:

$$\rho = \rho_T + \rho_i \qquad \textbf{(2.53)}$$

The elastic scattering is assumed to be independent of temperature for Mattheissen's rule. Detailed calculations show that there is no scattering of electron waves by a perfectly ordered crystal, and λ is assumed infinite. Thus scattering arises because of the imperfections in the lattice [117]. For dilute alloys, Mattheissen's rule holds well, but breaks down when large size differences are present and when the amount of impurity is too high [117]. Alloys rarely obey this law, and much interest has been directed toward measuring the deviations from Mattheissen's rule (DMR's). It is sometimes reasonable to

treat alloys as if they did obey this rule; for example, the resistivity of dilute alloys near room temperature. When temperatures and concentrations fall outside of restricted ranges, however, the resistivity must be determined experimentally [115].

For dilute solutions, the impurity resistivity is often considered to be proportional to the concentration. At higher concentrations, the impurity term is sometimes expressed by Nordheim's rule:

$$\rho_i = \frac{\overline{\rho}_i x(1-x)}{100} \qquad \textbf{(2.54)}$$

where $\overline{\rho}_i$ is the resistivity increase for the 1 at% impurity, and x is the atom percent of solute in the alloy [59]. This is the isothermal impurity resistivity of a solid solution of a binary alloy as a function of atom percent. Solid solutions whose constituents are both in the same column of the periodic table of the elements are often in agreement with Nordheim's rule. Homogeneous random solid solutions often follow this rule. Solid solutions containing transition elements usually do not follow this rule. This rule holds true for disordered solid solutions, but is not valid for solutions with SRO or LRO [119]. The ordering process occurs below a certain critical temperature, and results in a considerable decrease in ρ. Nordheim's rule holds approximately for disordered solid solutions but is not valid if SRO or LRO is present because then the resistivity decreases with increased ordering [119]. As order increases, ρ of a solid solution decreases a great deal. The resistivity is less dependent on the vacancy concentration than on the degree of order. Dislocations, especially at low temperatures, can have a significant effect on ρ.

Nordheim's rule does not allow for changes in the density of states with composition. There is an isothermal density of states model that gives ρ as a function of

concentration in concentrated alloys involving transition metal components, as long as the components are not magnetic. This model cannot be easily quantified into a mathematical relationship to calculate ρ. More refined theories also exist but have failed to give a mathematical relationship so that ρ can be calculated as a function of temperature and concentration with any degree of precision [115].

The alloy of primary interest of this proposal is Ni_4Mo, which is composed of two transition elements. The alloy undergoes order-disorder phenomena and displays a negative temperature coefficient of resistivity in certain temperature ranges. For transition metals, the most accepted electrical resistivity theory is probably based on the innerband scattering model presented by Mott and Jones [120]. Transition metals usually have higher electrical resistivity, and also have many unusual properties. All transition metals have partially filled d-shells. It is typical of these metals to have a high specific heat and electrical resistivity compared to the monovalent and divalent metals. They are strongly paramagnetic, and some are ferromagnetic and antiferromagnetic in some limited temperature ranges. Bloch waves at the Fermi level are more concentrated around the ion cores of transition metals and rare earth metals than they are concentrated around the ion cores of noble, alkali, and group II metals. This suggests that there is a considerable mixing of 's' and 'd' wave functions so that the Fermi momentum is effectively larger. The probability of an electron being between the atoms is decreased and hence it is more difficult for electrons to travel through the lattice [119]. Mott and Jones [120] suggested that the d-band electrons contribute very little to ρ. Electrons can be scattered into unoccupied energy states of the d-band. Those s-d transitions will add greatly to the scattering probability and thus to the resistivity. The valence electrons are shared between

a wide, low density of states s-band, and a narrow high density of states d-band. The d-band electrons contribute very little to the conductivity because they have a large effective mass [117].

Most alloys experiencing order-disorder phase transitions will exhibit anomalies in ρ and in $d\rho/dT$ around the critical point. Another anomaly may be a negative temperature coefficient of resistivity. This is not consistent with Bloch theory. In some alloys, this may be attributed to a rapid decrease in the density of the d-band states near the Fermi level which results in a reduction of the average d-band states within k_BT of the Fermi level as the temperature increases. Another contribution to ρ arises from scattering of conduction electrons with unpaired electrons such as the rare earth metals and some transition metals. The total magnetic resistivity above the curie temperature is:

$$\rho_m = CS(S+1) \qquad \textbf{(2.55)}$$

where S is the spin of the 3d or 4f electrons, and C is a constant which depends on whether it is a rare earth metal or a transition metal [120].

In most cases, the electrical resistivity as a function of temperature is independent of the direction of current flow, particularly in cubic metals, so that single crystals are not required to get data. In cubic metals the mean square displacement averaged along any crystal direction is the same. In non-cubic metals, there are some differences reported at room temperature, but these may be due to variations of the phonon vibrational amplitudes with crystal direction [117].

Much work has been done in trying to formulate electrical resistivity behavior. For example, Nicholson and Brown [112] attempted to theoretically model the

ρ behavior of the Ni_4Mo alloy based on first principles from a quantum mechanical description. They observed that:

> 1. The random alloys have more current flowing through them in weak fields.
> 2. The current is greater between Mo-Mo pairs, which are more plentiful in the random alloys.
> 3. The current is depressed between Mo-Ni pairs, which are more plentiful in SRO alloys.

They state: "Our understanding of the "K-state" effect depends, first on having a Fermi energy located on the upper d band edge, second, on the presence of SRO, so that it can be eliminated by cold work, and third, on the minority components being larger and having weaker d scattering at the Fermi level. This is precisely the situation in the prototypical K-state alloys, Ni-Cr, Ni-Mo, and Pd-W. "

The resistivity of many monovalent, divalent, and dilute metals can be described mathematically as a function of composition and temperature. However, Shröder [115] mentions that "..., the resistivity of most concentrated alloys for application purposes has to be obtained from experimental data and cannot, with some exceptions, be calculated from a standardized functional relationship." Some exceptions are selected alloys usually involving elemental constituents from the same column in the periodic table and do not involve transition metal components. Also, even though the resistivity is rather sensitive to ordering, there is not a general expression relating the degree of ordering to the change in electrical resistivity.

2.4.2 Electrical Resistivity Behavior in Ni_4Mo

Several investigators at the University of Tennessee have studied the electrical resistivity of Ni_4Mo in various initial states. Lampe [38] used a potentiometric method where the circuit was connected to the sample with the sample enclosed in a tube furnace.

He used two heating rates; 16 °C/min and 1.5 °C/min. He used a cooling rate of about 6 °C/min. Chang [57] used essentially the same method as Lampe to verify the results of Lampe. He used heating and cooling rates of 5 °C/min and 3.5 °C/min, respectively, on a sample that was initially in the LRO condition before heating, and used a heating rate of 25 °C/min on a sample that was initially the SRO condition before heating.

Lei [58] used direct current to heat the samples for electrical resistivity measurements with a computer to control the process. The equipment was capable of taking four readings per tenth of a second, and could heat up to 20 °C/min. Figure 2.18 shows results from Lei, the heating rate being about 10 K per minute for all three curves. For Curve 1 the sample was pre-treated by cooling slowly to have all β as the initial state. The electrical resistivity, ρ, starts out at about 45 $\mu\Omega$-cm at 25 °C but increases sharply and continuously all the way to the transforomation temperatue, where it peaks out at about 135 $\mu\Omega$-cm. This sharp increase is attributed to a decrease in the LRO as the temperature increases. Above the critical temperature (868 °C), no LRO exists, and only SRO exists. The SRO decreases with increased temperature to the melting point. Since there is less SRO scattering centers, the resistivity decreaes. In this case, the SRO effects are masking the thermal contributions, which would have resistivity increasing with temperature. At higher temperatures, ρ then decreases with temperature. Curve 2 is for SRO α as the initial state. The curve starts at about 145 $\mu\Omega$-cm at 25 °C. Above about 600 °C , the resistivity decreases with an increase in temperature due to the SRO to LRO transformation. Curve 3 is for the same heat treatment as for Curve 2, but was cold-worked to about 75%. The cold-work process introduces defects but destroys SRO clusters. The overall effect of this is a decrease in the electrical resistivity. From 25 to 600

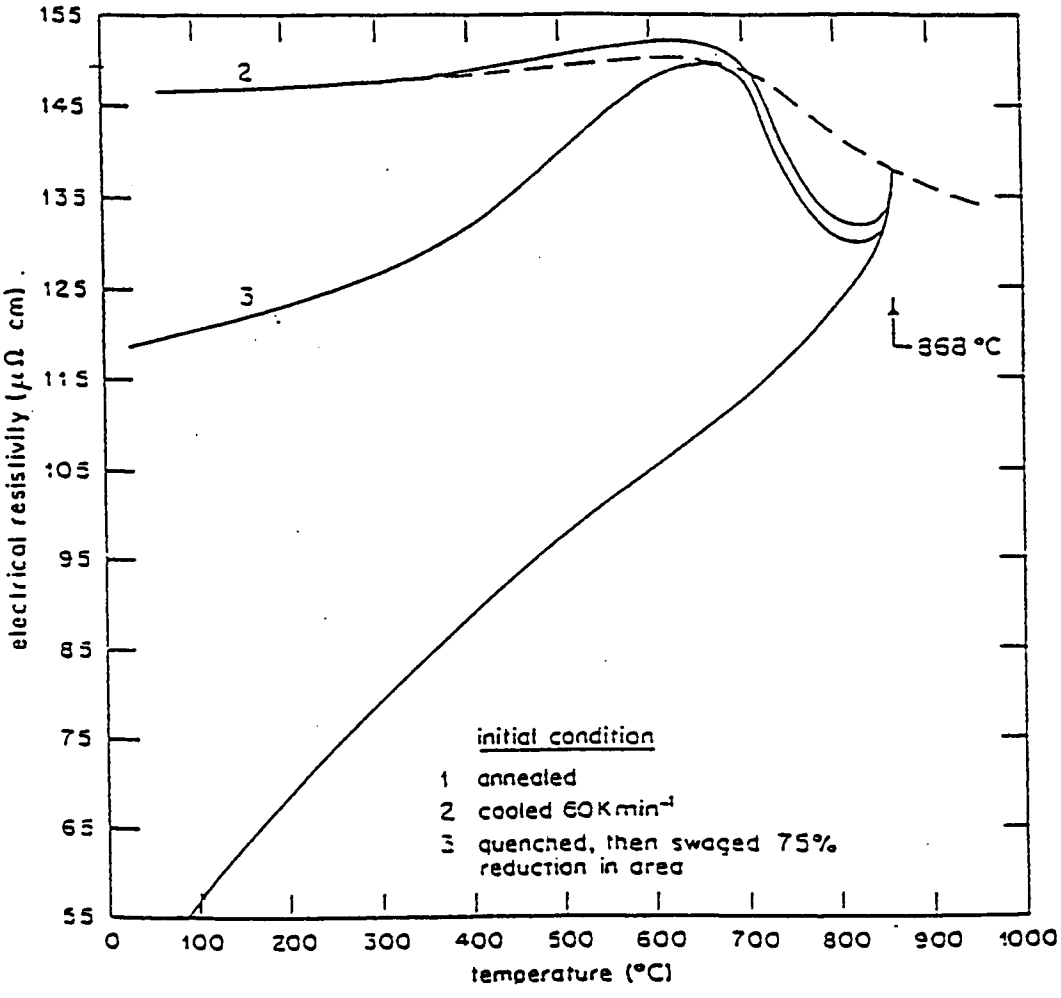

Figure 2.18 Electrical resistivity versus temperature data for Ni_4Mo from slow heating. The data shows three different initial conditions obtained from DC heating. Curve 1 represents resistivity for a sample that was annealed so that it was in the LRO β condition. Curve 2 represents resistivity data for a sample that was quenched from above Tc (868 °C) so that it is initially SRO α. Curve 3 represents resistivity data from a sample that was quenched to SRO α, and then cold-worked to 75% reduction in area. The heating rate was about 10 °C per minute. The dashed line represents resistivity data during cooling. Data is from Lei [58].

°C , ρ increases, and there is a return to SRO during this stage. At the recrystallization temperature, there is a contribution from the removal of defects to decrease the electrical resistivity [121]. If new SRO forms it will increase ρ, although it may be masked by other effects. Beyond 600 °C , ρ decreases as temperature increases because of the α to β transformation. This dominates the electrical resistivity behavior in this temperature region.

Vasudevan [37] measured the electrical resistivity of Ni_4Mo at elevated temperatures and various percentages of cold-work using ohmic heating techniques similar to Lei. He was able to obtain heating rates of up to 30 °C/min. His results were similar to Lei's.

Basak [121] performed electrical resistivity measurements on a Ni_4Mo alloy using the technique recommended in this proposal: a pulse-heating calorimeter. He attempted three initial conditions: cold-worked SRO, SRO, and LRO. The specimens were pulse-heated from room temperature to 1500 K, with heating rates from 50 to 75 °C per **second**. His data are shown in Figure 2.19. For the LRO β initial condition (Curve 1), ρ starts at about 75 μΩ-cm and rises sharply until T_c is reached. It then passes through a maximum at about 130 μΩ-cm at the order-disorder temperature of 1141 K, and then decreases gradually. Curve 2 shows data for the SRO initial condition. At 25 °C ρ is about 140 μΩ-cm. The SRO resistivity is much higher than the LRO resistivity because SRO clusters serve as sites for scattering of electrons. As the temperature increases, ρ gradually increases until a maximum at about 950 K.

A still further increase in temperature decreases the resistivity, even beyond the critical temperature. For the 14 % cold-worked initial SRO specimen (Curve 3), at 25 °C

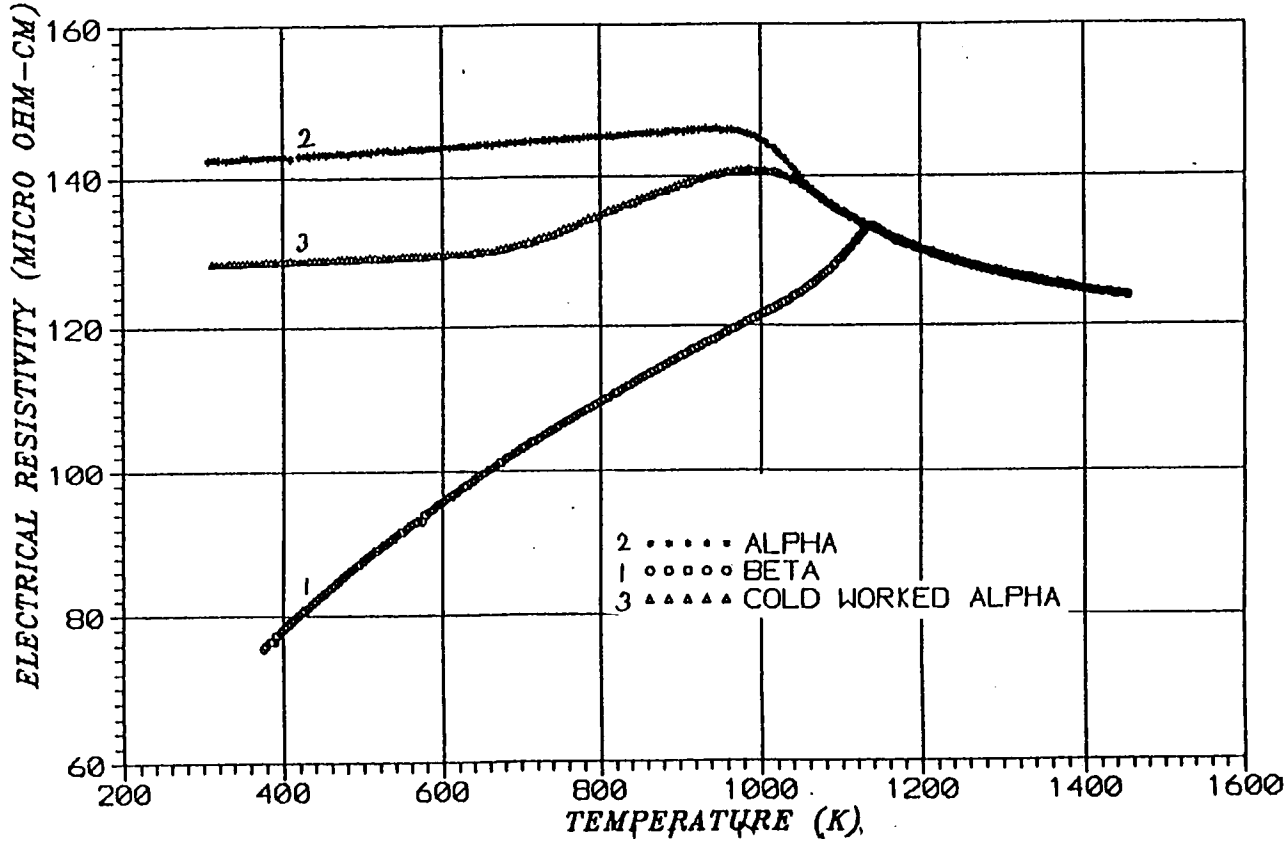

Figure 2.19 Electrical resistivity data versus temperature data for Ni_4Mo from pulse-heating. Curve 1 represents resistivity data from a LRO β initial condition sample. Curve 2 represents resistivity data from a SRO α initial condition sample. Curve 3 represents resistivity data from a sample that was converted to SRO α and then cold-worked to 14% reduction in area prior to obtaining the resistivity data. The heating rate used in obtaining this data was about 60 K per second. Data is from Basak [121].

ρ is about 130 $\mu\Omega$-cm; about 10 % less than the non cold-worked sample. This is attributed to the break-down of SRO clusters which more than compensates for the increase of resistivity due to electron scattering from defects. As the temperature rises from room temperature to about 690 K, the resistivity gradually rises. This is attributed to dominant thermal scattering. The slope then increases until a maximum is reached, and then resistivity decreases and merges with Curves 1 and 2. Between 690 to about 1000 K, the SRO is increasing above the initial cold worked structure. Beyond 1000 K the dominant factor is the decrease in SRO as temperature increases. This causes ρ to decrease smoothly and merge with that of the non-cold worked condition above T_C. Recovery and recrystallization also decrease the electrical resistivity due to removal of defects. Once the recrystallized grains form, there is a possibility for SRO to form within the grains, since it is thermodynamically stable at this temperature. These SRO clusters increase the resistivity.

The resistivity curve for the 14% cold work α did not clearly reveal recovery and recrystallization in Figure 2.19, but recovery and recrystallization are evident in the power versus temperature curve (Figure 2.20). The dips are due to release of heat. They were not present in the annealed (non-cold worked) samples.

Basak [121] also did a slower heating rate pulse at 1 K/s which showed a resistivity value lower than Lei's data. Lei used a heating rate of about 10 K/min. The results of the two heating rates are contrasted in Figure 2.21. The heating rate of Basak was slow enough to approach the equilibrium resistivity value. Basak's sample had less SRO, thus it had a lower resistivity up to about 1000 K. The data demonstrate that the pulse-heating method at 50 to 75 K/s is fast enough to avoid the α to β phase

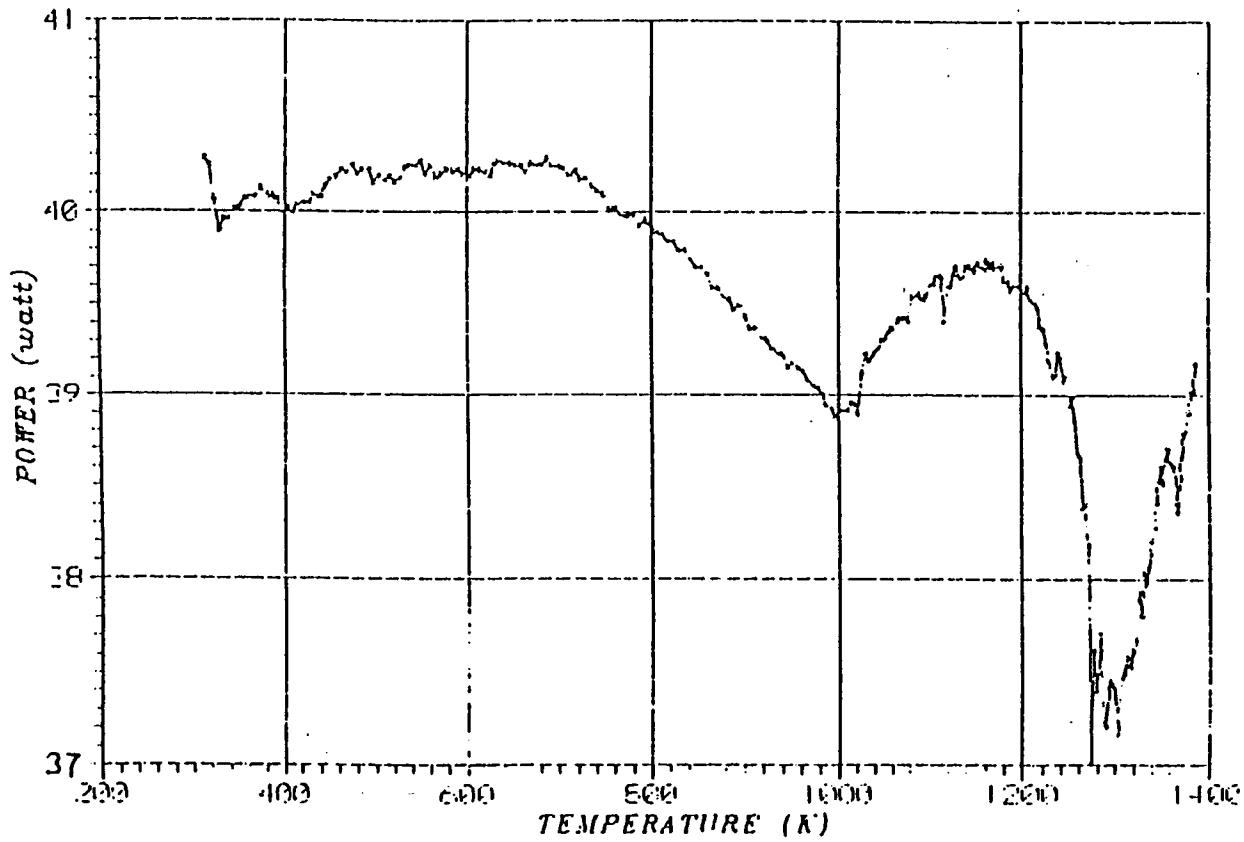

Figure 2.20 Power versus temperature data for cold-worked Ni_4Mo. Data was obtained from a pulse-heating calorimeter by Basak [121] on a sample cold-worked by 14 % R.A. The first minimum in the curve is attributed to recovery, and the second minimum is attributed to recrystallization.

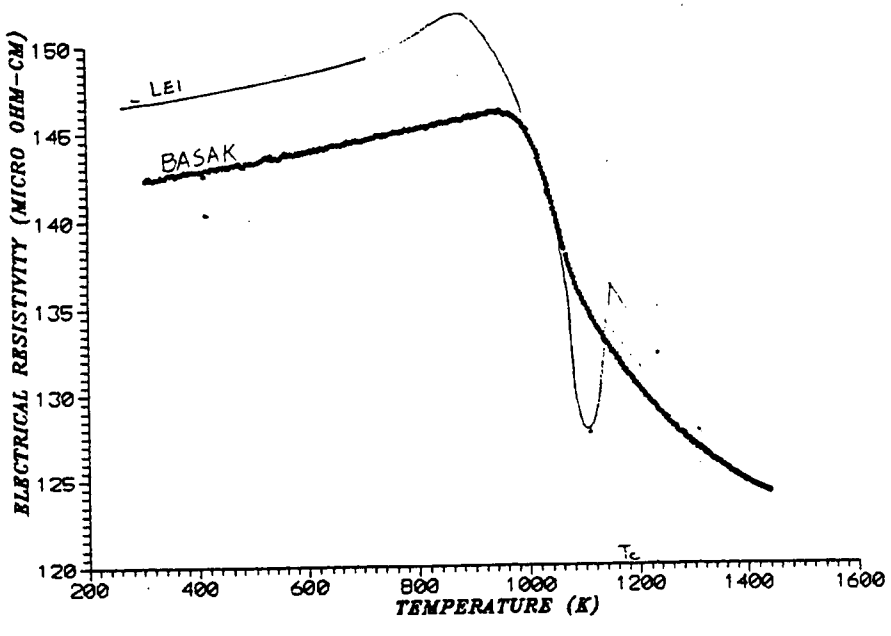

Figure 2.21 Comparison of electrical resistivity data on SRO α obtained from two different methods. Data was obtained at about 10 K per minute from Lei [58] and at about 60 K per minute from Basak [121] by slow heating in the pulse calorimeter. The initial condition for both samples was SRO α, but the slight difference in initial room temperature resistivity may be due to differences in amount of SRO due to Lei quenching his sample, and Basak allowing his sample to normalize in the calorimeter vacuum chamber. Adapted from Basak [121].

transformation.

Besides rapid heating capabilities, the pulse-heating calorimeter system is also capable of obtaining isothermal data using PID computer algorithms [121]. From the electrical resistivity data of these types of runs, it is possible to detect the change of phase as a function of time and temperature. Basak performed isothermal tests on Ni_4Mo for which the data depict the transformations of α to β at 700 °C and 750 °C. These data are shown in Figure 2.22.

2.5 Determination of Specific Heat

2.5.1 Specific Heat Theory

The majority of the presentation of the specific heat theory is adapted from Miiller [53] and Kollie [54]. The heat capacity of a system of arbitrary mass is defined in terms of the limit:

$$c \equiv \lim_{\Delta T \to 0} \frac{\Delta Q}{\Delta T} \tag{2.56}$$

where ΔQ is the quantity of heat that must be added to the system to raise its temperature by an amount ΔT. Dividing by the mass, m, gives the specific heat of the system:

$$C = \frac{c}{m} = \frac{\delta q}{dT} \tag{2.57}$$

where δq is the quantity of heat required to raise the temperature of a unit mass of the system by an amount dT. δ is an infinitesimal amount and not an exact differential.

There are two principle specific heats that have been defined; C_P and C_V for specific heat at constant pressure and constant volume, respectively:

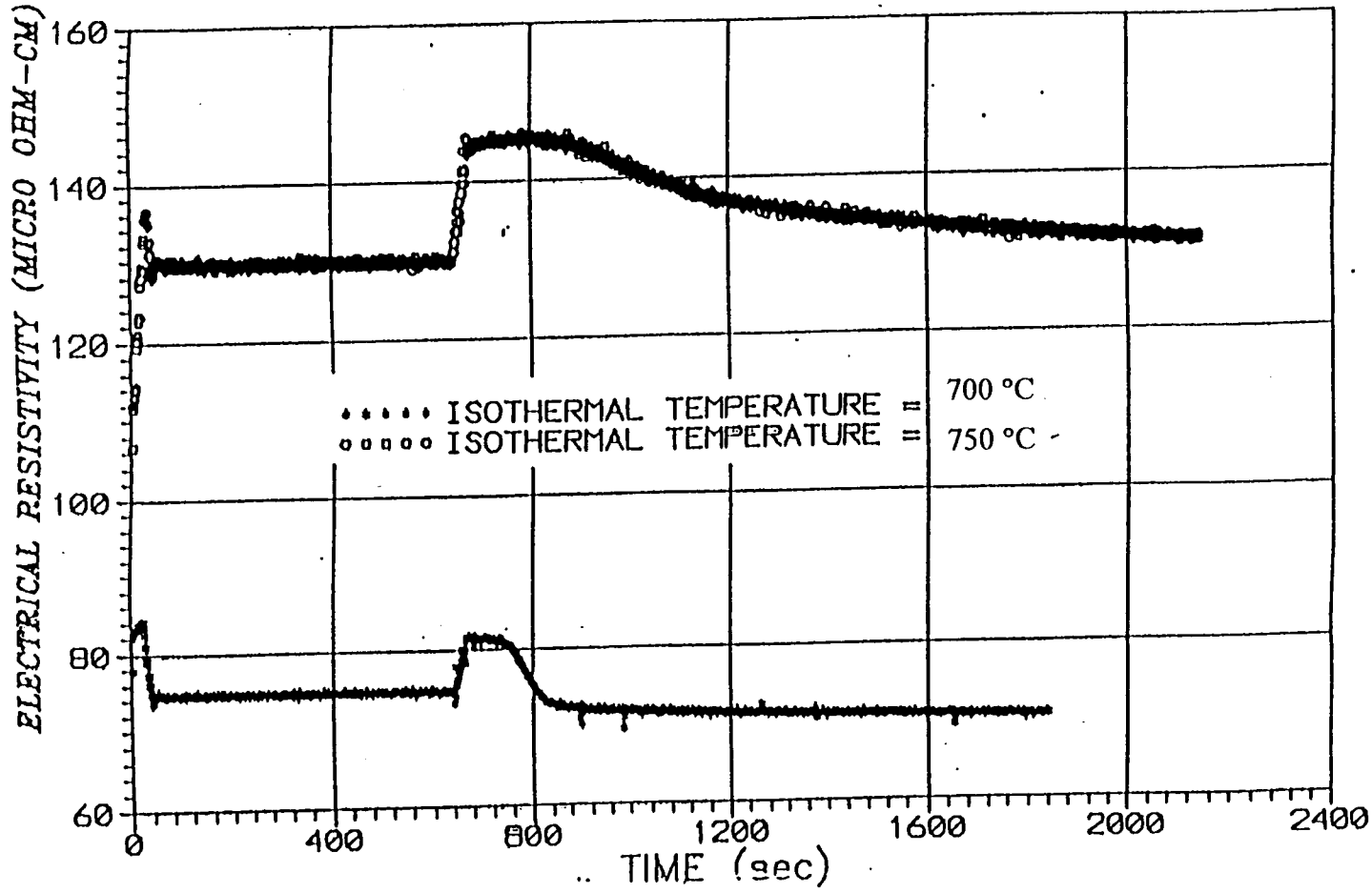

Figure 2.22 Isothermal electrical resistivity data for Ni_4Mo at 700 °C and 750 °C. These type of curves can be used to construct TTT diagrams by assuming locations on each curve where the point of the transition begins and ends. Data is from Basak [121]

$$C_P = \left(\frac{\delta q}{dT}\right)_P \text{ and } C_V = \left(\frac{\delta q}{dT}\right)_V \quad \textbf{(2.58)}$$

Under isobaric conditions, dH = TdS = δQ, therefore

$$C_P = \left(\frac{\partial H}{\partial T}\right)_P \quad \textbf{(2.59)}$$

C_P and C_V must both tend to zero at absolute zero, according to the Third Law of thermodynamics. Heating a substance through a temperature rise dT requires heat to increase the internal energy and also requires heat to do work in expanding against an internal pressure. Under constant volume conditions, no external work is done and less heat is required to obtain the same temperature rise. Thus, $C_P - C_V$ is often referred to as the dilation contribution, C_D. C_P is always larger than C_V.

C_P is usually measured since C_V is more difficult to obtain experimentally. One mathematical relationship between C_V and C_P is:

$$C_P = C_V + C_D \quad \textbf{(2.60)}$$

and thus C_D is defined as

$$C_D \equiv \frac{\beta^2 V_m T}{\kappa} \quad \textbf{(2.61)}$$

where V_m is the molar volume, β is the coefficient of volumetric thermal expansion, and κ is the isothermal compressibility. For isotropic solids, β is related to the coefficient of linear thermal expansion, α, as $\beta = 3\alpha$. β is defined as [41]

$$\beta \equiv \frac{1}{V}\left(\frac{\partial V}{\partial T}\right)_P \quad \textbf{(2.62)}$$

and κ is defined as

$$\kappa \equiv -\frac{1}{V}\left(\frac{\partial V}{\partial T}\right)_T \qquad \textbf{(2.63)}$$

Data are often available for α, but compressibility data are usually only available at or near room temperatures. The dilation contribution at other temperatures can be obtained [122] from the relation

$$\beta = G\frac{\kappa C_V}{V_m} \qquad \textbf{(2.64)}$$

where G is the Grüneisen parameter, assumed to be independent of temperature. Thus

$$C_D = GC_V\beta T \qquad \textbf{(2.65)}$$

Another method [123] to obtain the dilation contribution is to use the Nernst-Lindemann relation

$$C_D = A(C_P)^2 T \qquad \textbf{(2.66)}$$

where A is a constant. A is calculated from values of V_m, β, κ, and C_P at some reference temperature, and is then used to calculate C_P over a range of temperatures.

One way to estimate the specific heat is the Kopp-Neumann law [42]:

$$C_P = \sum_i f_i c_{Pi} \qquad \textbf{(2.67)}$$

where f_i is the mass fraction and c_{pi} is the specific heat of the ith constituent element.

The main contributions to C_V are mentioned by Kollie [124]. Each micro-mechanism leads to changes in the internal energies of a substance, and hence the specific heat.

C_{VV} = vibrational contribution

C_{VE} = electronic contribution

C_{VW} = re-arrangement contribution

C_{VN} = nuclear contribution

C_{VT}= translational motion contribution

C_{VR}= rotational motion contribution

C_{VI} = interaction contribution

The C_{VW} term includes contributions from configurational ordering effects and from vacancy formation effects. The C_{VE} term includes contributions from valence electrons and from alignment of spin in magnetic effects. It is negligible for almost all insulators, and is very small for most metals. C_{VE} can, however, be large for transition metals. The electronic contribution from the second-order ferromagnetic to paramagnetic transformation (Curie transition) can be very large. For example, at the Curie temperature for Fe, the magnetic portion can contribute 75% of the overall specific heat [124]. In practice, the magnetic portion of the electronic specific heat is considered as a separate contribution, C_{VM}. The vibrational term, C_{VV}, is usually separated into the harmonic portion, C_{VH} and the anharmonic portion, C_{VA}. Because the interaction contribution, C_{VI}, is very complex, it is often considered to be negligible for simplicity. Often other terms are modified to take into account the interactions between the different contributions.

Above about 10 K, the C_{VN} contribution becomes negligible. The theory of Schottky anomaly and nuclear contribution to specific heat is not discussed in this thesis, other than to mention that the general form of this nuclear contribution is proportional to T^{-2} . For solids, assuming that the atoms are relatively fixed is reasonable, and the translational and rotational motion is limited. Thus the C_{VT} and C_{VR} terms can be assumed negligible, and are also not discussed in this investigation. There are also some magnetic contributions mentioned by Miiller [42] that are not discussed in this research. These are

spin fluctuations, single-impurity effects, and spin-glass effects. Super-conducting electronic effects also have a different formalism than normal electronic effects, and are not discussed.

With the above assumptions, the specific heat at constant pressure can be approximately stated as

$$C_P = C_V + C_D = (C_{VH} + C_{VA}) + (C_{VE} + C_{VM}) + C_{VW} + C_D \quad \textbf{(2.68)}$$

The theory behind the individual terms of this equation are discussed in more detail below.

2.5.1.1 Historical Development of Specific Heat Theory

Early theories of specific heat were given by Dulong & Petit [125] and Kopp & Neumann [53]. Dulong and Petit showed that the heat capacity was about the same for all elements, about 3R, where R is the gas constant. Kopp & Neumann [42] showed that the heat capacity per gram molecular weight of a compound is approximately the sum of the atomic heats of the constituent elements. Thus diatomic and triatomic solids are expected to have specific heats of 6R and 9R, respectively [125].

Boltzmann [126] gave a theoretical explanation of the Dulong-Petit law based on the theory of equipartition of energy. An example of Boltzmann's theory is to look at a 3-dimensional oscillator. A simple model of the solid is to view the atoms oscillating about their lattice sites. This has 6 degrees of freedom, and the internal energy, U, is $3k_BT$, where k_B is Boltzmann's constant. One mole of a monotomic solid has a total energy of $3N_Ak_BT$, which is 3RT. Because $C_V = (dU/dT)_V$ Then C_V is found to be 3R, which is the Dulong-Petit value.

There were experimental exceptions to the Dulong-Petit law, which indicated that all substances approaches the 3R value if the temperature is high enough. At high temperatures, C_v approaches this value experimentally, but at low temperatures, C_v approached absolute zero very rapidly. Nernst [123] and others suggested that the specific heat of solids must go to zero at absolute zero temperature. Einstein [127] proposed that the solid should be composed of independent oscillators, where the energy was quantized. (This idea led Einstein to receive the Nobel prize.) The classical free electron gas model predicted an excessively large contribution to specific heat from the conduction electrons, and did not predict that C_v approached zero at 0 K. Hence, the classical theory failed to predict the specific heat of solids at low temperatures. This brought about further studies in lattice dynamics. Sommerfeld [128] was able to explain the relatively small magnitude of the electronic contribution. It is now generally accepted that only the electrons near the Fermi energy absorb heat and therefore contribute to the electronic specific heat [118].

Different theoretical models for the different modes of energy in a solid provide a means of estimating and separating their contributions to the observed specific heat.

2.5.1.2 Vibrational (Lattice) Contributions to Specific Heat

The early development of the vibrational contributions were based on the interactions of the lattice, and these vibrational contributions are often referred to as lattice contributions. The basis of almost all lattice dynamic theories is the harmonic approximation. At low temperatures, the vibrations of the atoms may be considered to be in harmonic motion, and therefore have potential energies proportional to the square of their displacements from the equilibrium positions. The description of the lattice specific heat on the basis of the harmonic approximation is thus expected to become more

accurate as the temperature decreases since the vibrational amplitudes will become smaller.

Einstein first developed a harmonic theory in 1907. He assumed that all atoms vibrate harmonically with the same characteristic frequency, ν_E, and he departed from classical theory and adopted Planck's rule that the energy of any one oscillator must take on quantized values [120]. The energy of a linear harmonic oscillator of frequency ν is:

$$\varepsilon_n = (n + \frac{1}{2})h\upsilon \tag{2.69}$$

where h is Planck's constant and n is an integer (0 to ∞). The solid is treated as a collection of independent uncoupled linear harmonic oscillators, each vibrating with the same frequency. The number of oscillators is selected to be the same as the number of degrees of freedom. Einstein demonstrated that the rapid reduction of specific heat with decreasing temperature was due to a quantization of the atomic vibrations. The collective properties of such oscillators can be determined by statistical methods. The average energy is

$$\langle \varepsilon \rangle = \left(\langle n \rangle + \frac{1}{2} \right) h\nu, \tag{2.70}$$

where

$$\langle n \rangle = \frac{1}{\exp(\frac{h\nu}{k_B T}) - 1} \tag{2.71}$$

<n> is the average quantum number, and k_B is Boltzmann's constant. At high temperature, n varies as $k_B T/h\nu$, and the average oscillator energy approaches the classical value $k_B T$. At very low temperatures, <n> approaches zero, and <ε> approaches

(1/2)hν, which is the energy of the oscillator at 0 K. For one mole of atoms, there are 3 moles of oscillators, and the internal energy is:

$$U = 3N_A\varepsilon = 3N_A(\langle n\rangle + \frac{1}{2})h\nu_E \tag{2.72}$$

where ν_E is a common frequency. Thus

$$C_V = \left(\frac{dU}{dT}\right)_V = \frac{3N_A k_B\left(\frac{\Theta_E}{T}\right)^2 \exp\left(\frac{\Theta_E}{T}\right)}{[\exp\left(\frac{\Theta_E}{T}\right) - 1]^2} \tag{2.73}$$

where θ_E ,the characteristic Einstein temperature, is (h ν/ k_B), and R =$N_A k_B$. θ_E is a scaling factor. At very high temperatures, C_V approaches the 3R value. At moderately high temperatures,

$$C_V \cong 3R\left[1 - \frac{1}{12}\left(\frac{\Theta_E}{T}\right)^2 + \cdots + \right] \tag{2.74}$$

At temperatures much less than θ_E,

$$C_V = 3R\left(\frac{\Theta_E}{T}\right)^2 \exp\left(\frac{-\Theta_E}{T}\right) \tag{2.75}$$

so C_V of a solid approaches zero as the temperature approaches absolute zero. Data showed that the Einstein model gave a specific heat decreasing to zero more rapidly than measured experimentally. Two assumptions that the model made were the non-coupled atoms and the same frequency of oscillation for all of the atoms.

Nernst and Lindemann modified Einsteins's theory at low temperatures to include two equally distributed frequencies: $\nu_E/\sqrt{2}$ and ν_E.

The Debye model was more rigorous. The model assumed that the solid can be treated as if it were an elastic continuum for all possible vibrational modes, from 0 to the cut-off frequency, ν_D. He chose a parabolic spectrum for the isotropic elastic continuum. The number of normal modes $g(\nu)d\nu$ whose frequencies range from ν to $d\nu$ is

$$g(\nu)d\nu = BV\nu^2 d\nu \tag{2.76}$$

where B is a function of the longitudinal and transverse wave velocities in the continuum. Debye assumed that at the characteristic frequency ν_D, the modes of $g(\nu)$ fell rapidly to zero. With 3 degrees of freedom maximum per atom, there are $3N_A$ modes of vibration per mole of solid. Integration over the allowed modes led to:

$$3N_A = \int_0^{\nu_D} g(\nu)d\nu = \int_0^{\nu_D} BV\nu^2 d\nu = \frac{BV}{3}(\nu_D)^3 \tag{2.77}$$

Debye then found that

$$g(\nu) = \frac{9N_A\nu^2}{(\nu_D)^3}d\nu \tag{2.78}$$

He then used Einstein's assumption of the quantization to get the energy per mole, and then the harmonic specific heat:

$$C_{VH} = 9R\left(\frac{T}{\Theta_D}\right)^3 \int_0^{\frac{\Theta_D}{T}} \frac{(x)^4 \exp(x)}{[\exp(x)-1]^2}dx\,;\; x = \frac{h\nu}{k_B T} \tag{2.79}$$

where θ_D ,the Debye characteristic temperature, is $h\nu_D/k_B$. This is defined in terms of a cut-off frequency. The Debye function is usually represented as $(3T/\theta_D)$ and is tabulated [129].

At high temperatures, a power series expansion of the harmonic contribution is

$$C_{VH} = 3R\left(1 - \frac{x_D^2}{20} + \frac{x_D^4}{560} - \frac{x_D^6}{18144} + \cdots\right) \tag{2.80}$$

C_{VH} for the Debye model eventually approaches the 3R value. At very low temperatures, the expression reduces to being proportional to T^3

$$C_{VH} = \frac{12}{5}\pi^4 R\left(\frac{T}{\Theta_D}\right)^3 \tag{2.81}$$

which is in good experimental agreement with values obtained below about one tenth of θ_D. Above about $\theta_D/50$, an expansion method works best. The Debye theory continues to be used extensively in the thermal description of solids, particularly at low temperatures. It does not accurately predict the specific heat over the entire temperature range. This may be attributed to the fact that real solids are composed of discrete atoms.

Modern lattice dynamics is based on a 3-dimensional model of a solid, which was presented by Born and Von Kármán [130] in 1912. They assumed the harmonic approximation and also that the atoms in the lattice wee bound together by elastic forces. They assumed the thermodynamic functions are additive functions of the normal mode frequencies, and they assumed the adiabatic approximation. Without showing any intermediate developments, their results showed that the harmonic contribution to the specific heat of a crystal is

$$C_V = k_B \int_0^{\nu_m} \frac{\left(\frac{h\nu}{k_B T}\right)^2 \exp\left(\frac{h\nu}{k_B T}\right)}{\left[\exp\left(\frac{h\nu}{k_B T}\right) - 1\right]^2} g(\nu) d\nu \tag{2.82}$$

where ν_m is the maximum frequency. C_V can be calculated once $g(\nu)$, the frequency distribution function, is determined. The Born & Von Kármán model is very difficult to

work with but can be used to compute a realistic vibrational spectrum from neutron scattering data.

As the temperature increases, anharmonic oscillations are introduced whose potentials energies are proportional to the third and fourth power of their displacements. The effect of the potential energy on the specific heat is controversial. Different theories agreeably predict that the C_{VA} term is directly proportional to temperature, but disagreeably predict whether the effect is positive or negative [42].

A common approach to studying anharmonic effects is to separate the thermodynamic properties into quasi-harmonic and explicitly harmonic contributions. This method leads to a functional relationship:

$$C_{VA} = -T\frac{\partial^2}{\partial T^2}[F_3 + F_4] = 3RAT \tag{2.83}$$

where F_3 and F_4 are the cubic and quartic terms of the Hemholtz energy, respectively. The A term is a volume-dependent coefficient whose value is determined by the particular force model selected for the anharmonic calculations. C_{VA} is sensitive to the form of the inter-atomic potential because of the large degree of cancellation that often occurs between F_3 and F_4, which have opposite signs.

Another method takes into account the total vibrational (harmonic plus anharmonic) lattice entropy or lattice specific heat, which can sometimes be derived from neutron spectroscopic data. The functional form provided here is derived from the lattice specific heat at constant pressure. This is specific heat result is

$$C_L^P = T\left(\frac{\partial S}{\partial T}\right)_P = k_B \sum_S \csc h^2 x_s \left(1 - \frac{T}{v_s}\frac{dS}{dT}\right) \tag{2.84}$$

where S is

$$S = -\left(\frac{\partial F}{\partial T}\right)_V = k_B \sum_S x_S \coth x_S - \ln\left[2\sinh x_S\right] \; ; \; x_S = \frac{h\nu_S}{k_B T} \qquad \textbf{(2.85)}$$

2.5.1.3 Electronic Contribution to Specific Heat

The C_{VE} of a solid is due to the change in energy distribution of the electrons with temperature. The total energy per unit volume of electrons is

$$U = 2\int_0^\infty N(E)F(E)EdE = 2\int_0^\infty \frac{N(E)EdE}{\left(\exp\left(\frac{E-\zeta}{k_B T}\right)+1\right)} \qquad \textbf{(2.86)}$$

where N(E) is the electronic density of states having energies between E and E+dE. ζ is the thermodynamic potential per electron, and is a function of temperature. The determination of N(E) is the most difficult task of evaluating C_{VE}. In analogy to determining g(ν), various approximations for N(E) have been made to make the energy equation more easily solvable. The most common approximation is the parabolic approximation, which leads to

$$C_{VE} = \left(\frac{\pi^2 n k_B}{2T_F}\right)T\left(1 - \frac{3\pi^2}{10}\left(\frac{T}{T_F}\right)^2\right) = \gamma T\left(1 - \frac{3\pi^2}{10}\left(\frac{T}{T_F}\right)^2\right) \qquad \textbf{(2.87)}$$

which describes well C_{VE} for some metals such as the alkali metals, and is valid at low temperatures or above the Curie temperature. n is the effective number of electrons or holes, and T_F is the Fermi temperature, E_F/K_B.

Only electrons near ζ contribute to C_{VE}. This is important in understanding the high C_{VE} of transition metals. For transition metals, the density-of-states of the d-band

electrons is much larger than that of the s-bands or of those of the free electrons. The result is that a large number of electrons are excited when the temperature of a transition metal is raised and results in an abnormally high C_{VE} contribution.

Fermi-Dirac statistics play a fundamental role in determining the temperature dependence of the electronic specific heat. The electronic specific heat is proportional to the electronic density of states, which in turn may be determined from a given model of electronic structure. The variation of the Fermi-Dirac distribution explains the relatively small contribution of the conduction electron gas to the specific heat of metals at ordinary temperatures. If the fraction of electrons which gain about k_BT is of the order of T/T_F, where T_F is the Fermi temperature, then the increase in internal energy per mole is approximately given by $N_A(T/T_F)\, k_BT$. Hence the electronic specific heat is approximately

$$C_V = \frac{2RT}{T_F} \qquad \textbf{(2.88)}$$

In metals, T_F is of the order of 10^4 to 10^5 K, which indicates that at room temperature, C_{VE} is only about 1% of the lattice contribution to the specific heat. The variation of C_{VE} with temperature can be seen to be linear. At low temperatures with a few reasonable assumptions,

$$C_V = \frac{\pi^2}{3} n(\varepsilon_F) k_B T \equiv \gamma T \qquad \textbf{(2.89)}$$

This electronic contribution is the temperature multiplied by a constant. The exact form of C_{VE} with temperature depends on the functional dependence of $N(\varepsilon)$ on ε over the

entire energy range, and calculations need to be done numerically by means of the above equation.

The Fermi surface energy of a sphere is given by:

$$\varepsilon_F = \frac{\hbar^2}{2m_e}\left(\frac{3\pi^2 N}{V}\right)^{\frac{2}{3}} \tag{2.90}$$

where V is the volume of the cell, $\hbar$ is Planck's constant divided by 2π, and N is the number of electrons in the system. The Fermi energy depends only on the electron density. For a metal, this is of the order of about 10^{23} electrons per cm^3, which corresponds to a Fermi energy of about 7.9 eV and T_F of about $9x10^4$ K.

$$N(\varepsilon_F) = \frac{m}{\pi\hbar}\left(\frac{3zN_A V_m^{\,2}}{\pi}\right)^{\frac{1}{3}} \tag{2.91}$$

where z is the conduction electron-to-atom ratio, N/N_A, and V_m is the molar volume. Therefore,

$$C_V = \gamma_0 T\left(1 - \frac{3\pi^2}{10}\left(\frac{T}{T_F}\right)^2\right) \tag{2.92}$$

where

$$\gamma_0 = \frac{m}{\hbar^2}(zN_A)^{\frac{1}{3}}\left(\frac{\pi V_m}{3}\right)^{\frac{2}{3}} k_B^{\,2} \tag{2.93}$$

2.5.1.4 Magnetic Contribution to Specific Heat

Even though the Ni_4Mo alloy in this research does not undergo significant magnetic transitions in the temperature range of the investigation, magnetic formalism is discussed here. This is due to the similarity between the specific heat effect of second

order magnetic transitions and effects on specific heat due to configurational order-disorder transformations.

Heisenberg [131] was able to show that the ordered magnetic state was the result of a quantum-mechanical exchange interaction between neighboring electron spins. Except for simple antiferromagnets, all other spin arrangements have a spontaneous magnetization even in the absence of a magnetic field. This ordered arrangement begins to break down at higher temperatures due to the increased thermal agitation, and at some critical temperature, the spins become completely disordered. For ferromagnetics and ferrimagnetics, the critical temperature is called the Curie temperature, and for antiferromagnets, this critical temperature is called the Neel temperature.

Complete order among atomic spins exists only at absolute zero. At low temperatures, the oscillations in the orientations of the spins may be regarded as a superposition of spin waves. The Heisenberg model treats magnetism as coming entirely from unpaired electron spins localized at the atomic lattice sites. The usual approach to assume spin-wave theory is to approximate the magnetic spin system by a system of linear harmonic oscillators. As a result, the spin-waves are quantized in energy units of $\hbar\omega$ known as magnons, and are characterized by a frequency-wave vector dispersion relation $\omega(q)$. The average energy of an oscillator with frequency ν_q is $\langle n\rangle\nu_q$, where $\langle n\rangle$ is the

Bose-Einstein population factor. The total energy of the system is then

$$U = \sum_q \frac{\hbar\omega_q}{\exp\left(\frac{\hbar\omega_q}{k_B T}\right) - 1} \qquad \textbf{(2.94)}$$

If the sum extends over all allowed modes q (the first Brillouin zone), then the number of modes with wave vectors between q and q + dq is

$$n(q)dq = \left(\frac{dN}{dq}\right)dq = \frac{V}{2\pi^2}q^2 dq \tag{2.95}$$

where V is a representative volume of the solid. The continuous sum is then

$$U = \frac{V}{2\pi^2}\int_0 \frac{\hbar\omega_q q^2 dq}{\exp\left(\frac{\hbar\omega_q}{k_B T}\right)-1} \tag{2.96}$$

The energy of the spin system in a ferromagnet may be expressed as

$$U = \frac{V}{2\pi^2} b^{-3/2}(k_B T)^{5/2}\int_0^\infty \frac{x^4}{\exp(x^2)-1} \tag{2.97}$$

where

$$x^2 = \frac{q^2 b}{k_B T}; b = 2\alpha_f JSa^2 \qquad x^2 = \frac{q^2 b}{k_B T}; b = 2\alpha_F JSa^2 \tag{2.98}$$

The magnetic specific heat is determined to be

$$C_m = c_f N_A k_B \left(\frac{k_B T}{2JS}\right)^{\frac{3}{2}} \tag{2.99}$$

where c_f is a geometrical shape factor, which depends on the type of lattice, J is the isotopic exchange integral, related to the overlap of the charge distribution of atoms, and S is the spin. At low temperatures, the ferrimagnetic specific heat is also proportional to $T^{3/2}$.

In ferrimagnets and non-metallic ferromagnets, the observed specific heat consists of contributions only from the lattice vibrations and the spin waves. At very low temperatures $C_V = C_P$ and

$$C_p = \delta T^{\frac{3}{2}} + \beta T^3 \tag{2.100}$$

In a metallic ferromagnet, there is an additional contribution of the conduction electrons to the specific heat:

$$C_p = \gamma T + \beta T^3 + \delta^{\frac{3}{2}} \tag{2.101}$$

The electronic term dominates the temperature variation of C_p and makes it difficult to resolve the spin-wave term.

In antiferromagnets, in the absence of anisotropy effects, the spin system energy is given by Miiller [42] as:

$$U = 2\frac{V}{2\pi^2} b^{-3} (k_B T)^4 \int_0^{\infty} \frac{x^3}{\exp(x\ ) - 1} \tag{2.102}$$

where

$$x = \frac{qb}{k_B T}; b = 2\alpha_a J' S a^2 \qquad U = \frac{V}{2\pi^2} b^{-3} (k_B T)^4 \int_0^{\infty} \frac{x^3 dx}{\exp(x\ ) - 1} \qquad x = \frac{q\ b}{k_B T}; b = 2\alpha_a J' S a^2 \tag{2.103}$$

Evaluation of the integral gives the magnetic contribution as

$$C_{VM} = c_a N_A k_B \left(\frac{k_B T}{2J'S}\right)^3 \tag{2.104}$$

The geometrical constant, c_a, can be found for several crystal structures. Because the C_{VM} in this case is proportional to T^3, it is impossible to separate this contribution from the low temperature lattice term in of metallic antiferromagnets [42].

2.5.1.5 Contribution Due to Configurational Ordering

At high enough temperatures, the ordered ferromagnetic, ferrimagnetic, and antiferrimagnetic states are transformed into the disordered paramagnetic state by the randomizing effects of thermal agitation on spin alignment. In the critical temperature region, the order to disorder transition is accompanied by rapid changes in specific heat. The specific heat approaches infinity as the temperature approaches the critical temperature from above and below. This is referred to as a λ-type singularity, which is a characteristic of second-order phase transitions, and is also typical in order-disorder changes in binary alloys, such as Ni_4Mo.

A number of approximate methods have been developed by Weiss [132] and Bragg & Williams [50] to study the magnetic transitions and other order-disorder problems, but are too lengthy to be discussed here. There are also statistical methods, namely the Heisenberg model and the Ising model, to study critical behavior. The statistical approach to the study of critical behavior involves the evaluation of the partition function of the system, which requires knowledge of either the total energy or the Hamiltonian.

Recent interest [133-136] in model systems has related to describing various thermodynamic quantities near the critical point. One important quantity for order-disorder alloys is the order parameter, discussed in section 2.3. The specific heat variation near Tc then exhibits an inverse power-law singularity of the form:

$$C_M \approx A\left(T - T_c\right)^{-\alpha}; T > T_c \qquad \textbf{(2.105)}$$

$$C_M \approx A'\left(T_c - T\right)^{-\alpha'}; T < T_c \qquad \textbf{(2.106)}$$

where α and α' are the critical exponents. A number of relationships have been developed to reduce the number of independent exponents to only two fundamental unknowns [42].

As Kollie [124] mentions, the configurational order-disorder transformations in binary alloys occur by diffusion and hence are dependent on the vacancy concentration and on the atomic mobility within the alloy. These both vary exponentially with temperature, and the kinetics of order-disorder transformations are strongly temperature dependent. Under assumed equilibrium conditions,

$$C_{VW} = \frac{d}{dT}\left(U_{od}(T)N(T)\right) = N(T)\frac{dU_{od}(T)}{dT} + U_{od}(T)\frac{dN(T)}{dT} \qquad \textbf{(2.107)}$$

where $U_{od}(T)$ is the energy of formation of one mole of ordered alloy at constant volume at temperature, T , and N(T) is the equilibrium mole fraction of ordered atoms at T. If $U_{od}(T)$ is assumed independent of T, then

$$C_{VW} = U_{od}\frac{dN(T)}{dT} \qquad \textbf{(2.108)}$$

Values of U_{od} and N(T) can be determined by, for example, the Bragg-Williams approximation. Due to the slow kinetics of order-disorder transformations at low temperatures, and due to the finite heating rates of most experimental methods, C_{VW} obtained from experiments is not an equilibrium value. The total energy, U_{od}, is calculated from experimental results. From the above relationship and assumptions, one finds [124]

$$Uod = \frac{1}{\left(\int_{T_i}^{T_f} C_{VW}\,dT\right)\left(N(T_f) - N(T_i)\right)} \qquad \textbf{(2.109)}$$

where T_f is the experimental temperature above which C_{VW} vanishes, and T_i is the

experimental temperature starting temperature. If perfect order exists at T_i, then N (at T_i) must be unity. If the value of N evaluated at T_f is assumed to be zero, then

$$U_{od} = -\left(\int_{Ti}^{Tf} C_{VW} dT \right) \tag{2.110}$$

As mentioned previously, the vacancy contributions are also included in the C_{VW} term of the specific heat. Vacancies cause a rapid rise in the specific heat prior to melting in numerous solids, and are particularly prominent in refractory metals. This is attributed to higher order anharmonic contributions and/or contributions from the lattice vacancies which are present in solids at the melting temperature. The increase in the energy arising from the formation of defects is

$$U_{vac} = n_v N_A Q_F \tag{2.111}$$

where n_v is

$$n_v = \exp\left(\frac{-S_F}{T}\right)\exp\left(\frac{-Q_F}{k_B T}\right) \qquad n_v = \exp\left(\frac{S_F}{k_B T}\right)\exp\left(\frac{-Q_F}{k_B T}\right) \tag{2.112}$$

S_F is the entropy of vacancy formation, and Q_F is the energy of vacancy formation. Thus

$$C_{vac} = \frac{dU_{vac}}{dT} = R\left(\frac{-Q_F}{k_B T}\right)^2 n_v \tag{2.113}$$

It is often difficult to distinguish vacancy contributions from anharmonic contributions.

Theoretical expressions for the different specific heat terms are summarized by Miiller [42] for low, moderate, and high temperatures. These are only approximations based on assumed models. The results for various conditions are shown in Table 2.2. A graphical depiction of the various contributions is shown in Figure 2.23 for nickel [124].

2.5.2 Specific Heat Behavior of Ni_4Mo

Table 2.2 Functional forms of the various contributions to specific heat. Adapted from Miiller [42].

Contribution	Temperature Range in Terms of the Debye Temperature ($\Theta_D = h\nu/k_B$)		
	$T < \Theta_D/50$	$\Theta_D/50 < T < \Theta_D$	$T > \Theta_D$
Dilation	$C_D = \frac{\beta^2 V_m T}{\kappa}$		
Harmonic Vibration	$C_{VH} = \frac{12}{5}\pi^4 R\left(\frac{T}{\Theta_D}\right)^3$	$C_{VH} = 9R\left(\frac{T}{\Theta_D}\right)^3 \int_0^{\frac{\Theta_D}{T}} \frac{(x)^4 \exp(x)}{(\exp(x)-1)^2} dx$	$C_{VH} = 3R\left(1 - \frac{xD^2}{20} + \frac{xD^4}{560} - \frac{xD^6}{18144} + \ldots\right)$
Anharmonic Vibration			$C_{VA} = -T\frac{\partial^2}{\partial T^2}(F_3 - F_4) = 3RT$
Electronic	$C_V = \frac{\pi^2}{3} n\varepsilon_F k_B T \equiv \gamma T$		$C_V = \gamma_0 T\left(1 - \frac{3\pi^2}{10}\left(\frac{T}{T_F}\right)^2\right)$
Ferromagnetic and Ferrimagnetic Spin Waves	$C_m = c_f N_A k_B \left(\frac{k_B T}{2JS}\right)^{3/2}$		
Anti-ferromagnetic Spin Waves	$C_{VM} = c_a N_A k_B \left(\frac{k_B T}{2J'S}\right)^3$		
Second Order Transition/Critical Region	$C_M \approx A(T - Tc)^{-\alpha}; T > Tc$		$C_M \approx A'(T - Tc)^{\alpha}; T < Tc$
Lattice Monovacancy			$C_{VAC} = \frac{dU_{VAC}}{dT} = R\left(\frac{Q_F}{k_B T}\right)^2 n_{VAC}$
Nuclear Schottky	$C_{VN} = DT^{-2}$		

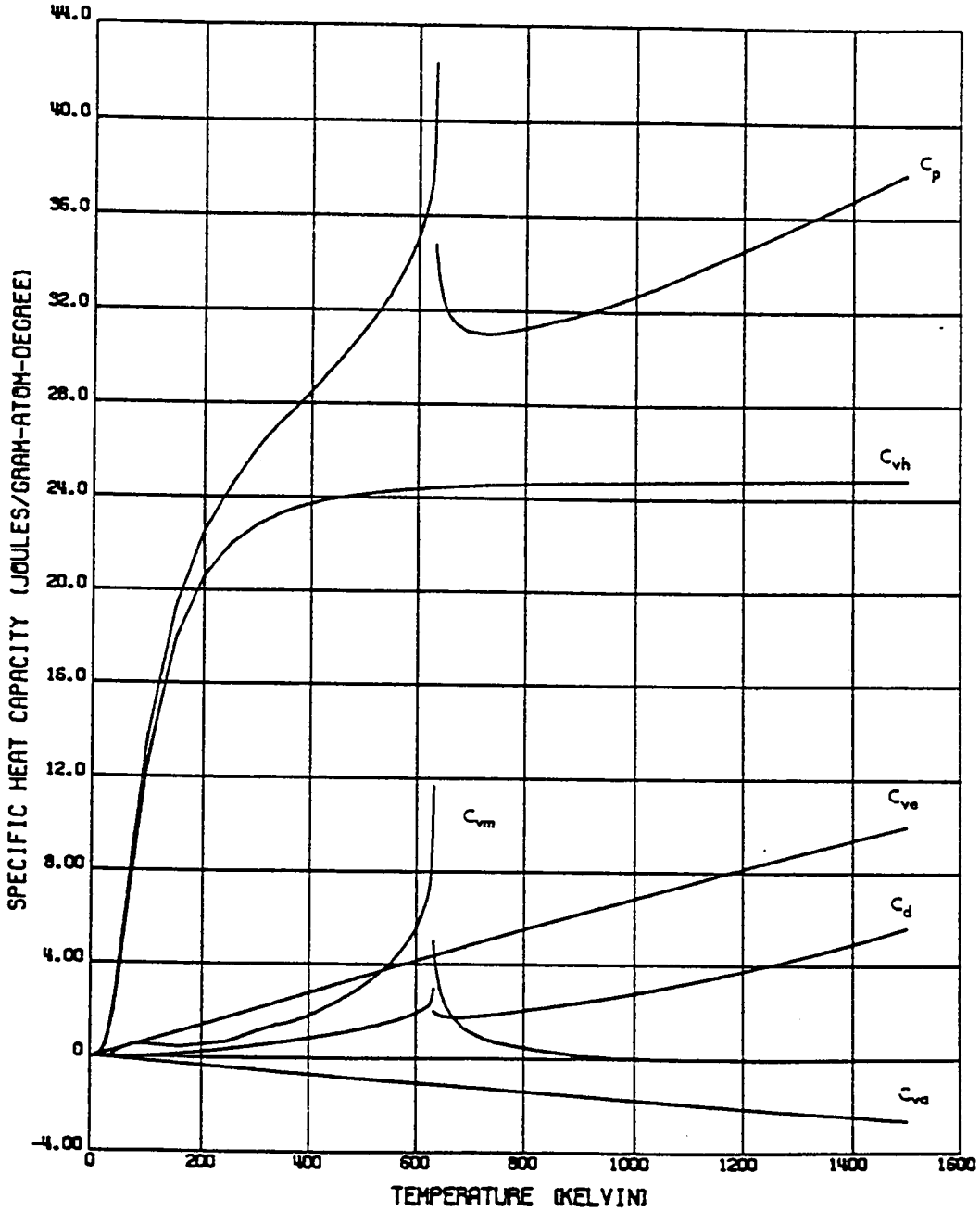

Figure 2.23 Various contributions to the specific heat of pure nickel. C_{vh} is the harmonic contribution, C_{va} is the anharmonic contribution, C_{ve} is the electronic contribution, C_{vm} is the magnetic contribution, and C_d is the dilation term. C_p is the overall experimental curve, being the superposition of the other curves. Data from Kollie [124].

The specific heat of Ni_4Mo was determined by Norem [137] using an adiabatic calorimeter for initial conditions of slowly cooled Ni_4Mo (all β) and quenched (SRO α). These results are shown in Figure 2.24. The dashed line is data for the α initial condition, and the solid line is data for the all β initial condition. The heating rate used to obtain the data was about 10 K per minute. The β sample shows Cp to be fairly constant until the transformation temperature is approached. Then there is a sharp increase associated with the decrease of LRO as the critical temperature is approached. This peak corresponds to an enthalpy change of about 2900 J/mol [137]. The metastable α initial condition (quenched) indicates two heat effects, as shown by the two dips in the dashed curve. Brooks et al. [13] suggest that the first minimum is due to the formation of additional SRO and initial LRO ordering. The second minimum at about 740 °C is attributed to the intensification of LRO. These mechanisms both release energy. As T_C is approached, LRO decreases and specific heat increases sharply. Above T_C there is a sharp decrease and then a gradual increase of specific heat with temperature where the sample is now in the equilibrium α state. The specific heat of α increases gradually with temperature in the temperature range shown.

Basak [121] determined the specific heat of Ni_4Mo using the pulse-heating calorimeter for similar initial conditions as Norem. The heating rate Basak used was between 50 to 75 °C per second as compared to Norem's data, which were obtained at about 10 °C per minute. These data are shown in Figure 2.25. For the LRO (β) initial condition, the curve gradually increases to the critical temperature. It then rises very sharply, which is due to the transition. Above T_C , the curve decreases sharply and then rises again. For the initial SRO (α) condition the curve is similar to the β curve up to

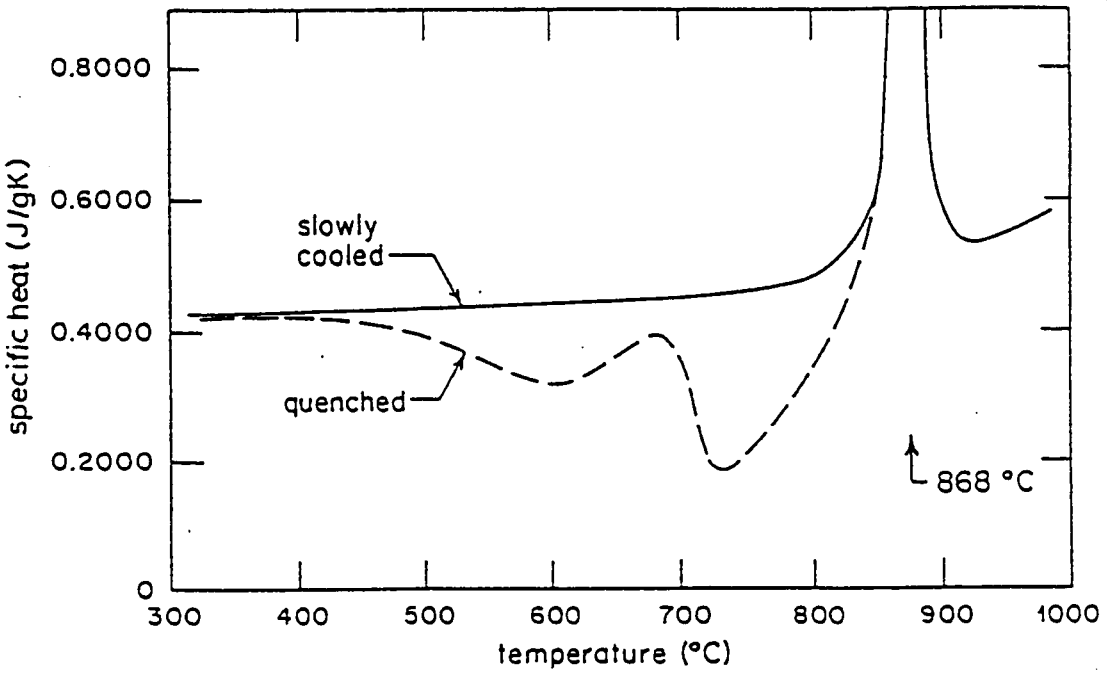

Figure 2.24 Specific heat versus temperature for Ni_4Mo from an adiabatic calorimeter. The solid line represents data from LRO β initial condition. The dashed line represents data from the SRO α initial condition. The heating rate used to obtain the data was about 10 °C per minute. From Norem [137].

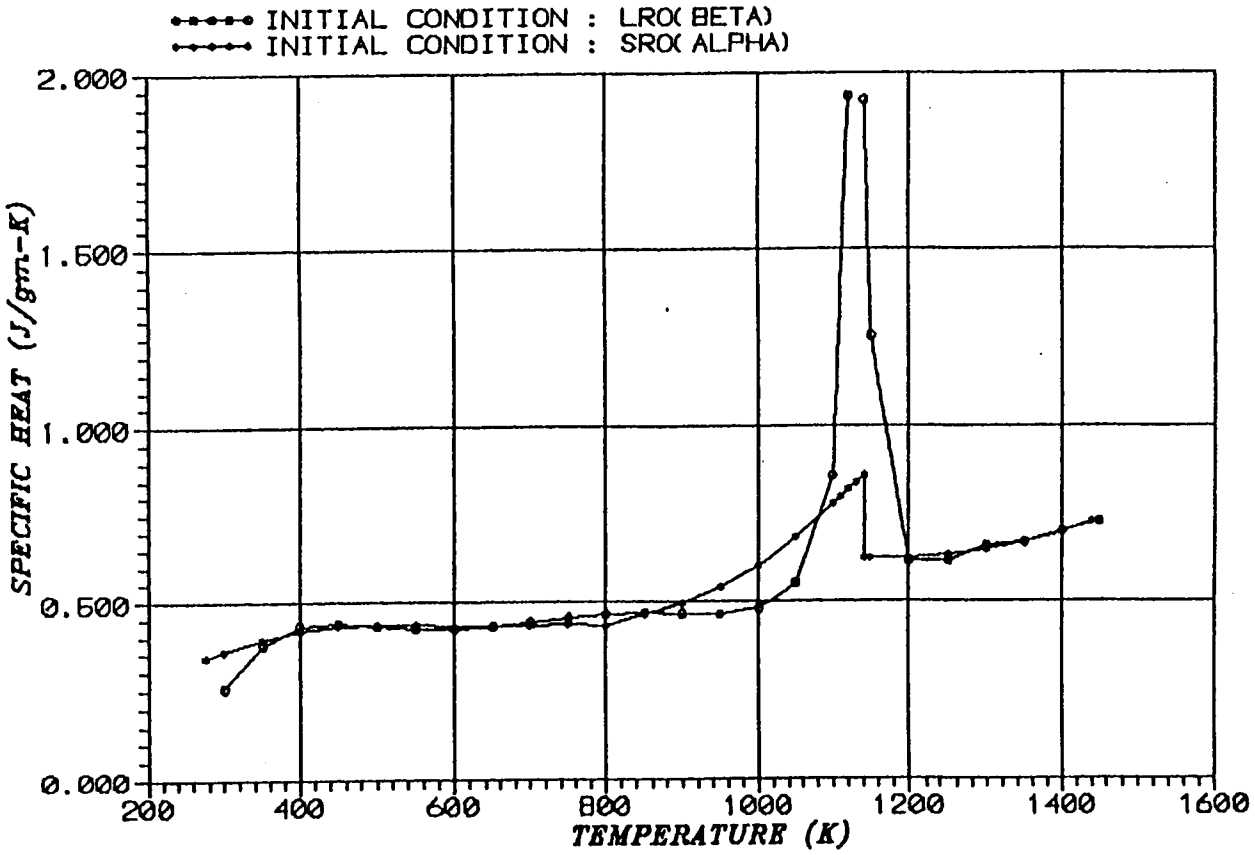

Figure 2.25 Specific heat versus temperature for Ni_4Mo from a pulse-heating calorimeter. The heating rate used in obtaining this data was about 60 K per second. From Basak [121].

about 850 K, then becomes steeper. C_p does not rise to as a high a value as it does for the β initial condition at T_C. The α and β curves merge above T_C (both are then SRO α).

Basak's data and Norem's data for specific heat of the LRO initial conditions compare very similarly. However, Basak's data for the SRO initial condition does not show the two dips in the curve due to heat energy release that are in Norem's slow-heating data (Figure 2.24). It is concluded that the heating rate for Basak's data was too high to provide the sample enough time to undergo the transformations depicted in Norem's data.

CHAPTER 3. Experimental Procedures

3.1 General Description of The Pulse-Heating Calorimeter

The equipment that was be used to obtain the specific heat and electrical resistivity data was a pulse-heating calorimeter. This type of calorimeter has advantages compared to conventional methods of speed, accuracy, extended higher temperature limit of measurement, and the ability to obtain data on metastable states [138].

In pulse-heating calorimetry, a high fixed current is passed through the specimen for a short period of time. The shape of the current-time curve is a square wave, as shown in Figure 3.1. The shape of the voltage, power and temperature as functions of time are also shown scematically in Figures 3.1b, 3.1c, and 3.1d, respectively. The specimen temperature rises due to resistive self-heating (Joule heating). The specimen is heated while the surroundings remaining at or near the ambient temperature. Rapid heating minimizes the heat losses during heating [121]. Because the specimen is in a vacuum, the two main heat losses pertinent to this situation are radiation heat loss from the specimen to the surroundings, and conduction heat loss through ends of the specimen and along the voltage taps and thermocouples. The conduction contribution becomes dominant at low temperatures. The temperature, current, and voltage drop across a section of the specimen are measured and recorded during the heating of the specimen. The power is then shut off and the temperature is recorded for the cooling of the specimen to use in correcting for heat losses.

The calorimeter used for this research was designed by Basak [139]. The system is controlled by a personal computer, which is capable of taking 20 data points per second.

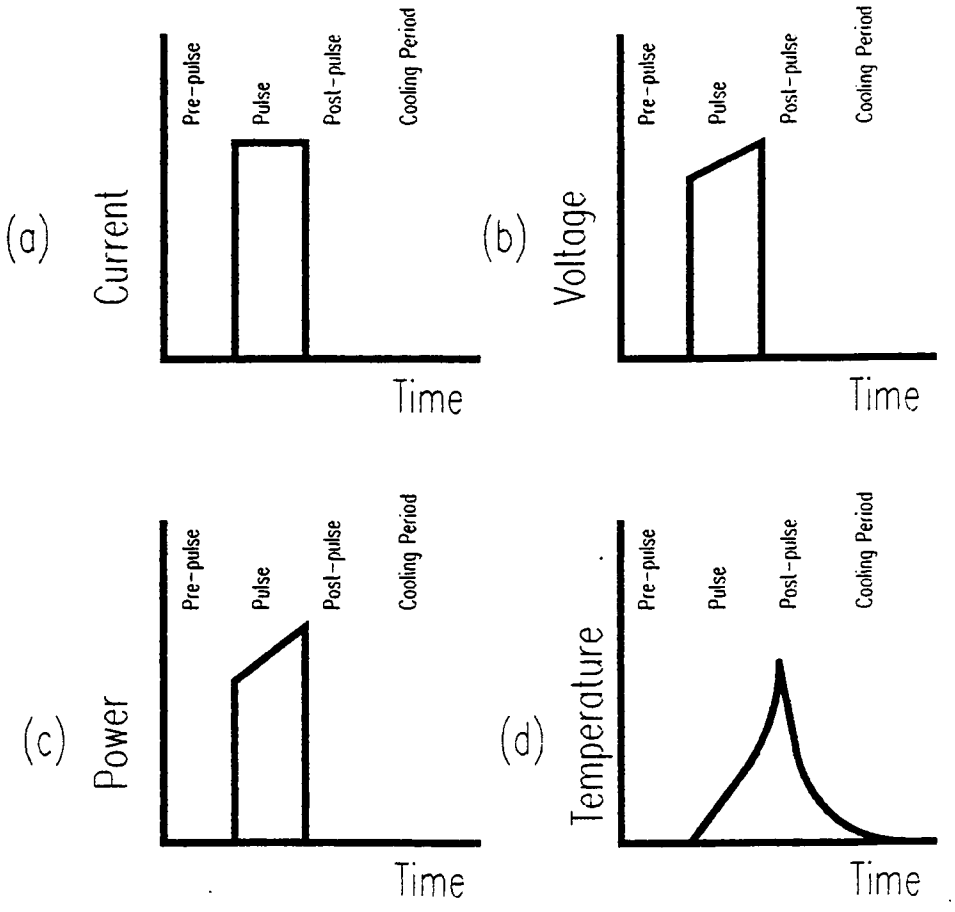

Figure 3.1 Schematic diagram showing how current, voltage, power, and temperature vary with time during the pulse. Adapted from Basak [121].

Figure 3.2 [121] shows a schematic of the calorimeter/computer arrangement. The specimen is in series with a standard resistor. The power is provided by a programmable DC power supply. The voltage drop across the standard resistor is measured to obtain the actual current, I, through the specimen. The voltage drop, E, across the specimen effective length, L, is determined by measuring the voltage drop across two leads, which are welded onto the specimen. The temperature is measured with a thermocouple welded to the specimen.

Figure 3.3 [121] shows a diagram of the specimen holder and vacuum chamber of the pulse-heating calorimeter. The thermocouple wires and voltage tap wires are welded directly to the specimen using a precision spot-welder. The thermocouple wires are centered between the voltage taps. This calorimeter arrangement uses R-type thermocouples, which use Pt and Pt-13%Rh wires. Thermal e.m.f. data are converted to temperature using conversion equations [140]. The voltage taps are made of nickel wire.

The vacuum system (Figure 3.4 [139]) is used to prevent reaction with atmospheric gases, prevent gas conduction and convection heat losses, and prevent disturbances due to air currents. The primary heat loss at lower temperatures is due to conduction through the ends of the specimen where it is clamped. At higher temperatures, radiation heat loss may become more prevalent. The vacuum chamber is a nickel tube about 100 cm in length and about 10 cm in diameter. The chamber is cooled by water coils surrounding it. A mechanical pump is used in conjunction with a diffusion pump. An ion gauge and thermocouple gauge are used to monitor the vacuum at low and medium pressures, respectively. The pressure at full pump-down is around 10^{-6} torr.

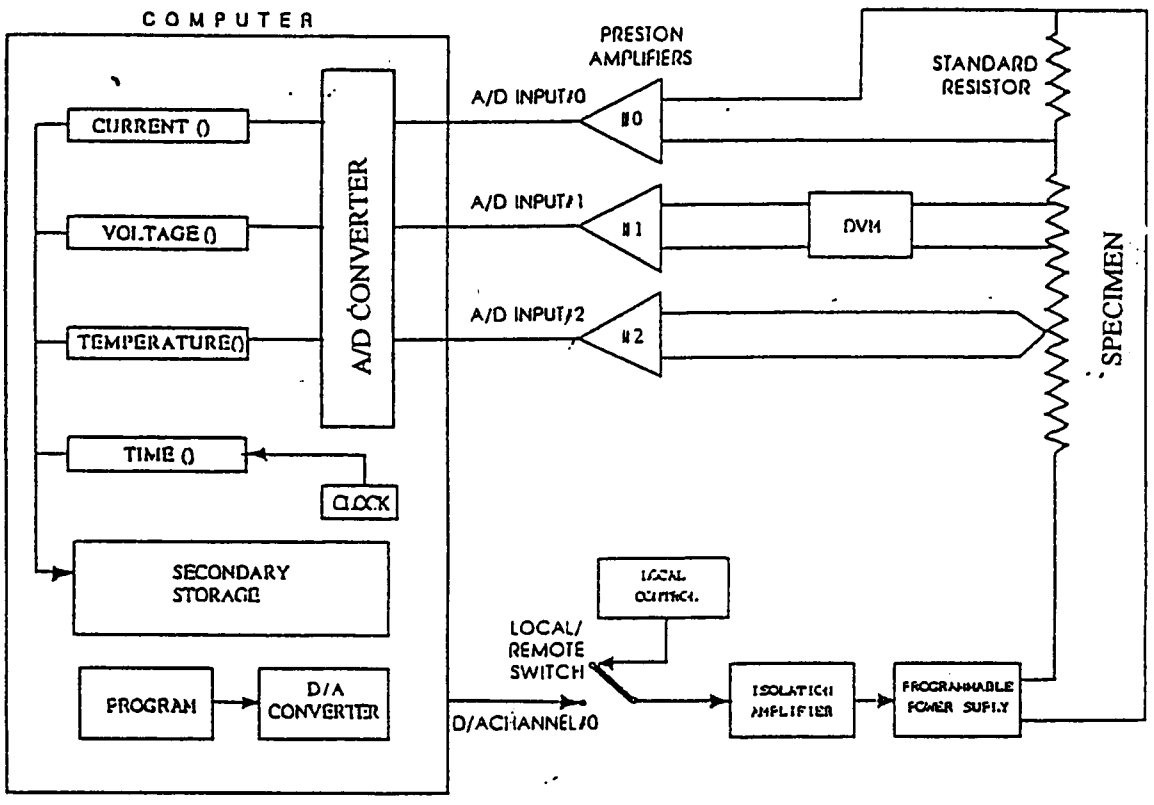

Figure 3.2 Schematic diagram of the relationship between the pulse-heating calorimeter and the personal computer [121].

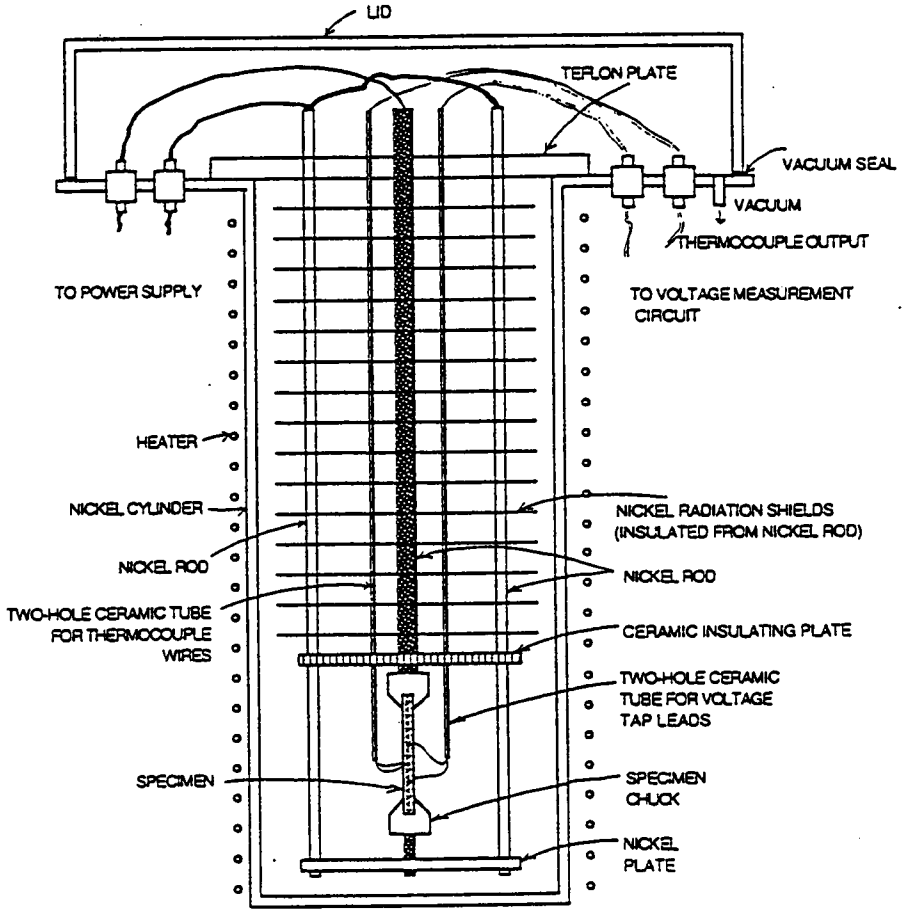

Figure 3.3 Cross-sectional view of the vacuum chamber and specimen holder in the pulse-heating calorimeter [121].

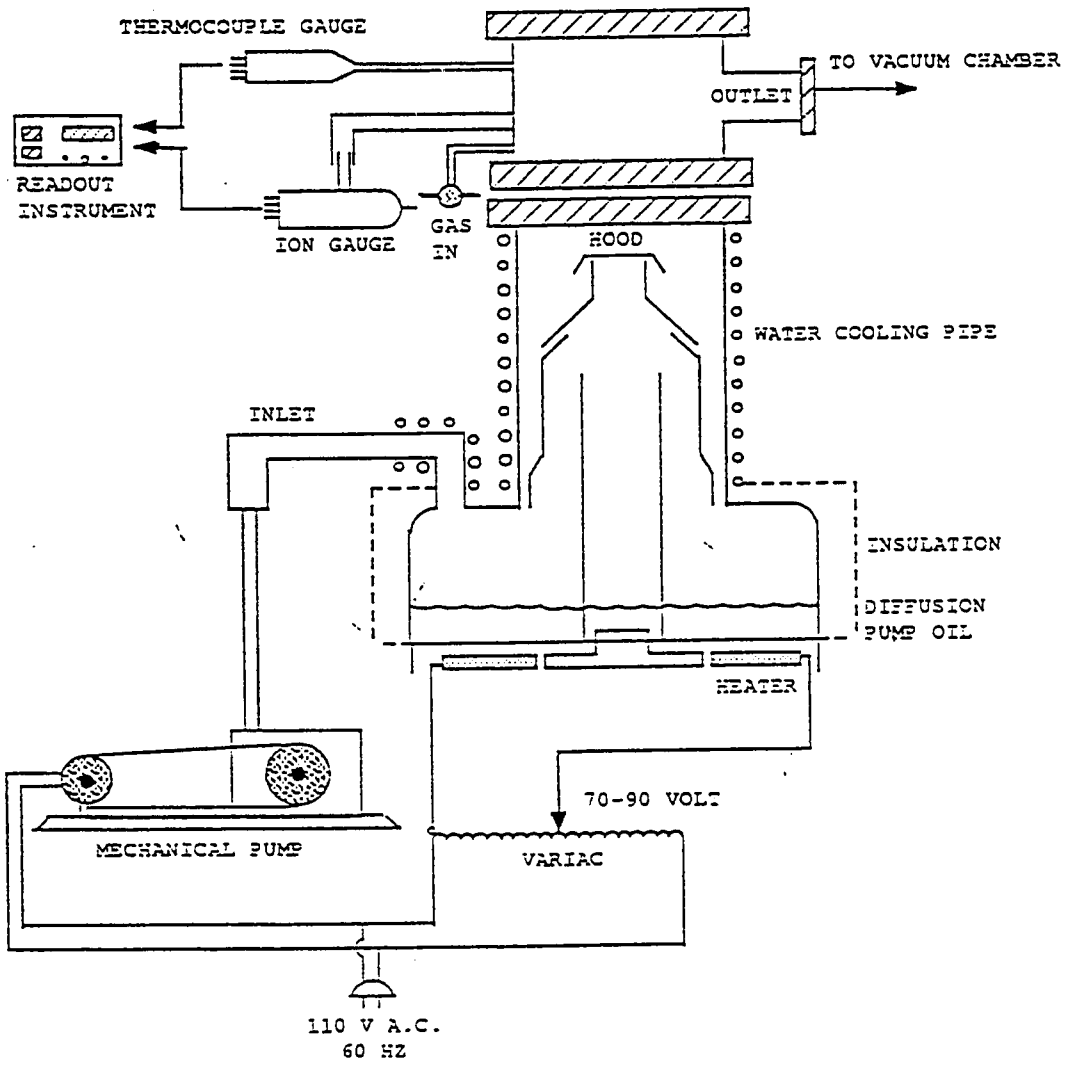

Figure 3.4 Diagram of the vacuum pumping system in the pulse-heating calorimeter [139].

The sample holder has Teflon™ flanges for keeping the holder centered in the vacuum chamber while keeping the holder electrically insulated from the vacuum chamber sides. There are four current leads of 1.25 cm nickel rod connecting to a bottom plate of nickel, which then connects to the lower specimen holder. One nickel rod current lead down the center connects the upper specimen holder. These leads connect to the power supply. The upper specimen holder is a threaded chuck with various collet sizes available. The lower chuck was also this threaded type of chuck during some tests on the long Ni_4Mo section. This caused the specimen to buckle from thermal expansion during one pulse since both ends were fixed. When the specimen was shortened, a flexible specimen holder was designed to allow expansion, shown in Figure 3.5. The bottom plate is connected to a nickel cable junction plate, where 6 flexible copper mesh cables are attached. These cables attach to another nickel cable junction, which is attached to a hollow chuck. The chuck side screws to hold the specimen in the tube.

A higher temperature can be obtained by increasing the pulse current or by increasing the pulse time. The time increase may not be an option if certain kinetic considerations are present. One other method may be to reduce the specimen size. There is a limit to size reduction however; for example the relative sizes of the thermocouple and the sample.

The calorimeter has one DC programmable power supply. This is rated at 90 A, 6 V. It can be remotely controlled from the PC, and has the option of being operated as either constant current or constant voltage. The present operation has been the constant current option.

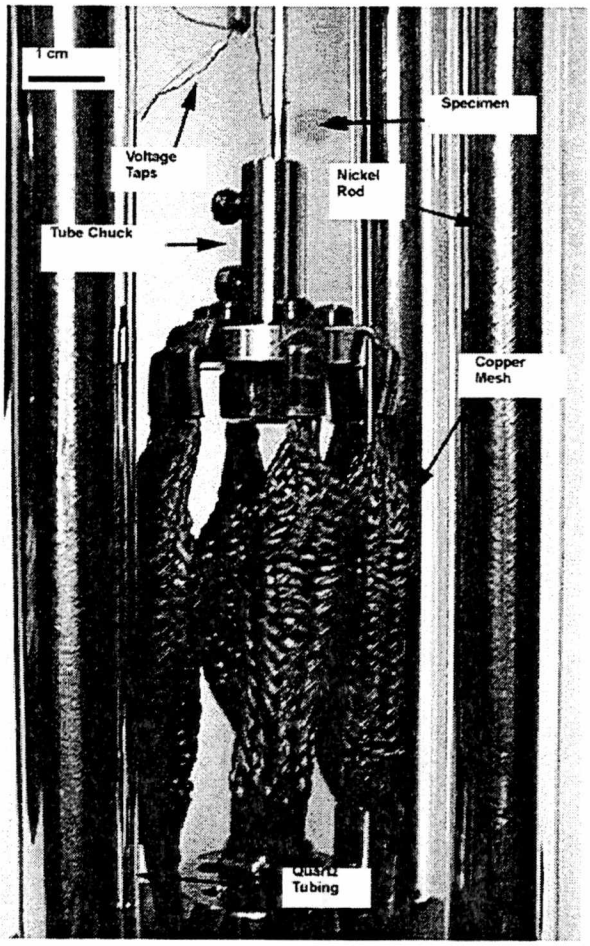

Figure 3.5 Flexible specimen holder which attaches the bottom end of the specimen to the bottom plate. This allows expansion to occur during heating.

Three Preston isolation amplifiers are used to increase the sensitivity of the current, voltage, and thermocouple e.m.f. signals. Gains of these are usually set to 1, 10, and 500, respectively. The leads from the voltage, current and thermal e.m.f. wires are connected to an 18 channel multiplexer. This chooses one signal at a time to send to a programmable gain amplifier, which boosts the signal and then sends it to a sample-and-hold circuit. A schematic diagram of the circuit is shown in Figure 3.6 [138]. The analog-to digital (A/D) signal conversion is done using DT 2821 series boards. These are high speed I/O boards designed for IBM compatible PC's. Two 12-bit boards are available, but only one is in use at present.

The data acquisition procedure is controlled by a FORTRAN program which sets the current to the specimen, calculates the electrical resistivity, and displays and records incoming data in real time. Several other BASIC and FORTRAN programs are also available to subsequently process the data. Examples of some tasks these programs perform are converting thermal e.m.f. data to degrees Kelvin, allowing graphical evaluation and regression analysis of the data (curve-fitting), and calculating the specific heat of the sample.

3.2 Specimen Preparation

The Ni_4Mo alloy specimen used in this thesis was prepared previously by Basak [121]. The composition is 29.51 wt% Mo, <0.01 wt% Al, 0.003 wt% O, remainder Ni. The specimen is in the shape of a cylindrical rod which is about 0.20 cm in diameter and initially was about 10 cm in length. The specimen was later cut into three sections of equal length. Appropriate specimen dimensions need to be selected to generate enough Joule-heating. The specimen was centerlessly ground to obtain a precise uniform

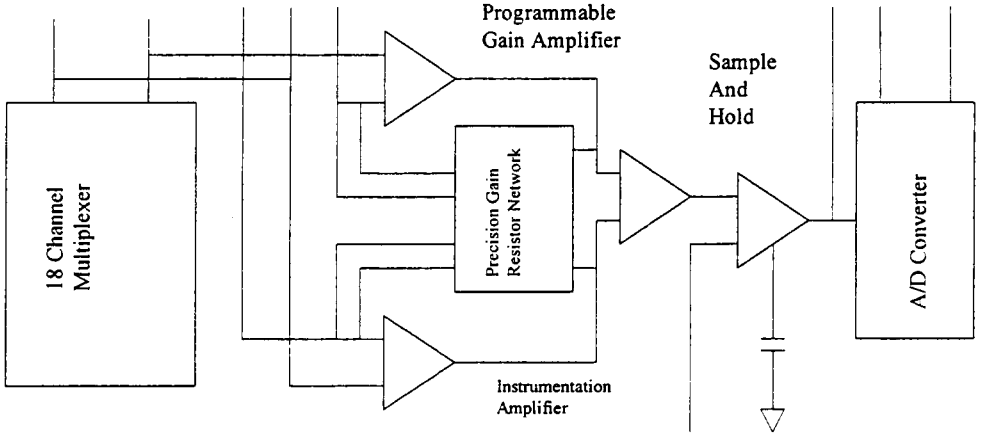

Figure 3.6 Schematic diagram of the sample-and-hold circuit and A/D converter. From Basak [139].

diameter, and the specimen effective length was made long enough to minimize the temperature gradient across its length due to end effects.

Basak [121] obtained his data with this same specimen. He prepared it from a forged rod. After being forged, a round specimen was machined from it. Because the βphase is very brittle, the specimen was alternately swaged, and then annealed in the ductile α phase until the diameter was down to about 0.36 cm. The annealing furnace was set to 950 °C and was argon purged and flushed. Each annealing time was one hour and then the sample was water quenched to room temperature to obtain SRO α, which is ductile and hence easier to cold-work. After a final swage to 14% cold-work, the specimen was centerless ground to 0.178 cm in diameter. Basak looked at the microstructure after processing, and no cracks or flaws were observed which could affect the data. See Appendix B for the exact swaging and annealing history of the specimen performed by Basak.

3.3 Experimental Procedures

The determination of specific heat using the equipment described above was broken into three main stages. The first stage was to determine some information that was needed prior to the pulse test. The next stage included processes that occurred during the pulse test. The final stage involved processing the data after the pulse test was concluded. These three stages were followed for each pulse test that was done.

3.3.1 Pre-pulsing Procedures

Several items were done prior to installing the sample into the calorimeter vacuum chamber. These included installing the voltage taps and thermocouple on the specimen, determining the mass to be used in the specific heat calculation, determining

the distance between the voltage taps, and determining the electrical resistivity at room temperature as a comparison value.

3.3.1.1 Attachment of Voltage Taps and Thermocouple to Specimen

The voltage taps were nickel wire 0.025 cm in diameter and were welded onto the specimen with a precision spot-welder. The wires were placed perpendicular to the axis such that they did not interfere with the specimen chucks that held the specimen at each end. The ends of the wires were trimmed so that there was no overhang.

The thermocouple that was used was a type-R thermocouple, which consisted of a junction between a pure platinum wire and a platinum-13% rhodium wire. The wire diameter used for the thermocouple was 0.013 cm. At about three inches from the specimen, the wire diameter was changed to 0.025 cm diameter wire. The small diameter wire near the specimen was used to minimize conduction heat losses. The Pt and Pt-13%Rh wires went all the way out of the vacuum chamber to the reference junction (0 °C ice water bath), where the wire changed to copper leads to the electronic instruments.

Basak [48] analyzed three different configurations of how the bare-wire thermocouples were attached to the specimen: 1. a welded bead method, 2. putting two wires at the same length but perpendicular to the specimen, and 3. putting one wire on top of the other. He concluded that the best method was to form a bead connecting the two wires first, and then to attach the whole bead to the specimen. This bead method was preferred because it is difficult to place the wires exactly at the same location along the length. If the wires are not at the exact same location along the length, there will be some voltage pick-up causing error in the e.m.f. signal. The bead method described above was used to attach the thermocouple to the specimen. The bead was formed with an arc

welder, and then a precision resistance spot welder was used to put the bead on the specimen.

3.3.1.2 Effective Mass Determination

The effective mass, M, of the specimen is the mass of the material between the voltage taps. The mass determination consisted of first measuring the voltage tap length L, and specimen diameter D (both discussed below). Then the volume of material between the voltage taps was calculated for a cylinder

$$V = \frac{\pi D^2}{4} L \tag{3.1}$$

And then the mass was found from the density, d

$$M = Vd \tag{3.2}$$

The method that was initially used to determine the density was the theoretical density method. The theoretical density is determined as the mass of atoms within the unit cell divided by the volume of the unit cell. The density determined from the LRO β unit cell to be 9.385 g/cm^3 is from the relationship

$$d = \frac{m_a}{a_0 a_0 c_0} \tag{3.3}$$

Here m_a is the mass of atoms in the BCT cell and a_0 and c_0 are the BCT lattice parameters. m_a is determined from a weighted average. If it is assumed that the alloy is exacly 20 at% Mo, then the weighted average is 8 Ni atoms per cell at 58.69 g/mole plus 2 Mo atoms per cell at 95.94 g/mole and then normalized for N_A atoms per mole. Thus m_a was calculated to be 1.098 x 10^{-21} grams. The lattice parameters determined by Guthrie and Stansbury [11] were used in the cell volume calculation; a = 5.727 Å and c = 3.566 Å.

Hence the cell volume was found to be 1.170×10^{-22} cm^3. This value was compared to the volume based on lattice parameter data from Casselton and Hume-Rothery [2], and the two values agreed within 0.9 %. This corresponds to a density of 9.385 g/cm^3

The volume of the FCC unit cell was found from $V = a^3$ where a is the FCC lattice parameter [13]:

$$a = 0.00406 \text{ at\% Mo} + 3.5242 \qquad \textbf{(2.1)}$$

The at% Mo for the actual sample (29.51 wt% Mo and assuming remainder Ni) is 20.39 at%. The lattice parameter is a = 3.6070 Å. The cell volume is $a^3 = 46.929$ $Å^3$ (4.6929×10^{-23} cm^3). In the FCC solution, there are four atoms per unit cell and, on the average, 20.39% of these Mo atoms and 79.61% are Ni atoms. Thus the mass of atoms in the cell is:

$$m_c = \frac{4(.7961)(58.69) + 4(.2039)(95.94)}{N_A} \qquad \textbf{(3.5)}$$

where N_A is Avagradro's number. The value calculated for was $m_c = 4.4028 \times 10^{-22}$ grams. Thus the density is 9.382 g/cm^3.

Another method to determine the density is to physically weigh the total sample with a balance and get the total mass, M_T. Then measure the total length of the sample and diameter of the sample, L_T. Then, if the voltage tap length, L is measured, the mass between the taps would be

$$M = \frac{M_T L}{L_T} \qquad \textbf{(3.6)}$$

This method assumes that the material from one end to the other is structurally uniform, which depends on how the sample was previously treated. For example, if the

sample previously pulsed to above Tc in the calorimeter and allowed to cool naturally, the center would be SRO. The structure at the ends however, would be uncertain because the chucks at the end of the sample are large and probably would keep the ends of the sample from exceeding Tc.

One way to ensure that the sample is uniform from end to end would be to heat-treat the sample prior the putting it in the calorimeter, by either quenching it to SRO α, or by annealing it to LRO β.

The density value that was finally used in the calculation was determined from measurements on the SRO state of the specimen and lattice parameter data for the FCC phase, as discussed above. First, the sample was heat-treated in the calorimeter to obtain the SRO α phase. This was achieved by heating it to above Tc, and then letting it cool naturally in the calorimeter, which is rapid enough to keep it in the SRO α condition. The specimen between the voltage taps would then be in the SRO α condition. Then, the specimen was removed from the calorimeter and D was measured with a precision micrometer (0.1775 cm) and L was measured with the knife-edge apparatus (2.5393 cm) in order to determine the volume (see Appendix D). The effective mass of the specimen was then found to be

$M = Vd = 0.06283\ cm^3 \times 9.382\ g/cm^3 = 0.5895\ g.$

3.3.1.3 Diameter Measurement

The diameter used in the volume calculation was determined from an average of several micrometer measurements. Ten measurements were made from one voltage tap to the other, and then the specimen was rotated 90 degrees, and ten more measurements were made between the voltage taps. An average of all 20 measurements was used in the

calculations for specific heat and electrical resistivity. For the tests on the short specimen, the diameter was determined to be 0.1760 cm. The long specimen value was originally determined by Basak [121] to be 0.1781 cm, and this value was used for calculations on the earlier tests on the long sample. A third diameter was determined to be 0.1775 cm that was used for the density and mass calulation because this is the value that was found after heat treating the sample to SRO α and measuring specifically to get an accurate density value. The dimensions apparently changed slightly or the difference is due to error in measurement (discussed in Section 3.4). One reason that these are slightly different may have been that after the data for the long specimen were obtained and before the specimen was cut, a high temperature pulse was done between fixed ends, which caused the specimen to buckle and deform slightly. To prevent buckling of the shortened specimen, a flexible specimen holder was designed, which was discussed in Section 3.1. The actual diameter measurements are shown in Appendix C.

3.3.1.4 Effective Length Measurement

The effective length L, was determined with a knife-edge apparatus. This equipment consists of an electrical circuit that puts a small current through the specimen, and then allows measurement of voltage drops at different locations along the specimen with a precision digital voltmeter. One distance that the potential was measured across is the known distance between the knife edges, L_K , which were placed in contact with the specimen. This potential is designated E_K. Another potential that is measured is E_T, which is the potential across the voltage taps. L can then be determined by the calculation

$$L = \frac{E_T}{E_K} L_K \tag{3.7}$$

Several measurements of the potentials were taken with the current in both directions and then averaged. Knife-edge data and example calculations are shown in Appendix D.

The knife-edge set that was used was 2.5339 cm between blades. This set was calibrated [121] in 1993, and the length was determined to range from 2.5527 cm to 2.5552 cm. An average distance was used. The value of L used for specific heat and electrical resistivity calculations on the short specimen was determined to be 2.5208 cm. For the long specimen L was determined to be 4.2972 cm.

3.3.1.5 Determining Electrical Resistivity at Room Temperature

One other application of the knife-edge apparatus is to determine the electrical resistivity at room temperature, separate from the pulse-heating calorimeter. This allows an outside check of the system to see if the resistivity data at room temperature are being calculated correctly by the pulse-heating calorimeter.

In addition to the potential measurements taken across the knife edge and across the voltage taps as discussed above, a third potential is measured across a standard resistor, designated E_R . This allows the current I, to be calculated through the sample from Ohm's Law:

$$I = \frac{E_R}{R_S} \tag{3.8}$$

where R_S is the resistance of the knife-edge standard resistor (0.999938 Ω the last time it was calibrated). The electrical resistivity is then calculated from the relationship

$$\rho = \frac{E}{I}\frac{\pi D^2}{4L} \tag{3.9}$$

where D is the sample diameter and L is the voltage tap length. Using this method, the resistivity was found to be about 144 μΩ-cm prior to putting the short sample into calorimeter. The initial condition from prior pulses should have produced SRO alpha, which is consistent with this value (see Figure 2.18, Curve 2). The knife-edge potential data and resistivity calculation are shown in Appendix D.

3.3.2 Processes During the Pulse-Heating Test

3.3.2.1 The Data Acquisition System

The pulse test itself consists primarily of:

-Entering data into the computer
-The computer setting the current through the sample
-The computer periodically measuring signals from the sample
-Calculating power and resistivity for each reading based on the signals
-Storing the data to a file

The user input data consist of the current values and time intervals of the square-wave pulse, the time of the cooling region, the sample effective length and the sample diameter, and the sampling time interval.

When the pulse program is executed, a digital signal is sent through the D/A converter to the power supply, setting the constant current it provides to the sample. This current level is set for the three steps of the square-wave pulse as described in Figure 3.1, and then the power supply sends no current during the cooling interval.

At the end of the cooling period, the acquisition stops and the user is given options on how to output the data. The usual option is to store the data in a data file for further processing.

3.3.2.2 Amplification of the Incoming Signals

There are three analog voltage signals from the system fed to the computer. One is from the standard resistor to determine current (channel 0), one is from the voltage taps (channel 1), and one is from the thermocouple (channel 2). These signals are amplified with gains of 10, 1, and 500, respectively, before entering the A/D converter. For more detailed discussion of the signal amplification and A/D conversion, see Basak [139].

The amplifiers were calibrated and found to have actual gains of 10.0106 x Vin + 0.0057, 0.99954x Vin + 0.0028192, and 499.412 x Vin + 0.008358 for channels 0, 1, and 2, respectively. The calibration data are presented in Appendix H. Before modifying the programs with these values, a check was made to see how much these values affected the results as compared to assuming the approximate gain values of 10, 1, and 500. It was found that these values had an insignicant effect on the calculated values based on the assummed values. Thus gains of 10, 1 and 500 were used in all calculations.

3.3.2.3 Calculation of Power and Electrical Resistivity

The power across the specimen is the rate of energy input to the specimen and is found from

$$P = EI \tag{3.10}$$

which is just a multiplication operation of the channel 1 signal and the channel 0 signal which is done by the computer for each signal reading. The result is then stored in a separate column.

The electrical resistivity ρ, is found from Equation 3.9 where D is the diameter of the specimen, L is the effective length of the specimen (D and L are values provided by

the user). In this case, E is the value from the voltage tap signal (channel 1) and I is the current signal (channel 0).

3.3.2.4 The Isothermal Control Program

The isothermal control program works similarly to the pulse program, but the computer uses a PID algorithm to maintain the temperature constant. There are three stages during the test. The first stage is a ramp-up interval. The second and third stages are isothermal hold intervals. The user inputs the ramp-up heating rate, the isothermal hold temperature values, and the sampling rate. The same three signals are recorded in this program that are recorded in the pulse program: for current, voltage, and temperature. The power and electrical resistivity are also calculated as described above.

The isothermal control program was used to anneal the sample below the critical temperate to transform the structure to the LRO β phase. A visual observation of the temperature-time data from the program showed that the range of temperature fluctuation was about ± 20 °C . This range was deemed acceptable, and the PID parameters within the program did not need to be adjusted. On one of the final annealing tests, however, it was noted that there was considerable noise in the temperature data during one of the isothermal runs, and in one case it was so variable that often there were temperature spikes above the critical temperature. This caused an incomplete transformation to the LRO phase. A second test needed to be done at a lower temperature anneal so that the temperature did not exceed Tc. The electrical resistivity versus time data from these tests were used to verify that he sample did transform. Electical resistivity versus time results for these isothermal tests are presented and discussed in Section 4.1.

3.3.3 Processing the Data Generated from a Pulse-Heating Test

The objective of processing the data generated by the pulse program is usually to determine the specific heat. This involves a calculation, but several other items must first be determined.

3.3.3.1 Time and Temperature Conversion

A couple of BASIC programs handle much of the calculation procedures. The main program, besides calculating specific heat, splits the data into two files, one consisting of heating data and the other consisting of cooling data. During the process of splitting the file, the time data are converted from a "time-tag number" unit used by the pulse program to units of seconds. This conversion is based on the sampling rates and interval times input by the user.

One other conversion that is done while splitting the data file is to convert thermal e.m.f. data from the thermocouple signal to degrees Kelvin. This is done in a subroutine that uses polynomial functions developed by NIST [140] from ITS-90 standards for type-R thermocouples. There are three polynomials; the one used depends on the e.m.f. range. Table 3.1 gives the e.m.f. ranges and their respective polynomial coefficients. Once the value in degrees Celsius is determined, it is converted to Kelvin scale by adding

Table 3.1 Polynomial coefficients used to convert thermal e.m.f. signals to degrees Celsius [140].

	e.m.f. Range (μV)		
Degree of Coefficient	0 to 3047	3047 to 11846	above 11846
0	6.414181	45.509556	-81.99599416
1	0.1586447	0.11284875	0.1553962042
2	-2.464001x10^{-5}	-2.8603978x10-6	-8.342197663x10-6
3	5.013749x10-9	8.5173702x10-11	4.279433549x10-10
4	-4.39642x1--13	-1.1440038x10-15	-1.19157791x10-14
5	0	0	1.492290091x10-19

the value in degrees Celsius to 273.15.

3.3.3.2 Determination of Specific Heat

The determination of specific heat, Cp, is a fairly complicated process because it involves curve-fitting to determine polynomials that best describe the data.

3.3.3.2.1 Overall Calculation

The calculation of specific heat is derived from an energy rate (power) balance. The amount of energy absorbed by the specimen is

MCpdT **(3.11)**

where M is the effective mass (between the voltage taps of the specimen), and Cp is the specific heat. The rate of energy absorbed is

MCp(dT/dt)h **(3.12)**

where $(dT/dt)_h$ is the time rate of change of temperature during the heating pulse (heating rate). Assuming that there are no heat losses (energy input equals rate of heat absorbed), then the specific heat at constant pressure is given by

$$C_P = \frac{EI}{M}\frac{1}{\left(dT/dt\right)_h} \quad \textbf{(3.13)}$$

where EI is the power (rate of energy input the specimen) Thus C_p is obtained at any temperature by taking the inverse of the derivative at that temperature and multiplying by EI/M.

However, there is some energy lost to the surroundings. This can be corrected for in the calculation by also measuring the time rate of change of temperature during cooling and subtracting out this portion. Thus the overall specific heat is

$$C_P = \frac{EI}{M}\left[\frac{1}{\left(dT/dt\right)_h - \left(dT/dt\right)_c}\right] \qquad \textbf{(3.14)}$$

where $(dT/dt)_c$ is the cooling rate.

Experimentally, the mass is determined separately and is a constant, but the EI curve (power), heating rate, and cooling rate must be determined as functions of temperature.

This method assumes that the energy rate losses on heating are the same as energy rate losses during cooling. This is known not to be true in certian circumstances during the tests. One reason is that on pulsing the the initial LRO β specimen the heat losses are due to the thermal conductivity of the β phase. At the critical temperature however, the specimen transforms to SRO α, which has a different thermal conductivity. The SRO α is retained on cooling so the heat losses on heating will not be the same as on cooling.

Another experimental problem is that heat losses at the beginning of the test when the calormeter is cold may be different than at the end of the test, when the calorimeter has warmed up. This problem also occurs when comparing two different tests, having to do with the time allowed between tests. For example, the tests on the shortened specimen in the LRO β initial condition at two different heating rates were done on the same day. The first test was done at the high heating rate in which the calorimeter and specimen were at room temperature at the start of the pulse. The next three tests were attempts to isothermally transform the specimen to LRO β by holding the specimen at high temperatures for over 30 minutes each. This increased the surrounding temperature during the final pulse test at lower current. Thus, the heat losses between the two different

tests may be different. Quantifying the effects of this problem has not been investigated in this thesis, but this problem may be apparent in some results, discussed in Section 4.4.

3.3.3.2.2 Curve-fitting Procedures

In order to describe the steps involved in getting a Cp versus T curve, an example using actual data will be used (pulse test 9/30/98, run #2), although the density value used in this analysis was not the value settled on in the final anlysis. This is just a description of the processes involved in curve-fitting. The sample pulse that will be evaluated was the pulse on the shortened Ni_4Mo sample that was initially in the SRO α phase (from a previous pulse above Tc and then naturally cooled), and pulsed at about 35 amps. The raw data file that was generated by the pulse program is shown in Appendix F, and the heating and cooling files that were generated from the processing program are in Appendix G.

The power, EI, was calculated at each temperature reading by the pulse program. Hence, a plot of power versus temperature was generated from the heating data file that was generated. Figure 3.7 shows a plot of power versus temperature of the data. The first three data points have zero power, and were recorded before the power supply was turned on. There were also about four reading just after the power supply came on where there was a spike in power before the signal stabilized. Thus, a decision was made to remove the first seven data points from the curve-fitting analysis. The curve shows a gradual increase in power with temperature until about 1000 K, where the curve drops fairly sharply at first and then continuously decreases but begins to level off at the higher temperature limit of the pulse.

A curve very similar to the power versus temperature (P-T) curve is the electrical

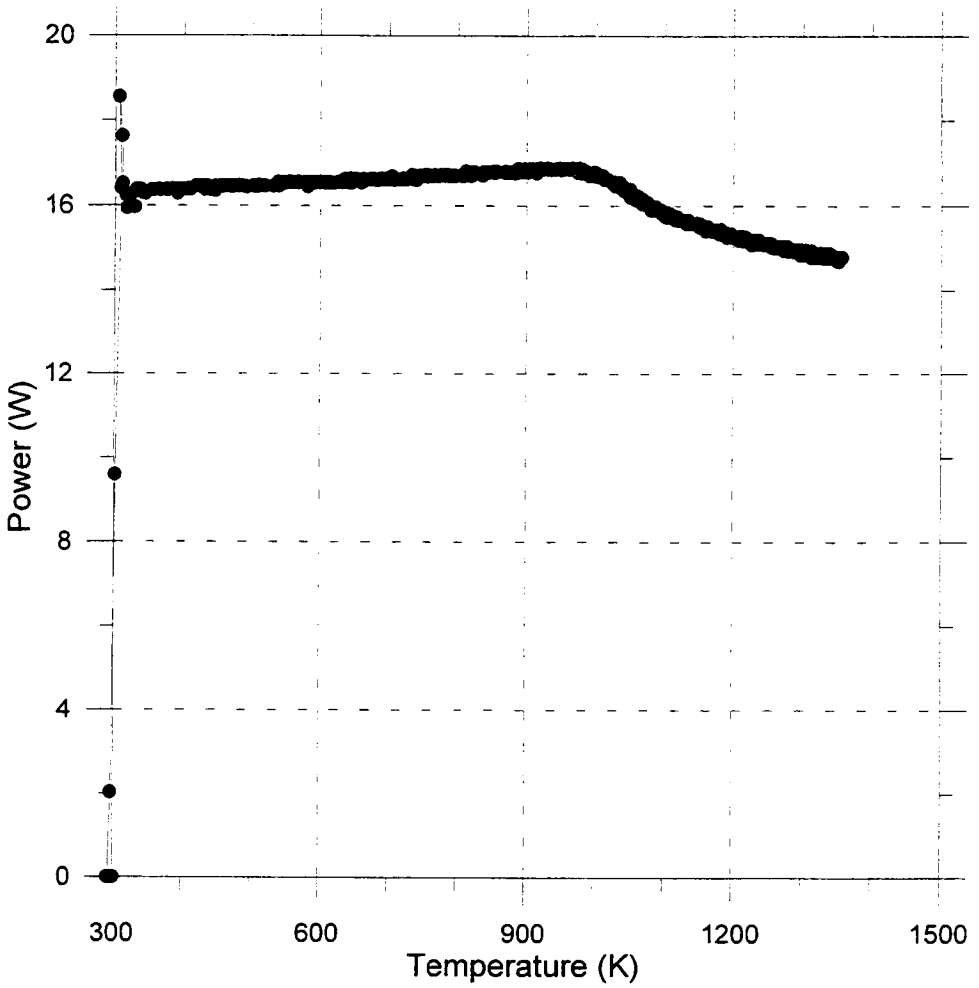

Figure 3.7 Power versus temperature from the raw data file generated from the pulsing program.

resistivity versus temperature (ρ-T) curve shown in Figure 3.8 (after deleting the first seven data points). The mechanisms dictating the shape of this curve were discussed in Section 2.4.

The temperature versus time (T-t) plot for the heating data is shown in Figure 3.9. There is a distinct change in behavior at about 1000 K for this curve. The curve is linear up to about 1000 K, where it changes slope and becomes non-linear.

The curve fitting introduces more artifacts when more complex curves are fitted. It was thus decided after looking at Figures 3.7 and 3.9 to split the data into two parts for curve-fitting; one interval from 300 K to 1000 K, and one from 1000 K to 1375 K.

Data were deleted up to, but not including, the 11.86 s data row of the heating file. Figure 3.10 shows the (T-t) plot for the modified heating data in the high temperature range. There appeared to be a change in behavior here at about 1180 K, therefore it was decided to split the data into four regions; 300-975 K, 950-1075 K, 1050-1180 K, and 1180-1375 K. It turned out later that the calculated specific heat was fairly constant through this region, and results would have been about the same by evaluating the wider range. Some overlap of the intervals was used, which was removed later during final evaluation of the specific heat versus temperature (Cp-T) curve. The highest interval was evaluated first, and the data below, but not including 17.63 s (1179.94 K), was removed from the analysis.

The decision of which degree polynomial to use for the fit was a difficult task. Basak [139] discusses this problem in more detail, and concluded that in most cases, a parameter that is the sum of the squares of the residuals, normalized to the number of data points, could be used to evaluate the fit. The lower value of this parameter would be the

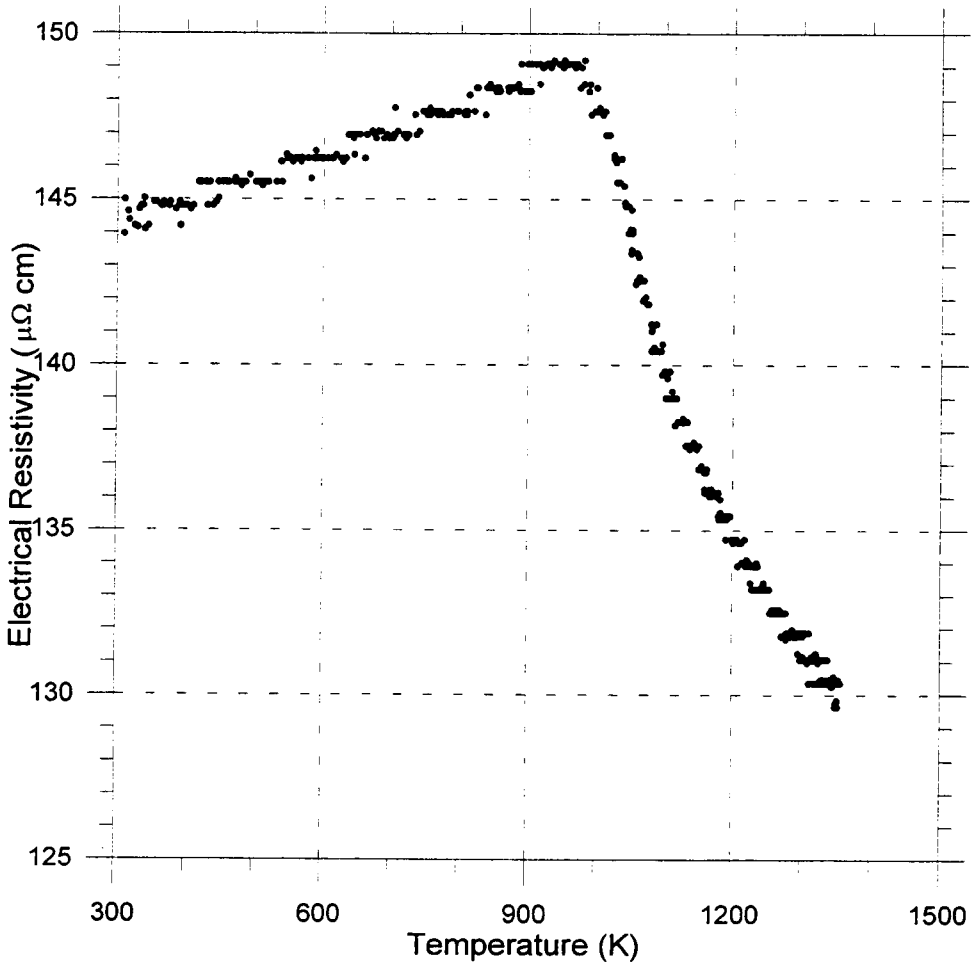

Figure 3.8 Electrical resistivity versus temperature for the Ni_4Mo specimen in the initial SRO α condition pulsed at 33 amps.

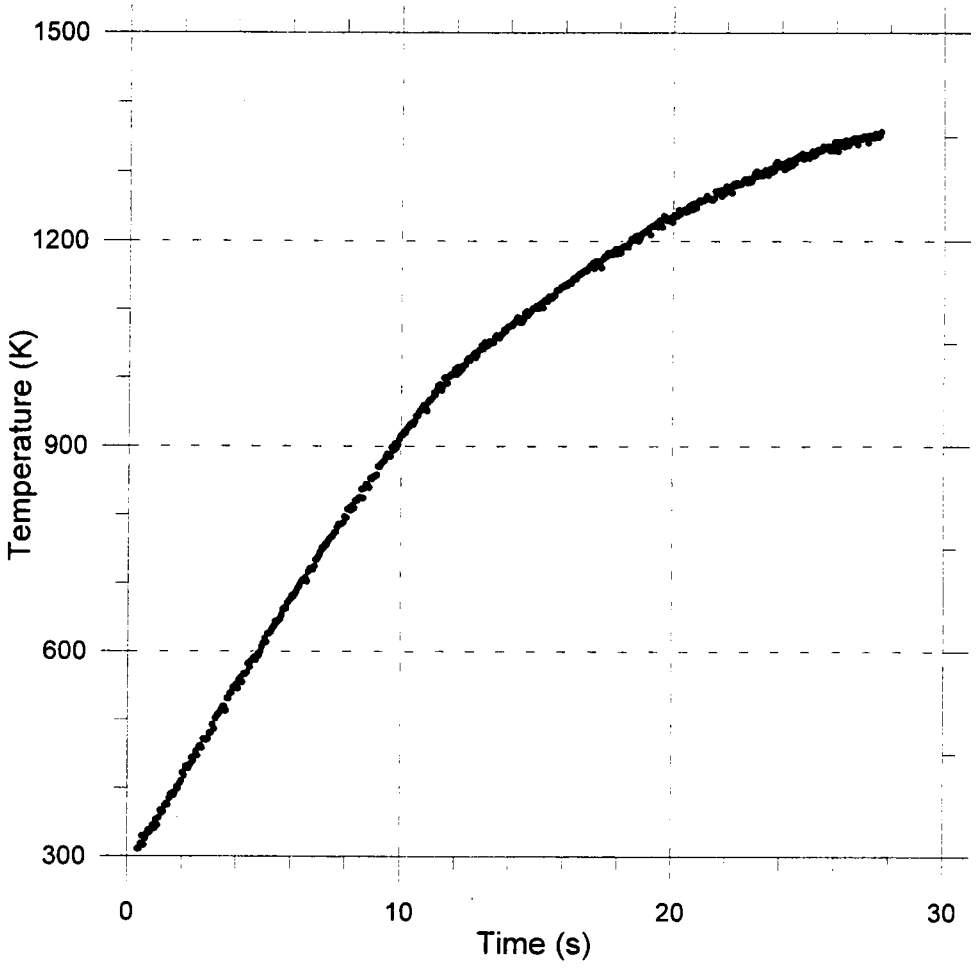

Figure 3.9 Temperature versus time upon heating over the entire temperature range of the pulse.

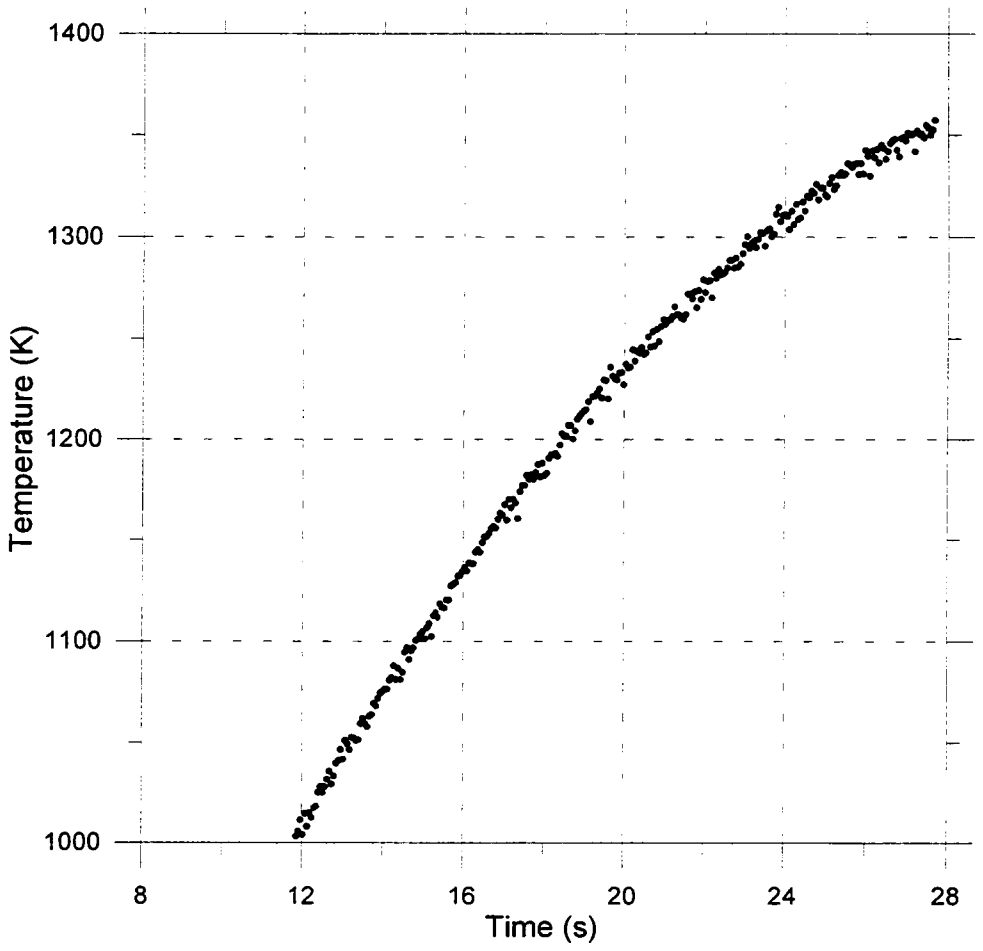

Figure 3.10 Temperature versus time plot for the high temperature interval for the curve-fitting example. There seemed to be a slight change in behavior at about 1150 K, thus a narrower temperature range was selected for the analysis.

more desirable. It was found for curve-fitting data for this thesis that in general, the lowest the value of the polynomial that visibly followed the trend of the data provided the best results. The reason for this was that using too high of a polynomial degree often picked up noise in the data causing artifacts in the calculations.

The P-T data for the high temperature interval are shown in Figure 3.11. The appearance of the multiple data values for a given P value due to the resolution of the A/D converter (2.44 mV). The data are digitized. A polynomial of the form

$$EI = P = a_1 + b_1T + c_1T^2 + d_1T^3 + ... \quad \textbf{(3.15)}$$

was generated. The polynomial coefficients of this curve were input into the processing program, and stored for final calculation of Cp. A second degree polynomial was selected to represent this data. The actual coefficients are listed in Table 3.2 along with the other coefficients that were determined for the high temperature interval analysis. The curve in Figure 3.11 is the generated second degree polynomial.

Figure 3.12 shows the T-t data for the high temperature region. A polynomial of the form

$$T = a_2 + b_2t + c_2t^2 + d_2t^3 + ... \quad \textbf{(3.16)}$$

was fitted to the data. A second degree polynomial was also used to describe this data, which is superimposed on the graph in Figure 3.12. The polynomial coefficients (Table 3.2) were entered into the processing program.

Then the polynomial was differentiated with respect to time to get a polynomial of the form

$$(dT/dt)_h = b_2 + c_2t + d_2t^2 + ... \quad \textbf{(3.17)}$$

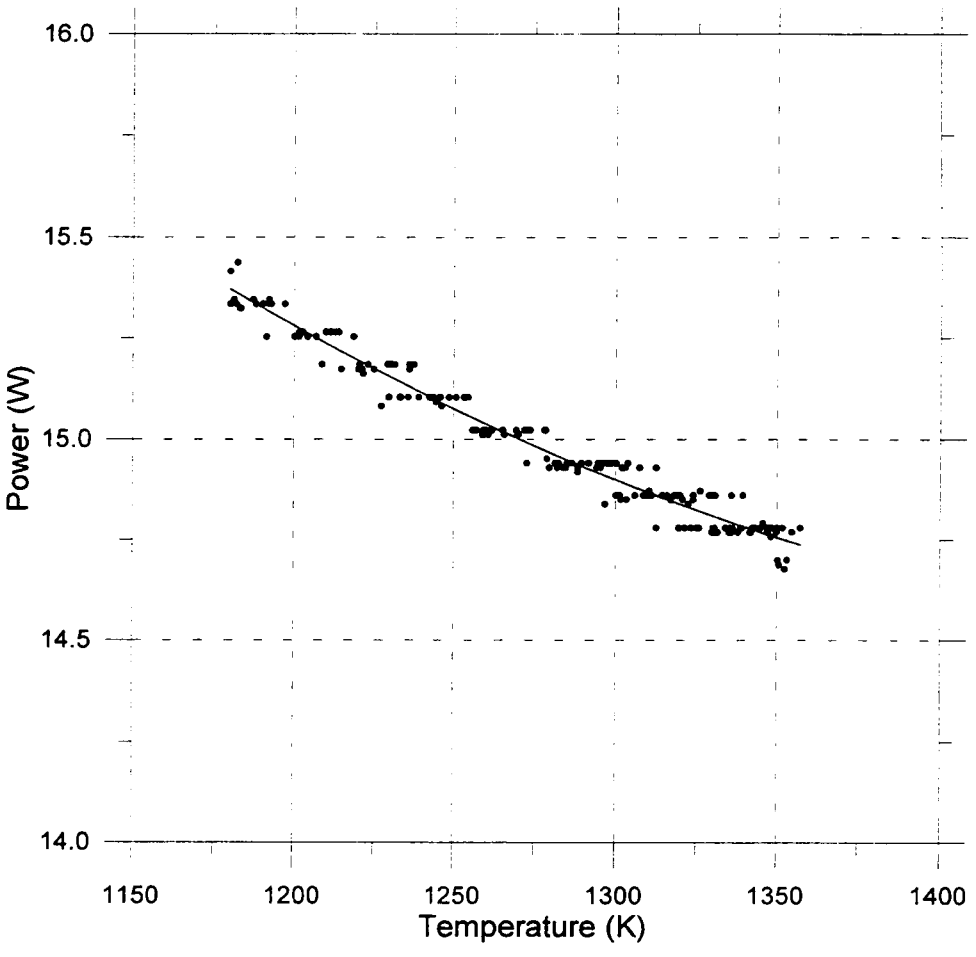

Figure 3.11 Power versus temperature for the high temperature interval. The best-fit curve shown is a second degree polynomial.

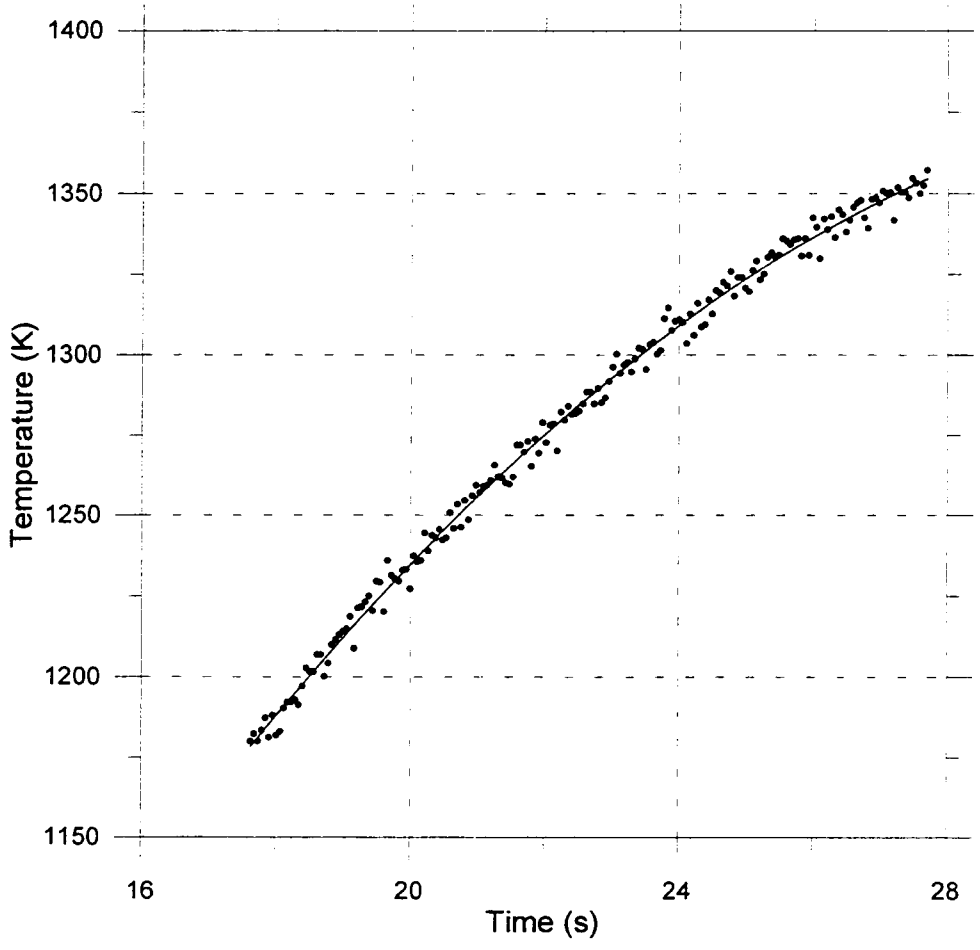

Figure 3.12 Temperature versus time on heating for the high temperature interval. The best-fit curve shown is a second degree polynomial.

For every value of t in the data set, a value for $(dT/dt)_h$ was then computed. These $(dT/dt)_h$ values were then plotted versus temperature, and a ($(dT/dt)_h$-T) curve was generated. The data are shown in Figure 3.13. The best-fit curve shown on the graph was selected to be a third degree polynomial of the form

$$(dT/dt)_h = a_3 + b_3T + c_3T^2 + d_3T^3 + ... \quad \textbf{(3.18)}$$

The polynomial coefficients for this polynomial (Table 3.2) were then entered into the processing program and stored for the final Cp calculation.

Once the heating rate data were analyzed, the heating file was closed and the cooling data file that was generated at the beginning of the analysis was opened (Appendix J). This file initially only included time and temperature data because when the power was zero, the current, voltage, and resistivity data were also zero. The file was later modified to include the cooling rate data as a part of the normal procedure. The data file was modified to include only the temperature range of the analysis by deleting data outside of the range of interest. It was also decided to discard one other data point, the highest temperature point. The reason for this was that the cooling had not quite started yet when the first data points were recorded. The T-t data for cooling in the high temperature range are shown in Figure 3.14, along with the superimposed best fit curve. The best-fit curve is a polynomial of the form

$$T = a_4 + b_4t+c_4t^2 + d_4t^3.... \quad \textbf{(3.19)}$$

In this case, a third degree polynomial was used. The coefficients of this curve (Table 3.2)

were input into the processing program, and the curve is shown in Figure 3.14. A cooling rate equation was found by differentiating the T-t polynomial with respect to t to get a

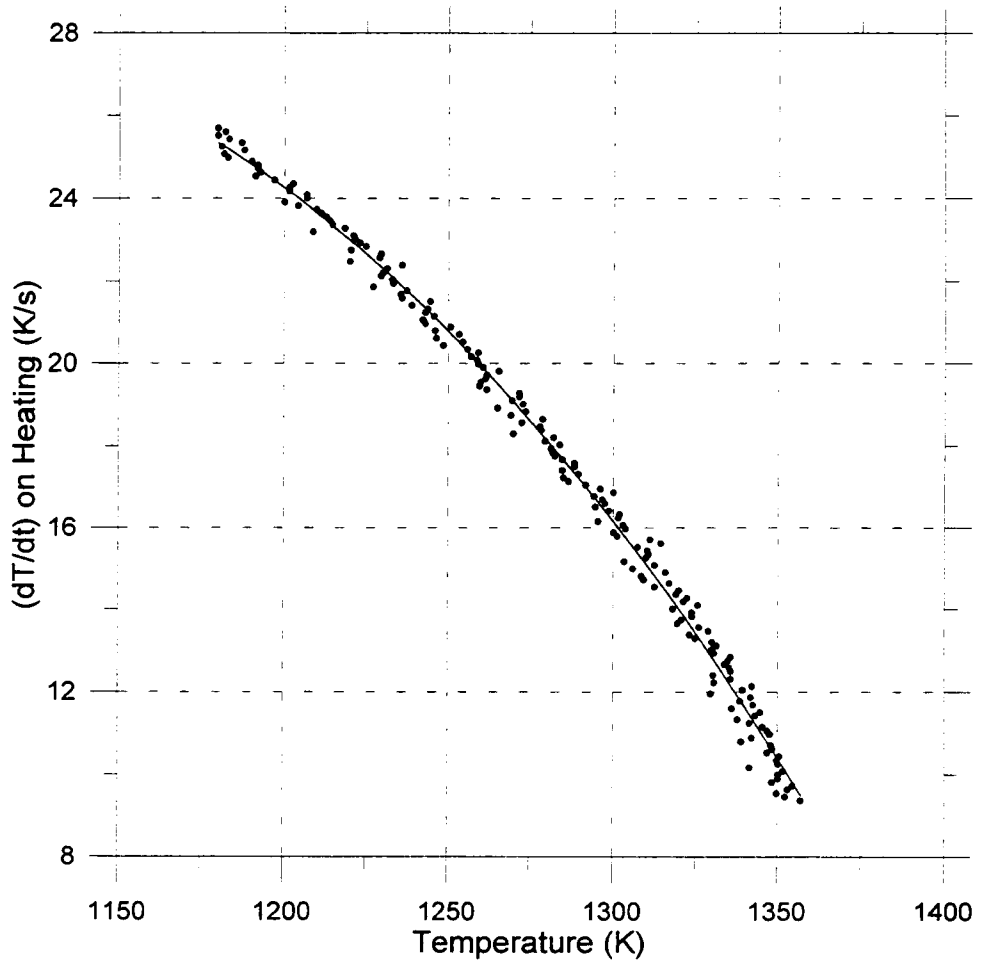

Figure 3.13 Heating rate versus temperature for the high temperature interval. The curve is a third degree polynomial generated from the data points.

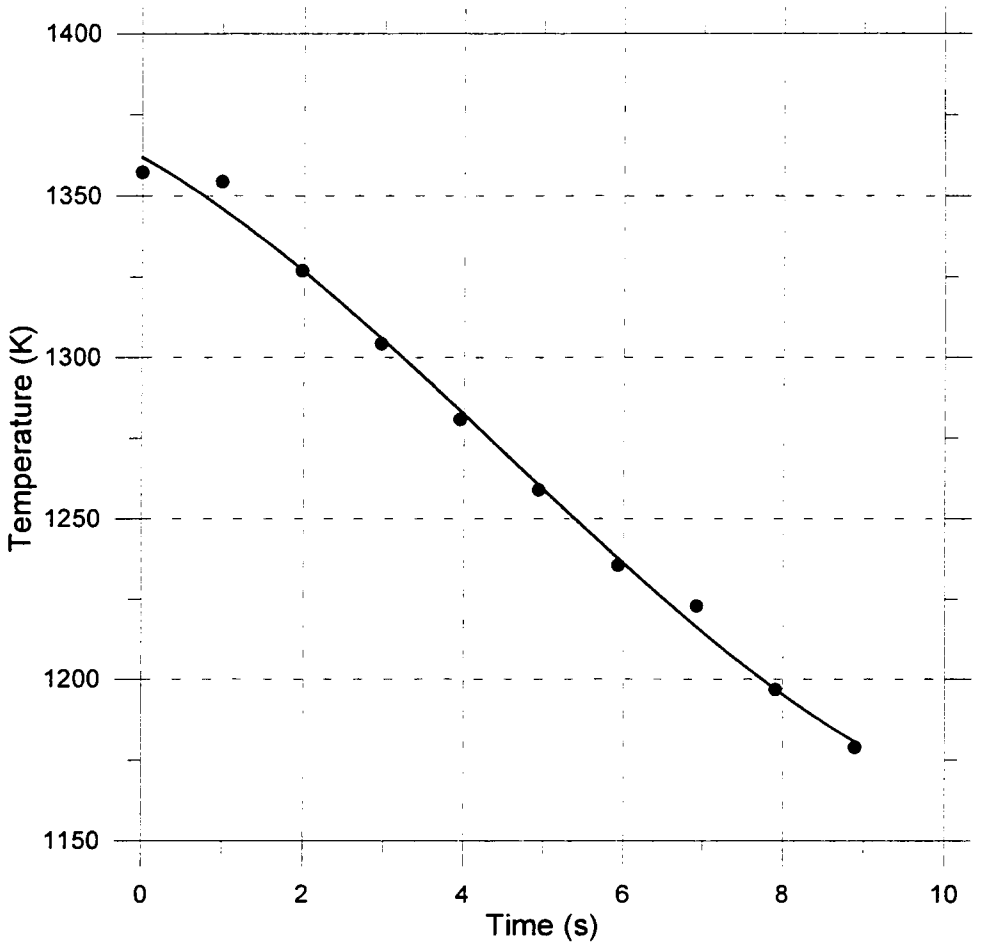

Figure 3.14 Temperature versus time during cooling for the high temperature interval. The best fit curve is a third degree polynomial generated from the data.

polynomial of the form

$$(dT/dt)_c = b_4 + c_4t + d_4t^2 + \ldots\ldots \quad \textbf{(3.18)}$$

For every value of time in the data set, a value for $(dT/dt)_c$ was calculated and then these were plotted versus temperature. This cooling rate versus temperature ($(dT/dt)_c$-T) curve was then plotted (Figure 3.15) and a best fit curve of the form

$$(dT/dt)_c = a_5 + b_5T + c_5T^2 + d_5T^3 + \ldots\ldots \quad \textbf{(3.19)}$$

was chosen to fit this data. A third degree polynomial was used to describe the cooling rate data, and the polynomial coefficients were entered into the processing program and stored for the final Cp calculation. The polynomial coefficients are listed in Table 3.2.

With the above mentioned ploynomial curves determined, the Cp as a function of T is then calculated using Equation 3.12 by substituting values in from Equations 3.13, 3.16, and 3.19. The temperature range of interest and increment are entered, and a file of specific heat and temperature is generated. For this particular example, the range from 1175 to 1360 K in 5 K increments was entered. The Cp results are plotted in Figure 3.16.

A similar procedure was followed for determining Cp in the lower temperature ranges. In the range 1050 K to 1180 K, a second degree polynomial was used for the P-T, T-t on heating, and (dT/dt)-T on heating curves. The T-t cooling curve in Figure 3.17 was first thought to be better represented by a higher degree polynomial, and a fifth degree polynomial was selected to represent this data. The resulting (dT/dt) - T on cooling curve was best described by a fifth degree polynomial curve, shown in Figure 3.18. Figure 3.19 shows the resulting Cp data that was generated from computed using those curve-fitting parameters. Using these curve fitting parameters produced a Cp-T curve that was lower than the expected values based on data from Basak [121] and Norem [137]. A slight

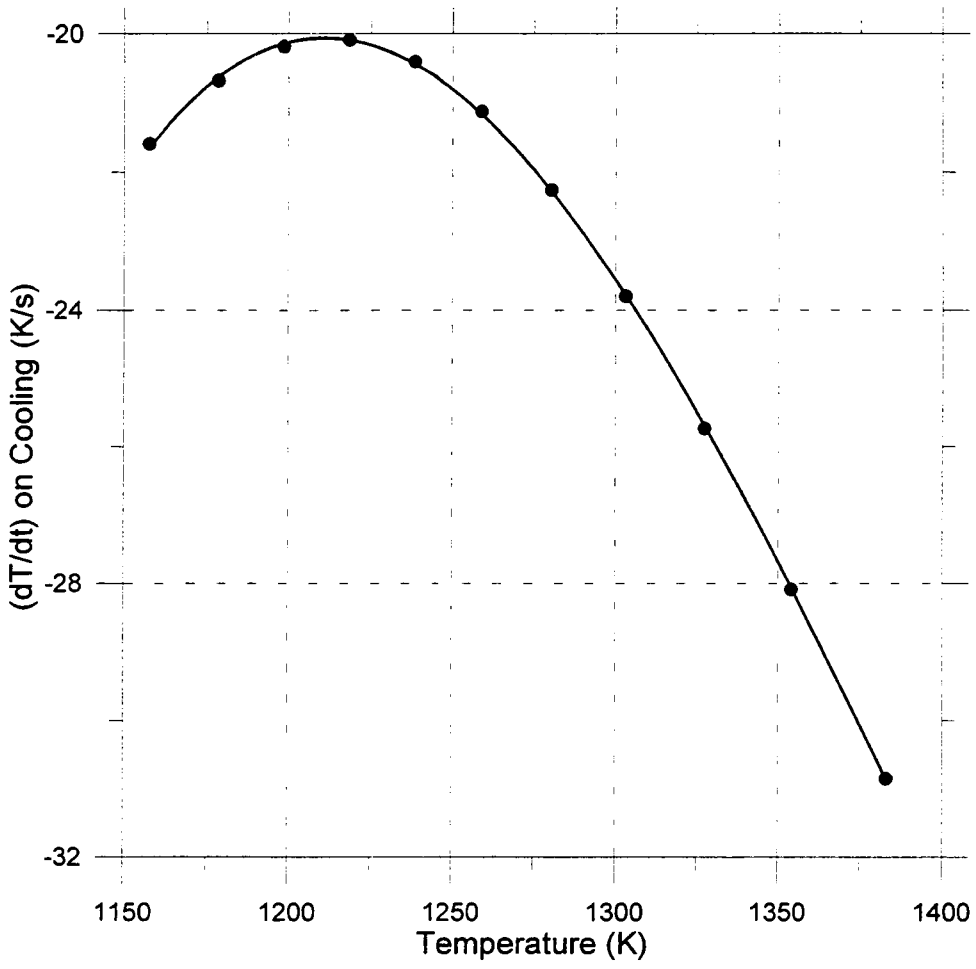

Figure 3.15 Cooling rate versus temperature for the high temperature interval. The curve is a third degree polynomial.

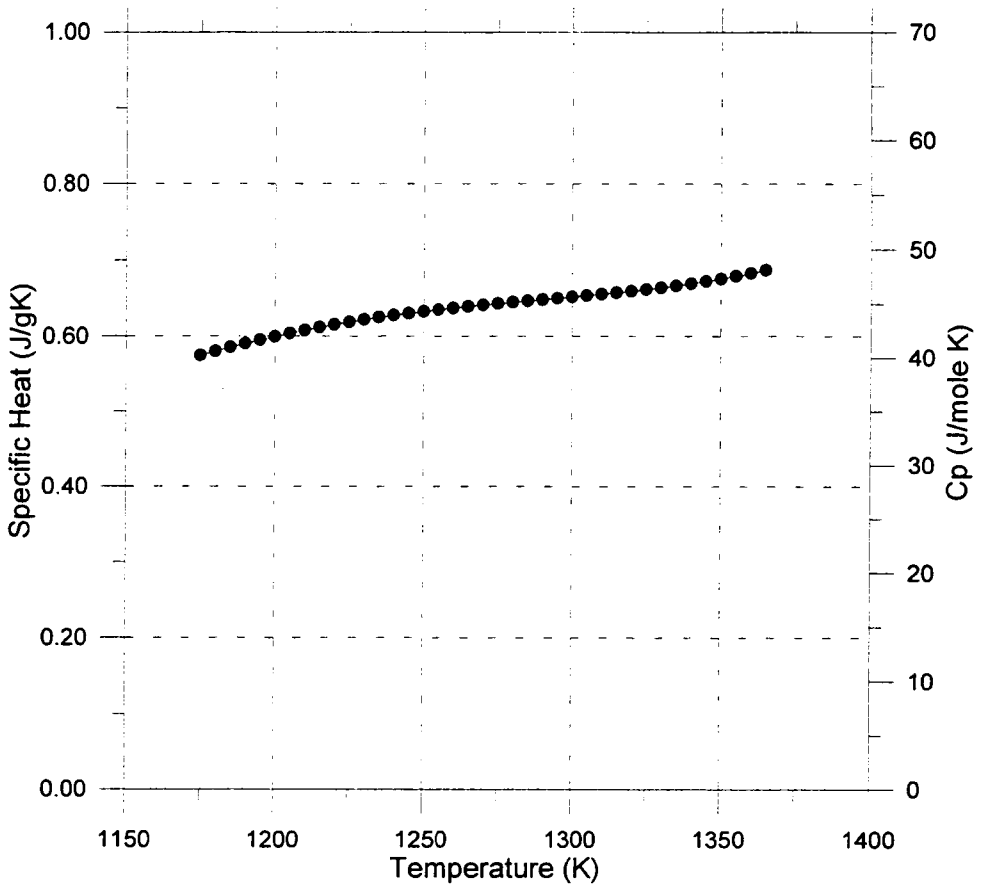

Figure 3.16 Specific heat versus temperature for the high temperature interval. Data is for Ni_4Mo in the SRO α initial condition pulse at 33 amps.

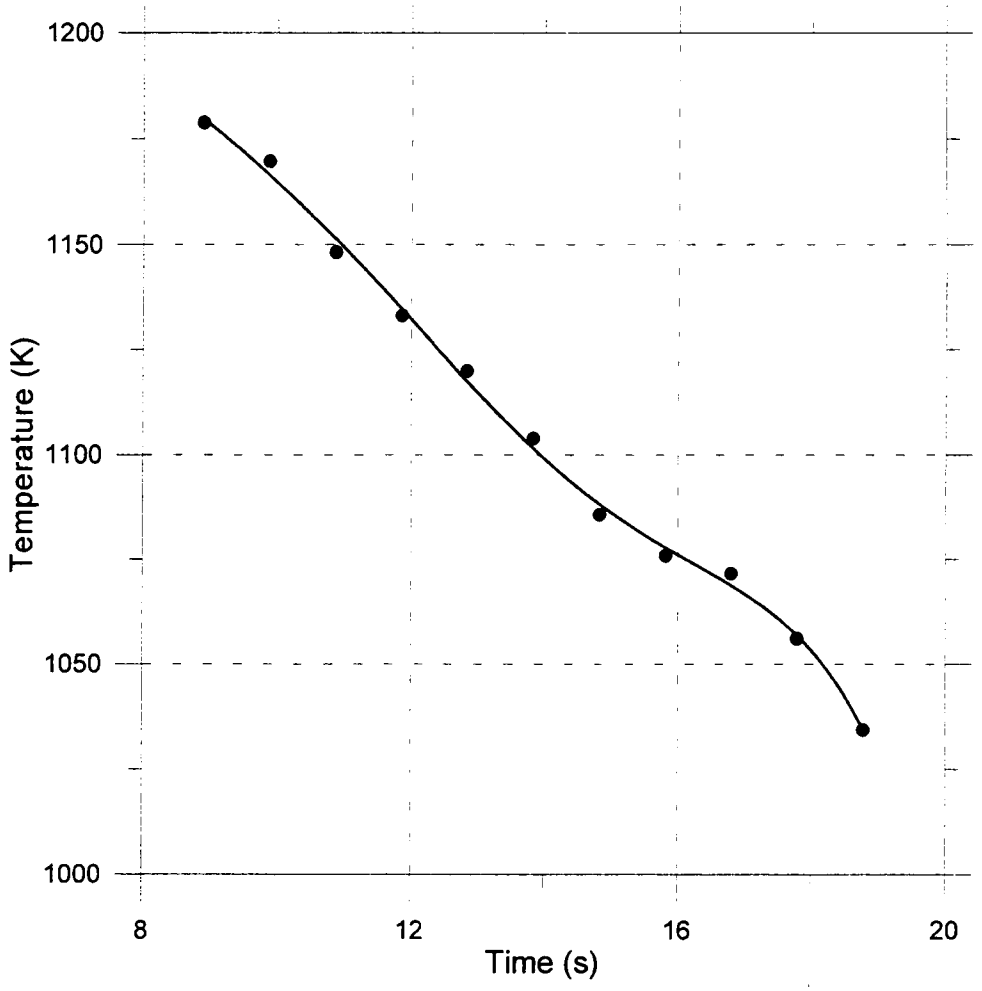

Figure 3.17 Temperature versus time on cooling for the medium-high temperature interval using a fifth degree polynomial best-fit curve for specific heat determination.

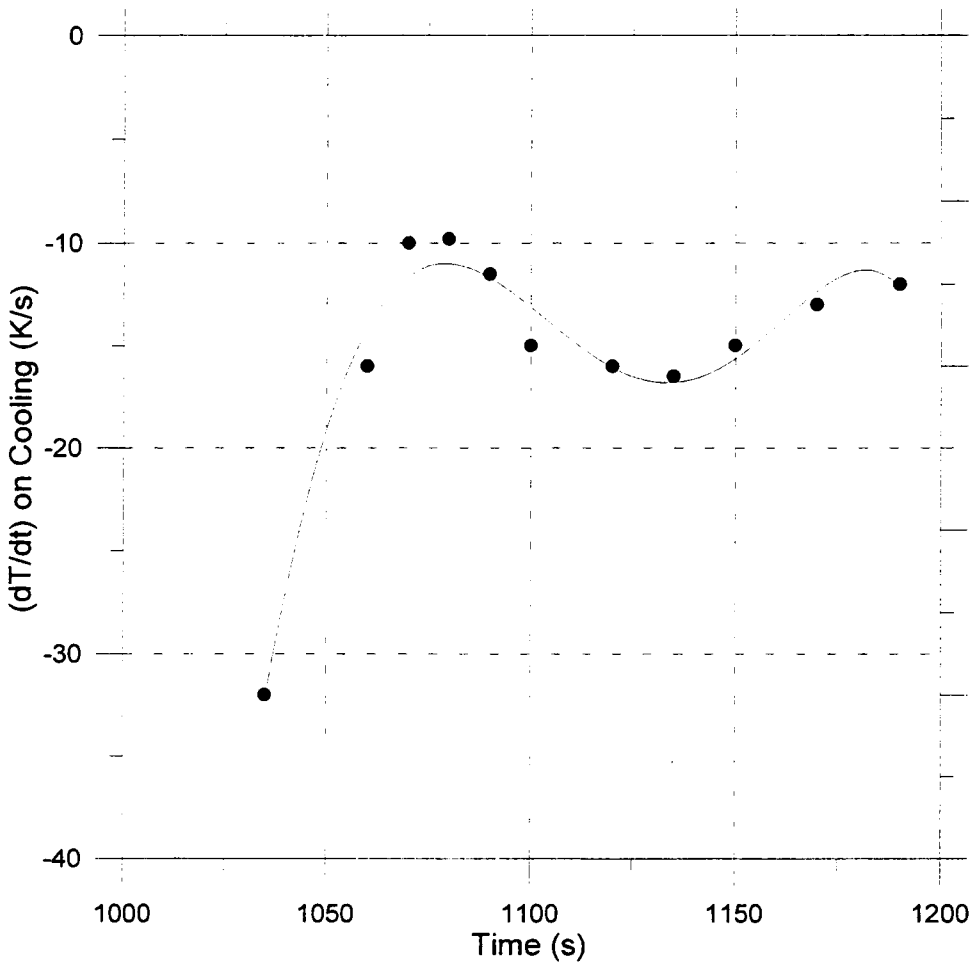

Figure 3.18 Cooling rate versus temperature for the medium-high temperature interval which resulted from the fifth degree polynomial best-fit temperature versus time on cooling curve.

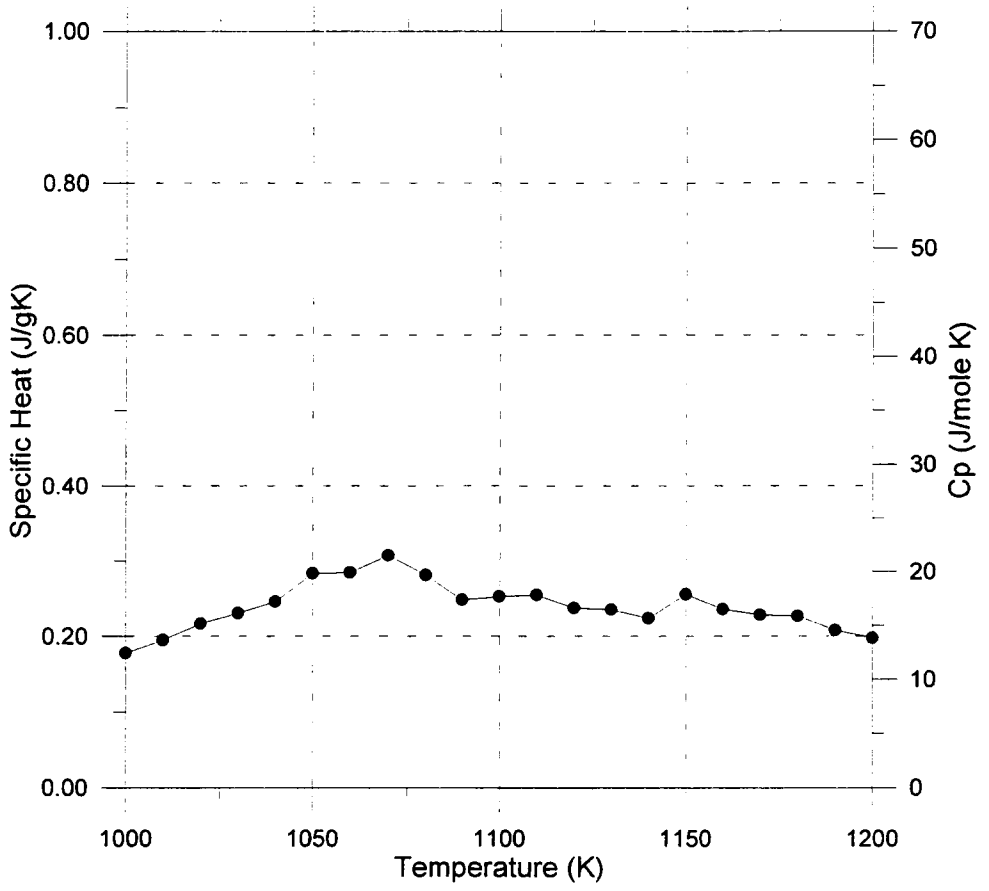

Figure 3.19 Specific heat versus temperature for the medium-high temperature interval resulting from a fifth degree polynomial fit of temperature versus time on cooling. These data a were rejected and data in Figure 3.22 were kept.

modification was done to the above curve-fitting parameters: a second degree polynomial was selected for the T-t on cooling curve, as shown in Figure 3.20. The coefficients found here corresponded to a lower degree polynomial in the (dT/dt) - T cooling curve (Figure 3.21) Figure 3.22 shows the Cp-T curve using the lower degree polynomial coefficients. A slight change in $(dT/dt)_c$ caused Cp to change by a factor of three. Data in Figure 3.22 is in closer agreement with the literature values. If no literature values are available for comparison, this problem may be difficult to resolve.

For the 950 to 1075 K range, the curve fitting plots are shown in Figure 3.23. A second degree polynomial was used for the P-T (Figure 3.23a), the T-t cooling (Figure 3.23d), and $(dT/dt)_c$-T (Figure 3.23e) curves. A third degree polynomial fit was selected for the T-t heating (Figure 3.23b) and $(dT/dt)_h$ -T (Figure 3.23c) curves. The specific heat data were then calculated from 925 to 1100 K in 5 K increments, shown in Figure 3.23f.

The specific heat at 300 to 950 K was evaluated using the following polynomial degrees:

P-T: 1st degree
T-t on Heating: 2nd degree
(dT/dt) on Heating: 2nd degree
T-t on Cooling: 6th degree
(dT/dt) on Cooling: 3rd degree

The corresponding plots for curve-fitting the specific heat are shown in Figure 3.24. An additional four data points were removed at low temperature to remove the initial spike in the P-T curve. The resulting specific heat data are shown in figure 3.24f. The temperature

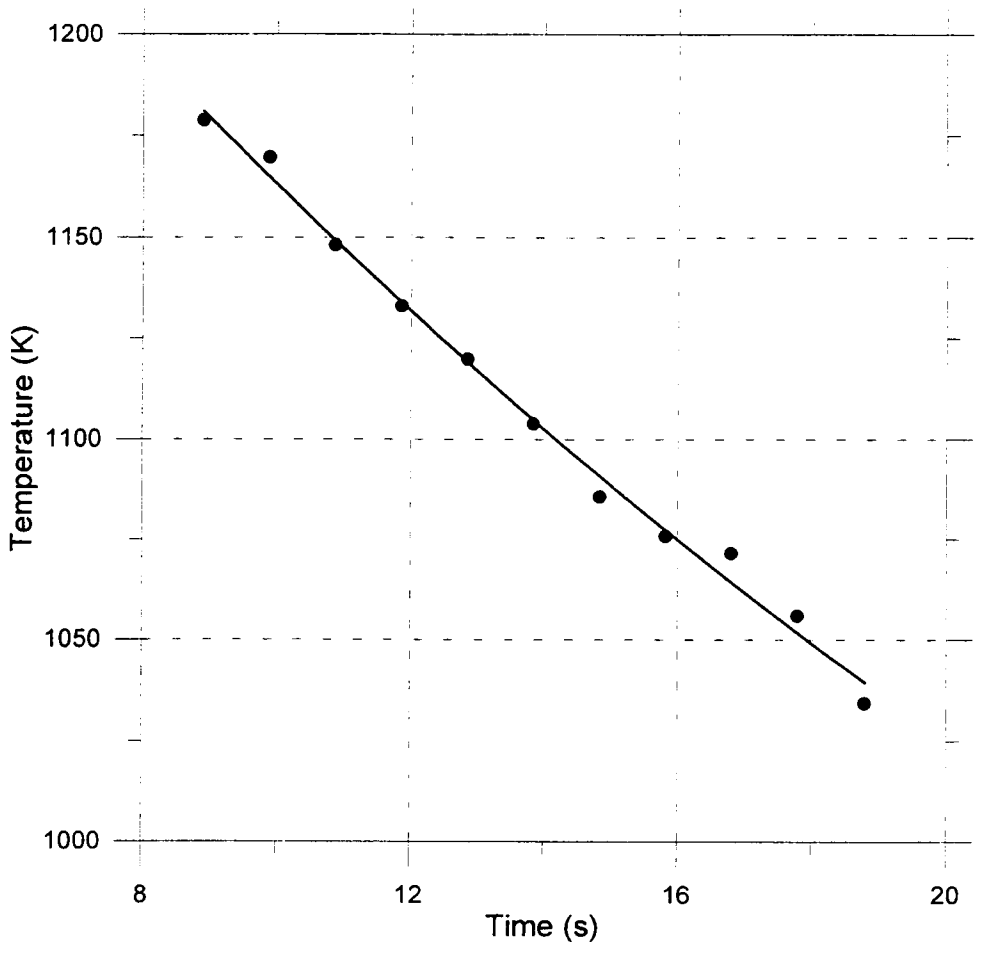

Figure 3.20 Temperature versus time on cooling for the medium-high temperature interval using a second degree polynomial fit for specific heat determination.

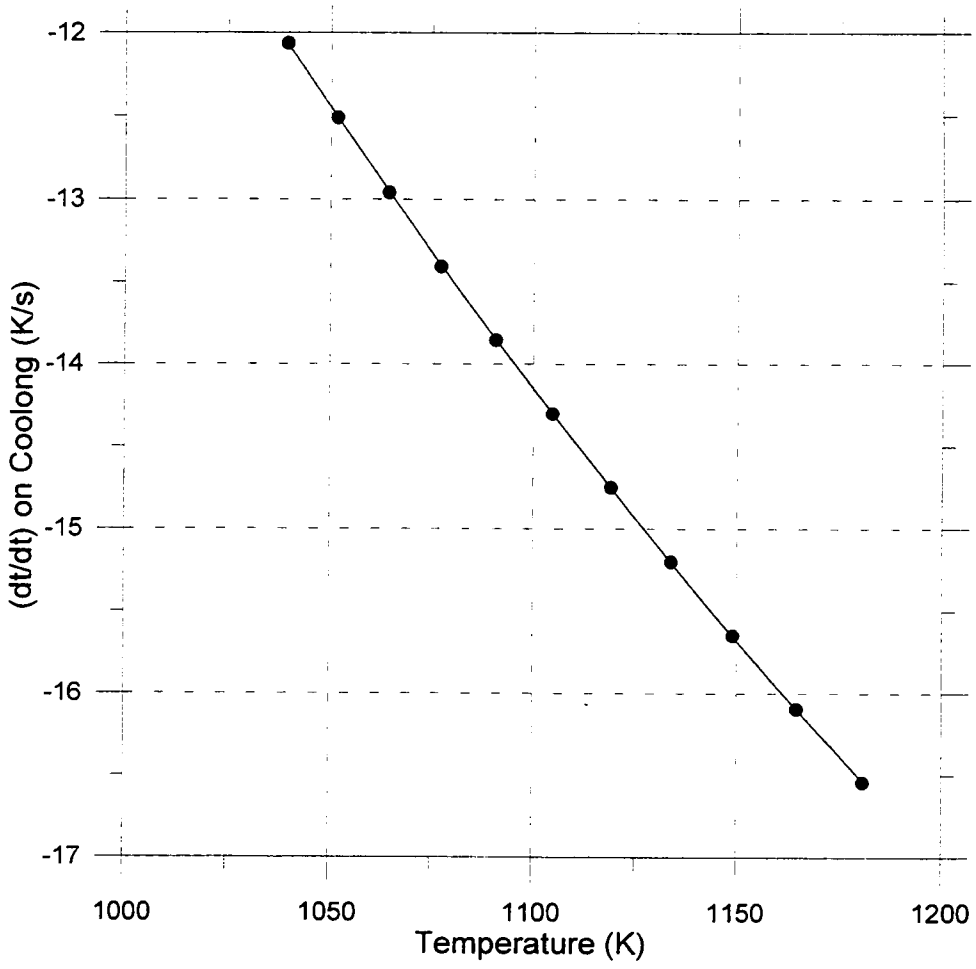

Figure 3.21 Cooling rate versus temperature for the medium-high temperature interval which resulted from the second degree polynomial fit temperature versus time on cooling curve.

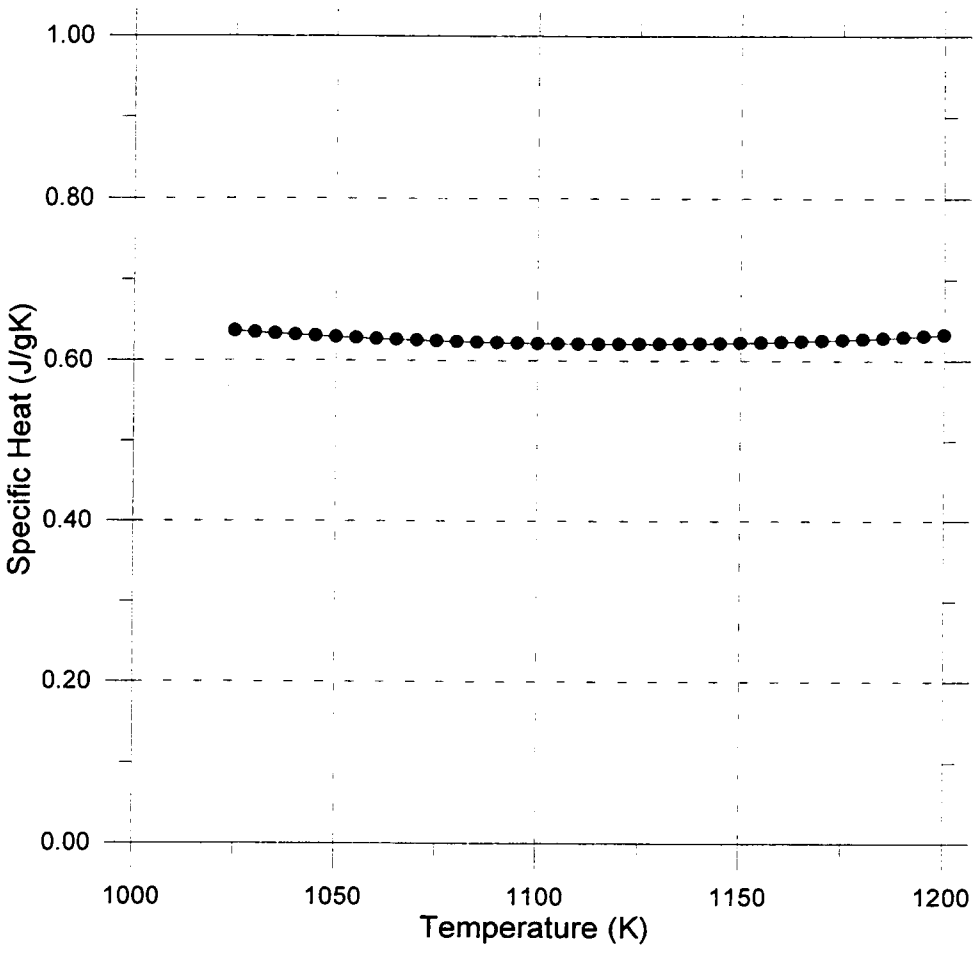

Figure 3.22 Specific heat versus temperature for the medium-high temperature interval resulting from a second degree polynomial fit of temperature versus time on cooling.

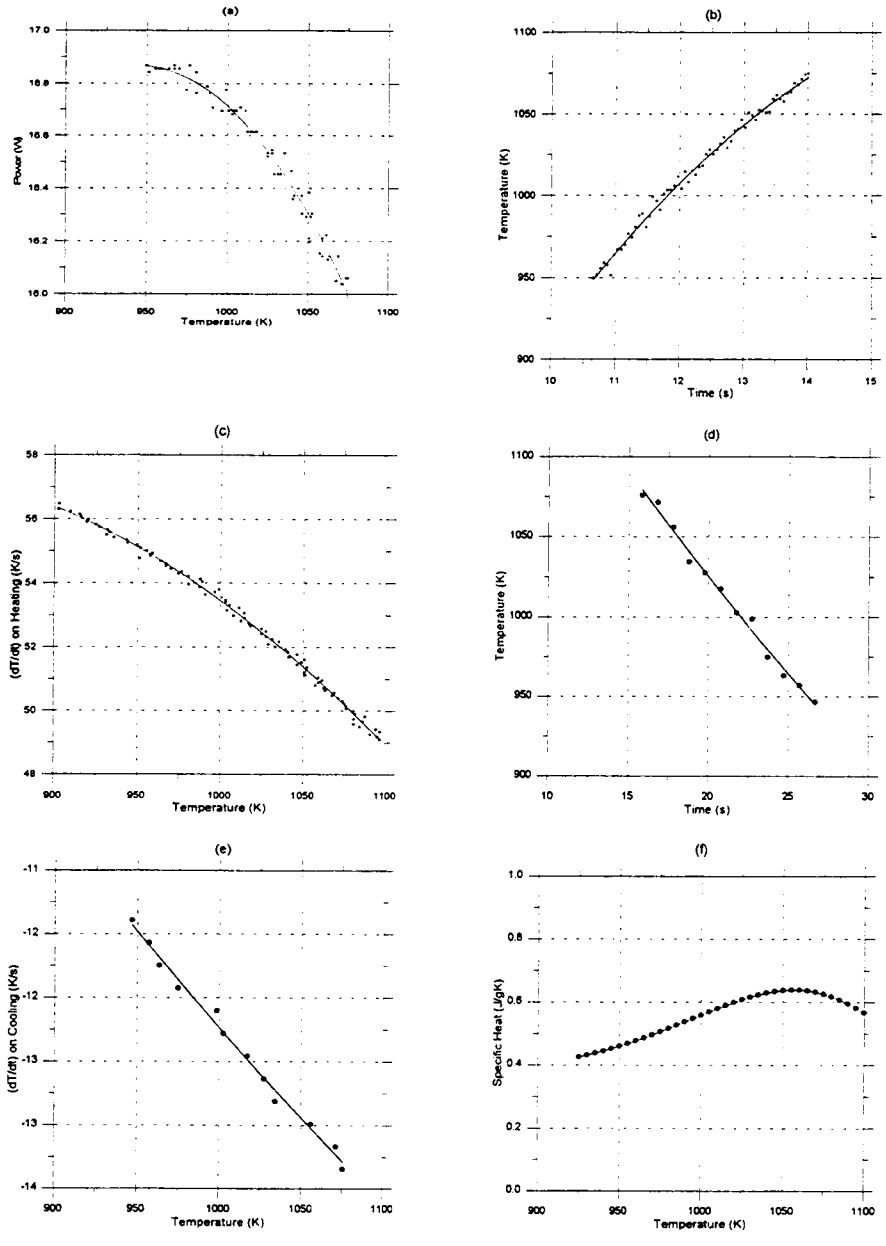

Figure 3.23 Data and polynomial curves used in the curve-fitting analysis for the medium-low temperature interval. a) P-T, b) T-t on heating, c) $(dT/dt)_h$-T, d) T-t on cooling, e) $(dT/dt)_c$-T, f) Cp versus T.

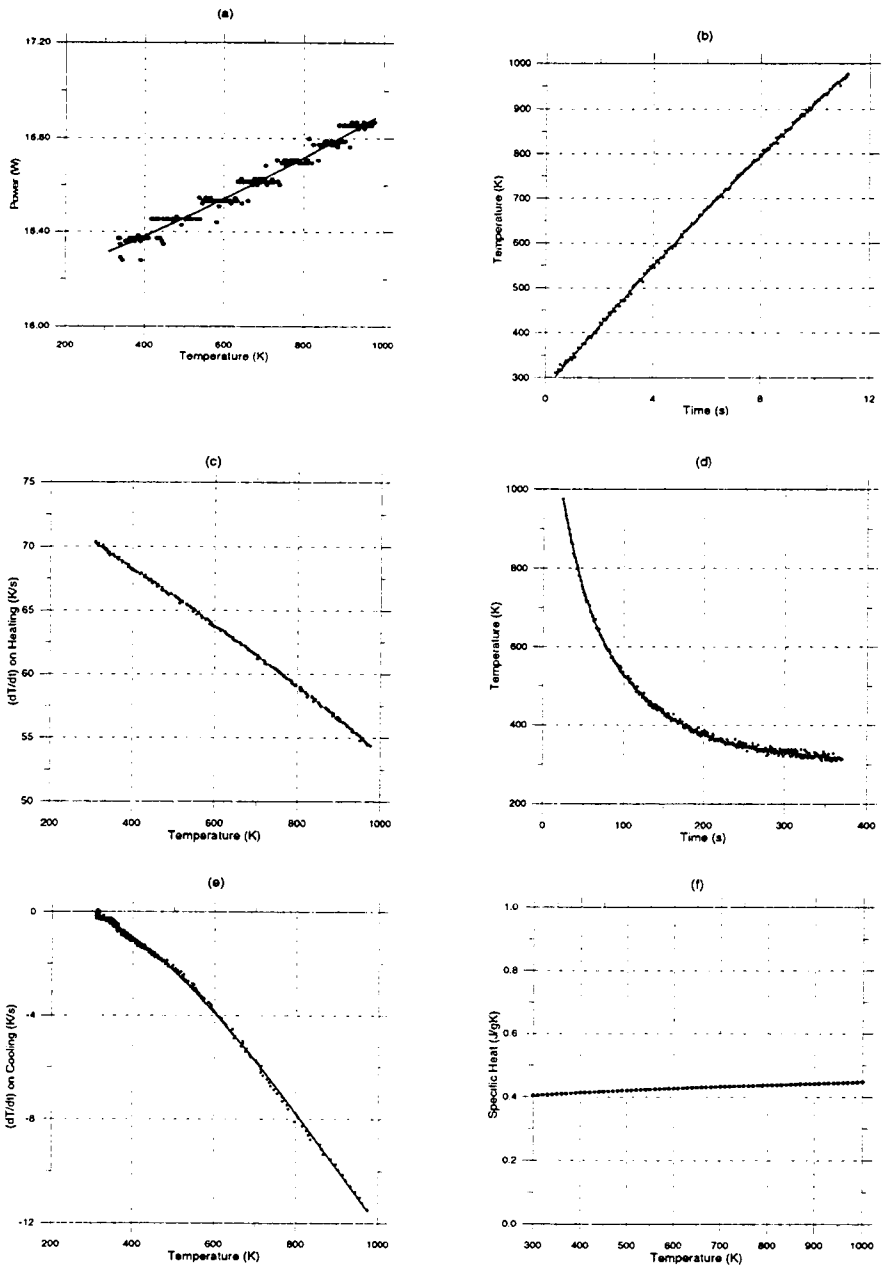

Figure 3.24 Data and polynomial curves used in the curve-fitting analysis for the low temperature interval. a) P-T, b) T-t on heating, c) $(dT/dt)_h$-T, d) T-t on cooling, e) $(dT/dt)_c$-T, f) Cp versus T.

Table 3.2 Polynomial coefficients for determining the specific heat in the high temperature range of the curve-fitting example. Data is from the shortened Ni_4Mo sample in the SRO α initial condition pulsed at 33 amps. Power is in watts, time is in seconds, and temperature is in degrees Kelvin.

	Best-Fit Curve				
Degree	P-T	T-t Heating	dT/dt -T Heating	T-t Cooling	dT/dt -T Cooling
0	29.4457	472.876	1375.67	1383.29	-2519.26
1	-0.0191937	54.3397	-3.32127	-30.8531	5.53968
2	6.15752×10^{-6}	-0.812408	0.00277497	1.49909	-0.00403785
3			-7.88104×10^{-7}	-0.0695161	9.6406×10^{-7}

range used for the calculation was 300 to 1000 K (allowing for some overlap), in 10 K increments. A sixth degree polynomial was used in the T-t on cooling curve to remove a deviation from the data at low temperature.

Figure 3.25 shows the specific heat data from all four temperature ranges. There is still overlaps and there still needs to be some smoothing analysis done on the curves. These types of decisions are discussed in Section 4.2.The results here were intended to illustrate the procedure that is performed for each pulse test to determin the specific heat.

3.3.4 Error Analysis

The overall performance of the calorimeter has shown to produce excellent results. One example of this was a strudy by Basak [139, 121] who determined the electrical resistivity and specific heat of pure nickel from 300 to 1200 K and the curie temperature. He compared his data to Kollie [124] and found the electrical resistivity to be within 1 % from 340 K to 1000 K. The Curie temperature obtained by Basak agreed with Kollie within 1 K. The specific heat data obtained by Basak agreed with Kollie agreed within 1% over most of the temperature range, and agreed within 2% just above the Curie temperature.

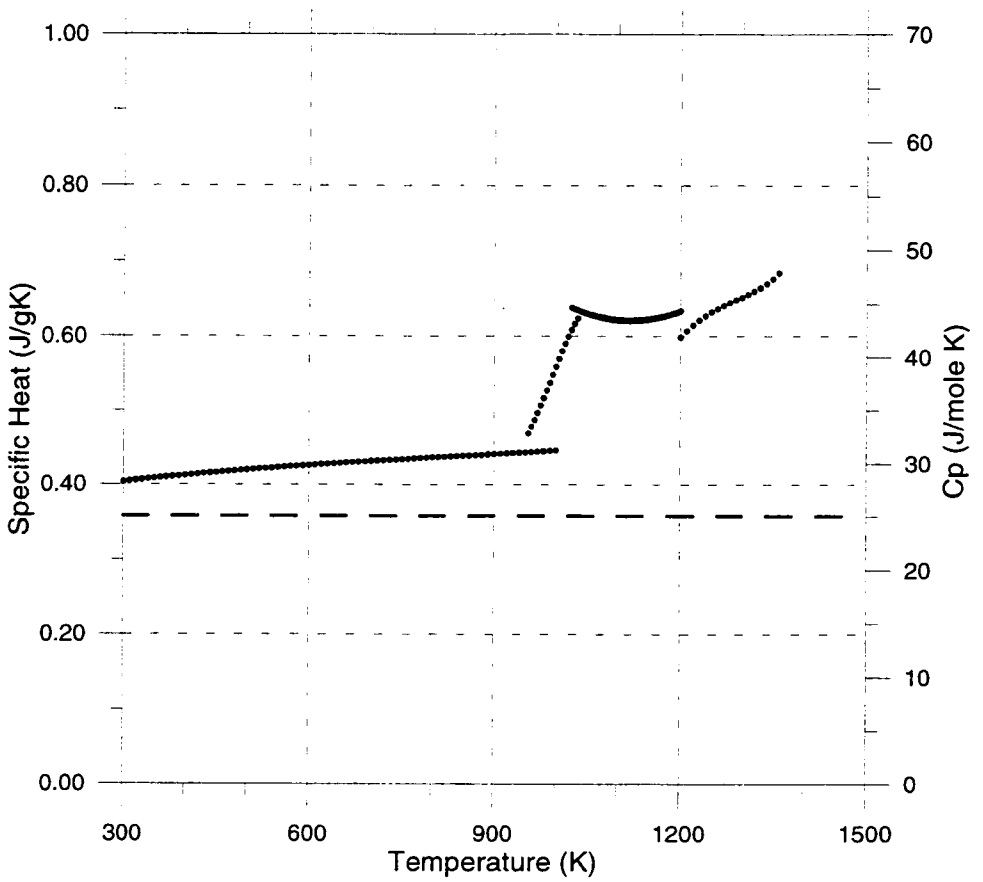

Figure 3.25 Specific heat versus temperature from the analysis of four different temperature intervals. Data is from test 9/30/98 #2 for Ni_4Mo in the Initial SRO α condition pulsed at 33 amps.

The error analysis in this thesis first presented error in the measured quantities, D, L, and d. Once the errors in D, L, and d were determined, their effects on the calculations of mass, electrical resistivity and specific heat were analyzed.

3.3.4.1 Diameter

The error in determination of the diameter D presents error in the calculation of the mass (and hence specific heat) and error in the electrical resistivity calculation. Another problem that compound the error in the specific heat and electrical resistivity calculations are that the value of D is a small number, and this value is squared when calculating mass and resistivity.

The actual D measurements are shown in Appendix F. The value used in the calculations for the shortened specimen was the average value of 20 measurements: 0.0693 inches (0.1760 cm). The standard deviation was found to be 0.0004 inches (0.0010 cm). A brief analysis similar to that of Basak [121] was done for D. If random error is assumed, then 2σ should contain about 95 % if the data, where σ is the standard deviation. Using the above value, 2σ x 100% = 0.20%. Since D is squared, 4σ x 100% = 0.4%. This is a rough estimate of the error in the mass and electrical resistivity due to error in the diameter.

3.3.4.2 Effective Length

Determination of the effective specimen length (voltage tap length) L involves two potential measurements and the length value of the knife-edge. The error for the voltage tap and knife-edge measurements from the Leeds and Northrup precision DVM was estimated from the standard deviations (see Appendix D). For example, a sample calculation using data from the shortend Ni_4Mo specimen showed that the average

potential across the voltage tap, E_T , was 13.508 mV and the average potential across the knife-edge, E_K, was 13.479 mV. Eight readins for each measurement were taken (four with the current in each direction). The standard deviations in the readings were $\Delta E_T \cong$ 0.006 mV and $\Delta E_K \cong$ 0.004 mV.

The knife-edge distance d_K was determined to be the average of the two extremes, from 1.0050 inches (2.5527 cm) to 1.0060 inches (2.5552 cm) [48]. The actual measurements were not provided, and so Δd_K was estimated to be half of the range, yielding a value of 0.0005 inches (0.0013) cm.

The error in L was then estimated from a propagation of errors analysis using the above values

$$\Delta L = \sqrt{\left(\frac{\partial L}{\partial E_T}\Delta E_T\right)^2 + \left(\frac{\partial L}{\partial E_K}\Delta E_K\right)^2 + \left(\frac{\partial L}{\partial d_K}\Delta d_K\right)^2} \qquad \textbf{(3.20)}$$

yielding $\Delta L \cong 0.0017$ cm (about 0.07 %) error in the length measurement. A sample calculation is shown in Appendix H.

3.3.4.3 Density

The value of density determined by FCC lattice parameter data was found to be 9.382 g/cm^3. FCC lattice parameter data from Brooks et al. [13] (Equation 2.1) is accurate to within 0.5 at% Mo. The range in lattice parameter of the 20.39 at% Mo sample was thus taken from 3.6050 to 3.6090 Å. The error in a, Δa, was then taken as half of the range. Thus a = 3.6070 ± 0.0020 Å, or about 0.06% error. It was assumed that the atomic numbers of nickel and molybdenum were exactly 58.69 and 95.94 grams/mole, respectively. The mass of atoms per unit cell was determined previously as m_c = 4.4028 x

10^{-22} g. The volume of the unit cell is $a^3 = 4.6929 \times 10^{-23}$ cm^3. A 0.06% error in one edge of the unit cell value, a, could lead to 0.18 % error in a^3, and hence a 0.18% error in density. Thus $\Delta d \cong 0.017$ g/cm^3

3.3.4.4 Effective Mass

The effective mass M is determined from the product of effective volume and density, d. The mass is

$$M = Vd = \left(\frac{\pi D^2 L}{4}\right)(d) \tag{3.21}$$

and the propagation of errors produces an error in mass of

$$\Delta M = \sqrt{\left(\frac{\partial M}{\partial D}\Delta D\right)^2 + \left(\frac{\partial M}{\partial L}\Delta L\right)^2 + \left(\frac{\partial M}{\partial d}\Delta d\right)^2} \tag{3.22}$$

where D = 0.1775 cm, ΔD = 0.0010 cm, L = 2.5393 cm, ΔL = 0.0017 cm, d = 9.382 g/cm^3, and Δd = 0.017 g/cm^3. Using these parameters, the error in effective mass was calculated (Appendix H) to be ΔM = 0.00674 g. This is about 1% of the effective mass.

3.3.4.5 Electrical Resistivity

Recall that the electrical resistivity is calculated from the expression

$$\rho = \frac{E}{I}\frac{\pi D^2}{4L} \tag{3.9}$$

In order to estimate the error in ρ, an estimate of the error in the channel 0 signal and channel 1 signal is needed. If ρ is determned as a function of temperature, then an error in the channel 2 signal is also needed. The error in the current, voltage, and temperature signals is limited by the resolution of the analog-to-digital converter and depends on the

gain of the amplifier for the particular channel. The A/D converter used was a 12-bit converter, and there are 2^{12} or 4096 counts. These counts are in a range of 10 V and so each count corresponds to 2.44 mV.

The percent error in the signal %ε, due to the resolution limitation is

$$\%\varepsilon = \frac{V/n}{V_S G}(100\%) \tag{3.23}$$

where V/n is the voltage per count (2.44 mV), V_S is the signal voltage, and G is the amplifier gain. The lowest voltage signals (and highest error) typically are of the order of 0.1V, 1V, and 0.001V for channels 0, 1, and 2, respectively. With the amplifer gains set to 10, 1, and 500 for the three channel signals, the error is about 0.25% for the current signal I, and voltage signal E, and about 0.5% in the thermal e.m.f. signal. The error in the temperature signal is more affected by voltage pick-up. The error in temperature is estimated to be ± 2 K in the final converted data [121] because the bare-wire thermocouples have not been calibrated.

The error in D and L were discussed above, and estimated to be 0.0010 cm and 0.0017 cm, respectively. The error in ρ can be estimated as

$$\Delta\rho = \sqrt{\left(\frac{\partial\rho}{\partial E}\Delta E\right)^2 + \left(\frac{\partial\rho}{\partial I}\Delta I\right)^2 + \left(\frac{\partial\rho}{\partial D}\Delta D\right)^2 + \left(\frac{\partial\rho}{\partial L}\Delta L\right)^2} \tag{3.24}$$

The typical ranges of ρ that were found in the Ni_4Mo sample were from about 80 μΩ cm to about 155 μΩ cm. A sample calculation using data from the pulsed Ni_4Mo on the α initial condition at 35 amps was performed (Appendix H) showed $\Delta\rho \cong \pm 1.8$ μΩ cm at 150 μΩ cm (about 1.2 %).

3.3.4.6 Specific Heat

The error in specific heat was primarily due to errors in determining the mass, current, and voltage. Error also occurs due to the determination of $(dT/dt)_h$ The temperature error is also present, as mentioned in the section on error in electrical resistivity. The error in determining the heating and cooling rates was investigated by Basak [47] and found to be negligeable. The error in Cp was estimated by

$$\Delta Cp = \sqrt{\left(\frac{\partial Cp}{\partial M}\Delta M\right)^2 + \left(\frac{\partial Cp}{\partial I}\Delta I\right)^2 + \left(\frac{\partial Cp}{\partial E}\Delta E\right)^2} \tag{3.25}$$

A sample calculation (Appendix H) using a typical value of Cp of 0.45 J/gK (29.6 J/mole K) found the error in Cp to be about 1.2 % (0.005 J/gK or 0.35 J/mole K).

Chapter 4. Results and Discussion

4.1 Electrical Resistivity

Several tests were performed on the Ni_4Mo specimen. The original total length of the specimen was about 22 cm, while the effective length was about 4.4 cm. A pulse test using about 32 A (7/15/98, #4) was done while the specimen was in the SRO α initial condition. The condition was known to be SRO α because the previous pulse test was done on the specimen to above Tc (1141 K) and allowed to cool naturally in the calorimeter. This natural cooling is rapid enough to obtain metastable α. The resulting structure from 7/15/98, #4 was also SRO α, and so a reproducibility test was done by pulsing the sample again (7/15/98, #5) at about 32 amps. The results of the electrical resistivity versus time data are shown in Figure 4.1 The resulting structure from 7/15/98, #5 was also SRO α.

The electrical resistivity increases approximately linearly from 147 μΩ cm at 300 K to about 152 μΩ cm at 950 K. The increase is attributed to the increase in SRO clusters with increased temperature. There is then a sharp decrease in resistivity from 950 K to 1400 K. This decrease is due to the progressive change from SRO to LRO. For further discussion of the shape of the electrical resistivity curves, see Section 2.4.

Next, an isothermal test (7/24/98, #1) was performed to transform the sample from SRO α to LRO β. A TTT curve of Brooks et al. [13] based on electrical resistivity measurements puts the nose of the curve at about 750 °C. Thus this was the temperature selected for the isothermal test. The specimen was heated from room temperature to about 900°C and held there for about 5 minutes. Then the temperature was dropped to about 750 °C and held there for about 30 minutes. The specimen was allowed to cool to room

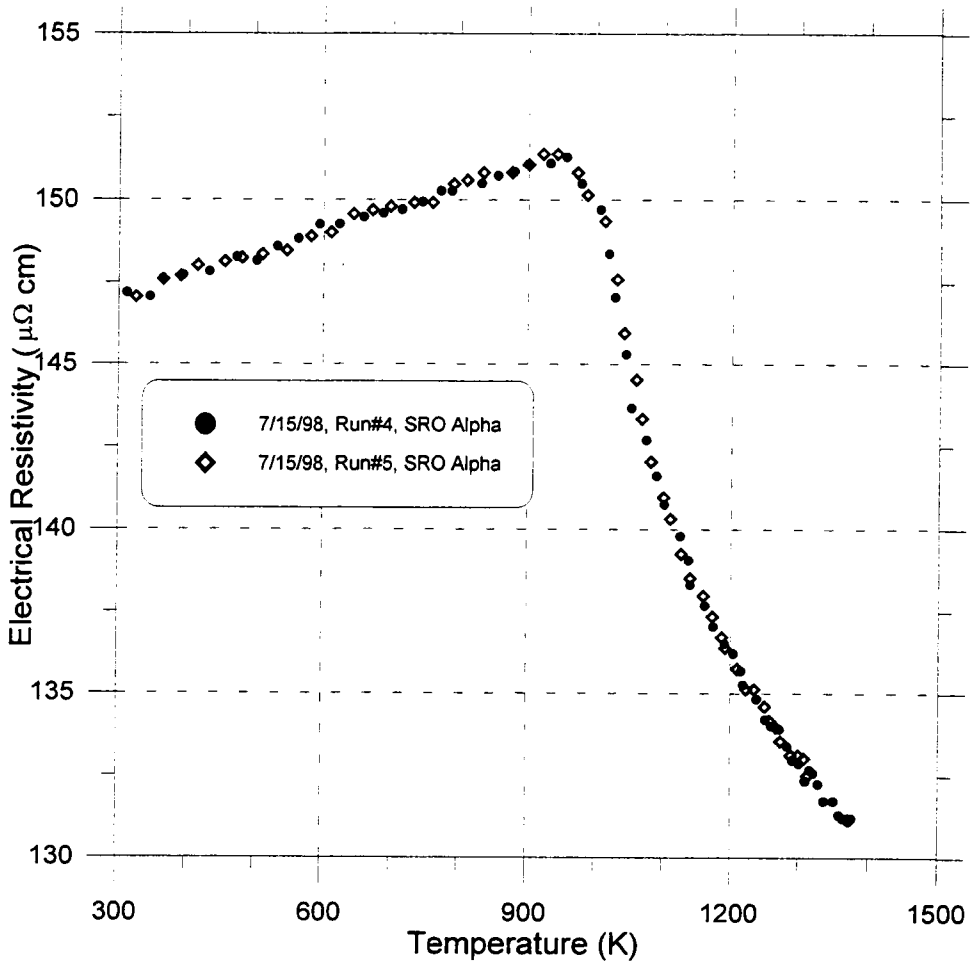

Figure 4.1 Electrical resistivity as a function of temperature for the SRO α initial condition pulsed at 33 amps. The current used in both tests was about the same. The two runs demonstrate the reproducibility of the data from the calorimeter.

temperature in the calorimeter. No data were taken during this last cool down stage. The isothermal data for this test is shown in Figure 4.2. The time-temperature data is in Figure 4.2a, and the electrical resistivity-time data is in Figure 4.2b. The resulting structure was assumed to be completely transformed to the LRO β phase. This assumption was based on the way the electrical resistivity data leveled off past 30 minutes test time in Figure 4.2b. It is difficult to determine if the curve has completely leveled off. A later test pulse the specimen in the LRO β initial condition showed that the electrical resistivity of β that corresponded to the 750 °C temperature was roughly 127 μΩ cm. This corresponded closely to the level-off region shown in the isothermal electrical resistivity data.

Once the sample was transformed to LRO β, it was pulsed at about 35 A for 30 s, and then allowed to cool naturally in the calorimeter. The electrical resistivity data for this test (7/29/98, #1) are shown in Figure 4.3. To check the reproducibility, a second pulse with the same parameters was done following an isothermal transformation to β. These data are also shown in Figure 4.3. The two runs agree very closely. The sharp drop at 140 μΩ cm corresponds very closely to the critical temperature of 1141 K. The general mechanisms leading to this type of electrical resistivity behavior are discussed in Section 2.4.2.

A very slow heating rate (about 45 K/min. on the average) test was done on the specimen using the ramp-up portion of the isothermal program (8/7/98 #2). The specimen was in the SRO α initial condition. The electrical resistivity versus temperature data are shown in Figure 4.4. This test was done to duplicate the slow heating rate results of Lei The transformation begins at about 8 minutes into the test where there is a sharp drop in ρ. [58] (See Figure 2.21). The dip in the curve corresponds to the specimen reverting

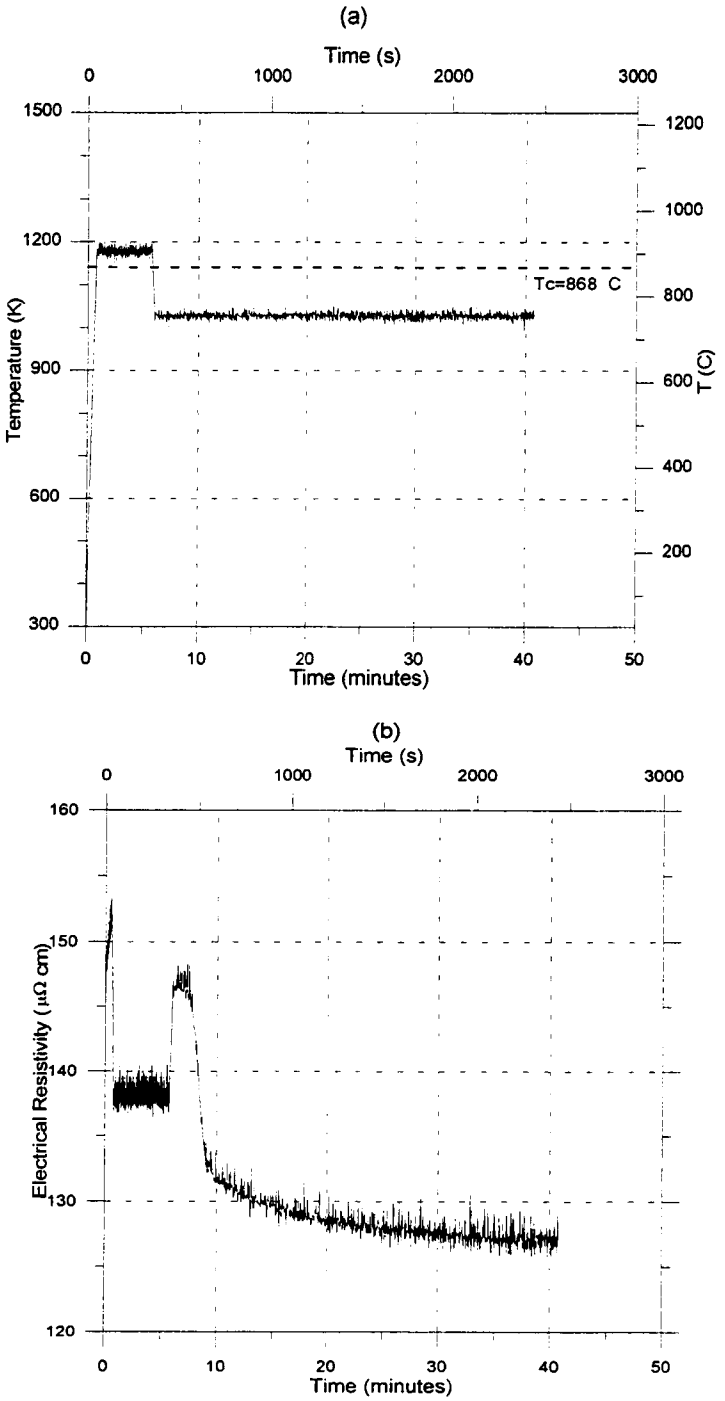

Figure 4.2 Isothermal transformation of Ni_4Mo from SRO α to LRO β at 750 °C. a) is a time-temperature history of the test. b) is the corresponding electrical resistivity during the test.

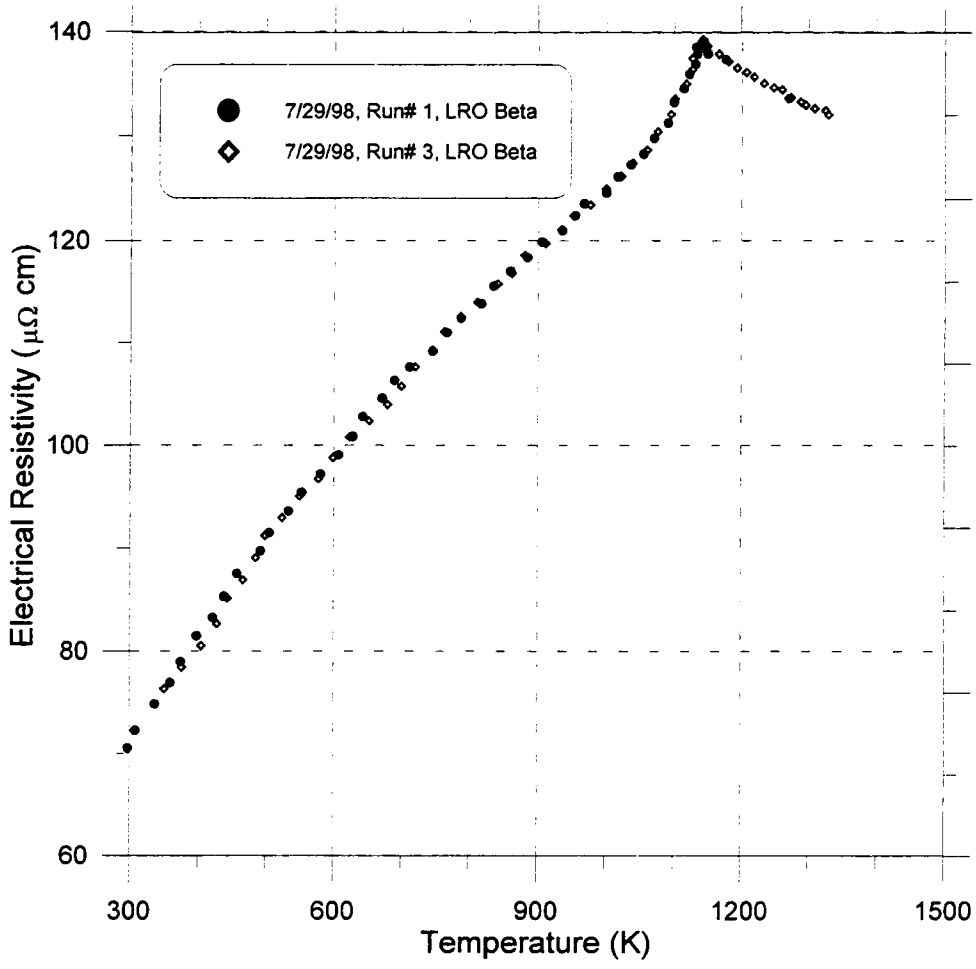

Figure 4.3 Electrical resistivity versus temperature for the LRO β initial condition pulsed at 33 amps. The specimen is in the LRO β condition from 300 to 1141 K and in the SRO α initial condition above 1141 K.

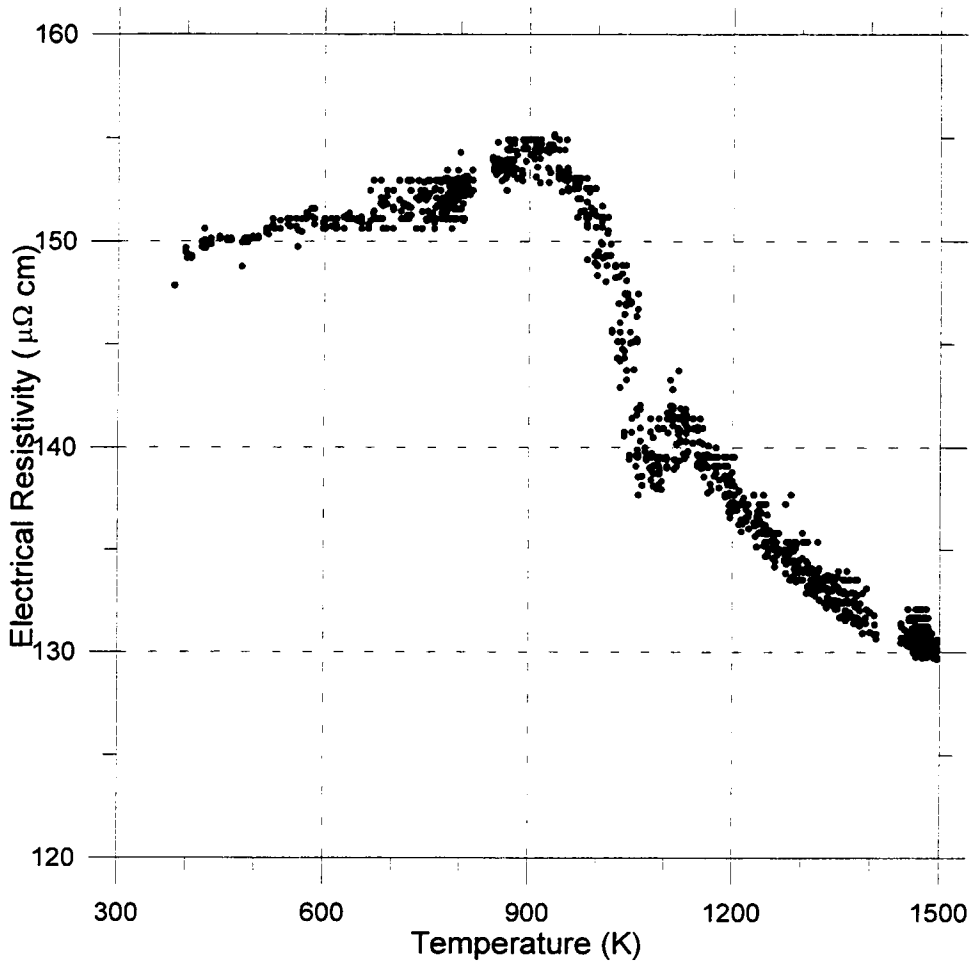

Figure 4.4 Electrical resistivity versus temperature of SRO α at very slow heating rates. The dip in the curve just prior to 1141 K is due to the sample transforming to the equilibrium β phase. Beyond 1141 K, the sample is in the equilibrium α phase.

back to the equilibrium β structure just below the critical temperature.

One other check on the reproducibility of the data and the system is to pulse the sample with the current in both directions through the sample. This was done on the specimen in the SRO α condition. Electrical resistivity data for the two runs (8/8/98, #3 and 8/8/98, #4) are shown in Figure 4.5. The actual current used in both cases was about 33 A.

The maximum current allowed on the long specimen was about 33 A. This limitation is due to the 6 V limitation of the power supply in conjunction with the overall resistance of the sample and the rest of the calorimeter system (totaling about 0.17 Ω). An estimate of the maximum current from Ohm's law predicts:

$$I = \frac{E}{R} = \frac{6V}{0.17\Omega} = 35A \qquad \textbf{(4.1)}$$

This estimate corresponds closely to the actual limit of 33 amps.

In order to increase the current and heating rate to further suppress the transformation, it was decided to reduce the length of the specimen. The specimen made up the majority of the total resistance (0.13 Ω). The 20.5 cm specimen was cut into three sections using an abrasive cut-off wheel. The three sections were each about 7.25 cm long. The first section that was pulsed was the middle section. It was pulsed to too high a temperature and was destroyed. The data presented in this section is from one of the end sections.

Several pulses were done gradually increasing the pulse current and time to work up to a safe high heating rate without destroying the sample. A range of 62 amps for about 8 seconds provided suitable data for the SRO α initial condition. A pulse with these parameters was done and the specimen was allowed to cool down naturally in the

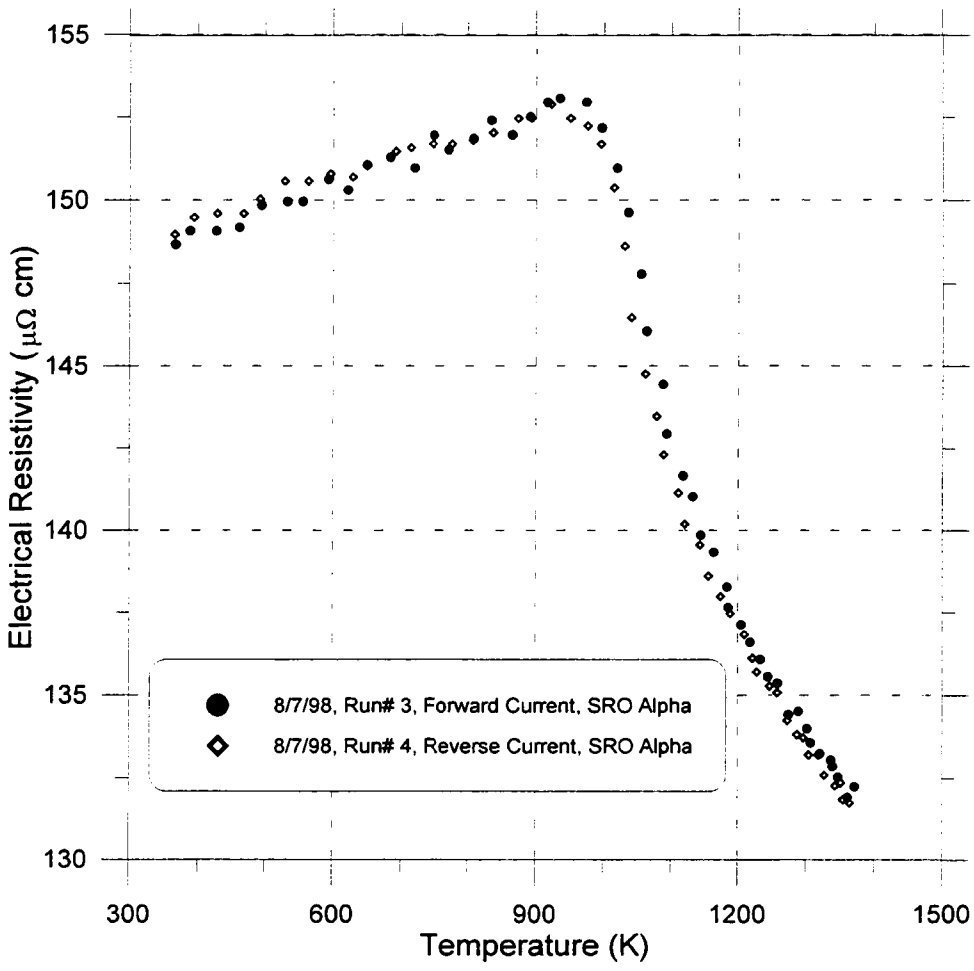

Figure 4.5 Electrical resistivity versus temperature data for the current in both directions obtained from the long specimen. The initial condition of the specimen was SRO α.

calorimeter from above Tc. Another pulse was done with these parameters for the final data test on the initial α shortened sample (9/25/98, #3). The electrical resistivity versus temperature data are shown in Figure 4.6. The resulting structure from this test was SRO α.

Another test was then done on the initial SRO α phase shortened specimen. A current value was chosen similar to the current that was used on the long specimen (33 A). The electrical resistivity versus temperature data for this test (9/30/98,#2) are also shown in Figure 4.6.

The next test that was done on the shortened specimen with the current reversed from the high current test of 9/25/98 #3. The initial condition was SRO α. Data for these two tests (9/25/98, #3 and 10/9/98, #1) are shown in Figure 4.7.

The shortened sample was then isothermally transformed (10/13/98, #2) to beta. Verification of this is shown by the electrical resistivity versus temperature data in Figure 4.8.

The specimen in the LRO β state was then pulsed at 68 amps for about 8 seconds (10/14/98, #1). Electrical resistivity versus temperature data for the LRO initial condition are shown in Figure 4.9.

The sample was then isothermally transformed to β. There were some problems with the isothermal tests at this point. There was a lot of noise in temperature, and the isothermal hold range actually exceeded Tc on one test, and hence a completed transformation was not obtained. A lower isothermal hold range (725 °C) was thus used to transform the specimen to β. The transformation time was also increased. Resistivity-temperature data for the final isothermal test (10/14/98, #4 data not shown) leveled off

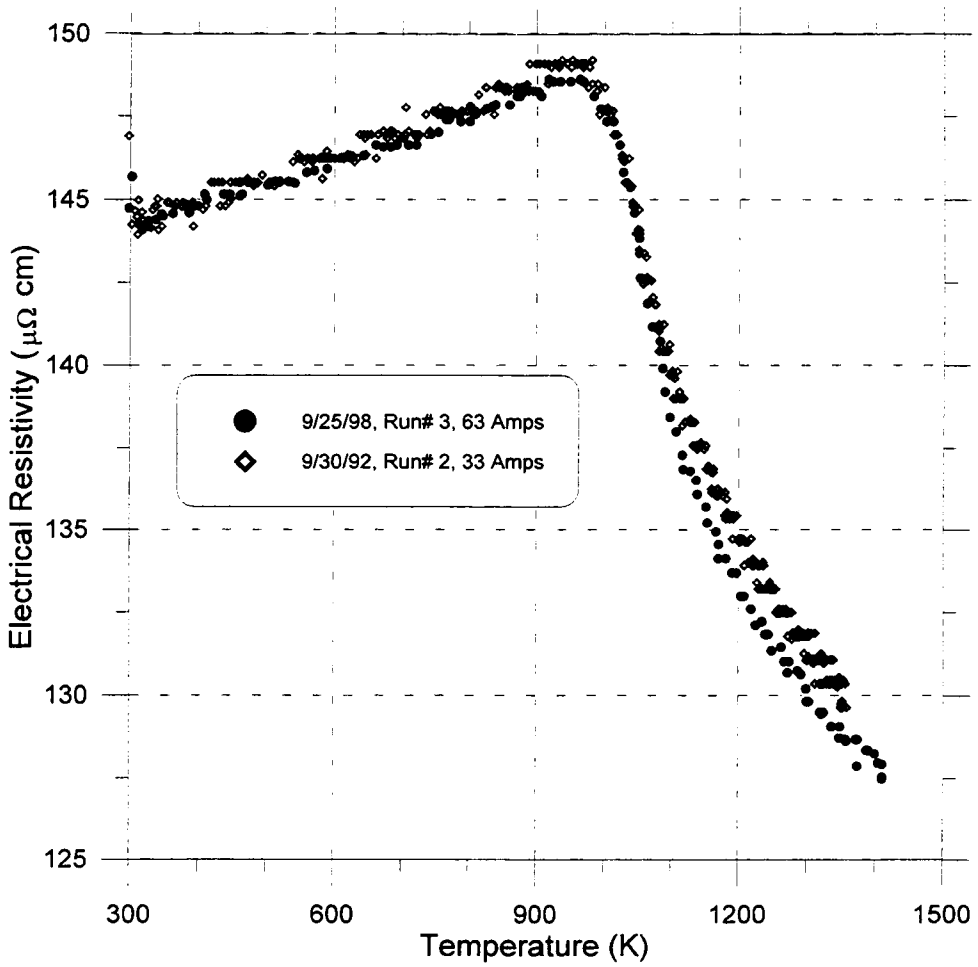

Figure 4.6 Electrical resistivity versus temperature of SRO α at two different pulse currents on the shortened specimen.

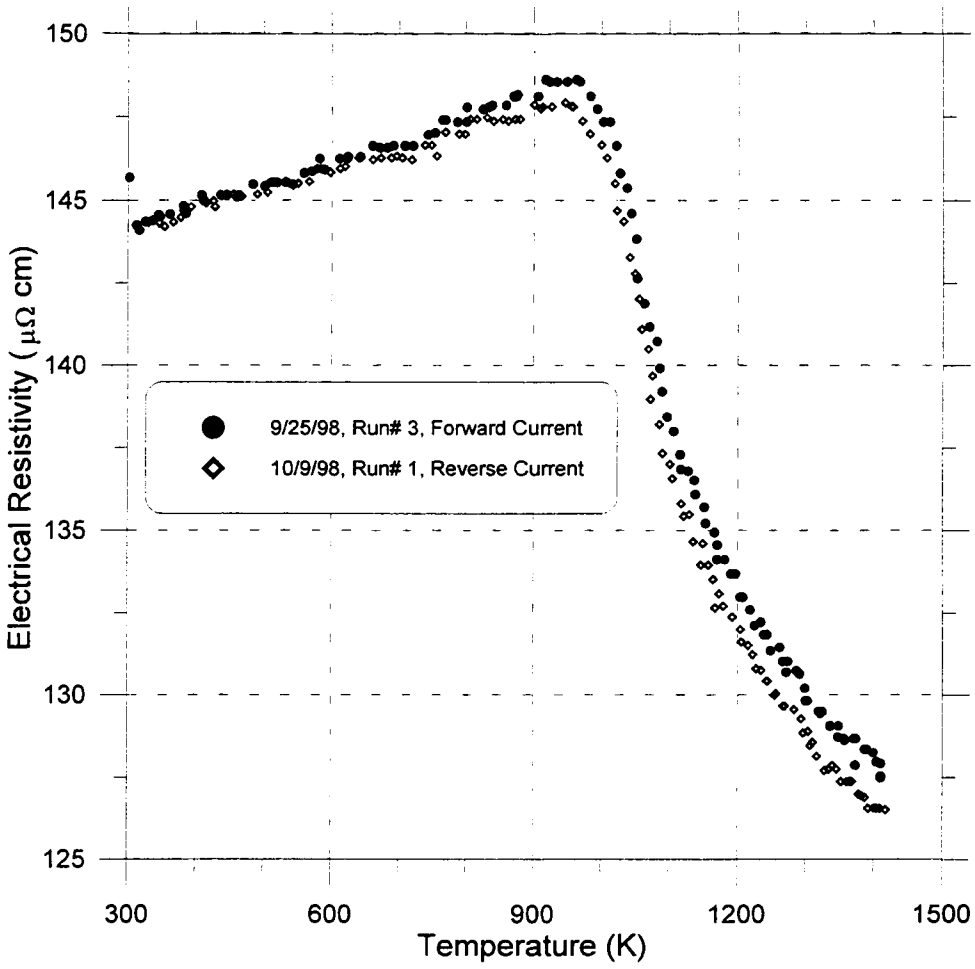

Figure 4.7 Electrical resistivity versus temperature data for the current in both directions obtained from the shortened specimen. The initial condition of the specimen was SRO α.

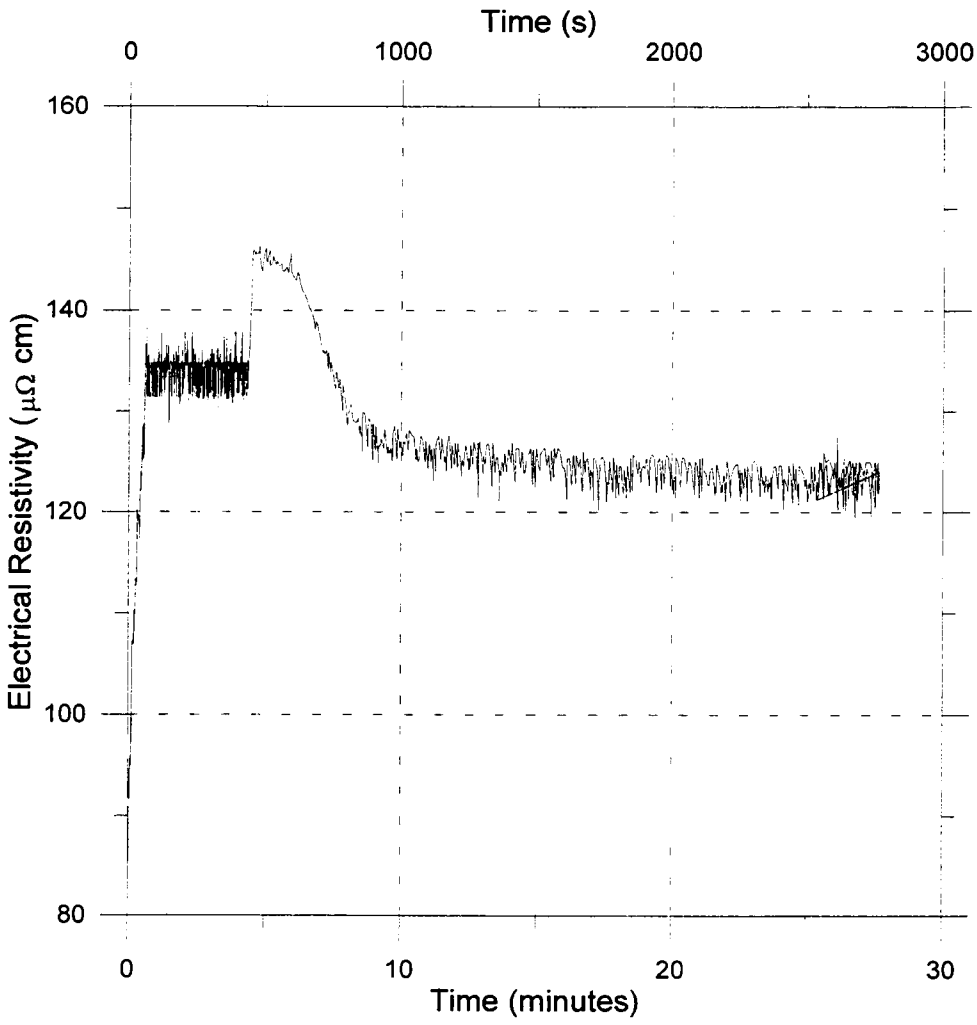

Figure 4.8 Isothermal transformation from SRO α to LRO β on the shortened specimen prior to pulsing LRO β at high current. The resistivity approaching a relatively constant value is an indication that the transformation is complete.

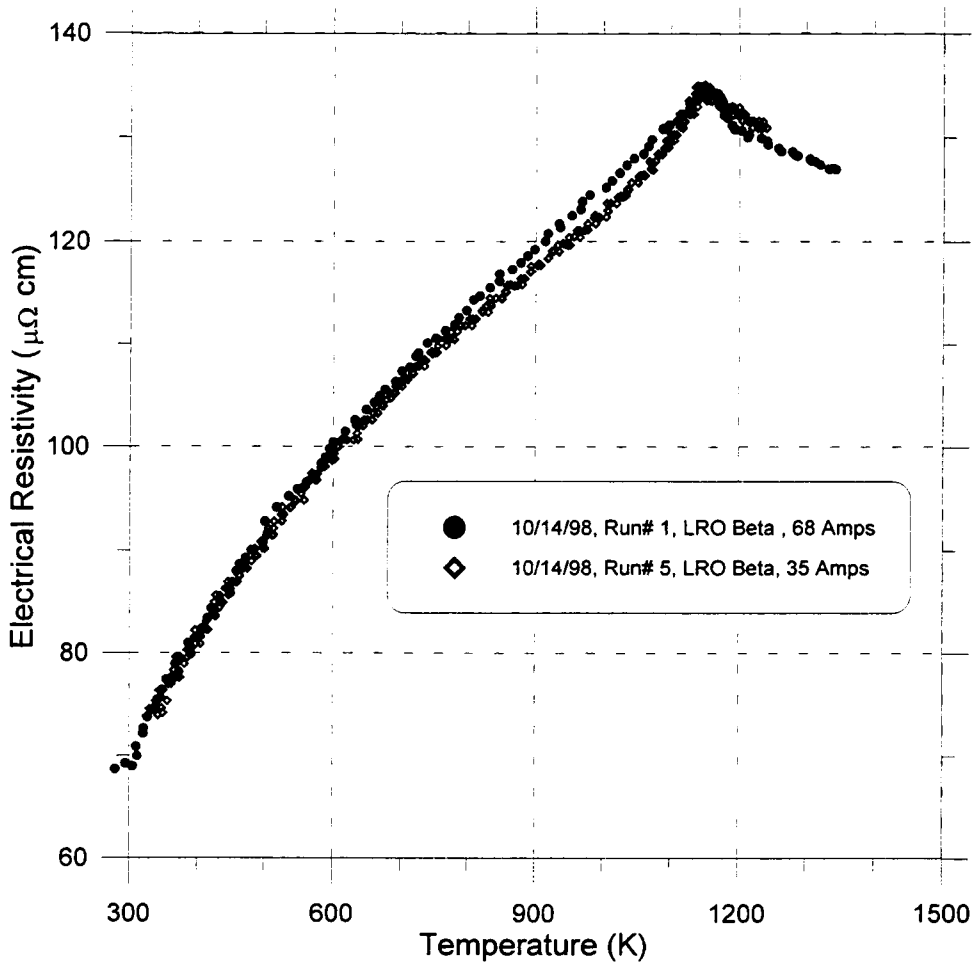

Figure 4.9 Electrical resistivity versus temperature of the shortened specimen in the LRO β initial condition at two different pulse currents. There is some splitting between the two heating rates from 700 K to the critical temperature.

Table 4.1 Summary of test parameters used for pulse-heating the Ni_4Mo alloy.

Specimen I.D.	Pulse Current (A)	Pulse Time (s)	Specimen Length
7/15/98, #4	32	25	Long
7/15/98, #5	32	25	Long
7/24/98, #1	N/A	N/A	Long
7/29/98, #1	35	25	Long
7/29/98, #3	34	30	Long
8/7/98, #2	N/A	N/A	Long
8/8/98, #3	33	25	Long
8/8/98, #4	33	25	Long
9/25/98, #3	62	7	Short
10/9/98, #1	62	7	Short
10/13/98, #2	N/A	N/A	Short
10/14/98, #1	68	7	Short
10/14/98, #5	36	24	Short

similarly to that in Figure 4.8.

The specimen in the LRO β condition was then pulsed at a lower current. The current selected (36 A) was similar to the current used in the long specimen tests. In this case, the pulse time was about 24 s. The data from this test (10/14/98, #5) are shown in Figure 4.9 with the high current data. A summary of the test parameters discussed in Section 4.1 is shown in Table 4.1.

Figure 4.10 contrasts the heating rates and initial conditions of the shortened specimen. A comparison of this data to Basak's [121] data was done and the data agree very closely. Basak's pulse-heating data for SRO α (Curve 2) and for LRO β (Curve 1) is shown in Figure 2.19. The heating rate from 33 amps and from 62 amps on the SRO α did not seem to have any affect on the electrical resistivity data. There is a minor splitting of the LRO β curves between 700 K and 1100 K. This has not been explained. Above 1141 K, all four curve closely agree, and should all be in the SRO α condition.

A comparison of the effect of specimen length on the electrical resistivity is

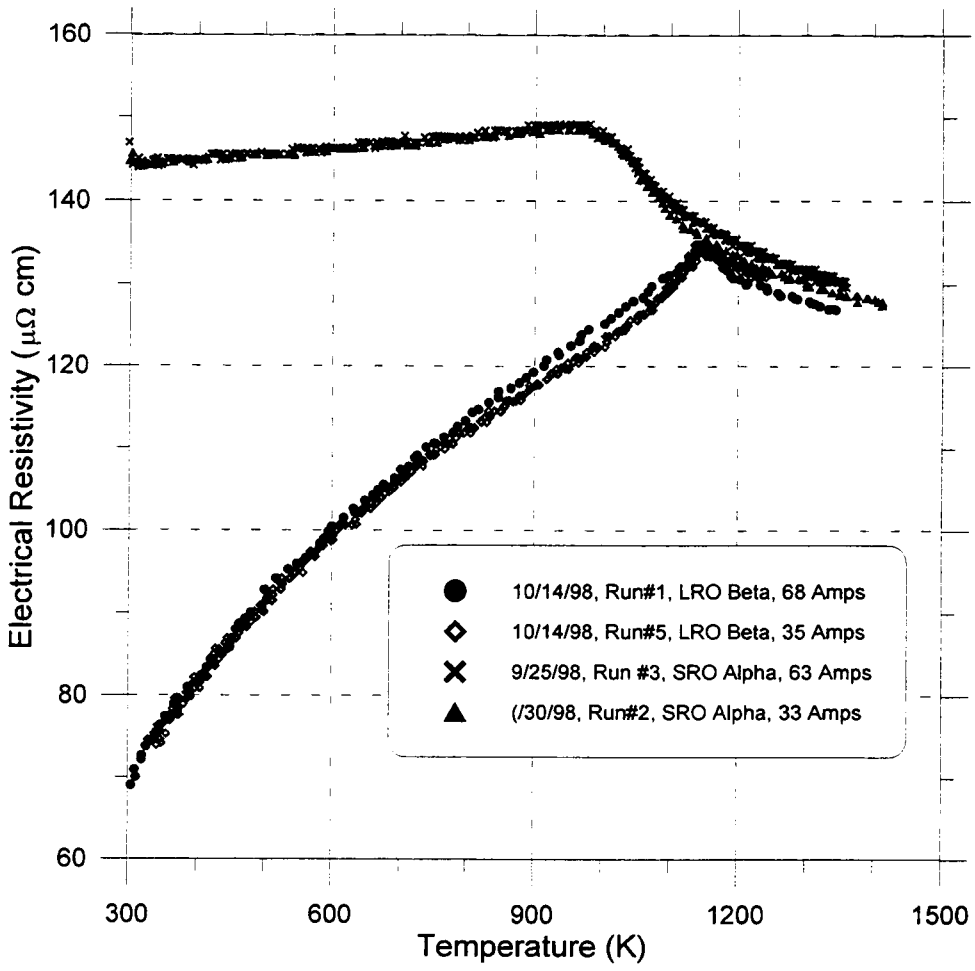

Figure 4.10 Electrical resistivity versus temperature of Ni_4Mo in the SRO α and LRO β initial conditions pulsed at low and at high currents.

shown in Figure 4.11. The data from the SRO α initial condition is shown in Figure 4.11a, and the LRO β data is shown in Figure 4.11b. Both initial conditions show a slight vertical shift, but this is thought to be caused by error in effective length calculation and diameter measurement. The error is assumed to be a vertical shift since the shape of the curves agree closely at each temperature.

4.2 Specific Heat

The specific heat data from the above mentioned tests were determined using the procedures discussed in Chapter 3. All of the raw data were obtained using the value of 9.360 g/cm^3 for the density.

The initially determined specific heat data are presented in Figures 4.12-4.17. It is shown by first plotting the various temperature range sections that resulted from the typical procedures, and then by smoothing the data into a continuous curve. This is done by determining a polynomial best-fit line, and then plotting the polynomial.

Figure 4.12 is the specific heat data for the long section SRO initial condition (7/15/98, #5). Figure 4.13 is specific heat data for the long section initial LRO β test (7/29/98, #3). The high current specific heat data for the shortened section in the SRO α initial condition are shown in Figure 4.14 (Test 9/25/98, #3). The low current data for the same condition are shown in Figure 4.15 (Test 9/30/98, #2). Figure 4.16 shows data for the high current LRO β test (10/14/98, #1) and Figure 4.17 shows data for the low current LRO β test (10/14/98, #5). Figure 4.18 is a plot of specific heat for SRO α for the shortened specimen at two heating rates. The 62 A pulse (9/25/98, Run #3) heated the specimen at about 220 K/s up to about 1000 K and then about 120 K/s from 1000 to 1400 K. The 33 A pulse heated the sample at about 60 K/s up to about 1000 K and then heated

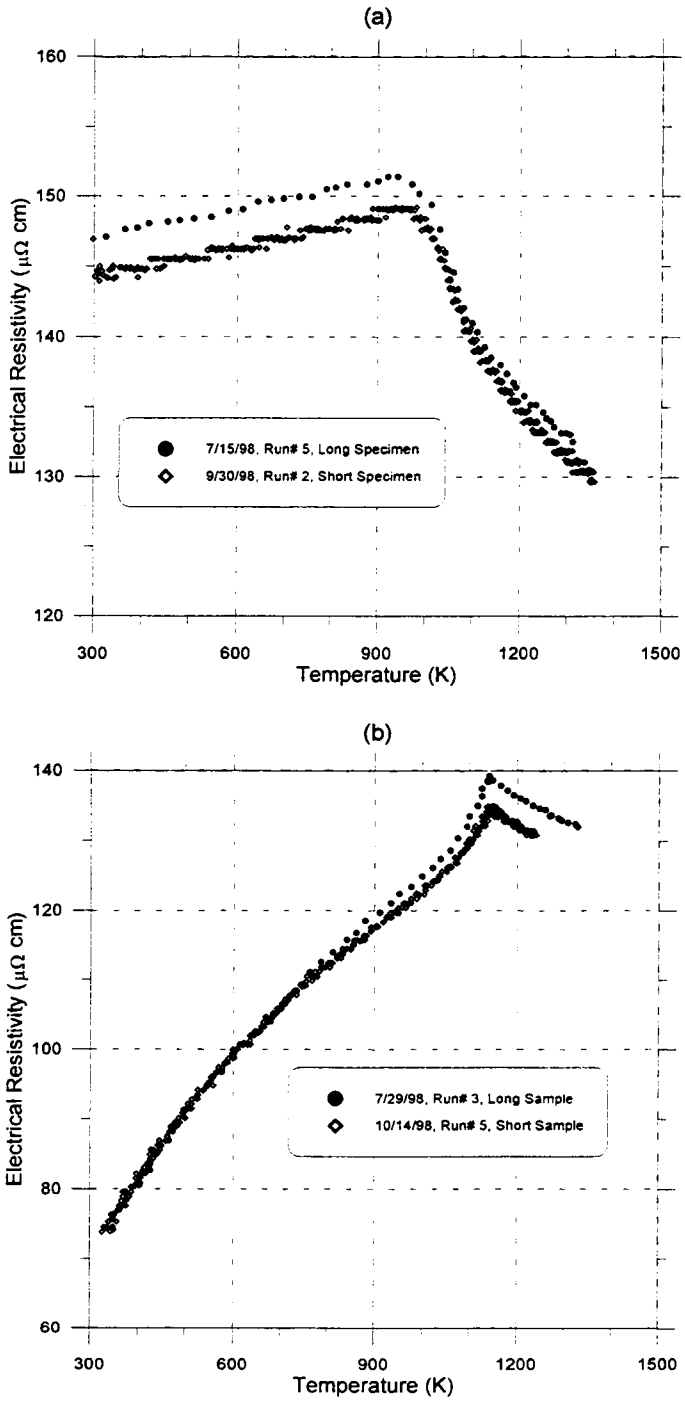

Figure 4.11 Electrical resistivity versus temperature of a) SRO α and b) LRO β on two different specimen lengths.

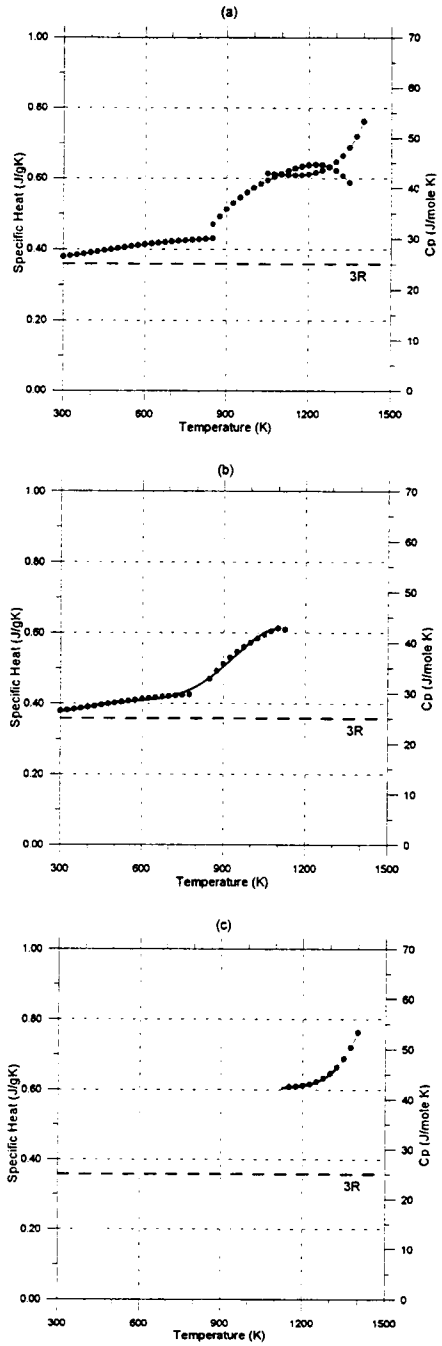

Figure 4.12 Specific heat versus temperature for the SRO α initial condition obtained from pulsing the long specimen. Data was obtained at about a 33 amp pulse. a) shows the three discontinuous segments that were obtained from initial curve-fitting process. b) shows a best-fit polynomial of the low temperature specific heat data. c) shows a best-fit polynomial of the high temperature data.

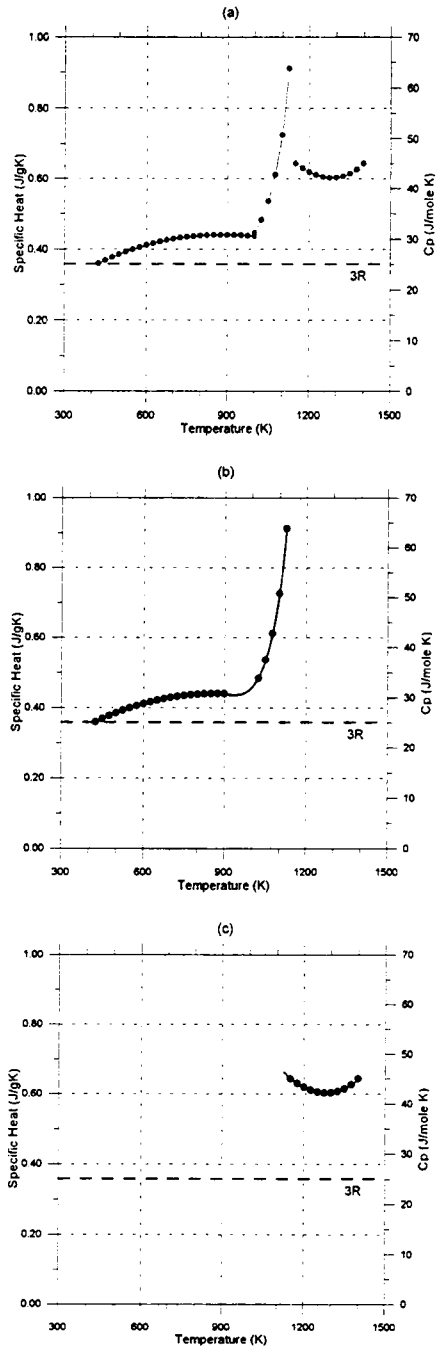

Figure 4.13 Specific heat versus temperature for the LRO β initial condition obtained from pulsing the long specimen. Data was obtained at about a 33 amp pulse. a) shows the three discontinuous segments that were obtained from initial curve-fitting process. b) shows a best-fit polynomial of the low temperature specific heat data. c) shows a best-fit polynomial of the high temperature data.

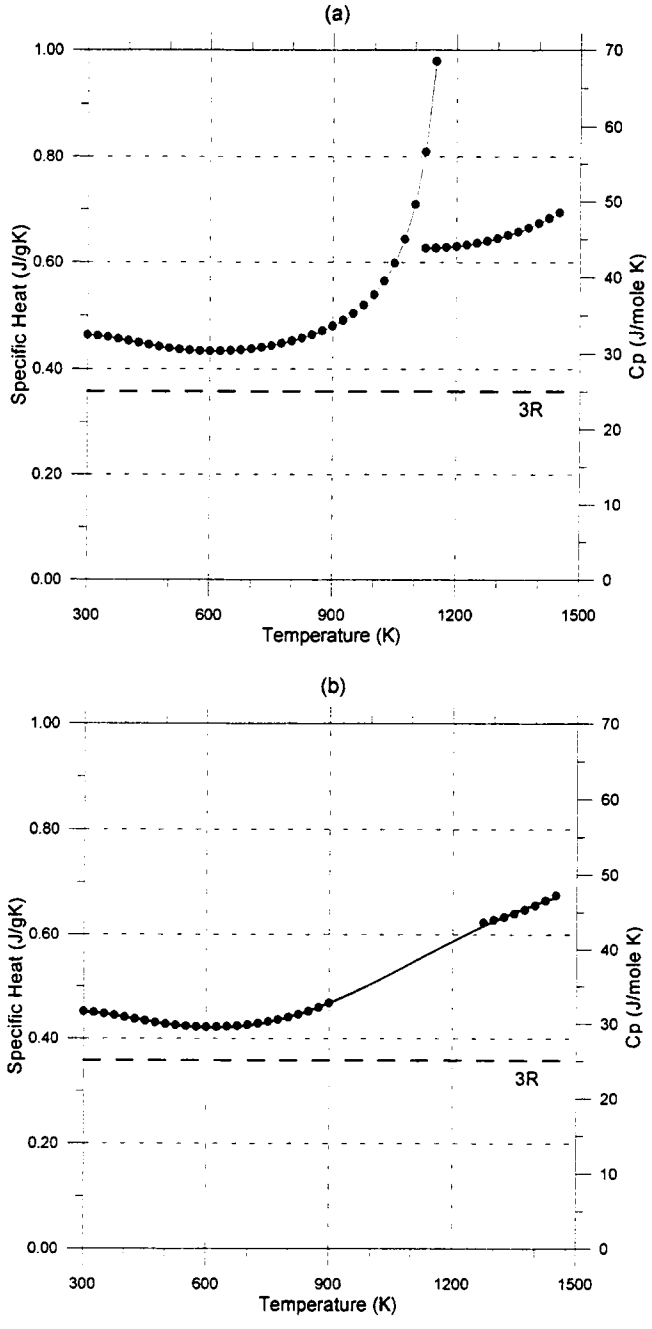

Figure 4.14 Specific heat versus temperature for the SRO α initial condition obtained from pulsing the shortened specimen at high current. Data was obtained at about a 63 amp pulse. a) shows the two discontinuous segments that were obtained from initial curve-fitting process. b) shows a best-fit polynomial of the specific heat data.

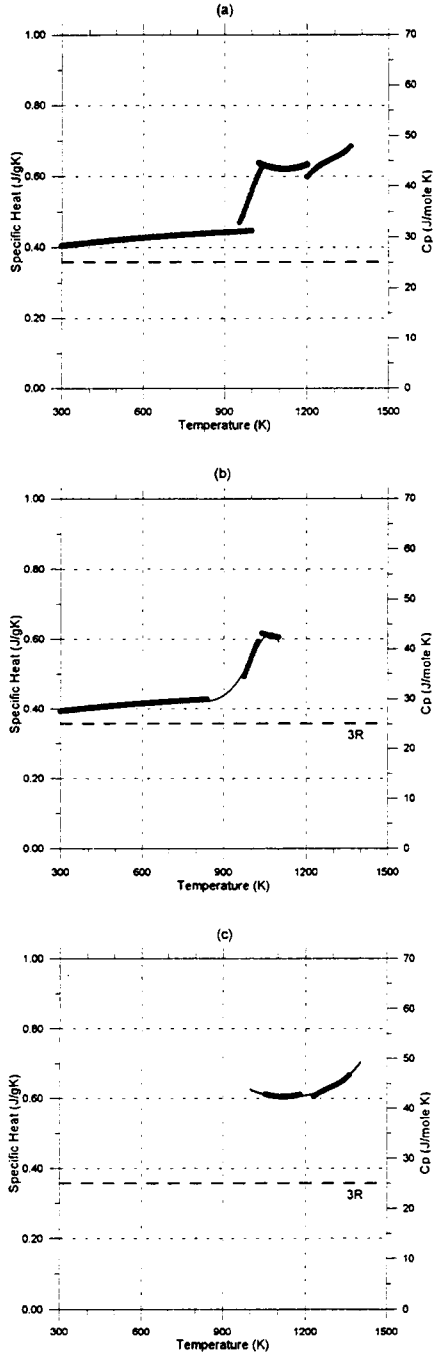

Figure 4.15 Specific heat versus temperature for the SRO α initial condition obtained from pulsing the shortened specimen at low current. Data was obtained at about a 33 amp pulse. a) shows the four discontinuous segments that were obtained from initial curve-fitting process. b) shows a best-fit polynomial of the low temperature specific heat data. c) shows a best-fit polynomial of the high temperature data.

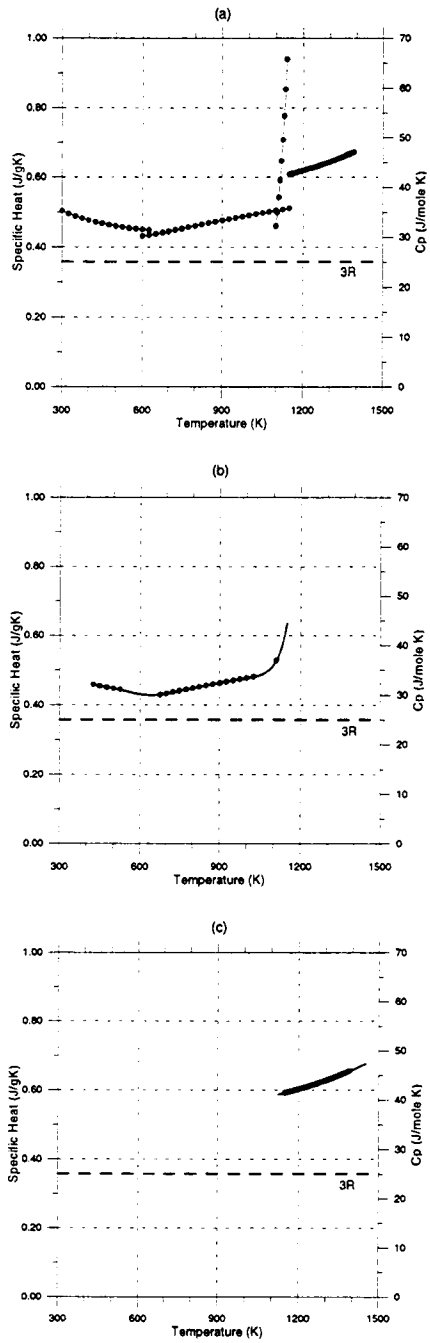

Figure 4.16 Specific heat versus temperature for the LRO β initial condition obtained from pulsing the shortened specimen at high current. Data was obtained at about a 68 amp pulse. a) shows the four discontinuous segments that were obtained from initial curve-fitting process. b) shows a best-fit polynomial of the low temperature specific heat data. c) shows a best-fit polynomial of the high temperature data.

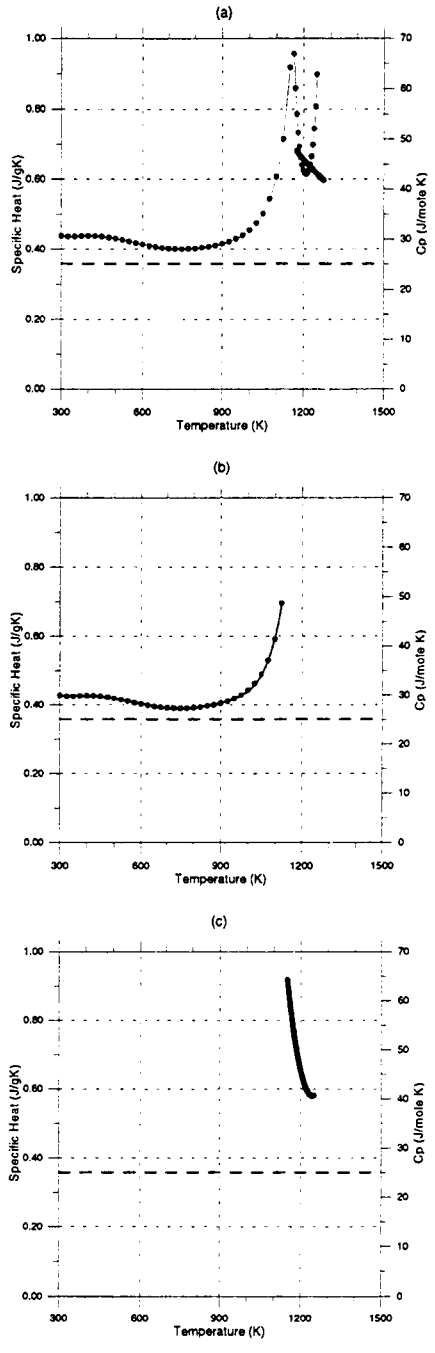

Figure 4.17 Specific heat versus temperature for the LRO β initial condition obtained from pulsing the shortened specimen at low current. Data was obtained at about a 35 amp pulse. a) shows the three discontinuous segments that were obtained from initial curve-fitting process. b) shows a best-fit polynomial of the low temperature specific heat data. c) shows a best-fit polynomial of the high temperature data.

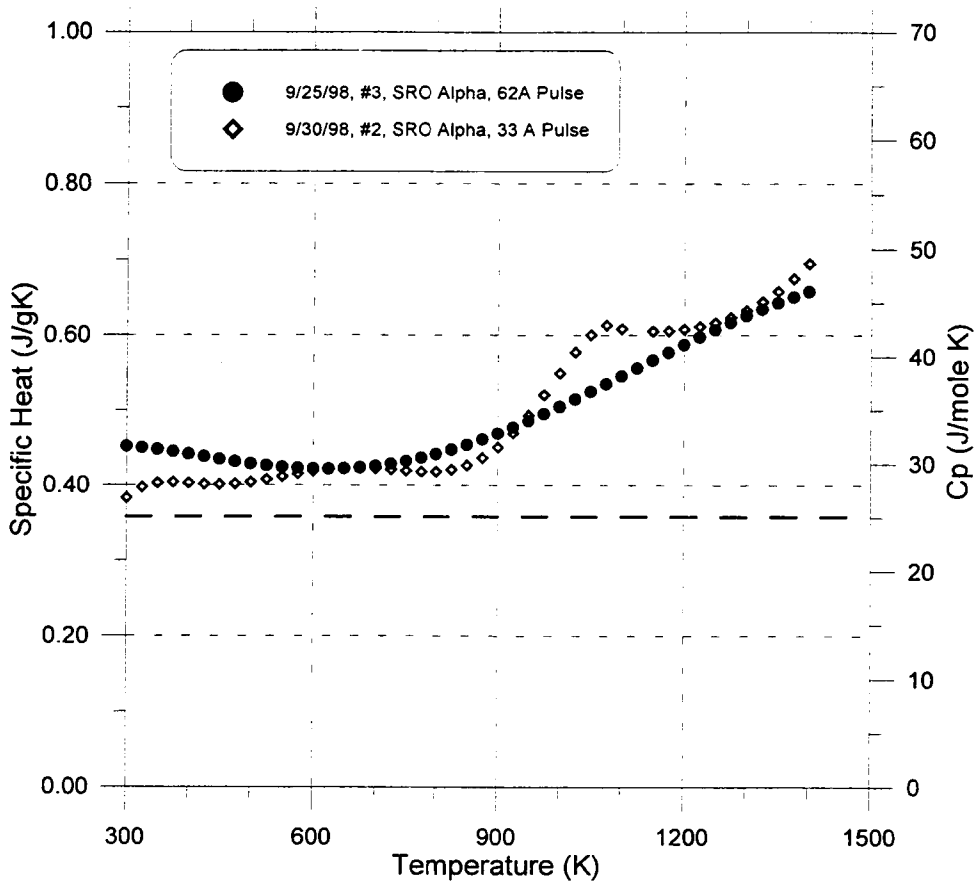

Figure 4.18 Specific heat versus temperature of the SRO α initial condition at two different pulse currents.

at about 20 K/s from 1000 to 1400K.

Figure 4.19 compares the specific heat of the shortened specimen in the initial LRO β condition. The high current pulse was about 68 A and the low current pulse was about 35 A.

A comparison of specific heat for the two different sample lengths was done. The SRO α initial condition results are shown in Figure 4.20. Both data sets were obtained using a current of about 33 A. The splitting between 700 and 1000 K may be due to the curve-fitting procedure. Figure 4.21 compares specific heat of the two specimen lengths for the LRO β initial condition.

Figure 4.22 is a comparison of the authors' high heating rate data (120-220 K/s) to other researchers for the SRO α initial condition. Basak [121] used a heating rate of about 60 K/s to obtain this data, and Norem [137] used a heating rate of about 0.17 K/s. The explanations of the shape of Norem's and Basak's curves are given in Section 2.5.2. The author's data (from Figure 4.14b) has been purposely made continuous through the whole temperature range. The initial un-smoothed data are shown in Figure 4.14a. Figure 4.23 compares the authors data in the initial LRO β condition to other researchers.

Figures 4.24, 4.25, and 4.26 show specific heat data for both phases for the various test conditions. Figure 4.24 is data for the shortened specimen at the high current pulses. Figure 4.25 is data for the shortened specimen at the low current pulses. Figure 4.26 is data from pulses on the long section.

There are also other curves superimposed on the graph in Figures 4.24-4.26. One curve (horizontal dashed line) is the value of 3R (24.9 J/mole K), where R is the gas constant. This is the value that the Debye specific heat approaches in the upper

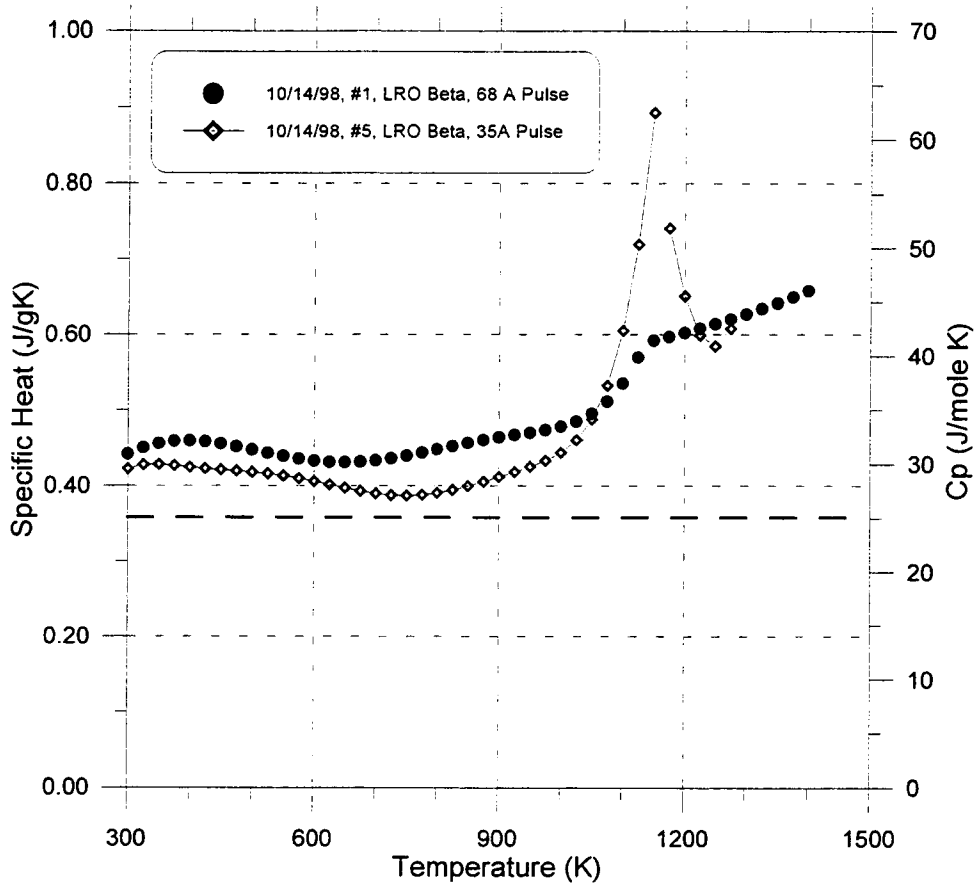

Figure 4.19 Specific heat versus temperature of the LRO β initial condition at two different pulse currents.

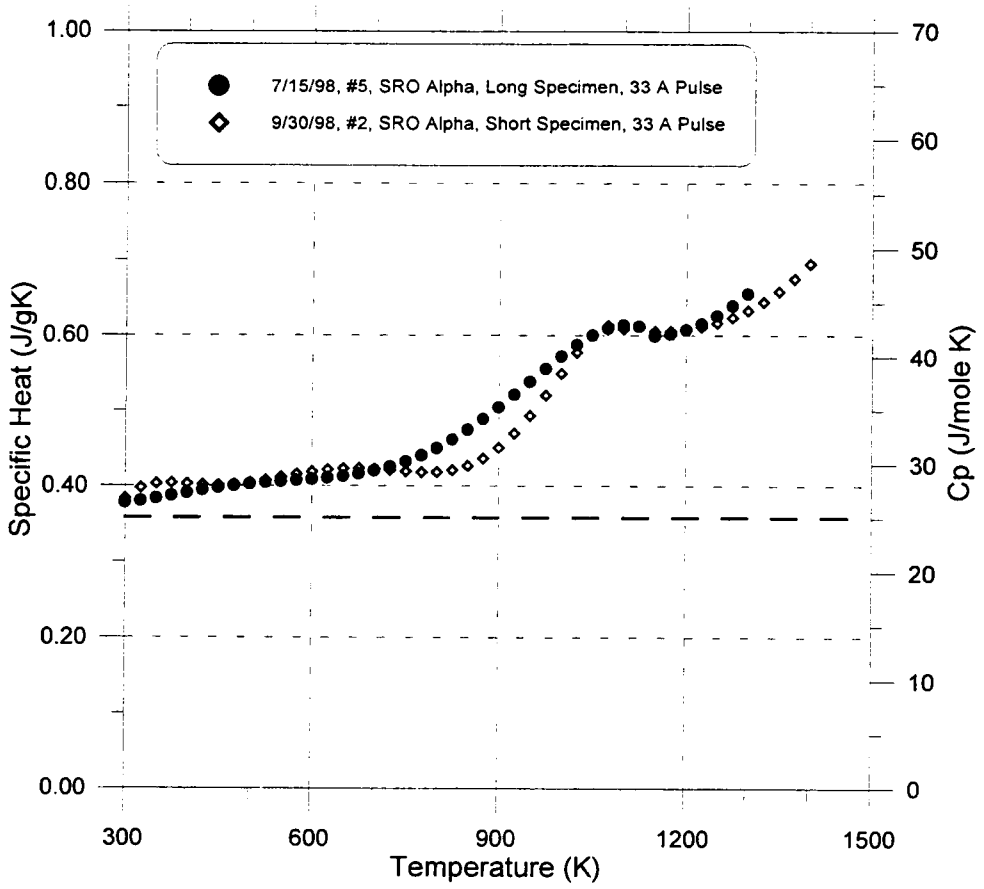

Figure 4.20 Specific heat versus temperature of the SRO α initial condition obtained from two different specimen lengths.

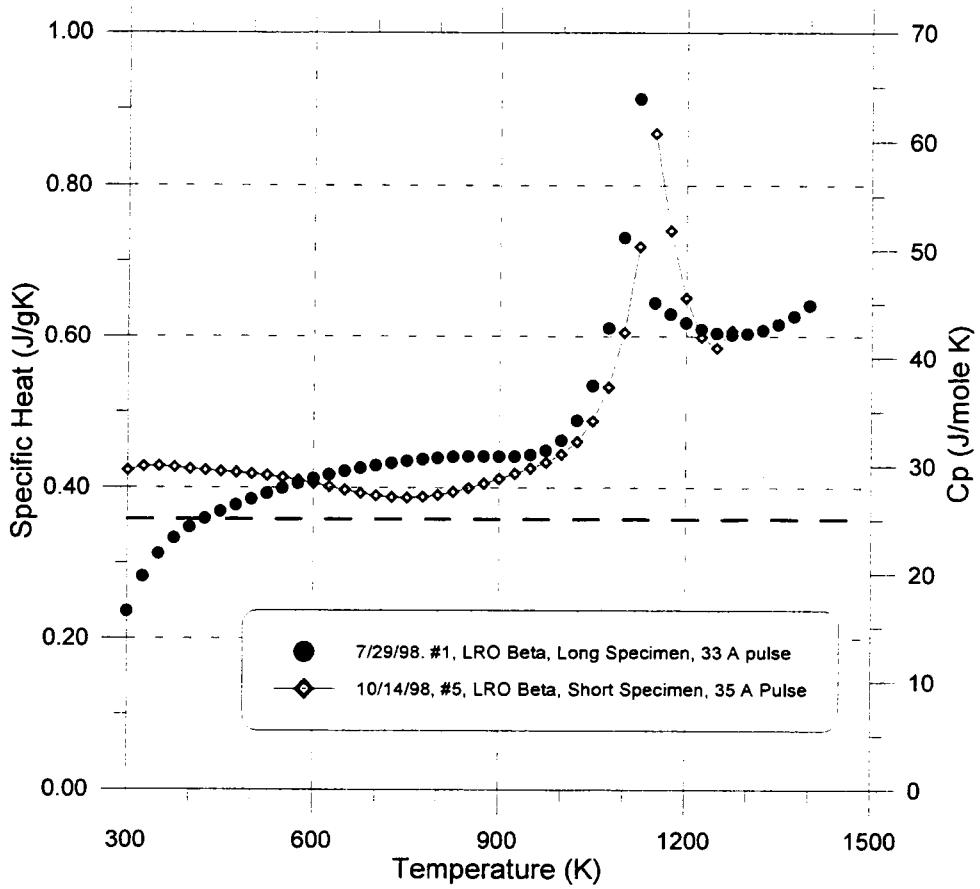

Figure 4.21 Specific heat versus temperature of the LRO β initial condition obtained from two different specimen lengths.

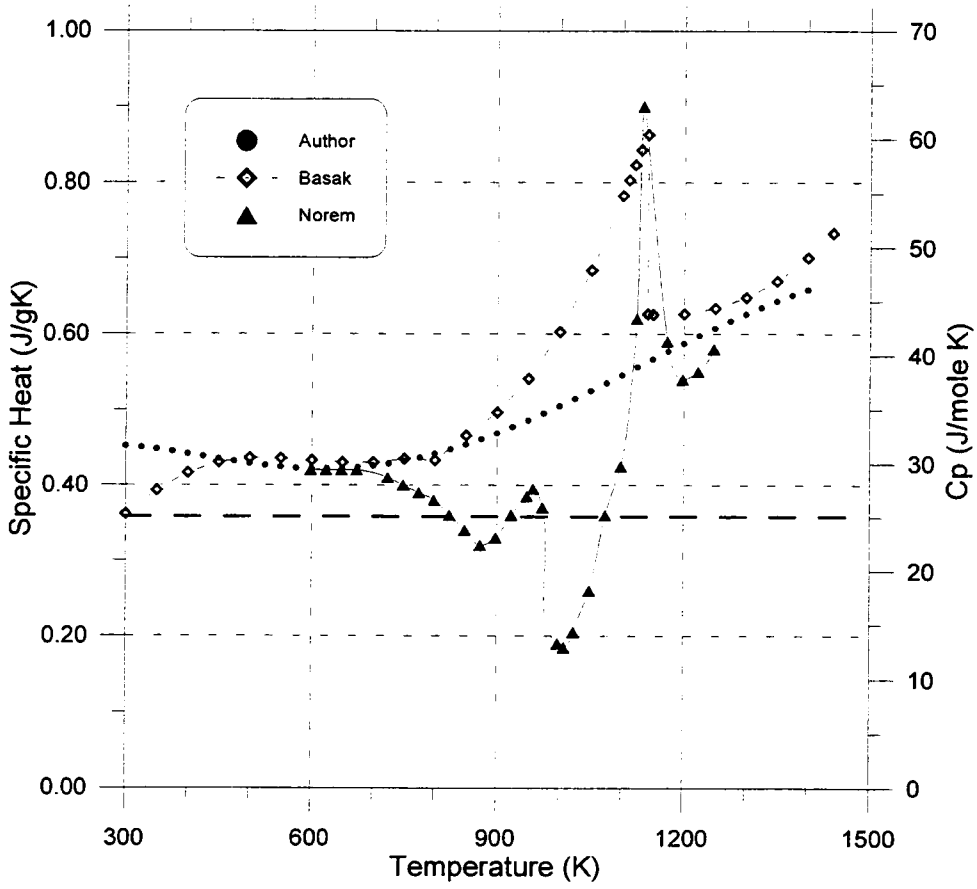

Figure 4.22 Specific heat of SRO α according to different researchers. Norem [137] used an adiabatic calorimeter with a heating rate of about 0.2 K/s. Basak [121] used a pulse heating calorimeter with a heating rate of about 60 K/s. The author obtained heating rates between 120 and 220 K/s during the pulse.

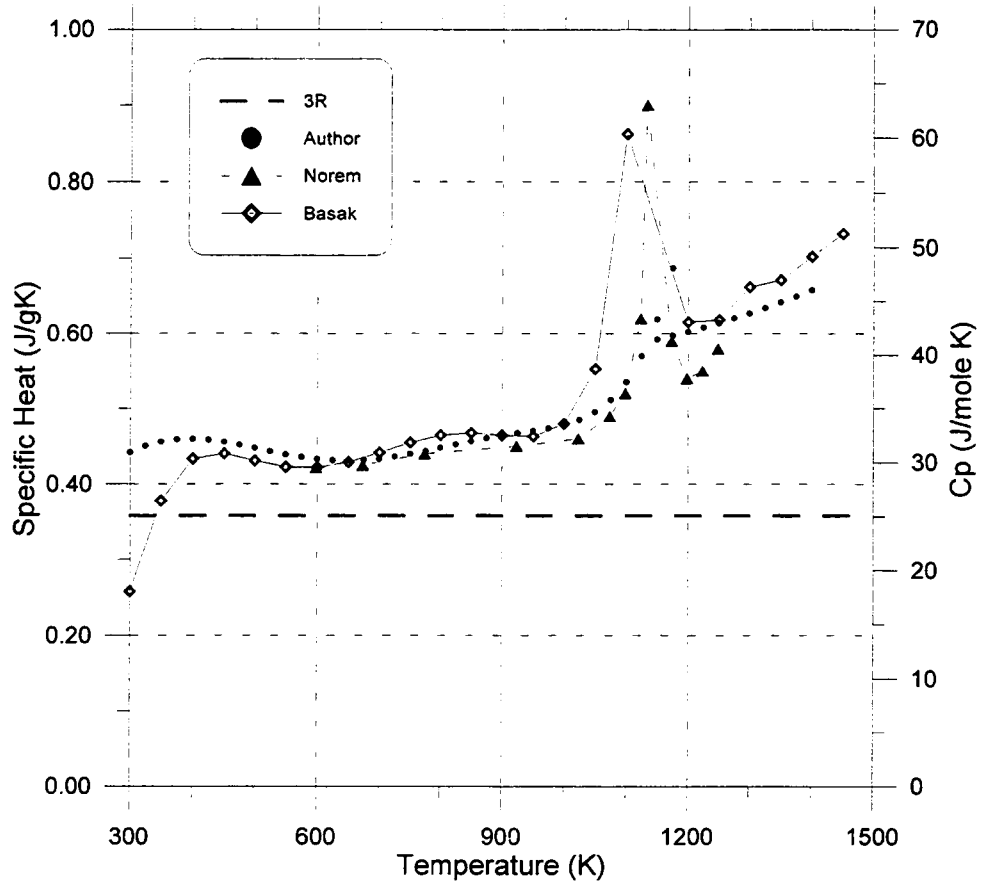

Figure 4.23 Specific heat of LRO β according to different researchers. Norem [137] used an adiabatic calorimeter with a heating rate of about 0.2 K/s. Basak [121] used a pulse heating calorimeter with a heating rate of about 60 K/s. The author obtained heating rates between 120 and 220 K/s during the pulse.

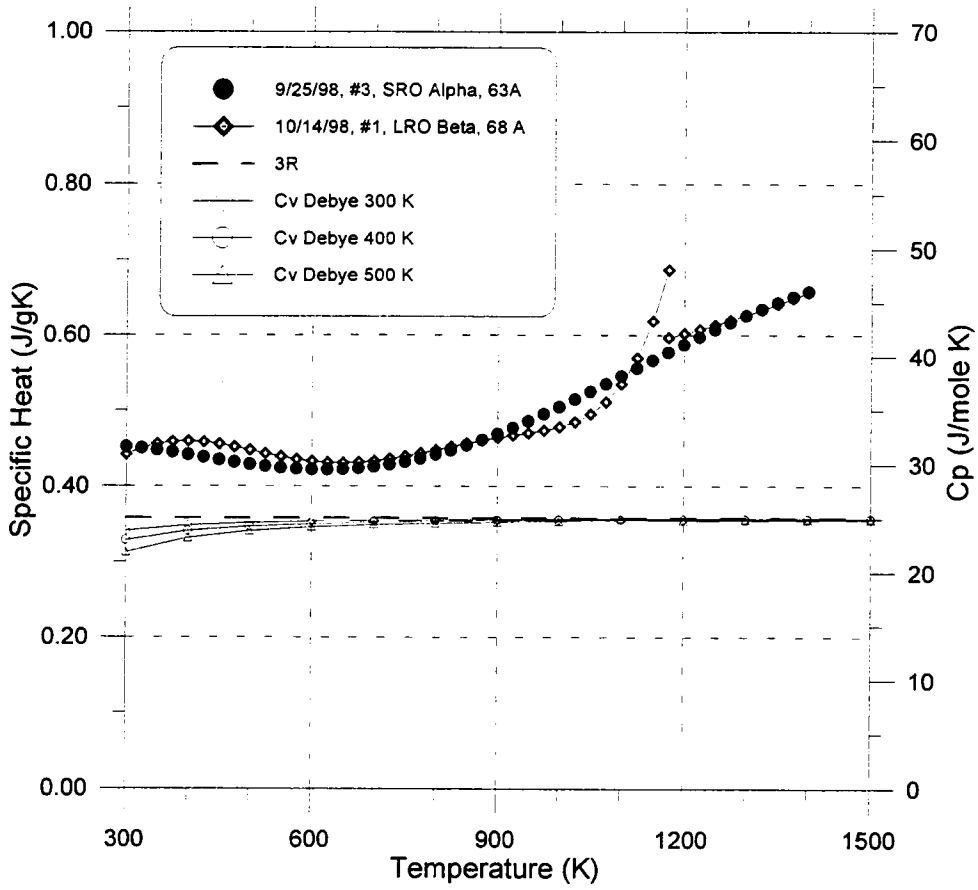

Figure 4.24 Specific heat of the SRO α and LRO β initial conditions obtained from high current pulses on the shortened specimen. Also depicted on the curve is the Debye specific heat at Debye temperatures of 300 K, 400 K, and 500 K. The dashed horizontal line is 3R.

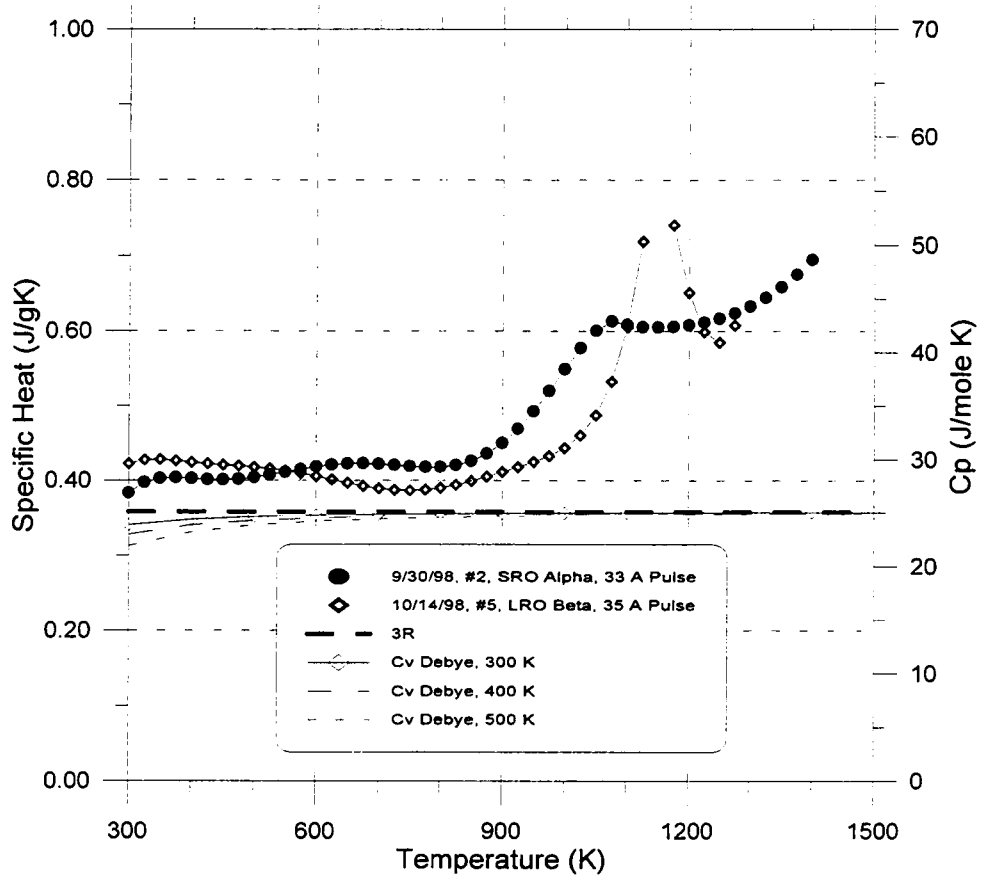

Figure 4.25 Specific heat of the SRO α and LRO β initial conditions obtained from low current pulses on the shortened specimen. Also depicted on the curve is the Debye specific heat at Debye temperatures of 300 K, 400 K, and 500 K. The dashed horizontal line is 3R.

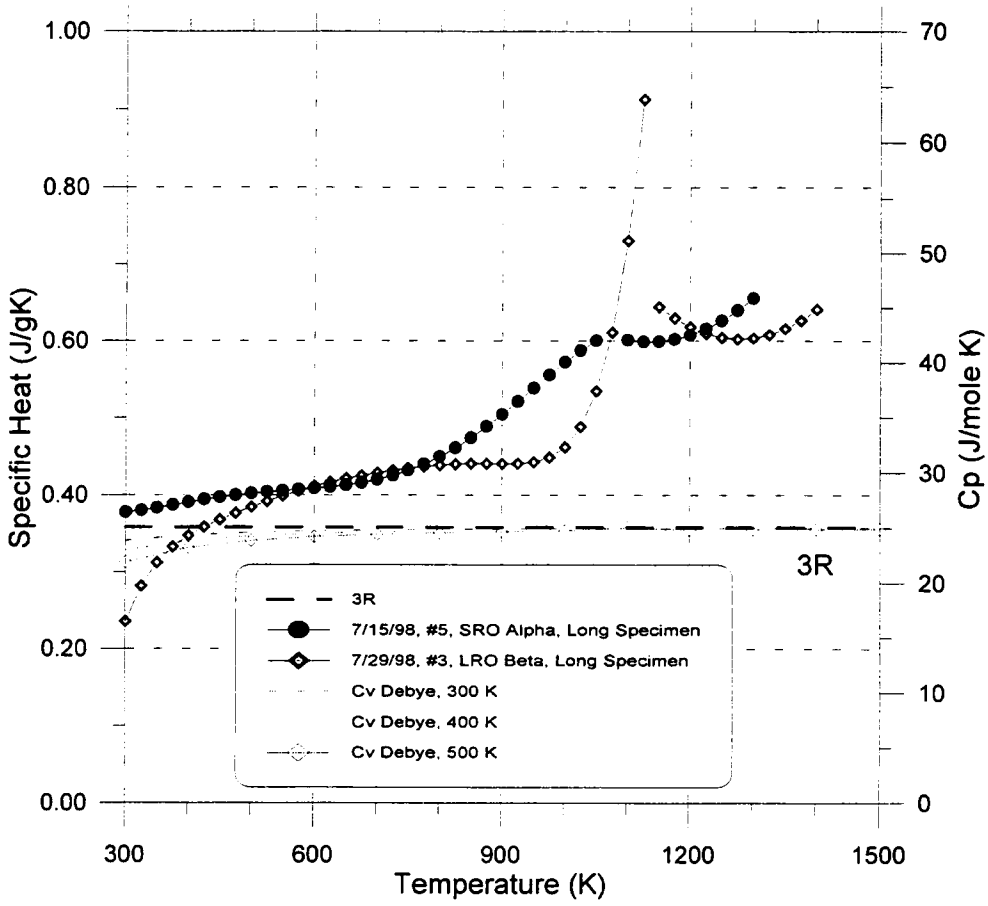

Figure 4.26 Specific heat of the SRO α and LRO β initial conditions obtained from low current pulses on the long specimen. Also depicted on the curve is the Debye specific heat at Debye temperatures of 300 K, 400 K, and 500 K. The dashed horizontal line is 3R.

temperature limit. Three other curves are also superimposed on the graphs which correspond to Debye temperatures, Θ_D, of 300 K, 400 K, and 500 K. Θ_D for nickel and molybdenum, as well as many other metals, lie in this range.

Tabulated data [141] were used to plot these three curves. The integral term in the Debye theoretical specific heat

$$C_V^D = 3R\left(\frac{12}{x^3}\int_0^x \frac{y^3 dy}{e^y - 1} - \frac{3x}{e^x - 1}\right); x = \frac{\Theta_D}{T} \qquad \textbf{(4.2)}$$

was approximated using the expression

$$\int_0^x \frac{y^3 dy}{e^y - 1} \cong \frac{\pi^4}{15} - x^4 \sum_1^\infty e^{-nx}\left(\frac{1}{nx} + \frac{3}{n^2x^2} + \frac{6}{n^3x^3} + \frac{6}{n^4x^4}\right) \qquad \textbf{(4.3)}$$

The lower part of the temperatrue range that these tests were done is right in the region where the Debye temperature approaches the 3R value.

One other interesting point about the SRO α curves is that they agree very closely in shape and value, even near the critical range. The odd shape is consistent with heating rate and specimen length. The curve-fitting procedures were fairly consistent and so the discontinuity at the critical temperature may be due to the procedures used.

4.3 Calculation of Gibbs Free Energy of the α to β Phase Transformation

The Gibbs free energy, $\Delta G^{\alpha\rightarrow\beta}$ in the range 300 to 1141 K can be determined from the specific heat data that was found. No specific heat data on the metastable LRO β phase was obtained above 1141 K, and so $\Delta G^{\alpha\rightarrow\beta}$ cannot be determined above 1141. The equation for $\Delta G^{\alpha\rightarrow\beta}$ that was used is from

$$G^\alpha = H^\alpha - TS^\alpha \qquad \textbf{(2.18)}$$

and

$$G^{\beta} = H^{\beta} - TS^{\beta} \tag{2.19}$$

Subtracting these two equations gives

$$\Delta G^{\alpha\to\beta} = G^{\beta} - G^{\alpha} = (H^{\beta} - H^{\alpha}) - T(S^{\beta} - S^{\alpha}) \tag{4.4}$$

where the enthalpies and entropies are calculated as follows

$$H^{\alpha} = H_0^{\alpha} + \int_{T_0}^{T} C_P^{\alpha} dT \tag{2.21}$$

$$H^{\beta} = H_0^{\beta} + \int_{T_0}^{T} C_P^{\beta} dT \tag{2.22}$$

$$S^{\alpha} = S_0^{\alpha} + \int_{T_0}^{T} \frac{C_P^{\alpha}}{T} dT \tag{2.23}$$

$$S^{\beta} = S_0^{\beta} + \int_{T_0}^{T} \frac{C_P^{\beta}}{T} dT \tag{2.24}$$

where H_0 and S_0 are the enthalpy and entropy, respectively at the transition temperature, T_0. From these equations

$$\Delta G^{\alpha\to\beta} = \int_{T0}^{T} \Delta Cp dT + \Delta H_0 - T \int_{T0}^{T} \frac{\Delta Cp}{T} dT - T\frac{\Delta H_0}{T_0} \tag{4.5}$$

which can be written as

$$\Delta G^{\alpha\to\beta} = \Delta H_0 \left[\frac{T_0 - T}{T_0}\right] + \int_{T0}^{T} \Delta Cp dT + -T \int_{T0}^{T} \frac{\Delta Cp}{T} dT \tag{4.6}$$

The value ΔH_0 was found [13] to be -2900 J/mole. The change in specific heat over the temperature range 300 to 1141 K was determined by finding a best-fit polynomial for the specific heat of each phase, and then subtracting Cp^{α} from Cp^{β}. The ΔCp value used in the

ΔG calculation was an average ΔCp value from three ΔCp values: the specific heat values of the short sample pulsed at high current, the short sample pulsed at low currents, and the long sample pulsed at low currents. The resulting polynomial was found to be

$$\Delta Cp = -3.502 + 0.0415T - 2.134x10^{-4}T^2 + 6.119x10^{-7}T^3 - 1.044x10^{-9}T^4 + 1.054x10^{-12}T^6 - 5.792x10^{-16}T^6 + 1.334x10^{-19}T^7 \quad \textbf{(4.7)}$$

over the temperature range from 300 K to 1141 K.

Dividing Equation 4.7 by T left the following equation:

$$\frac{\Delta Cp}{T} = \frac{-3.502}{T} + 0.0415 - 2.13x10^{-4}T + 6.119x10^{-7}T^2 - 1.044x10^{-9}T^3 + 1.054x10^{-12}T^4 - 5.792x10^{-16}T^6 + 1.334x10^{-19}T^6 \quad \textbf{(4.8)}$$

These equations were substituted into Equation 4.6 and evaluated from 1141 to 300 K. The analysis for determining $\Delta G^{\alpha \rightarrow \beta}$ is shown in Appendix I. The integral terms of Equation 4.6 were evaluated at 25 K increments from 300 to 1141 K. The enthalpy integral term varied from 0 to 10 J/mole, and the entropy integral term varied from –9 to 3 J/mole. Comparing these values to the ΔH_0 term, which varied from 0 to –2100 J/mole, it is seen that the integral terms are negligable ((< 0.5 % of the ΔH_0 term). The Gibbs free energy of the transformation from 300 to 1141 can thus be well approximated by

$$\Delta G^{\alpha \rightarrow \beta} = \Delta H_0 \left(\frac{T_0 - T}{T_0} \right) = -2900 + 2.54T \text{ [J/mole]} \quad \textbf{(4.9)}$$

4.4 Conclusions and Recommendations

A literature review of the Ni-Mo binary alloys was done. Particular emphasis was placed on the Ni_4Mo composition. This alloy undergoes an order to disorder phase transformation upon heating at 1141 K, where the LRO β phase (BCT) transforms to the SRO α (FCC) phase.

The electrical resistivity and specific heat of Ni_4Mo as a function of temperature was measured in the temperature range 300 K to 1400 K. Data were obtained on the metastable SRO α phase from 300 to 1141 K, on the equilibrium SRO α from 1141 to 1400 K, and on the equilibrium LRO β phase from 300 to 1141 K. The transformation from LRO β to SRO α upon heating occurred too rapidly to suppress, even at heating rates of over 200 K/s. The error in the specific heat and electrical resistivity was estimated to be about 1.2 %. This estimate was determined from a propagation of errors process. The error in temperature was estimated to be about ± 2 K. The bare-wire type R thermocouples were not calibrated.

The effect of sample length and heating rate on the electrical resistivity and specific heat was studied, and found to have little effect on the resulting data. Error in measurement of specimen dimensions was believed to be the cause of the electrical resistivity showing a slight difference in the results between the long and short specimen.

Heating rate had no noticeable affect on the specific heat data in the heating rate range investigated. Heating rate had a slight effect on the electrical resistivity data on the LRO β initial condition specimen, observed by some splitting of the data from about 700 K up to the critical temperature. The splitting in resistivity data may be due to the higher heating rates supressing the sharp increase in LRO as the critical temperature is approached. One other cause of the splitting may be an experimental problem related to a difference in temperature of the surroundings between the two tests. Details of this problem are mentioned in Section 3.3.3.2.

There was also a noticeable effect of heating rate on the temperature-time plot of the initial LRO β pulse. The transformation temperature in the high heating rate test was

about 1160 K shown by a thermal arrest stage in Figure 4.27. This is compared to the thermal arrest stage of 1141 seen in the low heating rate test of Figure 4.27.

The Gibbs free energy from 300 to 1141 K was determined as a function of temperature to be

$$\Delta G^{\alpha\rightarrow\beta} = \Delta H_0\left(\frac{T_0 - T}{T_0}\right) = -2900 + 2.54T \text{ [J/mole]} \qquad \textbf{(4.9)}$$

in which the integral terms for the enthalpy and entropy in Equation 4.6 were found to be negligeable.

The equipment used to obtain these data was a pulse-heating calorimeter. This equipment calculates electrical resistivity directly during the pulse, and specific heat is determined by a complicated curve-fitting process from the data that were stored from the test. The currents that were used to heat the sample ranged from about 33 amps to about 68 amps. The sample had to be shortened to about 7 cm from its original length of about 20 cm to obtain the high currents because of the power supply limitations. One shortened specimen (the original middle section) was destroyed during a trial and error process to obtain a high heating rate up to about 1400 K because the temperature of one of the pulses approached the melting temperature and pulled apart. An end section was then used to obtain data in the thesis. This type of overshoot occurred other times as well, causing a rough surface on the sample. Another type of damage to the sample was caused by buckling when the sample expanded between two fixed ends. A flexible sample holder was designed and built for subsequent measurements on the shorter specimens.

Modifications to the calorimeter system should include:

1. An emergency cut-off switch in the pulsing software to prevent temperature overshoot.

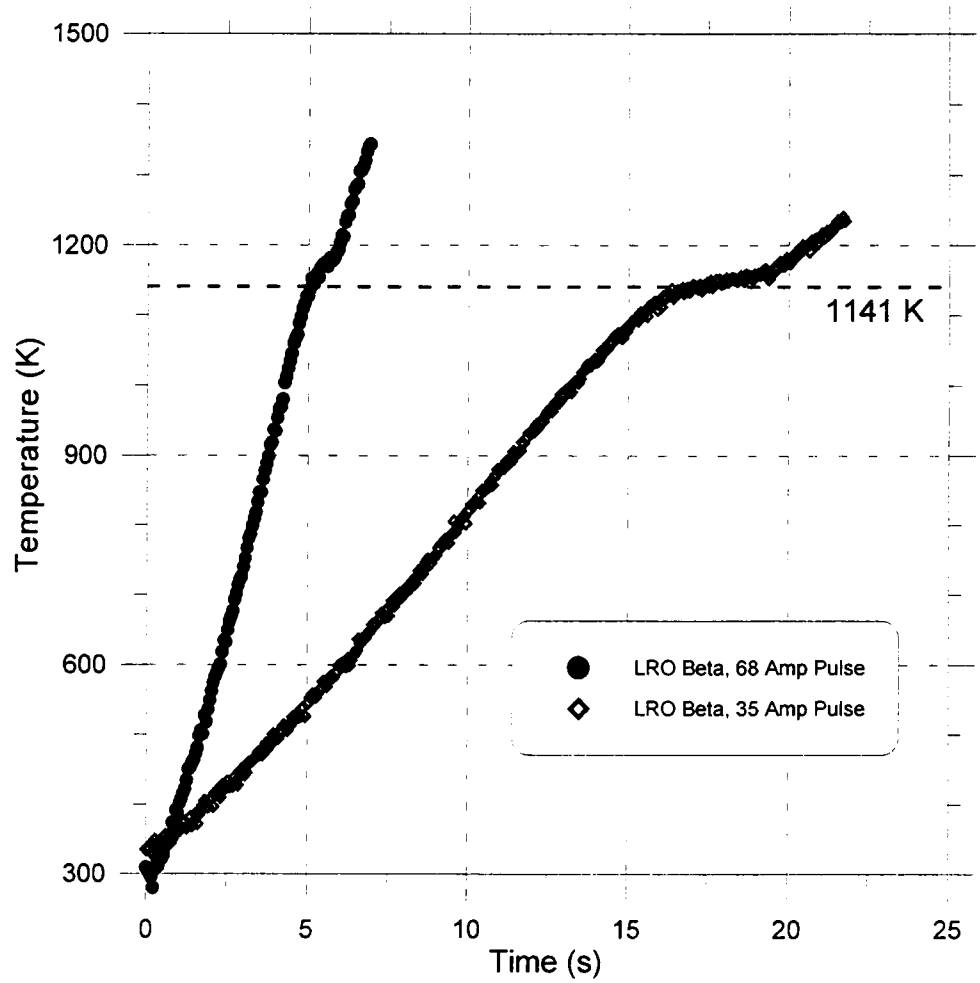

Figure 4.27 Temperature versus time on heating for the LRO β initial condition for two different heating rates. The thermal arrest has shifted to a slightly higher temperature in the faster heating rate pulse.

2. A larger power source to obtain data on higher resistance materials and data at higher heating rates.
3. A more user-friendly processing program to obtain data for the specific heat.

One other recommendation to obtain data on the metastable LRO β phase from 1141 to the melting temperature is to do a test on the sample using the millisecond pulse calorimeter facilities [141] at NIST, Gaithersberg. This equipment should have the power to heat the sample rapid enough to obtain the metastable data, but can only be used once per specimen since it destroys the specimen in the process.

REFERENCES

References

1. Singleton, M., and P. Nash, in "Binary Alloy Phase Diagrams, Volume 2", T.B. Massalski, ed. ASM, Metals Park, Ohio, 1986.

2. Casselton, R.E.W., and W. Hume-Rothery, J. Less Common Metals, 7, 212, 1964.

3. Wicker, A., C. Allibert, J. Driole, and E. Bonnier, C.R. Acad. Sci., 271, 273, 1970.

4. Heijwegan, C.P. and G.D. Rieck, Z. Metallkd., 64, 450, 1973.

5. Katayana, I., H. Shimitani, and Z. Kozuka, Z. Nippon Konzoku Gakkai-Shi, 37, 509, 1973.

6. Kang, S.L., Y.D. Song, W.A. Kaysser, and H. Hofman, Z. Metallkd., 75, 86, 1984.

7. Ellinger, F.H. Trans. ASM, 30, 607, 1942.

8. Elliot, R., "Constitution of Binary Alloys, First Supplement", McGraw-Hill, New York, 1965.

9. Hansen, M., and K. Anderko, "Constitution of Binary Alloys", McGraw-Hill, New York, 1969.

10. Bloom, D.S. and N.J. Grant, Trans. AIME, 200, 261, 1954.

11. Guthrie, P.V., and E.E. Stansbury, ORNL Report 3078, ORNL, Oak Ridge, Tennessee, 1961.

12. Gust, W., T. Nguyen-Tat, and B. Predel, Z. Metallkd. 70, 241, 1979.

13. Brooks, C.R., J.E. Spruiell, and E.E. Stansbury, International Metals Reviews, 29, 210, 1984.

14. Kozlov, E. and V. Kushnarenko, Phys. Met. Metallogr., 46, 75, 1978.

15. Frisk, Karin, CALPHAD, 14, 311, 1990.

16. Shoemaker, C.B. and D.P. Shoemaker, Acta Crystallogr., 16, 997, 1963.

17. Kaufman, L., and H. Nesor, "Treatise on Solid State Chemistry, Vol. 5", Plenum, New York, 1975.

18. Okamoto, H. J., J. Phase Equil., 12, 623, 1991.

19. Okamoto, H. and T.B. Massalski, J. Phase Equil., 12, 148, 1991.

20. Harker, D., J. of Chem. Phys., 12, 315, 1944.

21. Nosova, G. and N. Polyakova, Phys. Met. Metallogr., 46, 178, 1978.

22. Spruiell, J. and E. Stansbury, J. Phys. Chem. Solids, 26, 811, 1965.

23. Grube, G. and H. Schlect, Z. Electrochem., 44, 413, 1938.

24. Matveeva, N.M. and E.V. Kozlov, "Ordered Phases in Metallic Systems", Nova Science Publishers Inc., Cornmack, New York, 1996.

25. Grube, G., and O. Winkler, Z. Elecrochem., 44, 423, 1938.

26. Saito, S. and P.A. Beck, Trans. AIME, 15, Dec., 938, 1959.

27. Van Tendeloo, G. and S. Amelinckx, in "Electron Microscopy and Materials Science", 3rd Course of the Intl. School of Electron Microscopy, E. Ruedl and U. Valdre, eds., "Ettore Majorana" International Center for Scientific Culture, Luxembourg, 1976.

28. Ruedl, E. and S. Amelinckx, Mater. Res. Bull., 4, 361, 1969.

29. Shoemaker, C., A. Fox, and D. Shoemaker, Acta. Crys., 13, 585, 1960.

30. Van Tendeloo, G. and S. Amelinckx, Mater. Res. Bull., 8, 721, 1973.

31. Orbrowski, W., Naturwissenschaften, 46, 490, 1959.

32. Nash, P., S. Fidlding, and D. West, Met. Sci., 17, 192, 1983.

33. Miracle, D., K. Lark, V. Srinivsan, and H. Lipsitt, Metall. Trans., A15, 481, 1984.

34. Jin, Y., Y. Han, and M. Chaturvedi, Materials Letters, 23, 21, 1995.

35. Saburi, T., K. Komatsu, M. Yamamoto, S. Nenno, and Y. Mitzutani, Trans. AIME, 245, 2348, 1969.
36. Das, S.K. and G. Thomas, Phys. Status Solidi (a), 21, 177, 1974.
37. Vasudevan, K., M.S. Thesis, University of Tennessee, Knoxville, 1982.
38. Lampe, B.T., M.S. Thesis, University of Tennessee, Knoxville, 1963.
39. Richards, M. and J. Cahn, Acta. Metall., 19, 1263, 1973.
40. Van Tendeloo, G., R. Ridder, and S. Amelinckx, phys. stat. solidi, 27, 457, 1975.
41. DeHoff, R.T., "Thermodynamics in Materials Science", McGraw-Hill, New York, 1993.
42. Miiller, A.P., in "Specific Heat of Solids", (ed. C.Y. Ho), Hemishpere, New York, 1988.
43. Tammann, G., Z. Anorg. Chem., 107, 1, 1919.
44. Bain, E., Chem. & Met. Engr., 28, 65, 1923.
45. Muto, T. and Y. Takagi, " The Theory of Order-Disorder Transitions in Alloys", Academic Press, New York, 1955.
46. Bethe, H.A., Proc. Roy. Soc. (London), A150, 552, 1935.
47. Cowley, J.M., Phys. Rev., 77, 699, 1950.
48. Guttmann, L., "Order-Disorder Phenomena in Metals", Academic, New York, 1956.
49. Pedraza, A., Professor, University of Tennessee, Knoxville. MSE 530 Course Notes.
50. Bragg, W.L. and E.J. Williams, Proc. Roy. Soc. (London), A145, 699, 1934.
51. Porter, D.A., and K.E. Easterling, "Phase Transformations in Metals and Alloys", 2nd ed., Chapman Hall, London, 1992.

52. Landau. L.D. and E.M. Lifshitz, "Statistical Physics", Pergamon, London, 1958.

53. Hume-Rothery, W., "The Structure of Metals and Alloys", The Institute of Metals, 1947.

54. Kozlov, E.V. and V.M. Kushnarenko, Phys. Met. Metallogr., 46, 75, 1978.

55. Kao, H.P., PhD Thesis, University of Tennessee, Knoxville, 1987.

56. Kozlov, E.V., V.M. Kushnarenko, and G.V. Pushkareva, "Study of Ordering Kinetics and Properties of the NiMo Alloy" in "Proc. 4th All Union Conf. on Atomic Ordering and its Influence on Properties of Alloys", Tomsk, Tomsk Univ., Part 1, 232, 1974.

57. Chang, T.P., M.S. Thesis, University of Tennessee, Knoxville, 1965.

58. Lei, T.S., Ph.D. Thesis, University of Tennessee, Knoxville, 1979.

59. Dienes, J., Acta Metall., 3, 549, 1955.

60. Vineyard, G., Phys. Rev., 102, 981, 1956.

61. Sato, H., and R. Kikuchi, Acta Metall., 24, 797, 1976.

62. Yamuchi, H., and D. de Fontaine, in "Order-Disorder Transformations in Alloys", H. Warlimont, ed., Springer-Verlag, New York, 1974.

63. Cohen, J. in "Phase Transformations", ASM, Materials Park, OH, 1970.

64. Cook, H., J. Phys. Chem. Solids, 30, 2427, 1969.

65. Cook, H., Mater. Sci. Engr., 25, 127, 1976.

66. Irani, R., Contemp. Phys., 13, 559, 1972.

67. Kiriyenko, V., and L. Potapov, Fiz. metal. metalloved., 33, 436, 1972.

68. Kiriyenko, V., and L. Potapov, Fiz. metal. metalloved., 42, 817, 1974.

69. Kiriyenko, V., and L. Potapov, Fiz. metal. metalloved., 31, 548, 1971.

70. Vlasova, E., Y. Tyapkin, and V. Plakhtii, Sov.Phys. Dokl., 19, 321, 1974.

71. Tyapkin, Y., G. Nosova, Y. Vlasova, V. Ploykova, and V. Plakhtiy, Fiz. metall. metalloved., 41, 441, 1976.

72. Artsishevskaya, L., I. Malysheva, and Y. Selisskiy, Fiz. metal. metalloved., 33, 337, 1972.

73. Saburi, T. and S. Nenno, J. Less Common Metals, 37, 59, 1974.

74. Amelinckx, S., J. Less Common Metals, 28, 325, 1972.

75. Yamamoto, M., F. Massakai, S. Nenno, and S. Nakamura, J. Phys. Soc. Japan., 36, 1330, 1974.

76. Ling, F., R. Irani, and R. Cahn, Mat. Sci. Engr., 15, 181, 1974.

77. Spruiell, J.E. and E.E. Stansbury, J. Phys. Chem. Solids, 26, 811, 1965.

78. Chakravarti, B., E. Starke, C. Sparks, and R. Williams, J. Phys. Chem. Solids, 35, 1317, 1974.

79. Clapp, P., and S. Moss, Phys. Rev., 171, 754, 1968.

80. Clapp, P. and S. Moss, Phys. Rev., 142, 418, 1966.

81. Thomas, G. and R. Sinclair, Acta Metall., 25, 231, 1977.

82. Tanner, J. and H. Leamy, in "Order-Disorder Transformations in Alloys", H. Warlimont, ed., Springer-Verlag, New York, 1974.

83. Banerjee, S., Metals, Materials and Process, 5, 119, 1993.

84. de Fontaine, D., Acta. Metall., 23, 553, 1975.

85. Khachaturyan, A., Phys. Metall. Metallogr., 13, 493, 1963.

86. Kulkarni, U., S. Muralidhar, and S. Banerjee, phys. stat. solidi., 110, 331, 1988.

87. Mayer, J. and K. Urban, Acta Metall., 33, 539, 1985.

88. Chevlier, J., and W. Stobbs, Acta. Metall., 24, 535, 1976.

89. Chevalier, J. and W. Stobbs, Acta Metall. 27, 1197, 1979.

90. De Ridder, R., G. Van Tendeloo, and S. Amelinckx, Acta. Cryst., A32, 216, 1976.

91. Kikuchi, R., Phys. Rev., 81, 988, 1951.

93. Das, S., P. Okamoto, P. Fisher, and G. Thomas, Acta Metall., 21, 913, 1973.

94. Banerjee, S., in "Solid to Solid Phase Transformations", Johnson et al. ed., TMS, Warrendale PA, 1994.

95. Okamoto, P. and G. Thomas, Acta. Metall., 19, 825, 1971.

96. Thomas, G. and M. Goringe, "Transmission Electron Microscopy of Materials" John Wiley & Sons, New York, 1979.

97. Chevalier, J., J. of Microscopy, 119, 113, 1980.

98. Amelinckx, S., G. Van Tendeloo, and J. van Landyut, Mater. Sci. Forum, 3, 1985.

99. Van Tendeloo, G., S. Amelinckx, and D. de Fontaine, Acta. Cryst., B41, 281, 1985.

100. Stobbs, W. and S. Stobbs, Phil. Mag., 53B, 537, 1986.

101. Lee, K. K hiraga, D. Shindo, and M. Hirabayashi, Acta Metall., 36, 641, 1988.

102. Hata, S., S. Matsumura, N. Kuwano, and K. Oki, Acta Mater. 46, 881, 1998.

103. Stansbury, E.E., Mat. Res. Soc. Symp. Proc., 39, 93, 1985.

104. Lei, T.S., K. Vasudevan, and E.E. Stansbury, Mat. Res. Soc. Symp. Proc.

105. Brooks, C.R., and S. Cao, Phil. Mag. A, 65, 327, 1992.

106. Yamamoto, M., S. Nenno, M. Futomoto, and S. Nakanura, Jap. Jnl. of Appl. Phys., 2, 437, 1972.

107. Banerjee, S., K. Urban, and M. Wilkens, Acta. Met., 32, 299, 1984.

108. Stobbs, W.M. and J.P.A.A. Chevalier, Acta. Met., 26, 233, 1978.

109. Vasudevan, K., H. Kao, C. Brooks, and E. Stansbury, Met. Trans., 19A, 941, 1988.

110. Brooks, C. and M. Sanganeria, Scripta Met., 22, 1683, 1988.

111. Thomas, H. Z. Phys., 129, 219, 1951.

112. Nicholson, D.M.C. and R.H. Brown, Phys. Rev. Let., 70, 3311, 1993.

113. Tipler, P.A., "Elementary Modern Physics", Worth, New York, 1992.

114. Giancoli, D.C., "Physics for Scientists and Engineers", Prentice Hall, Englewood Cliffs, New Jersey, 1989.

115. Shröder, Klaus, "CRC Handbook of Electrical Resistivities of Binary Metallic Alloys", CRC Press, Boca Raton, Florida, 1983.

116. Cusack, N. "The Electrical and Magnetic Properties of Solids", Wiley, New York, 1958.

117. Meaden, George Terence, "Electrical Resistance of Metals", Plenum, New York, 1965.

118. Barrett, C.S. and T.B. Massalski, "Structure of Metals", 3rd ed., McGraw-Hill, New York, 1966.

119. Weiss, R.J., "Solid State Physics for Metallurgists", Pergamon Press, New York, 1963.

120. Blatt, Frank J., "Physics of Electronic Conduction in Solids", McGraw-Hill, New York, 1968.

121. Basak, D., Ph.D. Thesis, University of Tennessee, Knoxville, 1995.

122. Gruneisen, E., in Handbuch der Physic, Bd. 10, F, Berlin, Springer-Verlag, 1926.

123. Nernst, W., Akad. Wiss., Berlin, Sitzber, 52, 933, 1906.

124. Kollie, PhD Thesis, University of Tennessee, Knoxville, 1969.

125. Dulong, P.L. and A.T. Petit, Ann. Chem. Phys. (10), 395, 1819.

126. Boltzmann, L., Adad. Wissen. Wien., Sitzungsber, 63, 679, 1871.

127. Einstein, A., Ann. Physik, 22, 180, 1907.

128. Sommerfeld, A. and H. Bethe, in Handbuch der Physik, Geiger & Scheel, ed., Vol. XXIV/2, Springer-Verlag, Berlin, 1933.

129. Starke, W. and R. Kortzeborne, "A Convenient Tabulation of the Debye Energy, Heat Capacity, Free Energy, and Entropy for a Crystalline Solid", University of California Radiation Laboratory, UCRL-17225, 1966.

130. Born, M. and T. von Kármán, Phys. Z., 13, 297, 1912.

131. Heisenberg, W., Z. Phys., 49, 619, 1928.

132. Weiss, P., J. Phys. (Paris), 6, 661, 1907.

133. Rao, C. and K. Rao, "Phase Transitions in Solids", McGraw-Hill, New York, 1978.

134. Stanley, H., "Introduction to Phase Transitions and Critical Phenomena", Oxford University Press, Oxford, 1971.

135. Patashinka, A. and V. Pokrovskii, "Fluctuation Theory of Phase Transitions", Pergamon, New York, 1979.

136. Ma, S., "Modern Theory of Critical Phenomena", Benjamin, London, 1976.

137. Norem, W., Ph.D. Thesis, University of Tennessee, Knoxville, 1965.

138. Brooks, C., "A Pulse Heating system for Accurate Measurement of Specific Heat and Electrical Resistivity of Metallic Materials", University of Tennessee, Materials Science and Engineering Department Document, (Unpublished).

139. Basak, D., M.S. Thesis, University of Tennessee, Knoxville, 1992.

140. Burns, G., M. Scroger, G. Strouse, M. Croarkin, and W. Guthrie, "Temperature-Electromotive Force Reference Functions and Tables for the Letter-Designated Thermocouple Types Based on the ITS-90", NIST Monograph 175, U.S. Government Printing Office.

141. Beattie, J., Research Laboratory of Physical Chemistry, Report # 183, Massachusetts Institute of Technology, Cambridge.

142. Cezairliyan, A., J. of Research, NBS, 75c, 7, 1970.

APPENDICES

APPENDIX A- List of Symbols

α	Ni-Mo Phase; Linear TCE
α_i	SRO parameter
β	Ni-Mo phase; Volumetric TCE
δ	Ni-Mo phase
ε_n	Energy of oscillator
γ	Ni-Mo phase; Constant
κ	Isothermal compressibility; Thermal conductivity
λ	Mean free path
ν	Frequency
π	3.1415
θ	Angle between planes
θ_E	Einstein characteristic temperature
θ_R	General characteristic temperature
θ_D	Debye characteristic temperature
ρ	Electrical resistivity
ρ_T	Thermal electrical resistivity
ρ_i	Impurity electrical resistivity
ρ_m	Magnetic electrical resistivity
σ	Electrical conductivity; SRO parameter
τ	Average time between collisions
ψ	Wave function
a	Lattice parameter
$\vec{a}$	Acceleration
b	Lattice parameter
c	Lattice parameter, Heat capacity
c_f	Geometrical shape factor
c_a	Geometrical shape factor
d	Electron orbital; Innerplanar spacing
e	Charge of an electron
f	Electron orbital
f_A	Atom fraction
f_i	Mass fraction
h	Planck's constant
$\hbar$	$h/2\pi$
k	Wave number
k_B	Boltzmann's constant
m	Mass
m_e	Electron rest mass
m^*	Effective mass
n	Quantum number; Number of particles
n_i	Average number of atoms or ions
n_a	Number of particles
p	Probability
q	Electrical charge; Heat
r	Ion radius
$\vec{r}$	Radius vector
s	Electron orbital
t	Time
$\bar{v}$	Average velocity
v	Velocity
v_d	Drift velocity
v_{rms}	Root mean square velocity
v_F	Fermi velocity
x	Indice direction
y	Indice direction
z	Indice direction; Valence electron per atom
A	Area; General plane; General element
B	General plane; General element
C	General plane, Specific heat
D	General plane
E	General plane; Energy; Electrical potential
$\vec{E}$	Electric feild
E_F	Fermi energy
E_K	Kinetic energy
F	Fermi factor
$\vec{F}$	Force
G	Gibb's free energy; Grunsein parameter
H	Enthalpy
J	Isothermal exchange integral
J'	Exchange constant
K	"komplex" state
L	Length
M	Specimen effective mass
N_A	Avagradro's number
Q	Heat
R	Gas constant
$\vec{R}$	Identity period
S	Entropy; spin
T	Temperature
T_C	Critical temperature
T_F	Fermi temperature
U	Potential energy
V	Volume
V_m	Molar volume

APPENDIX B- Swaging and Annealing History of the Ni_4Mo Specimen

Step #	Procedure	Comments
1	Purge furnace with argon	temperature = 950 °C
2	Anneal specimen for 1 hour	temperature = 950 °C
3	Quench in water	alpha phase retained
4	Swage specimen	Die size = 0.562 in.
5	Anneal specimen for 1 hour	temperature = 950 °C
6	Quench in water	alpha phase retained
7	Swage specimen	Die size = 0.500 in.
8	Anneal specimen for 1 hour	temperature = 950 °C
9	Quench in water	alpha phase retained
10	Swage specimen	Die size = 0.437 in.
11	Anneal specimen for 1 hour	temperature = 950 °C
12	Quench in water	alpha phase retained
13	Swage specimen	Die size = 0.406 in.
14	Anneal specimen for 1 hour	temperature = 950 °C
15	Quench in water	alpha phase retained
16	Swage specimen	Die size = 0.375 in.
17	Anneal specimen for 1 hour	temperature = 950 °C
18	Quench in water	alpha phase retained
19	Swage specimen	Die size = 0.312 in.
20	Anneal specimen for 1 hour	temperature = 950 °C
21	Quench in water	alpha phase retained
22	Swage specimen	Die size = 0.281 in.
23	Anneal specimen for 1 hour	temperature = 950 °C
24	Quench in water	alpha phase retained
25	Swage specimen	Die size = 0.218 in.
26	Anneal specimen for 1 hour	temperature = 950 °C
27	Quench in water	alpha phase retained
28	Swage specimen	Die size =0.187 in.
29	Anneal specimen for 1 hour	temperature = 950 °C
30	Quench in water	alpha phase retained
31	Swage specimen	Die size = 0.183 in.
32	Anneal specimen for 1 hour	temperature = 950 °C
33	Quench in water	alpha phase retained
34	Swage specimen	Die size = 0.163 in.
35	Anneal specimen for 1 hour	temperature = 950 °C
36	Quench in water	alpha phase retained
37	Swage specimen	Die size = 0.143 in.
38	Anneal specimen for 1 hour	temperature = 950 °C
39	Quench in water	alpha phase retained
40	Swage specimen	Die size = 0.123 in.

APPENDIX C- Specimen Diameter Measurements

Basak's Data on Long Specimen

Reading	Diameter (in.)
1	0.0700
2	0.0700
3	0.0701
4	0.0700
5	0.0701
6	0.0701
7	0.0701
8	0.0700
9	0.0700
10	0.0701
Average*	0.0701= 0.1781cm

*Average of six central readings

Short Specimen Measurements 9/24/98

Reading	Diameter A (in.)	Diameter B** (in.)
1	0.0688	0.0693
2	0.0692	0.0689
3	0.0692	0.0690
4	0.0690	0.0691
5	0.0695	0.0691
6	0.0698	0.0691
7	0.0698	0.0695
8	0.0694	0.0697
9	0.0694	0.0697
10	0.0698	0.0697
Average	0.06929 in. = 0.1760 cm	

Short Specimen Measurements 11/10/98

Reading	Diameter A (in.)	Diameter B**(in.)
1	0.0689	0.0689
2	0.0695	0.0698
3	0.0699	0.0700
4	0.0701	0.0691
5	0.0698	0.0699
6	0.0702	0.0700
7	0.0705	0.0700
8	0.0700	0.0702
9	0.0703	0.0701
10	0.0702	0.0701
Average	0.06988 in. = 0.1775 cm	

** B is measurements rotating 90 degrees from A

APPENDIX D-Knife Edge Potential Data and Sample Calculations of Effective Length and Room Temperature Electrical Resistivity

Long Specimen data

Potential Across....	Average of Forward Readings (mV)	Average of Reverse Readings (mV)	Average (mV)
Voltage Taps(E_T)	13.11	33.05	33.08
Standard Resistor(E_R)	1300.99	1300.99	1300.99
Knife Edges(E_K)	19.64	19.68	19.66

Knife-edge distance = 2.5339 cm Diameter = 0.178 cm
Standard Resistor = 0.999938 Ω

$$L = \frac{E_T}{E_K} d_K = \frac{33.08mV}{19.66mV} 2.5539cm = 4.2972cm$$

$$I_S = \frac{E_S}{R_S} = \frac{1.30099V}{0.999938\Omega} = 1.30107A$$

$$\rho = \left(\frac{E_T}{I_S}\right)\left(\frac{\pi D^2}{4L}\right) = \left(\frac{0.03308V}{1.30107A}\right)\left(\frac{\pi(0.178cm)^2}{4(4.2972cm)}\right) = 147\mu\Omega cm$$

Short Specimen data

Potential Across....	Average of Forward Readings (mV)	Average of Reverse Readings (mV)	Average (mV)
Voltage Taps(E_T)	13.813	13.270	13.487
Standard Resistor(E_R)	904.39	904.53	904.48
Knife Edges(E_K)	13.559	13.615	13.587

Knife-edge distance = 2.5339 cm Diameter = 0.176 cm
Standard Resistor = 0.999938 Ω

$$L = \frac{E_T}{E_K} d_K = \frac{13.487mV}{13.587mV} 2.5339cm = 2.5208cm$$

$$I_S = \frac{E_S}{R_S} = \frac{0.90448V}{0.999938\Omega} = 0.904536A$$

$$\rho = \left(\frac{E_T}{I_S}\right)\left(\frac{\pi D^2}{4L}\right) = \left(\frac{0.01348V}{0.904536A}\right)\left(\frac{\pi(0.176cm)^2}{4(2.5208cm)}\right) = 144\mu\Omega cm$$

Final Effective Mass Determination Data

Potential Across....	Average of Forward Readings (mV)	Average of Reverse Readings (mV)	Average (mV)
Voltage Taps(E_T)	13.243	13.773	13.508
Standard Resistor(E_R)	904.36	904.53	904.44
Knife Edges(E_K)	13.207	13.751	13.4797

Knife-edge distance = 2.5339 cm Diameter = 0.1775 cm
Standard Resistor = 0.999938 Ω

$$L = \frac{E_T}{E_K} d_K = \frac{13.508mV}{13.479mV} 2.5339cm = 2.5394cm$$

$$I_S = \frac{E_S}{R_S} = \frac{0.90444V}{0.999938\Omega} = 0.904496A$$

$$\rho = \left(\frac{E_T}{I_S}\right)\left(\frac{\pi D^2}{4L}\right) = \left(\frac{0.013508V}{0.904496A}\right)\left(\frac{\pi(0.1775cm)^2}{4(2.5394cm)}\right) = 146\mu\Omega cm$$

APPENDIX E-Amplifier Calibration Data

Fit Results

Fit 1: Linear, Y=B*X+A
Equation:
Y = 10.0106 * X + 0.00569486
Number of data points used = 8
Average X = 0.388875

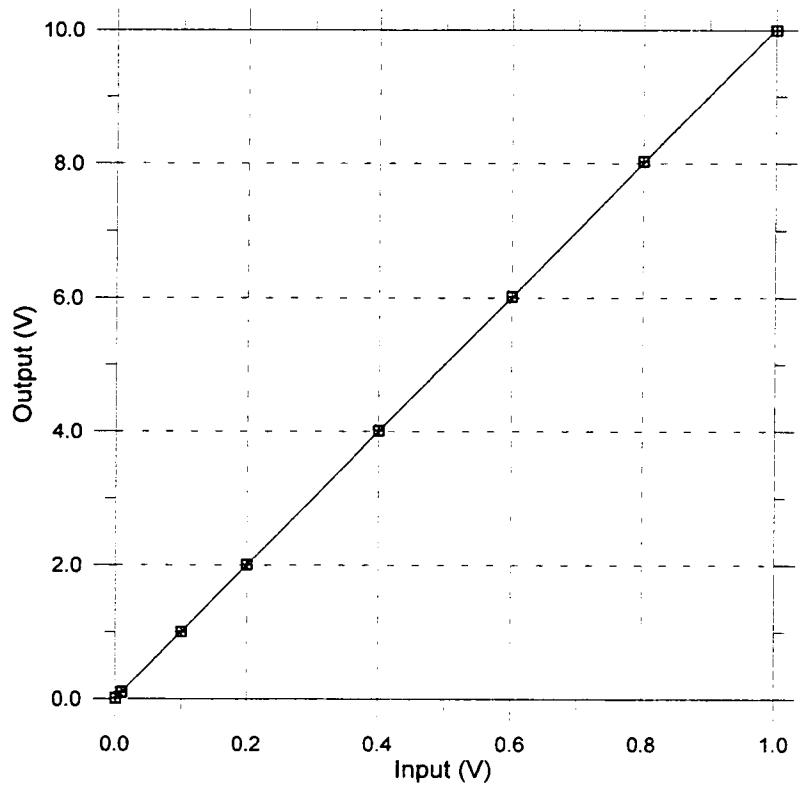

Ch 0	(Current)
V in	V out
0.00100	0.0126
0.01000	0.1026
0.10000	1.0051
0.20000	2.0080
0.40000	4.0129
0.60000	6.0177
0.80000	8.0320
1.00000	9.9976

Fit Results

Fit 2: Linear, Y=B*X+A
Equation:
Y = 0.999537 * X + 0.00281918
Number of data points used = 8
Average X = 3.87625

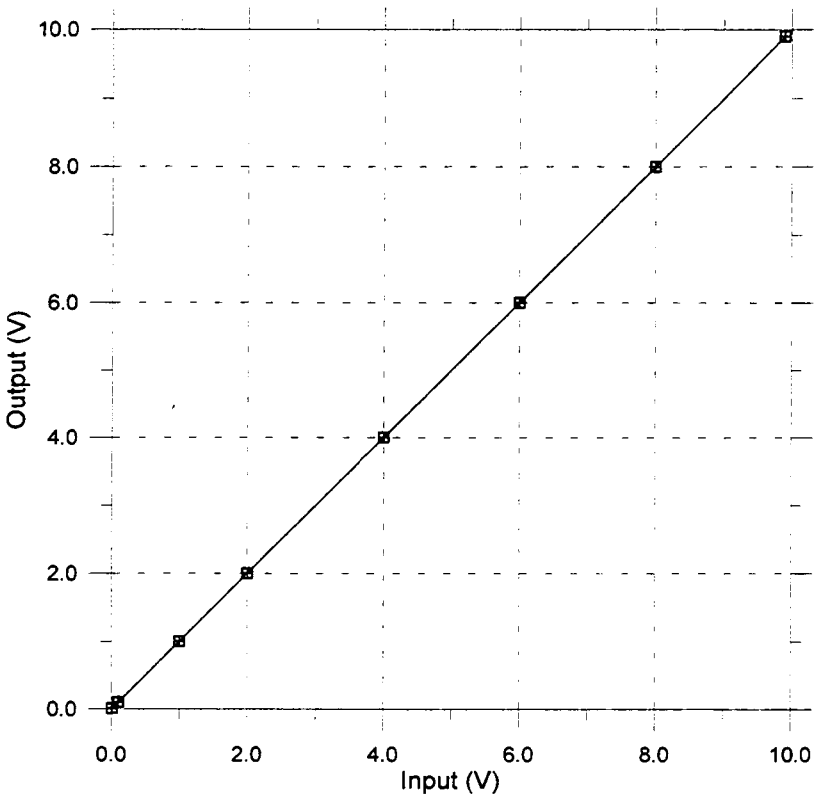

Ch 1 (Voltage)

V in	V out
0.01000	0.0124
0.10000	0.1030
1.00000	1.0028
2.00000	2.0019
4.00000	4.0014
6.00000	6.0001
8.00000	7.9986
9.90000	9.8984

Fit Results

Fit 3: Linear, Y=B*X+A
Equation:
Y = 499.412 * X + 0.00835815
Number of data points used = 13
Average X = 0.00853923

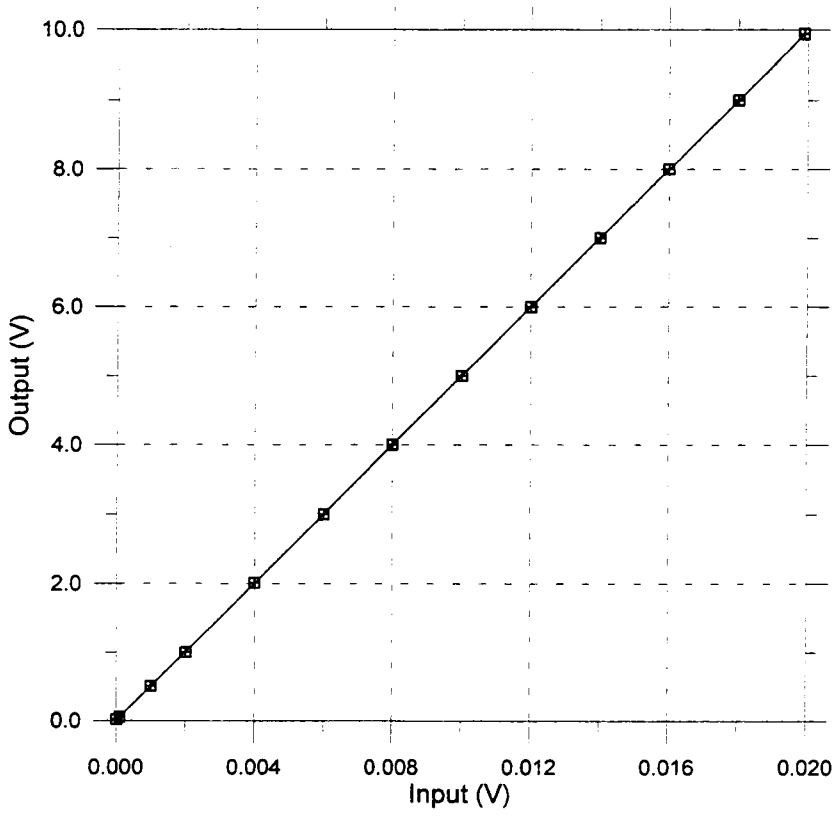

Ch 2 (Thermal emf)

V in	V out	V in	V out
0.00001	0.0216	0.01000	4.9999
0.00010	0.0569	0.01200	5.9999
0.00100	0.5070	0.01400	7.0014
0.00200	1.0000	0.01600	8.0018
0.00400	2.0130	0.01800	8.9988
0.00600	3.0014	0.01990	9.9464
0.00800	4.0004		

APPENDIX F- Example of Raw Data File Generated by the Pulse-Heating Program

Time (Time-Tag #)	Current (A)	Potential (V)	Temperature (e.m.f. mV)	Power (W)	Resistivity (μΩ cm)
1	0	0.00244	0.073	0	0
2	0	0.00244	0.151	0	0
3	0	0.00244	0.107	0	0
4	0	0.00244	0.088	0	0
5	0	0.00244	0.137	0	0
6	0	0.00244	0.112	0	0
7	0	0.00244	0.083	0	0
8	11.548	0.17578	0.112	2.03	146.909
9	25.317	0.37842	0.142	9.581	144.255
10	33.105	0.49561	0.19	16.407	144.482
11	35.181	0.52734	0.171	18.552	144.666
12	34.375	0.5127	0.2	17.624	143.944
13	33.154	0.49805	0.205	16.512	144.98
14	32.642	0.48828	0.249	15.938	144.369
15	32.69	0.48828	0.327	15.962	144.154
16	32.91	0.49316	0.239	16.23	144.623
17	33.008	0.49316	0.303	16.278	144.195
18	33.057	0.49561	0.347	16.383	144.695
19	33.032	0.49561	0.386	16.371	144.802
20	33.032	0.49561	0.366	16.371	144.802
21	32.983	0.49561	0.396	16.347	145.017
22	33.008	0.49316	0.439	16.278	144.195
23	33.032	0.49316	0.405	16.29	144.089
24	33.008	0.49561	0.498	16.359	144.909
25	33.008	0.49316	0.439	16.278	144.195
26	33.008	0.49561	0.518	16.359	144.909
27	33.008	0.49561	0.596	16.359	144.909
28	33.032	0.49561	0.571	16.371	144.802
29	33.032	0.49561	0.586	16.371	144.802
30	33.032	0.49561	0.654	16.371	144.802
31	33.008	0.49561	0.669	16.359	144.909
32	33.032	0.49561	0.659	16.371	144.802
33	33.057	0.49561	0.732	16.383	144.695
34	33.008	0.49561	0.776	16.359	144.909
35	33.008	0.49316	0.786	16.278	144.195
36	33.032	0.49561	0.767	16.371	144.802
37	33.032	0.49561	0.806	16.371	144.802
38	33.032	0.49561	0.859	16.371	144.802
39	33.032	0.49561	0.845	16.371	144.802
40	33.057	0.49561	0.903	16.383	144.695
41	33.032	0.49561	0.933	16.371	144.802

42	33.032	0.49805	1.03	16.452	145.515
43	33.032	0.49805	0.996	16.452	145.515
44	33.032	0.49561	1.104	16.371	144.802
45	33.032	0.49805	1.084	16.452	145.515
46	33.032	0.49805	1.084	16.452	145.515
47	33.032	0.49805	1.133	16.452	145.515
48	33.008	0.49561	1.211	16.359	144.909
49	33.032	0.49561	1.172	16.371	144.802
50	33.032	0.49805	1.235	16.452	145.515
51	33.032	0.49805	1.294	16.452	145.515
52	32.983	0.49561	1.24	16.347	145.017
53	33.032	0.49805	1.353	16.452	145.515
54	33.032	0.49805	1.367	16.452	145.515
55	33.032	0.49805	1.338	16.452	145.515
56	33.032	0.49805	1.45	16.452	145.515
57	33.008	0.49805	1.45	16.439	145.623
58	33.032	0.49805	1.44	16.452	145.515
59	33.032	0.49805	1.455	16.452	145.515
60	33.057	0.49805	1.528	16.464	145.408
61	33.032	0.49805	1.533	16.452	145.515
62	32.983	0.49805	1.641	16.427	145.731
63	33.032	0.49805	1.582	16.452	145.515
64	33.032	0.49805	1.724	16.452	145.515
65	33.032	0.49805	1.758	16.452	145.515
66	33.032	0.49805	1.777	16.452	145.515
67	33.057	0.49805	1.807	16.464	145.408
68	33.032	0.49805	1.836	16.452	145.515
69	33.032	0.49805	1.885	16.452	145.515
70	33.032	0.49805	1.885	16.452	145.515
71	33.032	0.49805	1.826	16.452	145.515
72	33.032	0.49805	1.997	16.452	145.515
73	33.032	0.49805	1.997	16.452	145.515
74	33.057	0.50049	2.061	16.544	146.121
75	33.032	0.49805	2.075	16.452	145.515
76	33.032	0.50049	2.148	16.532	146.229
77	33.032	0.50049	2.148	16.532	146.229
78	33.032	0.50049	2.188	16.532	146.229
79	33.008	0.50049	2.134	16.52	146.337
80	33.032	0.50049	2.261	16.532	146.229
81	33.032	0.50049	2.285	16.532	146.229
82	33.057	0.50049	2.222	16.544	146.121
83	33.057	0.50049	2.339	16.544	146.121
84	33.032	0.50049	2.339	16.532	146.229
85	33.032	0.50049	2.354	16.532	146.229
86	33.008	0.49805	2.485	16.439	145.623
87	33.032	0.50049	2.441	16.532	146.229
88	33.032	0.50049	2.524	16.532	146.229

89	32.983	0.50049	2.549	16.508	146.445
90	33.032	0.50049	2.578	16.532	146.229
91	33.032	0.50049	2.539	16.532	146.229
92	33.032	0.50049	2.612	16.532	146.229
93	33.032	0.50049	2.598	16.532	146.229
94	33.032	0.50049	2.661	16.532	146.229
95	33.032	0.50049	2.729	16.532	146.229
96	33.032	0.50049	2.783	16.532	146.229
97	33.008	0.50049	2.847	16.52	146.337
98	33.032	0.50049	2.798	16.532	146.229
99	33.032	0.50049	2.92	16.532	146.229
100	33.032	0.50049	2.925	16.532	146.229
101	33.057	0.50049	2.949	16.544	146.121
102	33.032	0.50049	2.993	16.532	146.229
103	33.032	0.50293	3.027	16.613	146.942
104	33.057	0.50293	3.101	16.625	146.834
105	33.032	0.50293	3.086	16.613	146.942
106	33.008	0.50049	3.115	16.52	146.337
107	33.032	0.50293	3.14	16.613	146.942
108	33.032	0.50293	3.198	16.613	146.942
109	33.032	0.50049	3.276	16.532	146.229
110	33.032	0.50293	3.306	16.613	146.942
111	33.032	0.50293	3.296	16.613	146.942
112	33.008	0.50293	3.384	16.601	147.051
113	33.032	0.50293	3.418	16.613	146.942
114	33.057	0.50293	3.442	16.625	146.834
115	33.008	0.50293	3.491	16.601	147.051
116	33.008	0.50293	3.486	16.601	147.051
117	33.008	0.50293	3.521	16.601	147.051
118	33.057	0.50293	3.564	16.625	146.834
119	33.032	0.50293	3.613	16.613	146.942
120	33.057	0.50293	3.647	16.625	146.834
121	33.057	0.50293	3.701	16.625	146.834
122	33.032	0.50293	3.73	16.613	146.942
123	33.008	0.50537	3.73	16.681	147.765
124	33.008	0.50293	3.774	16.601	147.051
125	33.032	0.50293	3.716	16.613	146.942
126	33.032	0.50293	3.867	16.613	146.942
127	33.032	0.50293	3.906	16.613	146.942
128	33.057	0.50293	3.906	16.625	146.834
129	33.032	0.50293	3.901	16.613	146.942
130	33.032	0.50293	3.945	16.613	146.942
131	33.057	0.50537	4.043	16.706	147.546
132	33.032	0.50293	4.067	16.613	146.942
133	33.008	0.50293	4.111	16.601	147.051
134	33.032	0.50537	4.17	16.694	147.655
135	33.057	0.50537	4.233	16.706	147.546

136	33.032	0.50537	4.224	16.694	147.655
137	33.057	0.50537	4.287	16.706	147.546
138	33.008	0.50537	4.277	16.681	147.765
139	33.032	0.50537	4.331	16.694	147.655
140	33.032	0.50537	4.37	16.694	147.655
141	33.057	0.50537	4.404	16.706	147.546
142	33.032	0.50537	4.414	16.694	147.655
143	33.032	0.50537	4.463	16.694	147.655
144	33.057	0.50537	4.482	16.706	147.546
145	33.057	0.50537	4.556	16.706	147.546
146	33.057	0.50537	4.604	16.706	147.546
147	33.057	0.50537	4.609	16.706	147.546
148	33.057	0.50537	4.609	16.706	147.546
149	33.032	0.50537	4.629	16.694	147.655
150	33.032	0.50537	4.727	16.694	147.655
151	33.032	0.50537	4.707	16.694	147.655
152	33.032	0.50537	4.844	16.694	147.655
153	33.057	0.50537	4.868	16.706	147.546
154	33.057	0.50537	4.829	16.706	147.546
155	33.081	0.50781	4.907	16.799	148.15
156	33.032	0.50537	4.868	16.694	147.655
157	33.032	0.50537	4.985	16.694	147.655
158	33.032	0.50537	4.985	16.694	147.655
159	33.032	0.50781	5.024	16.774	148.369
160	33.032	0.50781	5.034	16.774	148.369
161	33.057	0.50537	5.166	16.706	147.546
162	33.032	0.50781	5.024	16.774	148.369
163	33.032	0.50781	5.19	16.774	148.369
164	33.032	0.50781	5.249	16.774	148.369
165	33.008	0.50781	5.239	16.762	148.478
166	33.032	0.50781	5.195	16.774	148.369
167	33.032	0.50781	5.347	16.774	148.369
168	33.057	0.50781	5.342	16.787	148.259
169	33.032	0.50781	5.376	16.774	148.369
170	33.032	0.50781	5.386	16.774	148.369
171	33.057	0.50781	5.405	16.787	148.259
172	33.057	0.50781	5.547	16.787	148.259
173	33.032	0.50781	5.542	16.774	148.369
174	33.032	0.50781	5.591	16.774	148.369
175	33.032	0.50781	5.62	16.774	148.369
176	33.032	0.50781	5.64	16.774	148.369
177	33.008	0.50781	5.708	16.762	148.478
178	33.032	0.51025	5.752	16.855	149.082
179	33.057	0.50781	5.737	16.787	148.259
180	33.032	0.50781	5.713	16.774	148.369
181	33.032	0.51025	5.864	16.855	149.082
182	33.057	0.50781	5.815	16.787	148.259

183	33.032	0.51025	5.923	16.855	149.082
184	33.057	0.50781	5.859	16.787	148.259
185	33.057	0.50781	5.918	16.787	148.259
186	33.032	0.51025	6.001	16.855	149.082
187	33.008	0.50781	6.064	16.762	148.478
188	33.032	0.51025	6.074	16.855	149.082
189	33.057	0.51025	6.123	16.867	148.972
190	33.057	0.51025	6.113	16.867	148.972
191	33.032	0.51025	6.177	16.855	149.082
192	33.032	0.51025	6.201	16.855	149.082
193	33.032	0.51025	6.255	16.855	149.082
194	33.032	0.51025	6.27	16.855	149.082
195	33.057	0.51025	6.25	16.867	148.972
196	33.008	0.51025	6.304	16.842	149.192
197	33.032	0.51025	6.392	16.855	149.082
198	33.032	0.51025	6.396	16.855	149.082
199	33.057	0.51025	6.465	16.867	148.972
200	33.008	0.51025	6.489	16.842	149.192
201	33.032	0.51025	6.533	16.855	149.082
202	33.032	0.51025	6.572	16.855	149.082
203	33.032	0.51025	6.558	16.855	149.082
204	33.008	0.51025	6.484	16.842	149.192
205	33.032	0.51025	6.631	16.855	149.082
206	33.032	0.51025	6.67	16.855	149.082
207	33.057	0.51025	6.67	16.867	148.972
208	33.032	0.51025	6.704	16.855	149.082
209	33.057	0.51025	6.782	16.867	148.972
210	33.032	0.50781	6.758	16.774	148.369
211	33.008	0.51025	6.831	16.842	149.192
212	33.057	0.50781	6.914	16.787	148.259
213	33.008	0.50781	6.929	16.762	148.478
214	33.008	0.50781	6.831	16.762	148.478
215	33.057	0.50781	6.909	16.787	148.259
216	33.032	0.50781	7.051	16.774	148.369
217	33.032	0.50537	7.021	16.694	147.655
218	33.057	0.50537	6.953	16.706	147.546
219	33.032	0.50537	7.07	16.694	147.655
220	33.032	0.50537	7.1	16.694	147.655
221	33.008	0.50537	7.1	16.681	147.765
222	33.032	0.50537	7.129	16.694	147.655
223	33.032	0.50537	7.197	16.694	147.655
224	33.032	0.50537	7.109	16.694	147.655
225	33.032	0.50293	7.236	16.613	146.942
226	33.057	0.50537	7.158	16.706	147.546
227	33.032	0.50293	7.241	16.613	146.942
228	33.032	0.50293	7.212	16.613	146.942
229	33.032	0.50293	7.271	16.613	146.942

230	33.032	0.50293	7.28	16.613	146.942
231	33.008	0.50049	7.363	16.52	146.337
232	33.032	0.50049	7.397	16.532	146.229
233	33.032	0.50049	7.363	16.532	146.229
234	33.057	0.50049	7.397	16.544	146.121
235	33.032	0.49805	7.441	16.452	145.515
236	33.032	0.50049	7.49	16.532	146.229
237	33.032	0.49805	7.412	16.452	145.515
238	33.032	0.49805	7.461	16.452	145.515
239	33.057	0.49805	7.539	16.464	145.408
240	33.008	0.49561	7.554	16.359	144.909
241	33.032	0.49561	7.622	16.371	144.802
242	33.032	0.49561	7.563	16.371	144.802
243	33.057	0.49561	7.676	16.383	144.695
244	33.032	0.49316	7.656	16.29	144.089
245	33.057	0.49316	7.622	16.302	143.982
246	33.057	0.49316	7.695	16.302	143.982
247	33.032	0.49316	7.69	16.29	144.089
248	33.032	0.49072	7.676	16.21	143.376
249	33.008	0.49072	7.681	16.198	143.482
250	33.032	0.49072	7.778	16.21	143.376
251	33.057	0.49072	7.808	16.222	143.27
252	33.057	0.48828	7.778	16.141	142.557
253	33.081	0.48828	7.759	16.153	142.452
254	33.032	0.48828	7.822	16.129	142.662
255	33.057	0.48828	7.832	16.141	142.557
256	33.057	0.48828	7.9	16.141	142.557
257	33.032	0.48584	7.886	16.048	141.949
258	33.008	0.48584	7.93	16.037	142.054
259	33.057	0.48584	7.964	16.06	141.844
260	33.057	0.48584	7.974	16.06	141.844
261	33.057	0.48584	7.988	16.06	141.844
262	33.057	0.48584	7.988	16.06	141.844
263	33.032	0.4834	8.042	15.968	141.236
264	33.057	0.4834	8.057	15.98	141.131
265	33.032	0.4834	8.13	15.968	141.236
266	33.081	0.4834	8.047	15.991	141.027
267	33.057	0.48096	8.115	15.899	140.419
268	33.057	0.48096	8.047	15.899	140.419
269	33.032	0.48096	8.091	15.887	140.522
270	33.057	0.48096	8.213	15.899	140.419
271	33.008	0.48096	8.242	15.875	140.626
272	33.057	0.48096	8.169	15.899	140.419
273	33.057	0.48096	8.223	15.899	140.419
274	33.057	0.47852	8.242	15.818	139.706
275	33.032	0.47852	8.286	15.806	139.809
276	33.032	0.47852	8.296	15.806	139.809

277	33.057	0.47852	8.325	15.818	139.706
278	33.081	0.47852	8.34	15.83	139.603
279	33.057	0.47852	8.296	15.818	139.706
280	33.057	0.47607	8.364	15.737	138.993
281	33.032	0.47852	8.389	15.806	139.809
282	33.057	0.47607	8.311	15.737	138.993
283	33.057	0.47607	8.438	15.737	138.993
284	33.057	0.47607	8.457	15.737	138.993
285	33.008	0.47607	8.428	15.714	139.199
286	33.057	0.47607	8.511	15.737	138.993
287	33.057	0.47607	8.491	15.737	138.993
288	33.081	0.47363	8.486	15.668	138.178
289	33.057	0.47363	8.535	15.657	138.28
290	33.057	0.47363	8.535	15.657	138.28
291	33.057	0.47363	8.623	15.657	138.28
292	33.032	0.47363	8.633	15.645	138.382
293	33.057	0.47363	8.643	15.657	138.28
294	33.057	0.47363	8.682	15.657	138.28
295	33.057	0.47119	8.687	15.576	137.567
296	33.057	0.47363	8.711	15.657	138.28
297	33.057	0.47119	8.735	15.576	137.567
298	33.057	0.47363	8.716	15.657	138.28
299	33.057	0.47119	8.765	15.576	137.567
300	33.081	0.47119	8.76	15.588	137.466
301	33.057	0.47119	8.76	15.576	137.567
302	33.032	0.47119	8.833	15.565	137.669
303	33.057	0.47119	8.848	15.576	137.567
304	33.057	0.47119	8.833	15.576	137.567
305	33.081	0.47119	8.892	15.588	137.466
306	33.057	0.47119	8.926	15.576	137.567
307	33.057	0.46875	8.931	15.495	136.855
308	33.057	0.46875	8.95	15.495	136.855
309	33.032	0.46875	8.979	15.484	136.956
310	33.057	0.46875	8.994	15.495	136.855
311	33.057	0.46875	8.984	15.495	136.855
312	33.032	0.46631	9.038	15.403	136.242
313	33.057	0.46875	9.077	15.495	136.855
314	33.081	0.46875	9.067	15.507	136.754
315	33.081	0.46631	9.131	15.426	136.041
316	33.081	0.46875	9.033	15.507	136.754
317	33.081	0.46631	9.165	15.426	136.041
318	33.057	0.46631	9.111	15.415	136.142
319	33.032	0.46631	9.165	15.403	136.242
320	33.032	0.46631	9.141	15.403	136.242
321	33.057	0.46631	9.043	15.415	136.142
322	33.057	0.46631	9.214	15.415	136.142
323	33.081	0.46631	9.253	15.426	136.041

324	33.081	0.46631	9.253	15.426	136.041
325	33.057	0.46387	9.316	15.334	135.429
326	33.057	0.46631	9.292	15.415	136.142
327	33.105	0.46631	9.321	15.437	135.941
328	33.057	0.46387	9.292	15.334	135.429
329	33.032	0.46387	9.336	15.323	135.529
330	33.081	0.46387	9.385	15.345	135.329
331	33.081	0.46387	9.307	15.345	135.329
332	33.057	0.46387	9.395	15.334	135.429
333	33.057	0.46387	9.316	15.334	135.429
334	33.032	0.46387	9.331	15.323	135.529
335	33.057	0.46387	9.424	15.334	135.429
336	33.057	0.46387	9.448	15.334	135.429
337	33.081	0.46387	9.448	15.345	135.329
338	33.057	0.46387	9.458	15.334	135.429
339	33.057	0.46143	9.438	15.253	134.716
340	33.057	0.46387	9.512	15.334	135.429
341	33.081	0.46143	9.585	15.264	134.617
342	33.057	0.46143	9.57	15.253	134.716
343	33.081	0.46143	9.57	15.264	134.617
344	33.057	0.46143	9.639	15.253	134.716
345	33.057	0.46143	9.639	15.253	134.716
346	33.057	0.46143	9.551	15.253	134.716
347	33.057	0.46143	9.604	15.253	134.716
348	33.081	0.46143	9.678	15.264	134.617
349	33.081	0.46143	9.697	15.264	134.617
350	33.081	0.46143	9.717	15.264	134.617
351	33.081	0.46143	9.731	15.264	134.617
352	33.057	0.45898	9.741	15.172	134.003
353	33.057	0.46143	9.79	15.253	134.716
354	33.081	0.45898	9.663	15.184	133.905
355	33.057	0.45898	9.824	15.172	134.003
356	33.032	0.45898	9.829	15.161	134.103
357	33.081	0.45898	9.849	15.184	133.905
358	33.057	0.45898	9.873	15.172	134.003
359	33.081	0.45898	9.814	15.184	133.905
360	33.081	0.45898	9.932	15.184	133.905
361	33.081	0.45898	9.927	15.184	133.905
362	33.057	0.45898	9.81	15.172	134.003
363	33.057	0.45898	10.015	15.172	134.003
364	33.081	0.45898	9.956	15.184	133.905
365	33.081	0.45898	9.941	15.184	133.905
366	33.081	0.45654	9.932	15.103	133.192
367	33.081	0.45654	9.976	15.103	133.192
368	33.081	0.45654	9.98	15.103	133.192
369	33.032	0.45654	9.902	15.081	133.389
370	33.081	0.45898	10.034	15.184	133.905

371	33.081	0.45654	10.01	15.103	133.192
372	33.081	0.45898	10.015	15.184	133.905
373	33.057	0.45654	10.127	15.092	133.291
374	33.081	0.45654	10.054	15.103	133.192
375	33.081	0.45654	10.117	15.103	133.192
376	33.081	0.45654	10.107	15.103	133.192
377	33.081	0.45654	10.142	15.103	133.192
378	33.081	0.45654	10.098	15.103	133.192
379	33.081	0.45654	10.107	15.103	133.192
380	33.081	0.45654	10.21	15.103	133.192
381	33.081	0.45654	10.146	15.103	133.192
382	33.081	0.45654	10.244	15.103	133.192
383	33.032	0.45654	10.151	15.081	133.389
384	33.081	0.45654	10.259	15.103	133.192
385	33.081	0.45654	10.181	15.103	133.192
386	33.081	0.4541	10.278	15.022	132.48
387	33.081	0.4541	10.322	15.022	132.48
388	33.081	0.4541	10.293	15.022	132.48
389	33.057	0.4541	10.317	15.011	132.578
390	33.057	0.4541	10.322	15.011	132.578
391	33.057	0.4541	10.342	15.011	132.578
392	33.057	0.4541	10.405	15.011	132.578
393	33.081	0.4541	10.356	15.022	132.48
394	33.081	0.4541	10.352	15.022	132.48
395	33.081	0.4541	10.332	15.022	132.48
396	33.081	0.4541	10.327	15.022	132.48
397	33.081	0.4541	10.356	15.022	132.48
398	33.081	0.4541	10.488	15.022	132.48
399	33.081	0.4541	10.488	15.022	132.48
400	33.057	0.4541	10.459	15.011	132.578
401	33.081	0.4541	10.503	15.022	132.48
402	33.081	0.4541	10.4	15.022	132.48
403	33.081	0.4541	10.513	15.022	132.48
404	33.081	0.4541	10.454	15.022	132.48
405	33.105	0.45166	10.581	14.952	131.671
406	33.081	0.45166	10.498	14.941	131.768
407	33.081	0.4541	10.571	15.022	132.48
408	33.081	0.4541	10.576	15.022	132.48
409	33.057	0.4541	10.464	15.011	132.578
410	33.057	0.45166	10.625	14.93	131.865
411	33.057	0.45166	10.591	14.93	131.865
412	33.057	0.45166	10.649	14.93	131.865
413	33.081	0.45166	10.615	14.941	131.768
414	33.081	0.45166	10.62	14.941	131.768
415	33.081	0.45166	10.63	14.941	131.768
416	33.057	0.45166	10.659	14.93	131.865
417	33.057	0.45166	10.708	14.93	131.865

418	33.032	0.45166	10.708	14.919	131.963
419	33.057	0.45166	10.659	14.93	131.865
420	33.081	0.45166	10.723	14.941	131.768
421	33.081	0.45166	10.664	14.941	131.768
422	33.081	0.45166	10.684	14.941	131.768
423	33.081	0.45166	10.752	14.941	131.768
424	33.081	0.45166	10.811	14.941	131.768
425	33.081	0.45166	10.864	14.941	131.768
426	33.057	0.45166	10.786	14.93	131.865
427	33.032	0.44922	10.82	14.839	131.249
428	33.081	0.45166	10.83	14.941	131.768
429	33.081	0.45166	10.791	14.941	131.768
430	33.081	0.45166	10.845	14.941	131.768
431	33.057	0.45166	10.889	14.93	131.865
432	33.057	0.44922	10.884	14.85	131.152
433	33.057	0.45166	10.801	14.93	131.865
434	33.057	0.45166	10.903	14.93	131.865
435	33.081	0.45166	10.913	14.941	131.768
436	33.081	0.44922	10.864	14.861	131.056
437	33.081	0.44922	10.879	14.861	131.056
438	33.081	0.44922	11.011	14.861	131.056
439	33.081	0.44922	11.055	14.861	131.056
440	33.057	0.45166	10.962	14.93	131.865
441	33.105	0.44922	11.001	14.872	130.959
442	33.081	0.44922	11.006	14.861	131.056
443	33.081	0.44922	10.996	14.861	131.056
444	33.057	0.44922	10.908	14.85	131.152
445	33.057	0.45166	11.03	14.93	131.865
446	33.081	0.44922	10.942	14.861	131.056
447	33.081	0.44922	11.074	14.861	131.056
448	33.081	0.44922	10.977	14.861	131.056
449	33.081	0.44922	10.986	14.861	131.056
450	33.057	0.44922	11.089	14.85	131.152
451	33.081	0.44678	11.03	14.78	130.343
452	33.081	0.44922	11.128	14.861	131.056
453	33.081	0.44922	11.118	14.861	131.056
454	33.032	0.44922	11.162	14.839	131.249
455	33.081	0.44678	11.147	14.78	130.343
456	33.081	0.44678	11.206	14.78	130.343
457	33.081	0.44922	11.104	14.861	131.056
458	33.081	0.44922	11.182	14.861	131.056
459	33.057	0.44922	11.182	14.85	131.152
460	33.057	0.44922	11.138	14.85	131.152
461	33.081	0.44678	11.123	14.78	130.343
462	33.105	0.44922	11.211	14.872	130.959
463	33.081	0.44922	11.25	14.861	131.056
464	33.081	0.44678	11.172	14.78	130.343

465	33.081	0.44678	11.196	14.78	130.343
466	33.081	0.44678	11.265	14.78	130.343
467	33.057	0.44678	11.284	14.769	130.44
468	33.081	0.44922	11.265	14.861	131.056
469	33.081	0.44922	11.274	14.861	131.056
470	33.057	0.44678	11.343	14.769	130.44
471	33.057	0.44678	11.333	14.769	130.44
472	33.081	0.44678	11.318	14.78	130.343
473	33.081	0.44678	11.338	14.78	130.343
474	33.081	0.44678	11.343	14.78	130.343
475	33.081	0.44678	11.27	14.78	130.343
476	33.081	0.44922	11.343	14.861	131.056
477	33.057	0.44678	11.274	14.769	130.44
478	33.081	0.44678	11.431	14.78	130.343
479	33.081	0.44922	11.392	14.861	131.056
480	33.057	0.44678	11.26	14.769	130.44
481	33.057	0.44678	11.426	14.769	130.44
482	33.081	0.44678	11.382	14.78	130.343
483	33.081	0.44678	11.436	14.78	130.343
484	33.081	0.44678	11.348	14.78	130.343
485	33.081	0.44678	11.465	14.78	130.343
486	33.081	0.44678	11.445	14.78	130.343
487	33.057	0.44678	11.372	14.769	130.44
488	33.057	0.44678	11.421	14.769	130.44
489	33.105	0.44678	11.475	14.791	130.247
490	33.057	0.44678	11.494	14.769	130.44
491	33.081	0.44678	11.504	14.78	130.343
492	33.081	0.44678	11.431	14.78	130.343
493	33.081	0.44678	11.387	14.78	130.343
494	33.032	0.44678	11.509	14.758	130.536
495	33.081	0.44678	11.514	14.78	130.343
496	33.081	0.44678	11.494	14.78	130.343
497	33.057	0.44434	11.543	14.688	129.727
498	33.057	0.44678	11.533	14.769	130.44
499	33.081	0.44434	11.538	14.699	129.631
500	33.057	0.44678	11.421	14.769	130.44
501	33.081	0.44678	11.558	14.78	130.343
502	33.081	0.44678	11.538	14.78	130.343
503	33.081	0.44678	11.538	14.78	130.343
504	33.081	0.44678	11.514	14.78	130.343
505	33.057	0.44678	11.597	14.769	130.44
506	33.081	0.44434	11.577	14.699	129.631
507	33.081	0.44678	11.533	14.78	130.343
508	33.032	0.44434	11.567	14.677	129.823
509	33.081	0.44678	11.631	14.78	130.343
510	33.081	0.44434	11.655	14.699	129.631
511	31.299	0.42236	11.616	13.219	130.237

512	20.068	0.271	11.65	5.438	130.325
513	6.421	0.09033	11.582	0.58	135.776
514	0	0.00488	11.631	0	0
515	0	0.00488	11.592	0	0
516	0	0.00488	11.221	0	0
517	0	0.00488	10.918	0	0
518	0	0.00488	10.605	0	0
519	0	0.00488	10.317	0	0
520	0	0.00488	10.01	0	0
521	0	0.00488	9.844	0	0
522	0	0.00488	9.507	0	0
523	0	0.00488	9.277	0	0
524	0	0.00488	9.16	0	0
525	0	0.00488	8.887	0	0
526	0	0.00488	8.696	0	0
527	0	0.00488	8.53	0	0
528	0	0.00488	8.33	0	0
529	0	0.00488	8.105	0	0
530	0	0.00244	7.983	0	0
531	0	0.00488	7.93	0	0
532	0	0.00488	7.739	0	0
533	0	0.00488	7.476	0	0
534	0	0.00488	7.393	0	0
535	0	0.00244	7.271	0	0
536	0	0.00488	7.095	0	0
537	0	0.00244	7.046	0	0
538	0	0.00244	6.763	0	0
539	0	0.00488	6.626	0	0
540	0	0.00244	6.553	0	0
541	0	0.00244	6.431	0	0
542	0	0.00244	6.274	0	0
543	0	0.00244	6.143	0	0
544	0	0.00488	6.064	0	0
545	0	0.00244	5.913	0	0
546	0	0.00244	5.859	0	0
547	0	0.00244	5.718	0	0
548	0	0.00244	5.518	0	0
549	0	0.00244	5.474	0	0
550	0	0.00488	5.43	0	0
551	0	0.00488	5.171	0	0
552	0	0.00244	5.112	0	0
553	0	0.00244	5.059	0	0
554	0	0.00488	4.941	0	0
555	0	0.00488	4.741	0	0
556	0	0.00244	4.829	0	0
557	0	0.00244	4.756	0	0
558	0	0.00244	4.561	0	0

559	0	0.00244	4.526	0	0
560	0	0.00244	4.409	0	0
561	0	0.00244	4.404	0	0
562	0	0.00244	4.268	0	0
563	0	0.00244	4.185	0	0
564	0	0.00244	4.092	0	0
565	0	0.00244	4.063	0	0
566	0	0.00244	4.004	0	0
567	0	0.00244	3.896	0	0
568	0	0.00244	3.833	0	0
569	0	0.00244	3.838	0	0
570	0	0.00244	3.843	0	0
571	0	0.00488	3.755	0	0
572	0	0.00244	3.711	0	0
573	0	0.00488	3.569	0	0
574	0	0.00244	3.535	0	0
575	0	0.00244	3.447	0	0
576	0	0.00244	3.467	0	0
577	0	0.00244	3.33	0	0
578	0	0.00244	3.379	0	0
579	0	0.00244	3.369	0	0
580	0	0.00244	3.149	0	0
581	0	0.00244	3.169	0	0
582	0	0.00244	3.105	0	0
583	0	0.00244	3.066	0	0
584	0	0.00244	3.115	0	0
585	0	0.00244	2.964	0	0
586	0	0.00488	2.959	0	0
587	0	0.00244	2.9	0	0
588	0	0.00244	2.847	0	0
589	0	0.00244	2.847	0	0
590	0	0.00244	2.783	0	0
591	0	0.00244	2.72	0	0
592	0	0.00244	2.69	0	0
593	0	0.00244	2.646	0	0
594	0	0.00244	2.607	0	0
595	0	0.00488	2.573	0	0
596	0	0.00244	2.598	0	0
597	0	0.00488	2.568	0	0
598	0	0.00244	2.52	0	0
599	0	0.00244	2.397	0	0
600	0	0.00244	2.417	0	0
601	0	0.00244	2.407	0	0
602	0	0.00244	2.349	0	0
603	0	0.00244	2.295	0	0
604	0	0.00244	2.29	0	0
605	0	0.00244	2.246	0	0

606	0	0.00244	2.236	0	0
607	0	0.00244	2.188	0	0
608	0	0.00244	2.207	0	0
609	0	0.00244	2.129	0	0
610	0	0.00488	2.065	0	0
611	0	0.00244	2.168	0	0
612	0	0.00244	2.129	0	0
613	0	0.00244	2.007	0	0
614	0	0.00244	2.026	0	0
615	0	0.00244	1.963	0	0
616	0	0.00244	1.924	0	0
617	0	0.00244	1.924	0	0
618	0	0.00244	1.909	0	0
619	0	0.00244	1.89	0	0
620	0	0.00244	1.895	0	0
621	0	0.00244	1.934	0	0
622	0	0.00244	1.821	0	0
623	0	0.00244	1.787	0	0
624	0	0.00244	1.865	0	0
625	0	0.00244	1.758	0	0
626	0	0.00244	1.787	0	0
627	0	0.00244	1.724	0	0
628	0	0.00244	1.743	0	0
629	0	0.00244	1.655	0	0
630	0	0.00244	1.65	0	0
631	0	0.00244	1.577	0	0
632	0	0.00244	1.685	0	0
633	0	0.00244	1.685	0	0
634	0	0.00244	1.572	0	0
635	0	0.00244	1.509	0	0
636	0	0.00244	1.538	0	0
637	0	0.00244	1.523	0	0
638	0	0.00244	1.533	0	0
639	0	0.00244	1.445	0	0
640	0	0.00244	1.489	0	0
641	0	0.00244	1.548	0	0
642	0	0.00244	1.396	0	0
643	0	0.00244	1.431	0	0
644	0	0.00244	1.362	0	0
645	0	0.00244	1.387	0	0
646	0	0.00244	1.348	0	0
647	0	0.00244	1.289	0	0
648	0	0.00488	1.353	0	0
649	0	0.00244	1.265	0	0
650	0	0.00244	1.348	0	0
651	0	0.00244	1.255	0	0
652	0	0.00244	1.216	0	0

653	0	0.00244	1.265	0	0
654	0	0.00244	1.289	0	0
655	0	0.00244	1.201	0	0
656	0	0.00244	1.216	0	0
657	0	0.00244	1.279	0	0
658	0	0.00244	1.162	0	0
659	0	0.00244	1.226	0	0
660	0	0.00244	1.201	0	0
661	0	0.00244	1.211	0	0
662	0	0.00244	1.157	0	0
663	0	0.00244	1.187	0	0
664	0	0.00244	1.108	0	0
665	0	0.00244	1.172	0	0
666	0	0.00244	1.118	0	0
667	0	0.00244	1.055	0	0
668	0	0.00244	1.074	0	0
669	0	0.00244	1.079	0	0
670	0	0.00244	1.016	0	0
671	0	0.00244	1.099	0	0
672	0	0.00244	1.074	0	0
673	0	0.00244	0.996	0	0
674	0	0.00244	1.001	0	0
675	0	0.00244	0.938	0	0
676	0	0.00244	0.981	0	0
677	0	0.00244	0.962	0	0
678	0	0.00244	1.079	0	0
679	0	0.00244	0.957	0	0
680	0	0.00244	0.972	0	0
681	0	0.00244	0.972	0	0
682	0	0.00244	0.928	0	0
683	0	0.00244	0.923	0	0
684	0	0.00244	0.898	0	0
685	0	0.00244	0.918	0	0
686	0	0.00244	0.918	0	0
687	0	0.00244	0.967	0	0
688	0	0.00244	0.898	0	0
689	0	0.00244	0.908	0	0
690	0	0.00244	0.918	0	0
691	0	0.00244	0.82	0	0
692	0	0.00244	0.796	0	0
693	0	0.00244	0.791	0	0
694	0	0.00244	0.85	0	0
695	0	0.00244	0.864	0	0
696	0	0.00244	0.806	0	0
697	0	0.00244	0.825	0	0
698	0	0.00244	0.811	0	0
699	0	0.00244	0.757	0	0

700	0	0.00244	0.796	0	0
701	0	0.00244	0.718	0	0
702	0	0.00244	0.762	0	0
703	0	0.00244	0.723	0	0
704	0	0.00244	0.713	0	0
705	0	0.00244	0.723	0	0
706	0	0.00244	0.732	0	0
707	0	0.00244	0.762	0	0
708	0	0.00244	0.728	0	0
709	0	0.00244	0.669	0	0
710	0	0.00244	0.806	0	0
711	0	0.00244	0.693	0	0
712	0	0.00244	0.654	0	0
713	0	0.00244	0.63	0	0
714	0	0.00244	0.654	0	0
715	0	0.00244	0.728	0	0
716	0	0.00244	0.669	0	0
717	0	0.00244	0.723	0	0
718	0	0.00244	0.747	0	0
719	0	0.00244	0.645	0	0
720	0	0.00244	0.713	0	0
721	0	0.00244	0.664	0	0
722	0	0.00244	0.698	0	0
723	0	0.00244	0.625	0	0
724	0	0.00244	0.562	0	0
725	0	0.00244	0.625	0	0
726	0	0.00244	0.571	0	0
727	0	0.00244	0.62	0	0
728	0	0.00244	0.679	0	0
729	0	0.00244	0.649	0	0
730	0	0.00244	0.547	0	0
731	0	0.00244	0.547	0	0
732	0	0.00244	0.562	0	0
733	0	0.00244	0.581	0	0
734	0	0.00244	0.557	0	0
735	0	0.00244	0.547	0	0
736	0	0.00244	0.581	0	0
737	0	0.00244	0.581	0	0
738	0	0.00244	0.586	0	0
739	0	0.00244	0.532	0	0
740	0	0.00244	0.576	0	0
741	0	0.00244	0.532	0	0
742	0	0.00244	0.532	0	0
743	0	0.00244	0.508	0	0
744	0	0.00244	0.483	0	0
745	0	0.00244	0.503	0	0
746	0	0.00244	0.571	0	0

747	0	0.00244	0.488	0	0
748	0	0.00244	0.518	0	0
749	0	0.00244	0.503	0	0
750	0	0.00244	0.498	0	0
751	0	0.00244	0.488	0	0
752	0	0.00244	0.488	0	0
753	0	0.00244	0.513	0	0
754	0	0.00244	0.493	0	0
755	0	0.00244	0.464	0	0
756	0	0.00244	0.576	0	0
757	0	0.00244	0.449	0	0
758	0	0.00244	0.425	0	0
759	0	0.00244	0.439	0	0
760	0	0.00244	0.508	0	0
761	0	0.00244	0.435	0	0
762	0	0.00244	0.532	0	0
763	0	0.00244	0.469	0	0
764	0	0.00244	0.444	0	0
765	0	0.00244	0.42	0	0
766	0	0.00244	0.513	0	0
767	0	0.00244	0.488	0	0
768	0	0.00244	0.444	0	0
769	0	0.00244	0.435	0	0
770	0	0.00244	0.488	0	0
771	0	0.00244	0.361	0	0
772	0	0.00244	0.43	0	0
773	0	0.00244	0.43	0	0
774	0	0.00244	0.449	0	0
775	0	0.00244	0.435	0	0
776	0	0.00244	0.415	0	0
777	0	0.00244	0.42	0	0
778	0	0.00244	0.498	0	0
779	0	0.00244	0.435	0	0
780	0	0.00244	0.435	0	0
781	0	0.00244	0.396	0	0
782	0	0.00244	0.435	0	0
783	0	0.00244	0.391	0	0
784	0	0.00244	0.347	0	0
785	0	0.00244	0.474	0	0
786	0	0.00244	0.376	0	0
787	0	0.00244	0.376	0	0
788	0	0.00244	0.371	0	0
789	0	0.00244	0.366	0	0
790	0	0.00244	0.396	0	0
791	0	0.00244	0.391	0	0
792	0	0.00244	0.356	0	0
793	0	0.00244	0.381	0	0

794	0	0.00244	0.41	0	0
795	0	0.00244	0.278	0	0
796	0	0.00244	0.356	0	0
797	0	0.00244	0.303	0	0
798	0	0.00244	0.371	0	0
799	0	0.00244	0.405	0	0
800	0	0.00244	0.454	0	0
801	0	0.00244	0.337	0	0
802	0	0.00244	0.415	0	0
803	0	0.00244	0.376	0	0
804	0	0.00244	0.352	0	0
805	0	0.00244	0.322	0	0
806	0	0.00244	0.396	0	0
807	0	0.00244	0.337	0	0
808	0	0.00244	0.337	0	0
809	0	0.00244	0.356	0	0
810	0	0.00244	0.288	0	0
811	0	0.00244	0.342	0	0
812	0	0.00244	0.405	0	0
813	0	0.00244	0.366	0	0
814	0	0.00244	0.317	0	0
815	0	0.00244	0.371	0	0
816	0	0.00244	0.273	0	0
817	0	0.00244	0.391	0	0
818	0	0.00244	0.347	0	0
819	0	0.00244	0.322	0	0
820	0	0.00244	0.381	0	0
821	0	0.00244	0.371	0	0
822	0	0.00244	0.386	0	0
823	0	0.00244	0.317	0	0
824	0	0.00244	0.376	0	0
825	0	0.00244	0.269	0	0
826	0	0.00244	0.386	0	0
827	0	0.00244	0.278	0	0
828	0	0.00244	0.347	0	0
829	0	0.00244	0.313	0	0
830	0	0.00244	0.381	0	0
831	0	0.00244	0.386	0	0
832	0	0.00244	0.264	0	0
833	0	0.00244	0.361	0	0
834	0	0.00244	0.278	0	0
835	0	0.00244	0.298	0	0
836	0	0.00244	0.269	0	0
837	0	0.00244	0.288	0	0
838	0	0.00244	0.391	0	0
839	0	0.00244	0.234	0	0
840	0	0.00244	0.293	0	0

841	0	0.00244	0.283	0	0
842	0	0.00244	0.249	0	0
843	0	0.00244	0.381	0	0
844	0	0.00244	0.288	0	0
845	0	0.00244	0.347	0	0
846	0	0.00244	0.244	0	0
847	0	0.00244	0.249	0	0
848	0	0.00244	0.327	0	0
849	0	0.00244	0.278	0	0
850	0	0.00244	0.273	0	0
851	0	0.00244	0.249	0	0
852	0	0.00244	0.259	0	0
853	0	0.00244	0.249	0	0
854	0	0.00244	0.254	0	0
855	0	0.00244	0.342	0	0
856	0	0.00244	0.298	0	0
857	0	0.00244	0.288	0	0
858	0	0.00244	0.317	0	0
859	0	0.00244	0.293	0	0
860	0	0.00244	0.269	0	0
861	0	0.00244	0.278	0	0
862	0	0.00244	0.244	0	0
863	0	0.00244	0.225	0	0
864	0	0.00244	0.195	0	0
865	0	0.00244	0.288	0	0
866	0	0.00244	0.356	0	0
867	0	0.00244	0.308	0	0
868	0	0.00244	0.278	0	0
869	0	0.00244	0.205	0	0
870	0	0.00244	0.234	0	0
871	0	0.00244	0.259	0	0
872	0	0.00244	0.308	0	0
873	0	0.00244	0.205	0	0
874	0	0.00244	0.244	0	0
875	0	0.00244	0.21	0	0
876	0	0.00244	0.186	0	0
877	0	0.00244	0.229	0	0
878	0	0.00244	0.322	0	0
879	0	0.00244	0.21	0	0
880	0	0.00244	0.249	0	0
881	0	0.00244	0.229	0	0
882	0	0.00244	0.195	0	0
883	0	0.00244	0.239	0	0
884	0	0.00244	0.244	0	0
885	0	0.00244	0.254	0	0
886	0	0.00244	0.254	0	0
887	0	0.00244	0.229	0	0

888	0	0.00244	0.205	0	0
889	0	0.00244	0.225	0	0
890	0	0.00244	0.283	0	0

APPENDIX G- Example of Heating Data File and Cooling Data File Used for Determining the Specific Heat

Heating Data file

Time (s)	Temperature (K)	Power (W)	Resistivity (μΩ cm)
0	300.6988	0	0
5.49E-02	296.8803	0	0
0.109851	292.4148	0	0
0.164776	296.8803	2.03	146.909
0.219702	301.4591	9.581001	144.255
0.274627	308.701	16.407	144.482
0.329553	305.8466	18.552	144.666
0.384478	310.1969	17.624	143.944
0.439403	310.9433	16.512	144.98
0.494329	317.4647	15.938	144.369
0.549254	328.8266	15.962	144.154
0.60418	315.9898	16.23	144.623
0.659105	325.3571	16.278	144.195
0.71403	331.7001	16.383	144.695
0.768956	337.2584	16.371	144.802
0.823881	334.4154	16.371	144.802
0.878807	338.6741	16.347	145.017
0.933732	344.7184	16.278	144.195
0.988657	339.945	16.29	144.089
1.043583	352.9006	16.359	144.909
1.098508	344.7184	16.278	144.195
1.153434	355.6459	16.359	144.909
1.208359	366.2199	16.359	144.909
1.263284	362.8533	16.371	144.802
1.31821	364.8758	16.371	144.802
1.373135	373.9509	16.371	144.802
1.428061	375.9328	16.359	144.909
1.482986	374.6123	16.371	144.802
1.537911	384.1797	16.383	144.695
1.592837	389.8683	16.359	144.909
1.647762	391.1532	16.278	144.195
1.702688	388.7094	16.371	144.802
1.757613	393.7145	16.371	144.802
1.812538	400.4472	16.371	144.802
1.867464	398.6763	16.371	144.802
1.922389	405.978	16.383	144.695
1.977315	409.7197	16.371	144.802

2.03224	421.6615	16.452	145.515
2.087165	417.5022	16.452	145.515
2.142091	430.6196	16.371	144.802
2.197016	428.211	16.452	145.515
2.251942	428.211	16.452	145.515
2.306867	434.0962	16.452	145.515
2.361793	443.3565	16.359	144.909
2.416718	438.7425	16.371	144.802
2.471643	446.1803	16.452	145.515
2.526569	453.0731	16.452	145.515
2.581494	446.7671	16.347	145.017
2.63642	459.8991	16.452	145.515
2.691345	461.5094	16.452	145.515
2.746271	458.1698	16.452	145.515
2.801196	470.985	16.452	145.515
2.856121	470.985	16.439	145.623
2.911047	469.8497	16.452	145.515
2.965972	471.5521	16.452	145.515
3.020898	479.7844	16.464	145.408
3.075823	480.3452	16.452	145.515
3.130748	492.3653	16.427	145.731
3.185674	485.8202	16.452	145.515
3.240599	501.4901	16.452	145.515
3.295524	505.2016	16.452	145.515
3.35045	507.2692	16.452	145.515
3.405375	510.5247	16.464	145.408
3.460301	513.6613	16.452	145.515
3.515226	518.9386	16.452	145.515
3.570152	518.9386	16.452	145.515
3.625077	512.5808	16.452	145.515
3.680002	530.9007	16.452	145.515
3.734928	530.9007	16.452	145.515
3.789853	537.6776	16.544	146.121
3.844779	539.1548	16.452	145.515
3.899704	546.8268	16.532	146.229
3.954629	546.8268	16.532	146.229
4.009555	551.0101	16.532	146.229
4.06448	545.3593	16.52	146.337
4.119406	558.6091	16.532	146.229
4.174331	561.0977	16.532	146.229
4.229256	554.555	16.544	146.121
4.284182	566.6801	16.544	146.121
4.339107	566.6801	16.532	146.229
4.394033	568.2267	16.532	146.229
4.448958	581.6618	16.439	145.623
4.503884	577.1633	16.532	146.229
4.558809	585.6376	16.532	146.229

4.613734	588.1806	16.508	146.445
4.66866	591.1251	16.532	146.229
4.723585	587.164	16.532	146.229
4.778511	594.57	16.532	146.229
4.833436	593.1524	16.532	146.229
4.888361	599.5211	16.532	146.229
4.943287	606.3659	16.532	146.229
4.998212	611.78	16.532	146.229
5.053138	618.1726	16.52	146.337
5.108063	613.2806	16.532	146.229
5.162988	625.4321	16.532	146.229
5.217914	625.9282	16.532	146.229
5.272839	628.3065	16.544	146.121
5.327765	632.6575	16.532	146.229
5.38269	636.0108	16.613	146.942
5.437616	643.283	16.625	146.834
5.492541	641.8119	16.613	146.942
5.547467	644.6548	16.52	146.337
5.602392	647.101	16.613	146.942
5.657317	652.7595	16.613	146.942
5.712242	660.332	16.532	146.229
5.767168	663.2327	16.613	146.942
5.822093	662.2665	16.613	146.942
5.877019	670.7425	16.601	147.051
5.931944	674.0543	16.613	146.942
5.98687	676.3595	16.625	146.834
6.041795	681.0585	16.601	147.051
6.09672	680.5795	16.601	147.051
6.151646	683.9306	16.601	147.051
6.206571	688.0407	16.625	146.834
6.261497	692.7152	16.613	146.942
6.316422	695.9531	16.625	146.834
6.371348	701.086	16.625	146.834
6.426273	703.8376	16.613	146.942
6.481198	703.8376	16.681	147.765
6.536124	708.0061	16.601	147.051
6.591049	702.5096	16.613	146.942
6.645974	716.7916	16.613	146.942
6.7009	720.4656	16.613	146.942
6.755825	720.4656	16.625	146.834
6.810751	719.995	16.613	146.942
6.865676	724.1337	16.613	146.942
6.920602	733.3246	16.706	147.546
6.975527	735.5697	16.613	146.942
7.030453	739.68	16.601	147.051
7.085378	745.1799	16.694	147.655
7.140303	751.0378	16.706	147.546

7.195228	750.2019	16.694	147.655
7.250154	756.0469	16.706	147.546
7.305079	755.1203	16.681	147.765
7.360005	760.1203	16.694	147.655
7.41493	763.7247	16.694	147.655
7.469856	766.8623	16.706	147.546
7.524781	767.7843	16.694	147.655
7.579706	772.2968	16.694	147.655
7.634632	774.0441	16.706	147.546
7.689557	780.8368	16.706	147.546
7.744483	785.2321	16.706	147.546
7.799408	785.6893	16.706	147.546
7.854334	785.6893	16.706	147.546
7.909259	787.5179	16.694	147.655
7.964184	796.4565	16.694	147.655
8.01911	794.6351	16.694	147.655
8.074035	807.0827	16.694	147.655
8.128961	809.2564	16.706	147.546
8.183886	805.7231	16.706	147.546
8.238811	812.7843	16.799	148.15
8.293736	809.2564	16.694	147.655
8.348661	819.8238	16.694	147.655
8.403588	819.8238	16.694	147.655
8.458512	823.3356	16.774	148.369
8.513438	824.2351	16.774	148.369
8.568363	836.0771	16.706	147.546
8.623289	823.3356	16.774	148.369
8.678214	838.2238	16.774	148.369
8.73314	843.4924	16.774	148.369
8.788065	842.6002	16.762	148.478
8.842991	838.6707	16.774	148.369
8.897916	852.2175	16.774	148.369
8.952842	851.7731	16.787	148.259
9.007767	854.7932	16.774	148.369
9.062692	855.6807	16.774	148.369
9.117618	857.3661	16.787	148.259
9.172542	869.9236	16.787	148.259
9.227469	869.4826	16.774	148.369
9.282394	873.8009	16.774	148.369
9.337319	876.3531	16.774	148.369
9.392244	878.1116	16.774	148.369
9.44717	884.0806	16.762	148.478
9.502095	887.9348	16.855	149.082
9.557021	886.6216	16.787	148.259
9.611946	884.5188	16.774	148.369
9.666872	897.7174	16.855	149.082
9.721797	893.4426	16.787	148.259

9.776722	902.8548	16.855	149.082
9.831648	897.2817	16.787	148.259
9.886573	902.4198	16.787	148.259
9.941499	909.6293	16.855	149.082
9.996424	915.0872	16.762	148.478
10.05135	915.9524	16.855	149.082
10.10627	920.1872	16.867	148.972
10.1612	919.3236	16.867	148.972
10.21613	924.8456	16.855	149.082
10.27105	926.9131	16.855	149.082
10.32598	931.5585	16.855	149.082
10.3809	932.8472	16.855	149.082
10.43583	931.1288	16.867	148.972
10.49075	935.766	16.842	149.192
10.54568	943.304	16.855	149.082
10.6006	943.6461	16.855	149.082
10.65553	949.5394	16.867	148.972
10.71045	951.5859	16.842	149.192
10.76538	955.3334	16.855	149.082
10.82031	958.6502	16.855	149.082
10.87523	957.4601	16.855	149.082
10.93016	951.1598	16.842	149.192
10.98508	963.6594	16.855	149.082
11.04001	966.965	16.855	149.082
11.09493	966.965	16.867	148.972
11.14986	969.8432	16.855	149.082
11.20478	976.4333	16.867	148.972
11.25971	974.4074	16.774	148.369
11.31463	980.5642	16.842	149.192
11.36956	987.5459	16.787	148.259
11.42448	988.8055	16.762	148.478
11.47941	980.5642	16.762	148.478
11.53434	987.1259	16.787	148.259
11.58926	999.0269	16.774	148.369
11.64419	996.5173	16.694	147.655
11.69911	990.8196	16.706	147.546
11.75404	1000.615	16.694	147.655
11.80896	1003.121	16.694	147.655
11.86389	1003.121	16.681	147.765
11.91881	1005.54	16.694	147.655
11.97374	1011.205	16.694	147.655
12.02867	1003.872	16.694	147.655
12.08359	1014.447	16.613	146.942
12.13852	1007.957	16.706	147.546
12.19344	1014.863	16.613	146.942
12.24837	1012.452	16.613	146.942
12.30329	1017.354	16.613	146.942

12.35822	1018.101	16.613	146.942
12.41314	1024.979	16.52	146.337
12.46807	1027.791	16.532	146.229
12.52299	1024.979	16.532	146.229
12.57792	1027.791	16.544	146.121
12.63284	1031.426	16.452	145.515
12.68777	1035.467	16.532	146.229
12.7427	1029.031	16.452	145.515
12.79762	1033.076	16.452	145.515
12.85255	1039.502	16.464	145.408
12.90747	1040.736	16.359	144.909
12.9624	1046.322	16.371	144.802
13.01732	1041.476	16.371	144.802
13.07225	1050.75	16.383	144.695
13.12717	1049.111	16.29	144.089
13.1821	1046.322	16.302	143.982
13.23702	1052.306	16.302	143.982
13.29195	1051.896	16.29	144.089
13.34687	1050.75	16.21	143.376
13.4018	1051.159	16.198	143.482
13.45673	1059.092	16.21	143.376
13.51165	1061.541	16.222	143.27
13.56658	1059.092	16.141	142.557
13.6215	1057.54	16.153	142.452
13.67643	1062.683	16.129	142.662
13.73135	1063.498	16.141	142.557
13.78628	1069.035	16.141	142.557
13.8412	1067.896	16.048	141.949
13.89613	1071.475	16.037	142.054
13.95105	1074.236	16.06	141.844
14.00598	1075.048	16.06	141.844
14.06091	1076.184	16.06	141.844
14.11583	1076.184	16.06	141.844
14.17076	1080.561	15.968	141.236
14.22568	1081.776	15.98	141.131
14.28061	1087.678	15.968	141.236
14.33553	1080.966	15.991	141.027
14.39046	1086.466	15.899	140.419
14.44538	1080.966	15.899	140.419
14.50031	1084.526	15.887	140.522
14.55523	1094.373	15.899	140.419
14.61016	1096.709	15.875	140.626
14.66508	1090.826	15.899	140.419
14.72001	1095.179	15.899	140.419
14.77494	1096.709	15.818	139.706
14.82986	1100.248	15.806	139.809
14.88479	1101.052	15.806	139.809

14.93971	1103.382	15.818	139.706
14.99464	1104.586	15.83	139.603
15.04956	1101.052	15.818	139.706
15.10449	1106.511	15.737	138.993
15.15941	1108.515	15.806	139.809
15.21434	1102.257	15.737	138.993
15.26926	1112.439	15.737	138.993
15.32419	1113.959	15.737	138.993
15.37911	1111.639	15.714	139.199
15.43404	1118.274	15.737	138.993
15.48897	1116.677	15.737	138.993
15.54389	1116.277	15.668	138.178
15.59882	1120.19	15.657	138.28
15.65374	1120.19	15.657	138.28
15.70867	1127.202	15.657	138.28
15.76359	1127.998	15.645	138.382
15.81852	1128.794	15.657	138.28
15.87344	1131.894	15.657	138.28
15.92837	1132.291	15.576	137.567
15.98329	1134.197	15.657	138.28
16.03822	1136.101	15.576	137.567
16.09314	1134.594	15.657	138.28
16.14807	1138.48	15.576	137.567
16.203	1138.084	15.588	137.466
16.25792	1138.084	15.576	137.567
16.31285	1143.864	15.565	137.669
16.36777	1145.05	15.576	137.567
16.4227	1143.864	15.576	137.567
16.47762	1148.527	15.588	137.466
16.53255	1151.21	15.576	137.567
16.58747	1151.605	15.495	136.855
16.6424	1153.103	15.495	136.855
16.69732	1155.388	15.484	136.956
16.75225	1156.57	15.495	136.855
16.80718	1155.782	15.495	136.855
16.8621	1160.032	15.403	136.242
16.91703	1163.097	15.495	136.855
16.97195	1162.311	15.507	136.754
17.02688	1167.336	15.426	136.041
17.0818	1159.639	15.507	136.754
17.13673	1170.001	15.426	136.041
17.19165	1165.766	15.415	136.142
17.24658	1170.001	15.403	136.242
17.3015	1168.12	15.403	136.242
17.35643	1160.425	15.415	136.142
17.41135	1173.838	15.415	136.142
17.46628	1176.888	15.426	136.041

17.5212	1176.888	15.426	136.041
17.57613	1181.808	15.334	135.429
17.63106	1179.935	15.415	136.142
17.68598	1182.198	15.437	135.941
17.74091	1179.935	15.334	135.429
17.79583	1183.368	15.323	135.529
17.85076	1187.187	15.345	135.329
17.90568	1181.106	15.345	135.329
17.96061	1187.966	15.334	135.429
18.01553	1181.808	15.334	135.429
18.07046	1182.978	15.323	135.529
18.12538	1190.223	15.334	135.429
18.18031	1192.089	15.334	135.429
18.23524	1192.089	15.345	135.329
18.29016	1192.867	15.334	135.429
18.34509	1191.312	15.253	134.716
18.40001	1197.061	15.334	135.429
18.45494	1202.721	15.264	134.617
18.50986	1201.559	15.253	134.716
18.56479	1201.559	15.264	134.617
18.61971	1206.901	15.253	134.716
18.67464	1206.901	15.253	134.716
18.72957	1200.086	15.253	134.716
18.78449	1204.193	15.253	134.716
18.83942	1209.916	15.264	134.617
18.89434	1211.384	15.264	134.617
18.94927	1212.928	15.264	134.617
19.00419	1214.009	15.264	134.617
19.05912	1214.78	15.172	134.003
19.11404	1218.557	15.253	134.716
19.16897	1208.757	15.184	133.905
19.22389	1221.175	15.172	134.003
19.27882	1221.56	15.161	134.103
19.33374	1223.099	15.184	133.905
19.38867	1224.945	15.172	134.003
19.44359	1220.406	15.184	133.905
19.49852	1229.477	15.184	133.905
19.55344	1229.093	15.184	133.905
19.60837	1220.098	15.172	134.003
19.6633	1235.84	15.172	134.003
19.71822	1231.318	15.184	133.905
19.77315	1230.167	15.184	133.905
19.82807	1229.477	15.103	133.192
19.883	1232.852	15.103	133.192
19.93792	1233.158	15.103	133.192
19.99285	1227.173	15.081	133.389
20.04777	1237.295	15.184	133.905

20.1027	1235.457	15.103	133.192
20.15763	1235.84	15.184	133.905
20.21255	1244.405	15.092	133.291
20.26748	1238.825	15.103	133.192
20.3224	1243.642	15.103	133.192
20.37733	1242.878	15.103	133.192
20.43225	1245.551	15.103	133.192
20.48718	1242.19	15.103	133.192
20.5421	1242.878	15.103	133.192
20.59703	1250.737	15.103	133.192
20.65195	1245.856	15.103	133.192
20.70688	1253.327	15.103	133.192
20.76181	1246.238	15.081	133.389
20.81673	1254.469	15.103	133.192
20.87166	1248.526	15.103	133.192
20.92658	1255.915	15.022	132.48
20.98151	1259.26	15.022	132.48
21.03643	1257.056	15.022	132.48
21.09136	1258.88	15.011	132.578
21.14628	1259.26	15.011	132.578
21.20121	1260.78	15.011	132.578
21.25613	1265.561	15.011	132.578
21.31106	1261.843	15.022	132.48
21.36599	1261.539	15.022	132.48
21.42091	1260.02	15.022	132.48
21.47584	1259.64	15.022	132.48
21.53076	1261.843	15.022	132.48
21.58569	1271.848	15.022	132.48
21.64061	1271.848	15.022	132.48
21.69554	1269.653	15.011	132.578
21.75046	1272.983	15.022	132.48
21.80539	1265.181	15.022	132.48
21.86031	1273.74	15.022	132.48
21.91524	1269.274	15.022	132.48
21.97016	1278.878	14.952	131.671
22.02509	1272.605	14.941	131.768
22.08001	1278.123	15.022	132.48
22.13494	1278.501	15.022	132.48
22.18987	1270.032	15.011	132.578
22.24479	1282.199	14.93	131.865
22.29972	1279.633	14.93	131.865
22.35464	1284.008	14.93	131.865
22.40957	1281.444	14.941	131.768
22.46449	1281.821	14.941	131.768
22.51942	1282.576	14.941	131.768
22.57434	1284.762	14.93	131.865
22.62927	1288.452	14.93	131.865

22.68419	1288.452	14.919	131.963
22.73912	1284.762	14.93	131.865
22.79405	1289.581	14.941	131.768
22.84897	1285.139	14.941	131.768
22.9039	1286.645	14.941	131.768
22.95882	1291.763	14.941	131.768
23.01375	1296.196	14.941	131.768
23.06867	1300.172	14.941	131.768
23.1236	1294.318	14.93	131.865
23.17852	1296.871	14.839	131.249
23.23345	1297.622	14.941	131.768
23.28837	1294.694	14.941	131.768
23.3433	1298.747	14.941	131.768
23.39823	1302.047	14.93	131.865
23.45315	1301.672	14.85	131.152
23.50808	1295.445	14.93	131.865
23.563	1303.096	14.93	131.865
23.61793	1303.845	14.941	131.768
23.67285	1300.172	14.861	131.056
23.72778	1301.297	14.861	131.056
23.7827	1311.177	14.861	131.056
23.83763	1314.463	14.861	131.056
23.89255	1307.513	14.93	131.865
23.94748	1310.429	14.872	130.959
24.0024	1310.803	14.861	131.056
24.05733	1310.055	14.861	131.056
24.11225	1303.47	14.85	131.152
24.16718	1312.596	14.93	131.865
24.22211	1306.016	14.861	131.056
24.27703	1315.881	14.861	131.056
24.33196	1308.635	14.861	131.056
24.38688	1309.308	14.861	131.056
24.44181	1317	14.85	131.152
24.49673	1312.596	14.78	130.343
24.55166	1319.908	14.861	131.056
24.60658	1319.162	14.861	131.056
24.66151	1322.441	14.839	131.249
24.71643	1321.323	14.78	130.343
24.77136	1325.715	14.78	130.343
24.82629	1318.119	14.861	131.056
24.88121	1323.93	14.861	131.056
24.93614	1323.93	14.85	131.152
24.99106	1320.653	14.85	131.152
25.04599	1319.535	14.78	130.343
25.10091	1326.087	14.872	130.959
25.15584	1328.987	14.861	131.056
25.21076	1323.185	14.78	130.343

25.26569	1324.971	14.78	130.343
25.32061	1330.101	14.78	130.343
25.37554	1331.513	14.769	130.44
25.43047	1330.101	14.861	131.056
25.48539	1330.77	14.861	131.056
25.54031	1335.891	14.769	130.44
25.59524	1335.149	14.769	130.44
25.65017	1334.036	14.78	130.343
25.70509	1335.52	14.78	130.343
25.76002	1335.891	14.78	130.343
25.81494	1330.473	14.78	130.343
25.86987	1335.891	14.861	131.056
25.92479	1330.77	14.769	130.44
25.97972	1342.41	14.78	130.343
26.03464	1339.522	14.861	131.056
26.08957	1329.73	14.769	130.44
26.14449	1342.04	14.769	130.44
26.19942	1338.781	14.78	130.343
26.25435	1342.78	14.78	130.343
26.30927	1336.262	14.78	130.343
26.3642	1344.925	14.78	130.343
26.41912	1343.446	14.78	130.343
26.47405	1338.041	14.769	130.44
26.52897	1341.67	14.769	130.44
26.5839	1345.665	14.791	130.247
26.63882	1347.069	14.769	130.44
26.69375	1347.808	14.78	130.343
26.74867	1342.41	14.78	130.343
26.8036	1339.152	14.78	130.343
26.85853	1348.177	14.758	130.536
26.91345	1348.547	14.78	130.343
26.96838	1347.069	14.78	130.343
27.0233	1350.688	14.688	129.727
27.07823	1349.95	14.769	130.44
27.13315	1350.319	14.699	129.631
27.18808	1341.67	14.769	130.44
27.243	1351.795	14.78	130.343
27.29793	1350.319	14.78	130.343
27.35285	1350.319	14.78	130.343
27.40778	1348.547	14.78	130.343
27.4627	1354.672	14.769	130.44
27.51763	1353.197	14.699	129.631
27.57255	1349.95	14.78	130.343
27.62748	1352.46	14.677	129.823
27.68241	1357.178	14.78	130.343

Time (s)	Temperature (K)	Time (s)	Temperature (K)	Time (s)	Temperature (K)
0	1357.178	43.50093	781.295	87.00184	567.7113
0.988657	1354.304	44.48958	778.0854	87.9905	562.1332
1.977315	1326.831	45.47824	767.3234	88.97916	561.6155
2.965972	1304.219	46.4669	766.8623	89.96782	557.0513
3.954629	1280.69	47.45555	754.2858	90.95648	556.0118
4.943287	1258.88	48.44421	746.5761	91.94513	551.0101
5.931944	1235.457	49.43287	737.906	92.93379	552.9923
6.920602	1222.714	50.42153	735.1957	93.92245	544.8347
7.909259	1196.673	51.41018	729.6715	94.9111	538.0999
8.897916	1178.763	52.39884	719.5242	95.89976	548.9203
9.886573	1169.609	53.3875	713.5837	96.88842	544.8347
10.87523	1148.132	54.37615	714.0558	97.87708	531.9623
11.86389	1133.006	55.36481	714.5276	98.86573	533.9766
12.85255	1119.791	56.35347	706.2071	99.85439	527.2835
13.8412	1103.783	57.34213	702.0352	100.8431	523.1194
14.82986	1085.658	58.33079	688.5182	101.8317	523.1194
15.81852	1075.778	59.31944	685.2696	102.8204	521.5133
16.80718	1071.475	60.3081	676.8395	103.809	519.4755
17.79583	1055.906	61.29676	678.7582	104.7977	520.0122
18.78449	1034.313	62.28541	665.5483	105.7863	524.1886
19.77315	1027.46	63.27407	670.2625	106.775	512.0401
20.76181	1017.354	64.26273	669.3019	107.7637	508.3556
21.75046	1002.703	65.25138	647.9805	108.7523	516.7879
22.73912	998.6089	66.24005	649.9332	109.741	505.2016
23.72778	974.8296	67.2287	643.6751	110.7296	508.3556
24.71643	963.2354	68.21736	639.848	111.7183	501.4901
25.70509	957.0349	69.20601	644.6548	112.7069	503.566
26.69375	946.6373	70.19467	629.7912	113.6956	493.911
27.68241	933.1909	71.18333	629.2965	114.6843	493.3593
28.67106	921.9137	72.17198	623.4466	115.6729	485.2632
29.65972	915.0872	73.16065	618.1726	116.6616	497.2142
30.64838	901.9848	74.1493	618.1726	117.6502	497.2142
31.63703	897.2817	75.13796	611.78	118.6389	484.7058
32.62569	884.9571	76.12662	605.4617	119.6275	477.65
33.61435	867.3644	77.11528	602.444	120.6162	480.9055
34.60301	863.4763	78.10393	598.0071	121.6049	479.2233
35.59166	859.5818	79.09258	594.0638	122.5935	480.3452
36.58032	836.5246	80.08125	590.6178	123.5822	470.4175
37.56898	831.24	81.0699	593.1524	124.5708	475.397
38.55764	826.4827	82.05856	590.1104	125.5595	482.0251
39.54629	815.8554	83.04722	585.2303	126.5481	464.8338
40.53495	797.7305	84.03588	572.6507	127.5368	468.8264
41.52361	805.7231	85.02453	574.7036	128.5255	460.9347
42.51227	799.095	86.01318	573.6776	129.5141	463.8037

Time (s)	Temperature (K)	Time (s)	Temperature (K)	Time (s)	Temperature (K)
130.5028	459.3231	174.0037	407.8518	217.5046	360.9588
131.4914	452.4916	174.9923	395.5006	218.4933	359.6016
132.4801	459.8991	175.981	392.4353	219.4819	364.2025
133.4687	449.6937	176.9697	391.7946	220.4706	364.2025
134.4574	459.3231	177.9583	399.3093	221.4593	364.8758
135.4461	448.5245	178.947	401.0783	222.4479	357.5592
136.4347	443.9458	179.9356	393.7145	223.4366	363.5283
137.4234	449.6937	180.9243	396.1371	224.4252	357.5592
138.412	452.4916	181.913	394.353	225.4139	357.5592
139.4007	442.1765	182.9016	387.4189	226.4025	354.275
140.3893	443.9458	183.8903	392.4353	227.3912	350.8323
141.378	451.3272	184.8789	382.3576	228.3798	353.5883
142.3667	437.5543	185.8676	388.0645	229.3685	362.8533
143.3553	445.1228	186.8562	383.009	230.3572	351.5227
144.344	442.1765	187.8449	381.7054	231.3458	355.6459
145.3326	443.3565	188.8335	383.009	232.3345	353.5883
146.3213	436.9594	189.8222	384.1797	233.3231	352.9006
147.3099	440.5209	190.8109	388.0645	234.3118	351.5227
148.2986	431.1002	191.7995	383.6597	235.3005	351.5227
149.2873	438.7425	192.7882	375.9328	236.2891	354.9609
150.2759	432.3003	193.7768	393.7145	237.2778	352.2121
151.2646	424.7021	194.7655	379.0889	238.2664	348.2009
152.2532	427.0032	195.7542	373.9509	239.2551	363.5283
153.2419	427.6074	196.7428	370.7651	240.2437	346.1142
154.2306	419.9522	197.7315	373.9509	241.2324	342.7581
155.2192	430.0183	198.7201	383.6597	242.2211	344.7184
156.2079	427.0032	199.7088	375.9328	243.2097	354.275
157.1965	417.5022	200.6974	383.009	244.1984	344.1591
158.1852	418.1156	201.6861	386.1254	245.187	357.5592
159.1738	410.341	202.6748	372.7584	246.1757	348.8947
160.1625	415.6583	203.6634	381.7054	247.1643	345.4168
161.1511	413.3146	204.6521	375.2729	248.153	342.0563
162.1398	427.6074	205.6407	379.7442	249.1417	354.9609
163.1285	412.6963	206.6294	370.0991	250.1303	351.5227
164.1171	414.5492	207.618	361.6362	251.119	345.4168
165.1058	414.5492	208.6067	370.0991	252.1076	344.1591
166.0944	409.0977	209.5954	362.8533	253.0963	351.5227
167.0831	408.4751	210.584	369.4323	254.0849	333.7022
168.0718	405.3522	211.5727	377.25	255.0736	343.4591
169.0604	407.8518	212.5613	373.2888	256.0623	343.4591
170.0491	407.8518	213.55	359.6016	257.0509	346.1142
171.0377	413.9322	214.5386	359.6016	258.0396	344.1591
172.0264	405.3522	215.5273	361.6362	259.0282	341.3534
173.015	406.6033	216.516	364.2025	260.0169	342.0563

Time (s)	Temperature (K)	Time (s)	Temperature (K)	Time (s)	Temperature (K)
261.0055	352.9006	304.5065	337.2584	348.0074	332.9881
261.9942	344.1591	305.4951	327.3838	348.996	326.0819
262.9829	344.1591	306.4838	335.8388	349.9847	321.7182
263.9715	338.6741	307.4725	320.4019	350.9734	310.9433
264.9602	344.1591	308.4611	337.2584	351.962	315.2508
265.9488	337.9667	309.4498	321.7182	352.9507	318.9354
266.9375	331.7001	310.4384	331.7001	353.9393	326.0819
267.9262	349.5875	311.4271	326.8056	354.928	310.9433
268.9148	335.8388	312.4157	336.5491	355.9166	316.7278
269.9035	335.8388	313.4044	337.2584	356.9053	311.6886
270.8921	335.1276	314.393	319.6692	357.894	308.1014
271.8808	334.4154	315.3817	333.7022	358.8826	314.5107
272.8694	338.6741	316.3703	321.7182	359.8713	328.1057
273.8581	337.9667	317.359	324.6314	360.8599	311.6886
274.8468	332.9881	318.3477	320.4019	361.8486	317.4647
275.8354	336.5491	319.3363	323.1769	362.8373	314.5107
276.824	340.6497	320.325	337.9667	363.8259	309.4495
277.8127	321.7182	321.3136	315.2508	364.8146	315.9898
278.8014	332.9881	322.3023	323.9046	365.8032	316.7278
279.79	325.3571	323.291	322.4481	366.7919	318.2006
280.7787	335.1276	324.2796	317.4647	367.7805	318.2006
281.7673	339.945	325.2683	336.5491	368.7692	314.5107
282.756	346.8107	326.2569	323.1769	369.7579	310.9433
283.7447	330.2653	327.2456	331.7001	370.7465	313.9178
284.7333	341.3534	328.2342	316.7278		
285.722	335.8388	329.2229	317.4647		
286.7106	332.4161	330.2116	328.8266		
287.6993	328.1057	331.2002	321.7182		
288.6879	338.6741	332.1889	320.9874		
289.6766	330.2653	333.1775	317.4647		
290.6653	330.2653	334.1662	318.9354		
291.6539	332.9881	335.1549	317.4647		
292.6426	323.1769	336.1435	318.2006		
293.6312	330.9832	337.1322	330.9832		
294.6199	339.945	338.1208	324.6314		
295.6086	334.4154	339.1095	323.1769		
296.5972	327.3838	340.0981	327.3838		
297.5859	335.1276	341.0868	323.9046		
298.5745	320.9874	342.0755	320.4019		
299.5632	337.9667	343.0641	321.7182		
300.5518	331.7001	344.0527	316.7278		
301.5405	328.1057	345.0414	313.9178		
302.5292	336.5491	346.0301	309.4495		
303.5178	335.1276	347.0187	323.1769		

APPENDIX H- Example Calculations for the Error Analysis

Effective Length

$$\Delta L = \sqrt{\left(\frac{d_K}{E_K}\Delta E_T\right)^2 + \left(\frac{-E_T d_K}{(E_K)^2}\Delta E_K\right)^2 + \left(\frac{E_T}{E_K}\Delta d_K\right)^2}$$

$$\Delta L = \sqrt{\left(\frac{2.5339}{13.479}(0.006)\right)^2 + \left(\frac{-(13.508)(2.5339)}{(13.479)^2}(0.004)\right)^2 + \left(\frac{13.508}{13.479}(0.0013)\right)^2}$$

$$\Delta L = 0.0017 cm$$

Effective Mass

$$\Delta M = \sqrt{\left(\frac{2\pi DLd}{4}\Delta D\right)^2 + \left(\frac{\pi D^2 d}{4}\Delta L\right)^2 + \left(\frac{\pi D^2 L}{4}\Delta d\right)^2}$$

$$\Delta M = \sqrt{\left(\frac{2(\pi)(0.1775)(2.5393)(9.382)}{4}(0.0010)\right)^2 + \left(\frac{2(\pi)(0.1775)^2(9.382)}{4}(0.0017)\right)^2 + \left(\frac{2(\pi)(0.1775)^2(2.5393)}{4}(0.017)\right)^2}$$

$$\Delta M = 0.00674 g$$

Electrical Resistivity

$$\Delta\rho = \sqrt{\left(\frac{\pi D^2}{4IL}\Delta E\right)^2 + \left(\frac{-E\pi D^2}{4I^2 L}\Delta I\right)^2 + \left(\frac{2E\pi D}{4IL}\Delta D\right)^2 + \left(\frac{-E\pi D^2}{4IL^2}\Delta L\right)^2}$$

$$\Delta\rho = \sqrt{\left(\frac{\pi(0.1760)^2}{4(33.008)(2.5208)}(0.00128)\right)^2 + \left(\frac{-(0.51025)\pi(0.1760)^2}{4(33.008)^2(2.5208)}(0.08252)\right)^2 + \left(\frac{2(\pi)(0.1775)(.51025)}{4(33.008)(2.5208)}(0.017)\right)^2 + \left(\frac{-(\pi)(0.1760)^2(.51025)}{4(33.008)(2.5208)^2}(0.0017)\right)^2}$$

$$\Delta\rho = 1.78 \mu\Omega cm$$

Specific Heat

$$\left(\frac{\partial T}{\partial t}\right)_H \approx 63K/s$$

$$\left(\frac{\partial T}{\partial t}\right)_C \approx -4K/s$$

$$\frac{1}{\left(\frac{\partial T}{\partial t}\right)_H - \left(\frac{\partial T}{\partial t}\right)_C} \approx 0.0149$$

$$\Delta Cp = \sqrt{\left(\frac{0.0149\,I}{M}\Delta E\right)^2 + \left(\frac{0.0149\,E}{M}\Delta I)\right)^2 + \left(\frac{-0.0149\,EI}{M^2}\Delta M\right)^2}$$

$$\Delta Cp = \sqrt{\left(\frac{0.0149(33.032)}{0.5895}(0.001251)\right)^2 + \left(\frac{0.0149(0.50049)}{0.5895}(0.08258)\right)^2 + \left(\frac{-0.0149(0.50049)(33.032)}{(0.5895)^2}(0.00674)\right)^2}$$

$$\Delta Cp = 0.005J/gK$$

APPENDIX I- Calculation of Change in Gibbs Free Energy

Specific heat data for both phases for three different conditions
(Cp values in J/gK)

	High Current Pulse			Low Current Pulse			Long Specimen		
T(K)	Beta Cp	Alpha Cp	ΔCp	Beta Cp	Alpha Cp	ΔCp	Beta Cp	Alpha Cp	ΔCp
300	0.441	0.451	-0.010	0.422	0.383	0.039	0.235	0.377	-0.142
325	0.450	0.450	0.000	0.428	0.397	0.030	0.282	0.380	-0.098
350	0.455	0.447	0.008	0.428	0.403	0.025	0.312	0.383	-0.071
375	0.458	0.444	0.014	0.427	0.404	0.023	0.333	0.387	-0.054
400	0.459	0.441	0.018	0.424	0.403	0.022	0.347	0.390	-0.043
425	0.458	0.438	0.020	0.423	0.401	0.021	0.359	0.394	-0.035
450	0.455	0.434	0.021	0.421	0.401	0.020	0.368	0.397	-0.029
475	0.451	0.431	0.020	0.420	0.402	0.018	0.376	0.400	-0.023
500	0.447	0.428	0.019	0.418	0.404	0.014	0.384	0.402	-0.018
525	0.443	0.426	0.017	0.416	0.407	0.009	0.392	0.404	-0.012
550	0.439	0.424	0.015	0.413	0.411	0.002	0.399	0.405	-0.007
575	0.435	0.422	0.013	0.410	0.415	-0.005	0.405	0.407	-0.002
600	0.433	0.422	0.011	0.406	0.419	-0.013	0.411	0.408	0.003
625	0.431	0.421	0.010	0.401	0.421	-0.020	0.416	0.410	0.006
650	0.431	0.422	0.009	0.397	0.423	-0.026	0.421	0.413	0.008
675	0.431	0.423	0.008	0.393	0.423	-0.030	0.425	0.416	0.009
700	0.433	0.425	0.008	0.390	0.422	-0.033	0.429	0.420	0.009
725	0.436	0.428	0.008	0.387	0.421	-0.033	0.432	0.425	0.007
750	0.439	0.432	0.008	0.387	0.419	-0.032	0.435	0.432	0.003
775	0.443	0.436	0.007	0.388	0.418	-0.030	0.437	0.440	-0.003
800	0.448	0.441	0.006	0.390	0.418	-0.028	0.439	0.450	-0.011
825	0.452	0.447	0.005	0.394	0.421	-0.026	0.440	0.461	-0.021
850	0.456	0.453	0.003	0.399	0.426	-0.027	0.441	0.474	-0.033
875	0.460	0.461	-0.001	0.405	0.436	-0.031	0.441	0.488	-0.048
900	0.464	0.468	-0.005	0.412	0.450	-0.039	0.440	0.504	-0.064
925	0.467	0.477	-0.010	0.418	0.469	-0.051	0.441	0.521	-0.080
950	0.470	0.485	-0.016	0.425	0.493	-0.068	0.443	0.538	-0.095
975	0.473	0.495	-0.021	0.433	0.520	-0.087	0.448	0.555	-0.107
1000	0.478	0.504	-0.026	0.444	0.549	-0.105	0.462	0.572	-0.110
1025	0.485	0.514	-0.030	0.460	0.577	-0.117	0.488	0.587	-0.099
1050	0.495	0.524	-0.029	0.488	0.600	-0.113	0.534	0.600	-0.066
1075	0.511	0.535	-0.024	0.532	0.613	-0.081	0.611	0.609	0.002
1100	0.535	0.545	-0.010	0.605	0.608	-0.003	0.731	0.614	0.117
1125	0.570	0.556	0.014	0.719	0.577	0.142	0.913	0.612	0.301
1141	0.599	0.563	0.037	0.822	0.538	0.285	1.072	0.607	0.465

Average change in specific heat

T(K)	Avg Delta Cp
300	-0.0375
325	-0.02257
350	-0.01254
375	-0.00575
400	-0.00113
425	0.001958
450	0.003876
475	0.004845
500	0.005009
525	0.004492
550	0.003431
575	0.001986
600	0.000331
625	-0.00136
650	-0.00292
675	-0.00428
700	-0.00539
725	-0.00634
750	-0.00734
775	-0.00869
800	-0.0108
825	-0.01415
850	-0.01921
875	-0.02634
900	-0.03572
925	-0.04709
950	-0.05966
975	-0.07175
1000	-0.08056
1025	-0.0818
1050	-0.06925
1075	-0.03432
1100	0.034515
1125	0.152315
1141	0.262114

Plotted average change in specific heat with best fit 7th degree polynomial

Polynomial Coefficients
Degree 0: -3.50223
Degree 1: 0.0415017
Degree 2: -0.000213478
Degree 3: 6.1185E-007
Degree 4: -1.04456E-009
Degree 5: 1.05404E-012
Degree 6: -5.79231E-016
Degree 7: 1.33299E-019

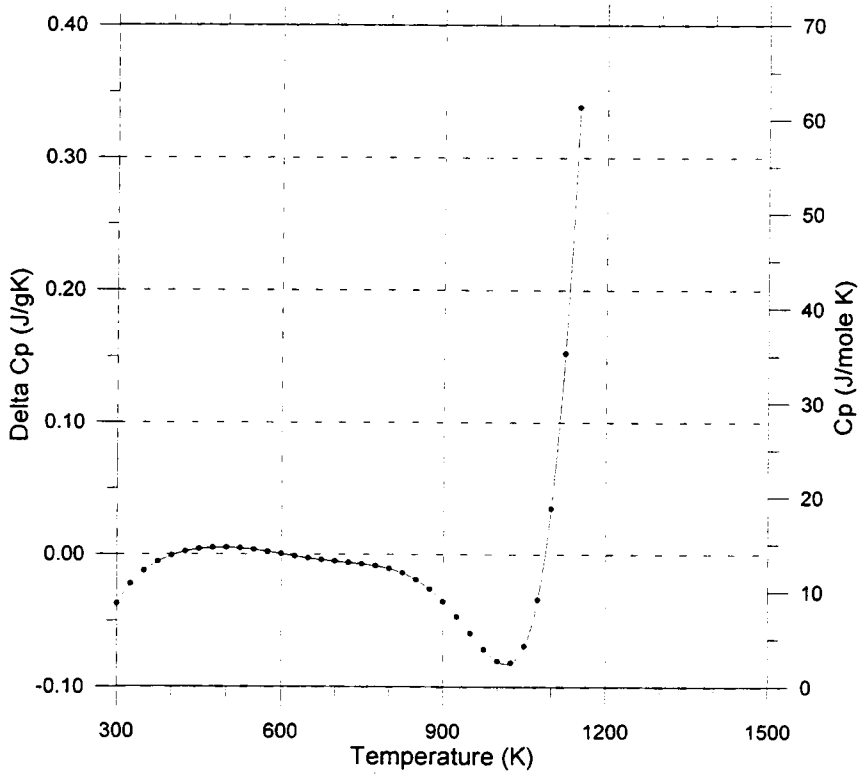

Calculation of different contributions to the Gibbs free energy

T(K)	integral delta Cp	-T*(integral delta Cp/T)	-2900* Delta T/T0	Delta G
300	9.8	-4.7	-2137.5	-2132.4
325	9.0	-4.3	-2074.0	-2069.2
350	8.6	-4.1	-2010.4	-2006.0
375	8.4	-4.2	-1946.9	-1942.7
400	8.3	-4.4	-1883.3	-1879.4
425	8.3	-4.7	-1819.8	-1816.2
450	8.4	-5.1	-1756.3	-1752.9
475	8.5	-5.4	-1692.7	-1689.7
500	8.6	-5.9	-1629.2	-1626.4
525	8.8	-6.3	-1565.6	-1563.2
550	8.9	-6.7	-1502.1	-1499.9
575	8.9	-7.1	-1438.6	-1436.7
600	9.0	-7.4	-1375.0	-1373.5
625	8.9	-7.7	-1311.5	-1310.2
650	8.9	-7.9	-1247.9	-1247.0
675	8.8	-8.2	-1184.4	-1183.8
700	8.7	-8.3	-1120.9	-1120.5
725	8.5	-8.5	-1057.3	-1057.3
750	8.4	-8.6	-993.8	-994.0
775	8.2	-8.7	-930.2	-930.8
800	7.9	-8.7	-866.7	-867.5
825	7.6	-8.7	-803.2	-804.2
850	7.2	-8.6	-739.6	-741.0
875	6.7	-8.2	-676.1	-677.7
900	5.9	-7.7	-612.5	-614.3
925	4.9	-6.9	-549.0	-551.0
950	3.5	-5.7	-485.5	-487.6
975	1.9	-4.2	-421.9	-424.2
1000	0.0	-2.4	-358.4	-360.8
1025	-2.1	-0.3	-294.8	-297.3
1050	-4.0	1.6	-231.3	-233.7
1075	-5.4	3.0	-167.7	-170.2
1100	-5.5	3.2	-104.2	-106.5
1125	-3.3	1.0	-40.7	-43.0
1141	0.0	-2.3	0.0	-2.3

APPENDIX J- Data for the Debye Specific Heat

Θ	T	X	cV/3R	cV(J/moleK)	Ni4Mo Cv(J/gK)
300	300	1.00	0.9517	23.7377	0.3407
	400	0.75	0.9724	24.2540	0.3481
	500	0.60	0.9822	24.4985	0.3516
	600	0.50	0.9876	24.6332	0.3535
	700	0.43	0.9908	24.7130	0.3547
	800	0.38	0.9928	24.7629	0.3554
	900	0.33	0.9946	24.8078	0.3560
	1000	0.30	0.9955	24.8302	0.3563
	1100	0.27	0.9963	24.8502	0.3566
	1200	0.25	0.9969	24.8651	0.3568
	1300	0.23	0.9974	24.8776	0.3570
	1400	0.21	0.9978	24.8876	0.3572
	1500	0.20	0.9980	24.8926	0.3572
Θ	T	X	cV/3R	cV(J/moleK)	Cv(J/gK)
400	300	1.33	0.9169	22.8697	0.3282
	400	1.00	0.9517	23.7377	0.3407
	500	0.80	0.9687	24.1618	0.3468
	600	0.67	0.9779	24.3912	0.3500
	700	0.57	0.9839	24.5409	0.3522
	800	0.50	0.9876	24.6332	0.3535
	900	0.44	0.9904	24.7030	0.3545
	1000	0.40	0.9920	24.7429	0.3551
	1100	0.36	0.9939	24.7903	0.3558
	1200	0.33	0.9946	24.8078	0.3560
	1300	0.31	0.9952	24.8227	0.3562
	1400	0.29	0.9958	24.8377	0.3565
	1500	0.27	0.9963	24.8502	0.3566
Θ	T	X	cV/3R	cV(J/moleK)	Cv(J/gK)
500	300	1.67	0.8733	21.7822	0.3126
	400	1.25	0.9260	23.0967	0.3315
	500	1.00	0.9517	23.7377	0.3407
	600	0.83	0.9664	24.1044	0.3459
	700	0.71	0.9752	24.3239	0.3491
	800	0.63	0.9804	24.4536	0.3509
	900	0.56	0.9844	24.5533	0.3524
	1000	0.50	0.9876	24.6332	0.3535
	1100	0.45	0.9989	24.9150	0.3576
	1200	0.42	0.9912	24.7230	0.3548
	1300	0.38	0.9928	24.7629	0.3554
	1400	0.36	0.9936	24.7828	0.3557
	1500	0.33	0.9946	24.8078	0.3560

VITA

Douglas Falcon was born in Boulder, Colorado, in the foothills of the Rocky Mountains. He attended public schools there until he was fifteen. His high school years were spent in California, Oregon, and then Eastern Colorado. He graduated from Deer Trail High School, and then attended trade school for three years in Colorado.

The author then took a job at a firearms manufacturing company in California for two years. It was here that he developed an interest in materials science and metallurgy. He entered a metallurgical and materials engineering program at the Colorado School of Mines, in Golden Colorado, and recieved his B.S. degree in 1994.

The author worked at several jobs, including an aluminum mill as a lab technician, and at a cast iron foundry as a metallurgist. Although he obtained invaluable work experience, he felt that a more thorough understanding was needed, and so he entered the graduate program at the University of Tennessee, Knoxville. He received his M.S. degree in metallurgical engineering in 1998.